Role of Catalyst Support and Continuity Additives on the Degree of Electrostatic Charging and Reactor Fouling in Polyethylene Gas-solid Fluidized Bed Reactors

by

Milad Taghavivand

uOttawa

A thesis submitted in partial fulfillment of the
requirements for a

DOCTOR OF PHILOSOPHY IN CHEMICAL ENGINEERING

Department of Chemical and Biological Engineering
Faculty of Engineering
University of Ottawa

Abstract

Electrostatic charging occurs in many gas-solid processes due to interparticle and particle-process vessel wall contacts during particle handling, transport, and processing. A commercial process adversely affected by electrostatic charging is ethylene gas-phase polymerization. In such a process, catalyst particles, which are periodically fed into the fluidized bed reactor could become electrostatically charged along with the produced polyethylene (PE) resin, resulting in their adhesion to the reactor walls, causing an operational challenge known as sheeting. Sheets can break off the reactor walls and block the distributor plate resulting in a significant economic loss due to reactor shutdown for clean up. Electrostatic charge generation in PE fluidized bed reactors has been the topic of research for several years. However, to date, the majority of the works have only considered PE resin charging behavior and thus the influence of catalyst charging on the extent of reactor wall fouling has received minimal attention. Catalyst particles which have different chemistry and particle size from the PE resin, are expected to have different triboelectrification behaviour and thus contribute to the reactor electrification. In addition, dry feeding of the catalyst into the PE fluidized bed reactor through narrow tubes could make them electrostatically charged upon entering the reactor due to their collisions with the conveying tube wall. The catalyst particles' initial charge upon entering the reactor in addition to the generated charge due to their contacts with the PE resin inside the reactor could affect the degree of bed electrification and consequently the extent of particles migration towards the reactor walls. A widely used technique to mitigate the sheeting formation in commercial PE gas-phase fluidized bed reactors is dry feeding of compounds referred to as continuity additives (CAs). Although CAs are hypothesized to reduce the charge build-up in PE reactors, their exact role in mitigating or controlling the reactor sheeting is unknown. This in turn has made their selection, in particular for processes with a newer catalyst generation, challenging and only based on trial and error.

This thesis aims at understanding the roles that catalyst and CAs play on the degree of PE fluidized bed electrification and wall fouling formation. First, a thorough investigation was carried out on particles' electrostatic charging behaviour during their pneumatic conveying by designing and building a pneumatic conveying apparatus equipped with two electrostatic charge measurement techniques, from which one was an online method. This apparatus was then attached to an atmospheric gas-solid fluidized bed enabling the direct pneumatic injection of the powders into a

PE fluidized bed. The entire experimental system for the first time allowed the electrostatic charge measurement of a number of additives while being pneumatically conveyed into a PE fluidized bed. The experimental apparatus also allowed measurements of the electrostatic charge generation inside the fluidized bed as well as the amount of fluidized bed wall fouling. Since a big portion of the catalysts utilized in the PE process is occupied by the support, in this thesis the charging behavior of a typical catalyst support (i.e., amorphous silica) was studied as a preliminary step to study catalyst particles in the future. In addition, five commercially available CAs including three ionic (aluminum distearate, calcium stearate, and zinc stearate) and two non-ionic (AS-990 and Chimassorb 944) solids were tested. Ion and electron transfer were proposed as the charging mechanism of the ionic and non-ionic powders, respectively.

The amorphous silica catalyst support was found to become highly charged due to pneumatic injection while the CAs gained a minimal amount of charge. The fluidized bed wall fouling magnitude was observed to be directly related to the bed bulk particles' specific charge magnitude. Among the tested combinations, those that reduced the net charge of the bulk of the bed to close to zero were successful in reducing the amount of wall fouling. The bed bulk charge and the wall fouling magnitude were observed to be influenced by the type of the powders added, while being independent of the powders' charge upon entering the fluidized bed. The findings of this thesis clearly emphasize the significance of having knowledge of the solids' surface chemistry involved in the process and its utilization as a predictive tool in determining the charging mechanism of the continuity additives in contact with the PE resin inside the reactor. Knowledge of the solids' charging mechanism enables the prediction of the dominant charge polarity within the reactor and in turn resulting in effectively mitigating the reactor sheeting.

Résumé

La charge électrostatique se produit dans de nombreux procédés gaz-solide en raison des contacts entre les particules, ainsi qu'entre les particules et les parois du réservoir de procédé, durant la manipulation, le transport et le traitement de ces particules. Le procédé commercial de la polymérisation de l'éthylène en phase gazeuse est négativement affecté par la charge électrostatique. Dans un tel procédé, les particules du catalyseur, périodiquement introduites dans le réacteur à lit fluidisé, ainsi que la résine de polyéthylène (PE) produite, peuvent devenir chargées électrostatiquement, résultant à leur adhérence aux parois du réacteur, ce qui cause un défi opérationnel connu sous le nom de "sheeting". Les "sheets" peuvent briser les parois du réacteur et bloquer la plaque de répartition, ce qui entraîne une perte économique importante due à l'arrêt du réacteur pour son nettoyage. La génération de charges électrostatiques dans les réacteurs à lit fluidisé de PE fait l'objet de recherches depuis plusieurs années. Cependant, à ce jour, la majorité des travaux n'ont considéré que le comportement de charge de la résine PE donc l'influence de la charge du catalyseur sur l'étendue de l'encrassement des parois du réacteur a reçu une attention minime. Les particules de catalyseur qui ont une chimie et une taille de particule différentes à celles de la résine PE, devraient avoir un comportement triboélectrique différent, contribuant ainsi à l'électrification du réacteur. De plus, une alimentation sèche du catalyseur dans le réacteur à lit fluidisé de PE à travers des tubes étroits pourrait les charger électrostatiquement lors de leur entrée dans le réacteur en raison de leurs collisions avec la paroi du tube de transport. La charge initiale des particules de catalyseur lors de leur insertion dans le réacteur, ainsi que la charge générée en raison de leurs contacts avec la résine PE à l'intérieur du réacteur, pourraient affecter le degré d'électrification du lit et par conséquent l'étendue de la migration des particules vers les parois du réacteur. Une technique couramment utilisée pour atténuer la formation de "sheeting" dans les réacteurs commerciaux à lit fluidisé de PE en phase gazeuse est l'alimentation sèche de composés appelés additifs de continuité (AC). Bien que les AC soient censés réduire l'accumulation de charge dans les réacteurs PE, leur rôle exact dans l'atténuation ou le contrôle de "sheeting" du réacteur est inconnu. Cela a rendu leur sélection difficile et basée uniquement sur des essais et des erreurs, particulièrement pour les procédés avec une nouvelle génération de catalyseur.

Cette thèse vise à comprendre les rôles que jouent le catalyseur et les AC sur le degré d'électrification du lit fluidisé de PE et la formation d'encrassement sur les parois du réservoir.

Tout d'abord, une enquête approfondie a été menée sur le comportement de charge électrostatique des particules lors de leur transport pneumatique en concevant et en construisant un appareil de transport pneumatique équipé de deux techniques de mesure de charge électrostatique, dont l'une était une méthode en ligne. Cet appareil a ensuite été fixé à un lit fluidisé gaz-solide atmosphérique permettant l'injection pneumatique directe des poudres dans un lit fluidisé de PE. L'ensemble du système expérimental a permis pour la première fois de mesurer la charge électrostatique d'un certain nombre d'additifs tout en étant transporté pneumatiquement dans un lit fluidisé de PE. L'appareil expérimental a également permis de mesurer la génération de charges électrostatiques à l'intérieur du lit fluidisé ainsi que la quantité d'encrassement sur les parois du lit fluidisé. Puisqu'une grande partie des catalyseurs utilisés dans le procédé PE est occupée par le support, dans cette thèse, le comportement de charge d'un support de catalyseur typique (c'est-à-dire la silice amorphe) a été étudié comme étape préliminaire pour l'étude de particules de catalyseur à l'avenir. De plus, cinq AC disponibles dans le commerce comprenant trois solides ioniques (distéarate d'aluminium, stéarate de calcium et stéarate de zinc) et deux solides non-ioniques (AS-990 et Chimassorb 944) ont été testés. Le transfert d'ions et d'électrons a été proposé comme mécanisme de charge des poudres ioniques et non-ioniques, respectivement.

Il a été observé que le support de catalyseur de silice amorphe devenait très chargé avec l'injection pneumatique tandis que les AC ne gagnaient qu'une quantité minimale de charge. Il a aussi été observé que l'amplitude de l'encrassement des parois du lit fluidisé était directement liée à l'amplitude de la charge spécifique des particules en vrac du lit. Parmi les combinaisons testées, celles qui réduisaient la charge nette du lit à près de zéro, ont réussi à réduire la quantité d'encrassement sur les parois du réservoir. Il a été observé que la charge en vrac du lit et l'amplitude de l'encrassement des parois du lit étaient influencées par le type de poudres ajoutées, tout en étant indépendant de la charge des poudres lors de leur entrée dans le lit fluidisé. Les résultats de cette thèse soulignent clairement l'importance d'avoir une connaissance de la chimie de surface des solides impliquée dans le processus et son utilisation comme outil prédictif pour déterminer le mécanisme de charge des additifs de continuité en contact avec la résine PE à l'intérieur du réacteur. La connaissance du mécanisme de chargement de solides permet la prédiction de la polarité de charge dominante à l'intérieur du réacteur et, à son tour, résulte à une atténuation efficace du "sheeting" dans le réacteur

Statement of Contributions of Collaborators

All chapters presented in this thesis were written solely by me with editorial comments provided by Dr. Mehrani and Dr. Sowinski with the exception of chapter 4 in which editorial comments were also received from Dr. K. Choi (National Institute of Occupational Safety and Health, Japan).

Chapter 2 is a manuscript published in a peer-reviewed academic journal. I designed the pneumatic conveying apparatus, performed all the experiments, and analyzed the results with assistance from an engineering co-op student, Bilal Elchamaa, who is mentioned as a co-author. Editorial comments were provided by Dr. Mehrani and Dr. Sowinski who are also listed as co-authors.

Chapter 3 is a manuscript published in a peer-reviewed academic journal. The experimental work and results analysis were conducted by me. Benjamin J. Cho (an undergraduate student who carried his Undergraduate Research Opportunity Program in our lab) assisted me in conducting a part of the experiments. Editorial comments were provided by Dr. Mehrani and Dr. Sowinski who are also listed as co-authors.

Chapter 4 is a manuscript published in a peer-reviewed academic journal. The experimental work and results analysis were conducted by me at the National Institute of Occupational Safety and Health in Tokyo, Japan, under the supervision of Dr. Kwangseok Choi. Editorial comments were provided by Dr. Mehrani, Dr. Sowinski, and Dr. Choi who are also listed as co-authors.

Chapter 5 is a manuscript submitted to a peer-reviewed academic journal. The experimental work and results analysis were conducted solely by me. Editorial comments were provided by Dr. Mehrani and Dr. Sowinski who are also listed as co-authors.

Chapter 6 is a manuscript submitted to a peer-reviewed academic journal. The experimental work and results analysis were conducted solely by me. Editorial comments were provided by Dr. Mehrani and Dr. Sowinski who are also listed as co-authors.

Table of Content

List of Tables

List of Figures

Nomenclature

C_o	Capacitance between two bodies, F
d_p	Mean particle diameter, m
E_F	Fermi level, eV
E_G	Energy gap, eV
E_{vac}	Vacuum level, eV
e	Elementary charge, C
I	Electric current, A
ID	Pipe inner diameter, m
L	Pipe length, m
$\dot{m}_s$	Solid flow rate, kg/s
Q	Charge, C
ΔQ	Exchanged charge, C
ΔQ_C	Exchanged charge between materials in a contact, C
t	Time, s
U_g	Superficial gas velocity, m/s
V	Potential difference, V
V_C	Contact potential difference, V
ρ_P	Particle density, kg/m^3
ϕ	Work function, eV

Acknowledgement

Prior to anyone else, I would like to express my deepest gratitude and appreciation to both my supervisors, Dr. Poupak Mehrani and Dr. Andrew Sowinski who continuously supported me by providing guidance and advice throughout this challenging project. As well, I would like to express my regards and thanks to Dr. Kwangseok Choi from the Japan National Institute of Occupational Safety and Health who kindly accepted me in his research group and provided me with experimental facilities to conduct research abroad.

I would like to thank John F. Szul, David M. Pearson, Dr. Chuan He, and Dr. Kishori Deshpande from Univation Technologies, LLC, and Dow Chemical Company for their guidance and support as well as for supplying all the samples used in this work.

I would also like to acknowledge my graduate student peers, Fahad Al Amin Chowdhury, Mohsen Isaac Nimvari, Christopher McIntyre, Fang Li, and Di Song for the productive discussions and their scientific input to this project. I would also like to thank the undergraduate students, Benjamin January Cho and Bilal Elchamaa who helped to perform the experiments.

This work could not have been completed without the help from the staff of the Department of Biological and Chemical Engineering at the University of Ottawa: Franco Ziroldo, Gérard Nina, James Macdermid, Francine Pétrin, Sylvie Saindon, and Chantal Dube for their kindness and assistance.

The financial supports provided by the Ontario Trillium Scholarship (OTS), Faculty of Engineering International Experience Scholarship (IES), Natural Sciences and Engineering Research Council (NSERC) of Canada, and Univation Technologies, LLC (USA) are acknowledged and appreciated.

Last but not least, I would like to express my warmest thanks to my parents and my wife, Parinaz Arjmandkia, who never stopped believing in me and showed her continuous support in every aspect of our lives.

Chapter 1 - Introduction

In many gas-solid processes, electrostatic charges are generated by the triboelectric charging phenomena due to particle-particle and particle-wall contacts during particle handling, transport, and processing. The generation of electrostatic charge can lead to operational challenges including particle-wall adhesion, particle agglomeration and segregation, and high-voltage electrical fields, which can cause explosions. The significant negative impact of electrostatic phenomena has been reported in many industries such as petrochemicals [1], oil and gas [2], and pharmaceuticals [3]. In particular, in the petrochemical industry, electrostatic charging has been clearly observed in the production of polyethylene (PE), which is conducted in catalytic gas-solid fluidized bed reactors. In this process, electrostatic charging of PE and catalyst particles results in their adhesion to the reactor wall and formation of "sheets" [4]. Sheeting is known to be a major drawback since particle sheets can break off and block the reactor, causing long shut down periods for clean-up. Reactor shut down results in significant economic losses due to decreased production and higher maintenance costs. Globally, there are over 100 reactors producing nearly 20 Mt/yr of PE (e.g., Dow Canada in Prentiss, AB, producing 750,000 t/yr). A fouling incident could result in 2 to 30 days of reactor downtime. A rough estimation of the economic loss due to such an occurrence for the Dow Canada Prentiss plant (Alberta) is nearly USD 2.0M/day.

The operational challenges resulting from electrostatics necessitate the understanding of the mechanisms contributing to particle charging in gas-solid fluidized beds, and in particular, in relation to the PE production process. Concerning PE fluid bed reactor electrification, in this work, it is hypothesized that charging of catalyst particles through pneumatic conveying into the reactor is a contributing factor to the overall reactor charging and migration of the particles to the reactor wall and their subsequent fouling.

1-1 Electrostatic Charge Generation

The very first detection of electrostatic charge generation may date back to as early as the sixth century BC in Greece when it was noticed that some light objects such as feathers are attracted by amber after rubbing against fur [5]. From then on and throughout the centuries, the electrostatic effects have been regarded as one of the influential contributors in numerous undesired incidents in many industrial and manufacturing processes dealing with particulates. Examples of processes

include grinding, sieving, mixing, solids conveying, solids transfer from bags to hoppers and silos, gas-solid fluidization, and pneumatic transport. In all processes, collisions between solids and the containing vessel, and/or collisions among solids themselves could be the cause of the generation of electrostatic charge. In relation to the hazardous effect of electrostatics, a study published in 2011 [6] has revealed that electrostatic discharge was responsible for almost 70% of 153 industrial accidents over a 50-year time span in Japan. Furthermore, according to statistics in Germany published in 2003, one dust explosion occurs each day and every tenth explosion is caused by static electricity [7]. Therefore, it is important to understand and distinguish the dominant charge generation mechanisms to help control or eliminate the negative impacts of static electricity in many processes.

1-1-1 Electron Energy and Energy Bands

This section briefly summarizes some of the fundamental concepts of electrons configuration in atoms, which are of great importance in charge transfer between solid materials.

In a single isolated atom, electrons with a certain amount of energy are rotating in orbits, known as energy levels, around the nucleus. Bringing isolated atoms together to form a solid will result in merging of the single energy levels and formation of less precisely defined energy levels known as energy bands as presented in **Figure 1-1** [8,9].

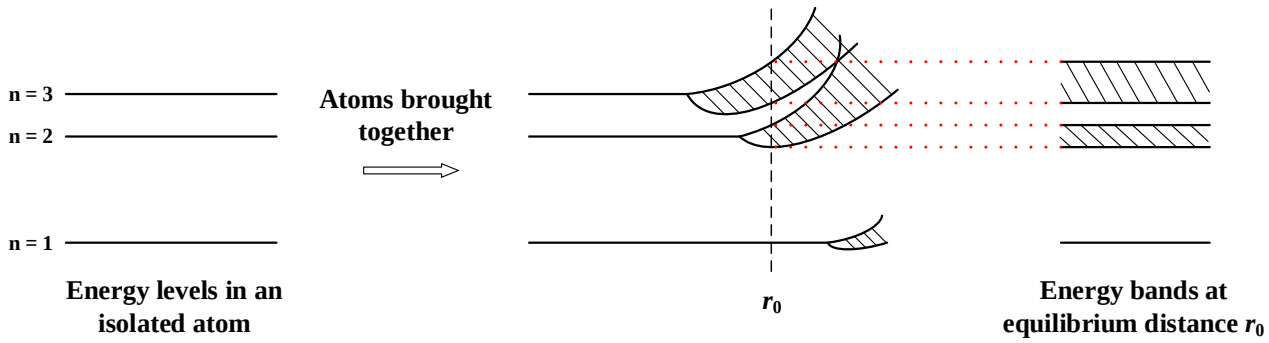

Figure 1-1 The formation of energy bands. The sharp energy levels of individual atoms widen as the atoms are brought together because of interactions between the electrons of different atoms [8].

The electrons located in these energy bands have a fixed range of energies, rather than a particular energy. The energy band which is the farthest from the nucleus is called the valence band and the electrons located in the valence band are called the valence electrons [8]. The conduction band is the last energy band that may exist and corresponds to the excited states of the outer electrons [8].

The gap between the two energy bands is the forbidden energy band or energy gap (E_G) in which no electron can exist [8]. **Figure 1-2** schematically shows energy bands structure in a material with a partially filled valence band.

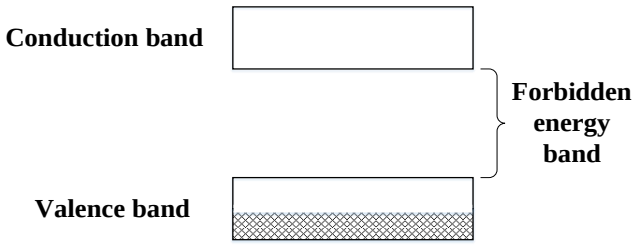

Figure 1-2 Schematic diagram of energy bands structure in a material.

Whether a material is electrically conductive, insulating or semi-conductive depends on the variation in the band structure. **Figure 1-3a** illustrates an insulator in which the movement of electrons is very limited. This can occur if the conduction band is empty but the valence band is completely full of electrons or if the energy gap is large (up to 12 eV) [8]. Electron volt (eV) is an energy unit and is defined as the energy gained (or lost) by the charge of a single electron moving across an electric potential difference of one volt. Semi-conductors, by their nature, have the same structure as the insulators with the exception that their energy gap is much smaller than that of insulators and is in the order of 1 eV (**Figure 1-3b**). Such a characteristic provides an opportunity for electrons to become excited and move from the valence band to the conduction band by obtaining a reasonable amount of either thermal or optical energy [8,9]. This electron transportation from the valence band to the conduction band leaves some unoccupied places in the valence band which are known as electron holes [9]. Therefore, aside from the electron movement between bands which assists a material to conduct electricity, depending on the number of formed holes in the valence band, the partially empty valence band could also facilitate the conductivity of the material. In metals, the valence band is either partially filled (**Figure 1-3c**) or the valence band and the conduction band overlap (**Figure 1-3d**). In both cases, electrons can easily increase their energy within the band and move. Such characteristic turns these materials into perfect conductors. Silver, copper, gold, and aluminum are a few examples of such materials [8].

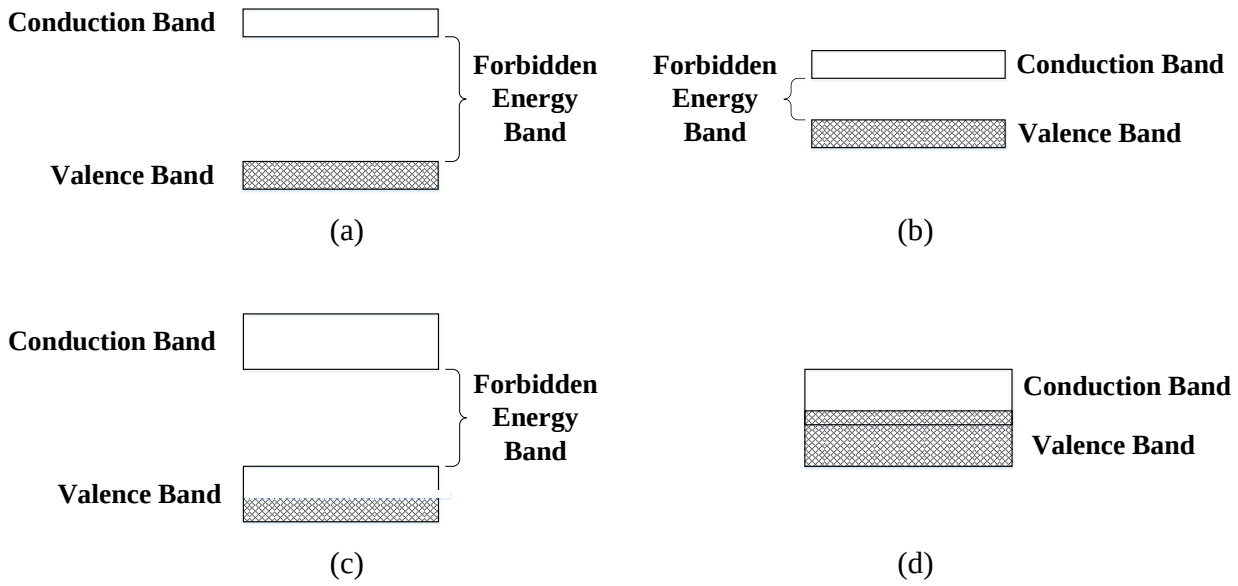

Figure 1-3 The band structure in (a) insulator, (b) semi-conductor, (c) conductor (partially filled valence band), (d) conductor (overlapping conduction and valence band).

The vacuum level (E_{vac}), a reference point where the electron has zero kinetic and potential energy, is another important (**Figure 1-4**). Electrons with positive energy are free to move and not bounded to the atom and poses certain kinetic energy, whereas the negative energy represents electrons that are bound to the atom and are located at a certain energy level in the atom [10].

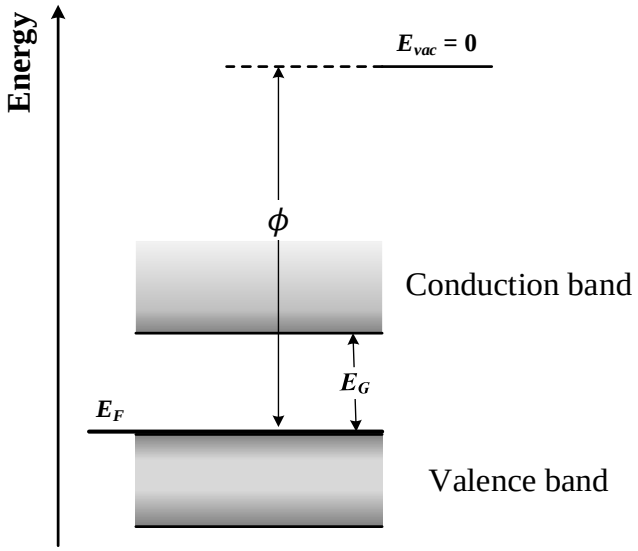

Figure 1-4 Energy diagram of a metal [10].

The work function (ϕ) is referred to as the energy required to transfer an electron from the Fermi level (E_F) – the occupied energy level at absolute zero temperature – to a point in infinity relative

to surface yet not so far away as to be affected by the ambient electric field, i.e. at E_{vac} [8,10,11]. The work function can be interpreted as the energy barrier which resists the transfer of an electron from the fermi level to vacuum level [10] and is widely used to describe the electrostatic charge transfer.

1-1-2 Charge Generation Mechanisms

Solids can be electrostatically charged due to three known mechanisms of (a) contact charging, (b) frictional charging (also known as tribocharging), and (c) induction charging.

- *Contact Charging:* Electrostatic charging can occur when two solids (of the same or different materials) are brought into contact and then separated as shown in **Figure 1-5**. At the point of contact, the difference in solids surface energy levels results in electrostatic charges to transfer between surfaces until an equilibrium state is reached. If the solids are then separated, the electrostatic equilibrium is destroyed, and two oppositely charged electrical layers will form on the surfaces of the solids [12–15]. This charging mechanism is known as contact charging or contact electrification [14].
- *Frictional Charging:* Also known as triboelectrification or tribocharging, which occurs when two solids are rubbed against each other [14]. The distinction between contact electrification and frictional electrification is difficult; therefore, the term triboelectric charging or tribocharging is widely used in the literature to describe both mechanisms.

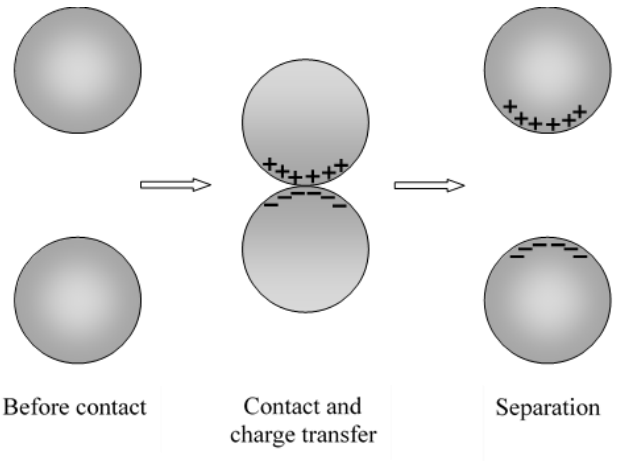

Figure 1-5 Schematic illustration of contact electrification.

- *Induction Charging*: As shown in **Figure 1-6**, induction charging involves a charged object that is brought close to an isolated object, which is electrically conductive and neutral. Depending on the polarity of the charged object, the electrons on the surface of the neutral object will move and accumulate on the side closer or further away from the charged object (**Figure 1-6b**). Grounding the neutrally charged object will then result in the object becoming either positively or negatively charged (gaining an opposite charge polarity to that of the inducing charge source) (**Figure 1-6c**). Disconnecting the ground source followed by moving the charged object away will turn the initially neutral object into a charged object with an opposite charge polarity to that of the inducing charge source (**Figure 1-6d**). It is important to note that in this case, an attractive force, known as the image force, can be created between the two oppositely charged objects.

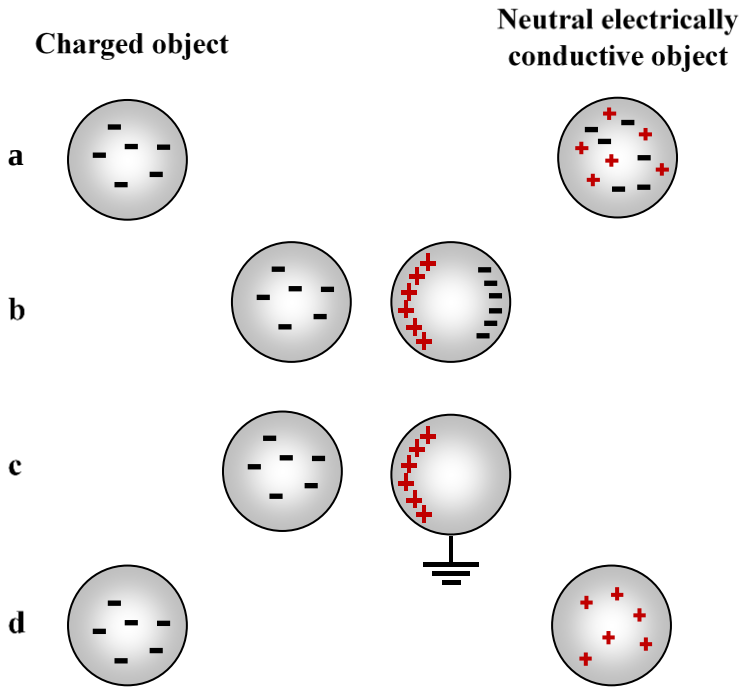

Figure 1-6 Induction charging by a negatively charged object. (a) Bringing a negatively charged and a neutral electrically conductive object to a close distance, (b) electron redistribution on the surface of the neutral object, (c) moving electrons from the neutral object to the ground source, (d) disconnecting the ground and separating the two objects.

Based on the surface conductivity, the contact between objects can then be divided into three categories: i) metal-metal contact; ii) metal-insulator contact; and iii) insulator-insulator contact.

1-1-2-1 Metal-Metal Contact

The cause of electron transfer during a metal-metal contact is the contact potential difference (V_c) which is a result of the difference in work functions of metals in contact [9].

$$V_c = -\frac{(\phi_1 - \phi_2)}{e} \qquad \textbf{(Eq. 1-1)}$$

where ϕ_1 and ϕ_2 are the work functions of metals (eV) and e is the elementary charge (C) [16] (see **Figure 1-7**).

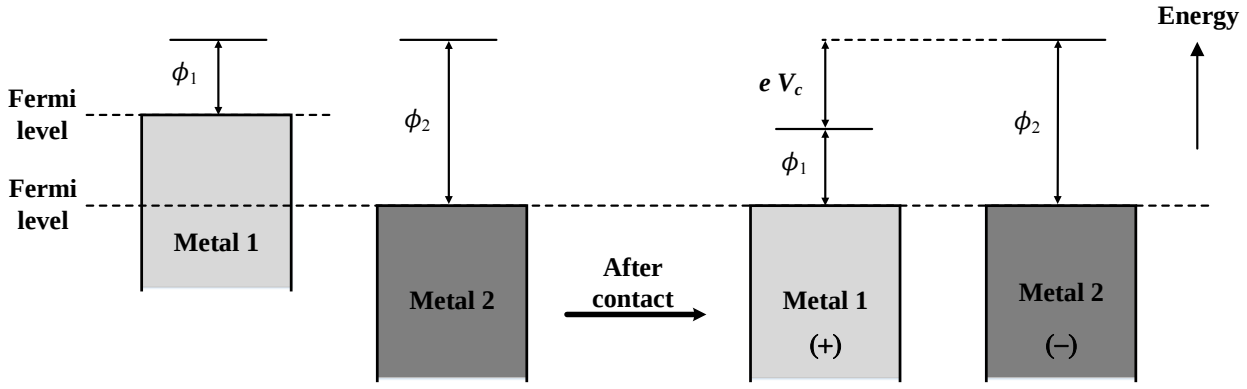

Figure 1-7 Electron potential energy for metal-metal contact.

According to the work function definition, the electron transfer from a metal with a lower work function to a metal with a higher work function will continue until the electron energy (chemical potential or Fermi energy level) reaches equilibrium [15]. In order to determine the amount of transferred charge, the condenser (capacitor) model can be applied [10]. This model suggests that the charge accumulation on the surfaces of materials in contact with each other is similar to charge build-up on a capacitor [9]. Therefore, using this model, the transferred charge between materials (ΔQ_c) can be calculated by:

$$\Delta Q_c = C_0 V_c \qquad \textbf{(Eq. 1-2)}$$

where C_0 is the capacitance between two bodies (F) at a distance where charge transfer stops, and V_c is the contact potential difference (V) [10].

1-1-2-2 Metal-Insulator and Insulator-Insulator Contacts

Due to the fact that insulator materials do not have free electrons in their valance band, aside from electron transfer, ion transfer and material transfer have been proposed to explain their charging mechanism as a result of contact between a metal or an insulator [16].

As mentioned earlier, the charge transfer mechanism for metals, which are electrically conductive, is believed to be dominantly electron transfer [17]. However, for insulators, depending on their surface nature, either of the three proposed mechanisms can be considered as a dominant charge transfer. As such, and to facilitate analyzing the charging mechanism for insulators, they are categorized as ionic and non-ionic solids [17,18]. It has been observed that polymeric solids covalently functionalized with ionic compounds develop a charge polarity similar to that of the covalently bonded side of the ionic compound upon contacting other materials, which were observed to develop a charge polarity similar to that of the mobile counterion [17–22]. Surface analysis such as X-ray Photoelectron Spectroscopy (XPS) confirmed the existence of the mobile counterion on the contacting surfaces [17]. There are several reported applications of using ionic compounds to tailor and control the transferred charge and its polarity in the electrophotographic industry [21,23–26].

As for the non-ionic solids, acidity/basicity of the solids' surface or their proton affinity (PA) were proposed as the driving forces for charge transfer [18,27–30]. Solids with an acidic surface (such as SiO_2, TiO_2, or sulfonated polystyrene) are typically regarded as materials with a high work function with a tendency to develop a negative charge by attracting electron pairs or adsorbing OH^- ions (i.e., Lewis definition), or losing H^+ ions (i.e., Bronsted definition) [27,28,30–33]. In contrast, solids with a basic surface (such as MgO, Al_2O_3, or De-acidite FF) would develop a positive charge by losing electron pairs or adsorbing H^+ ions (i.e., Lewis definition), or losing OH^- (i.e., Bronsted definition) [27,28,30–33]. The supply of H^+/OH^- in this charge transfer mechanism is assumed to be the hydroxide groups on the surface. Transferring H^+/OH^- is one specific case for ion transfer charging mechanism.

Another proposed charging mechanism for non-ionic solids is transferring of mobile H^+/OH^- ions resulted from the moisture present either in the environment or as separated patches adsorbed on the surface of the solids (even those with a high hydrophobic nature) [17,34,35]. However, in a

separate study, charge transfer was proven to be independent of the moisture presence; although moisture was observed to promote the transferred charge magnitude [36].

Material transfer is another mechanism that is applicable where a small piece from an object adheres to another object during contact [16,37,38]. Charge transfer occurs if the transferred piece carries an electrostatic charge.

1-1-3 Electrostatic Charge Measurement

Two commonly employed methods to measure the electrostatic charge include Faraday cups and electrostatic probes. The Faraday cup is used to measure the net charge of objects that are placed inside it, whereas electrostatic probes are used to determine the net cumulative charge at specific local points inside a system [39].

1-1-3-1 Faraday Cage Technique

A Faraday cage consists of two concentric vessels made of a conductive material such as copper, which are insulated from each other (**Figure 1-8**). The outer vessel is grounded and acts as a shield to prevent external electric fields from affecting the inner vessel and subsequently the electrostatic charge measurement. The inner vessel, which is used to determine the electrostatic charge, is connected to an electrometer that measures charge by detecting the voltage generated across a known capacitor.

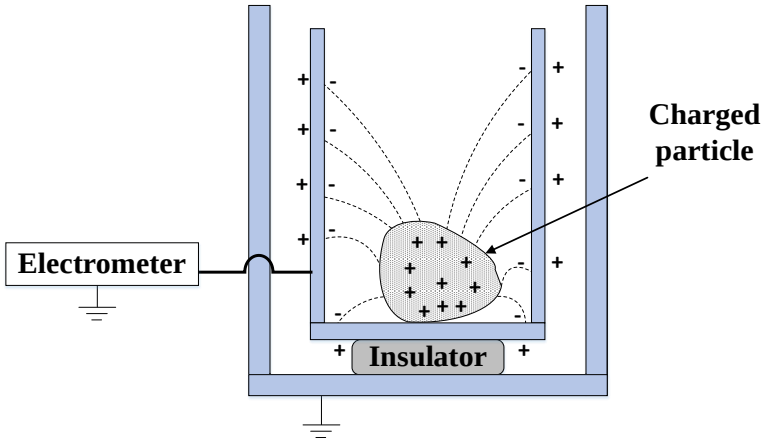

Figure 1-8 Faraday cage for measuring the electrostatic charge.

As an object is placed inside a Faraday cage, equal but opposite charges will accumulate on the inner wall of the inner vessel. This is due to induction charging between the object and the

conductive wall, which leads to charge build-up with the same magnitude and polarity as of the charged object on the outer wall of the inner vessel. It is important to note that for applications with particles, a Faraday cage measures the bulk net charge of particles placed inside it and does not provide any information about the charge of the single particles.

1-1-3-2 Electrostatic Probes

In principle, electrostatic probes measure electrostatic charge by reading the image charge induced on their conductive surfaces (**Figure 1-9**) [39,40]. When a charged object approaches an electrostatic probe, the object can induce an image charge of itself on the probe. This induced signal is measured using an electrometer as an electric potential, current, or charge. Unfortunately, the adhesion of particles to the tip of the probe can significantly influence the charge reading [41]. Also, in the case that particles collide with the probe, the contacts might introduce extra charge and eventually affect the accuracy of charge measurement over time [42].

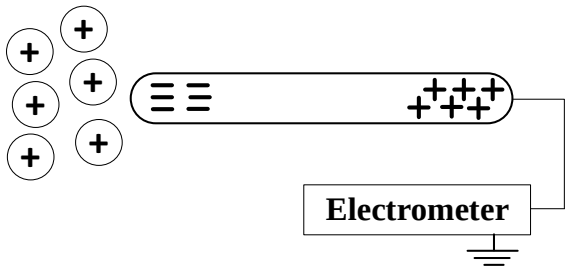

Figure 1-9 Electrostatic probe measurement technique.

1-2 Electrostatic Charging in Gas-Solid Fluidized Beds

Gas-solid fluidization is a process in which passing of a gas upward through a static bed of solid particles turns it into a dynamic fluid-like state. Gas-solid fluidized beds have a wide range of application in many industries such as petrochemical [43], oil and gas [44], food and agriculture [45], pharmaceutical [46,47], etc. due to their excellent characteristics of providing a high degree of heat and mass transfer, as well as good mixing.

The presence of electrostatic phenomenon in gas-solid fluidized beds, which results from repeated particle-particle collisions along with contacts of particles with the vessel wall, and its contribution to particle adhesion to the fluidization column wall were first reported in the early 1940s

[12,39,48,49]. Segregation and agglomeration of particles, adhesion of particles to the wall surface, and finally electrostatic discharge that can cause explosions are generally the problems associated with tribocharging in gas-solid fluidized beds [48–50]. Charged particles can attract or repel each other, resulting in segregation or formation of particle agglomerates (chunks), ultimately affecting the fluidization hydrodynamics [48,49]. Electrostatic discharge, which could lead to electrical shocks to operating personnel, damaging the manufacturing equipment and facilities, or even fires and explosions, are often the result of the generation of high-voltage electrical fields [49].

One industry that has significantly suffered from the operational challenges resulting from fluidized bed charging is the polyolefin industry and in particular ethylene gas-phase polymerization process to produce PE. PE is the most widely used plastic in the world [51]. A simplified diagram of this process, which was developed by Union Carbide (now owned by Univation Technologies) and named UNIPOL PE Process, is shown in **Figure 1-10**. The polymerization reaction is an exothermic catalytic reaction that requires ethylene as the reactant. Ethylene gas and its co-monomers (1-butene, 1-hexene, or 1-octene) are fed into the bottom of the fluidized bed reactor at a flow rate as high as 6 times the minimum fluidization velocity, corresponding to turbulent flow regimes [43].

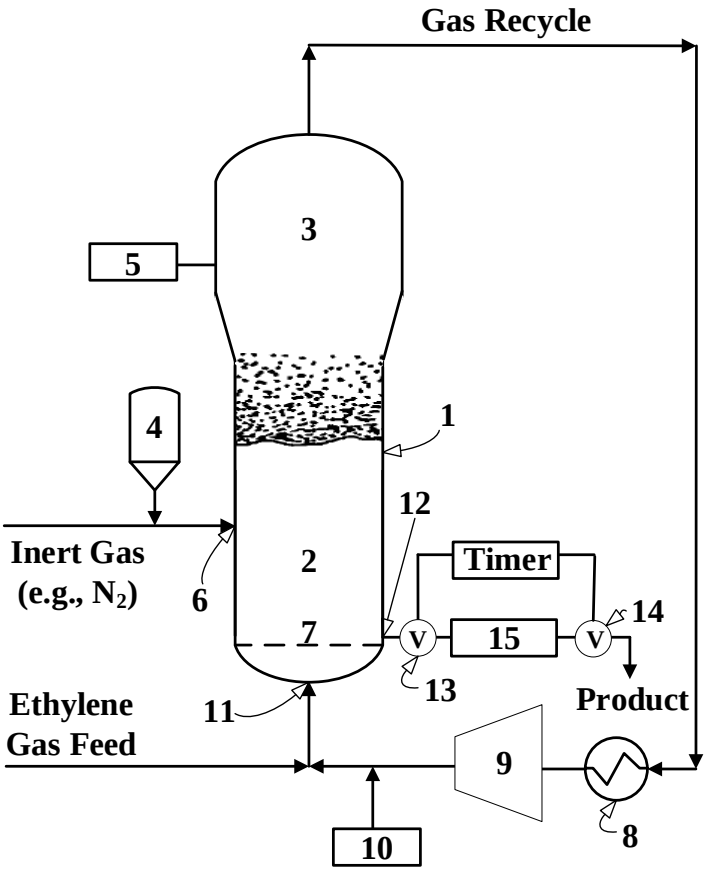

Figure Description	
1	Reactor
2	Reaction Zone
3	Disengagement Zone
4	Catalyst Reservoir
5	Gas Analyzer
6	Fluidization Ethylene Gas
7	Distributor Plate
8	Compressor
9	Heat Exchanger
10	Dispenser
11	Catalyst Injection Port
12	Product
13, 14	Valve
15	Segregation Zone

Figure 1-10 Schematic of Union Carbide (UNIPOL^{TM}) gas-solid PE fluidized bed polymerization reactor [4].

Three major catalysts used in ethylene polymerization are Ziegler-Natta, metallocene, and chromium-based (e.g., Phillips) catalysts. Ziegler-Natta catalysts typically comprise a transition metal salt of metals from groups IV-VIII (e.g., titanium, vanadium, chromium, and zirconium) and a co-catalyst/activator which is a metal alkyl of a base metal from group I-III (e.g., triethyl aluminum also referred to as TEAl) [52,53]. The third component in Ziegler-Natta catalysts which is employed to increase the catalysts activity and/or stereoselectivity is an electron donor and could be chosen from amines, ethers or esters (e.g., ethyl benzoate) [53]. $TiCl_4$ and $TiCl_3$ are examples of Ziegler-Natta catalyst. Phillips catalysts, which do not require a co-catalyst and their activation is in-situ during polymerization, are composed of chromium oxide (CrO_x) or vanadium oxide (VO_x) which is generally impregnated on an amorphous silica support [54]. Metallocene catalysts, which belong to the single site catalyst family, are organometallic compounds with a transition metal (e.g., titanium, zirconium or hafnium) at the center bounded to one or two cyclopentadienyl (Cp) rings or substituted cyclopentadienyl rings [53,54]. Methylaluminoxane (MAO) and trityl

tetrakis (pentafluoro phenyl) borate are two typical co-catalysts/activators for a majority of the metallocene catalysts [53,55]. In an industrial scale, Ziegler-Natta and metallocene catalysts can be used in either supported (heterogeneous) or non-supported (homogenous as soluble in reaction solvent) form, whereas the Phillips catalyst, as explained, exists in the supported form. Magnesium dichloride ($MgCl_2$) and amorphous silica (SiO_2) are two of the commonly used materials for catalyst supports [54]. With respect to ethylene gas-phase polymerization, a supported form of these catalysts should be utilized. Further information on Ziegler-Natta and metallocene catalysts is provided in **Appendix B**.

In commercial gas-phase PE processes, catalyst particles are periodically injected into the reactor in either slurry or dry solid form. However, there are a number of problems associated with slurry feeding including the uneven distribution of catalyst particles inside the reactor after the injection, the need for an additional slurry making equipment and procedure, as well as possible impacts on catalyst activity [56]. In the dry feeding systems, catalyst particles, which are stored in a catalyst reservoir under a nitrogen blanket, are pneumatically conveyed into the reactor at a rate equal to PE production through narrow and long tubes (typically stainless-steel tubes with a 4.75×10^{-3} m inner diameter) at ¼ to ¾ of the bed height above the distributor plate [43].

The polymerization reaction takes place on the surface of the catalyst particles through fragmentation process by which the growing chains rupture the support and entrap the active catalyst sites at their center. As the PE resins grow, they drop down to the bottom of the bed and discharge as the product. Polymerization heat is removed by a heat exchanger before the unreacted portion of the ethylene gas is recycled back to the reactor using a compressor to improve the conversion rate. With the current technology, the reactor operating pressure is between 20 to 30 atm, and the temperature ranges from 75 ^{o}C to 110 ^{o}C [43].

In the gas-phase PE production, if the PE resin and catalyst particles become electrostatically charged, they could adhere to the fluid bed reactor walls while the exothermic reaction progresses. Due to the poor reaction heat removal from the reactor walls, the localized temperature rise melts the growing PE resin causing the formation of sheets along the reactor wall. Such sheets, which are shown schematically in **Figure 1-11** and have been reported to be up to 0.05 m thick, over 0.5 m wide and up to 1.5 m long, can break off the reactor wall and block the distributor plate and

impose a long reactor shut down period for clean-up (i.e., process discontinuity), resulting in significant production and economic losses [4,48,57–59].

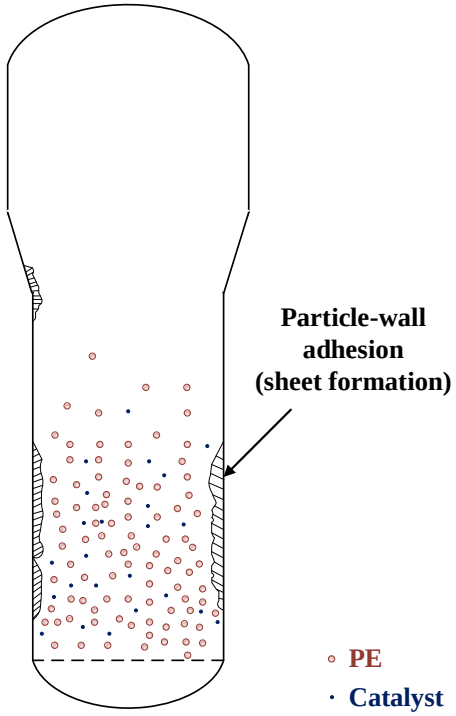

Figure 1-11 Schematic of the wall sheeting in a PE production fluidized bed reactor.

1-2-1 Controlling the PE Gas-Solid Fluidized Bed Reactors Sheeting

The above-mentioned challenges resulting from fluidized bed electrification necessitate the understanding, measurement, and reduction or elimination of electrostatic charge build-up from both process operation and safety standpoints. Attempts have been made by the industry to determine ways to reduce or prevent the reactor charge build-up. Operating under condensed mode to enhance the reaction heat removal by introducing an inert condensing agent (ICA) such as iso-pentane at a temperature just below its dew point, treating the reactor inner wall prior to polymerization by chromium-containing compounds, suppression of the fines by introducing a hydrocarbon, redesigning the fluidized bed reactor (e.g., redesigning the distributor plate and reactor expanded zone) and using sound waves were other techniques used to eliminate the reactor sheeting [4,60–64].

The addition of continuity additives (CAs), formerly known as static control agents, to the reactor during operation is another widely used technique. Although some of the CAs have been reported

to adversely affect the catalyst productivity, they have shown promising results in controlling the reactor sheeting [65]. Inorganic metal oxides such as MgO and SiO_2, very low concentrations of water, alcohols, ketones, oxygen and nitric oxide, metal carboxylate salts (e.g., aluminum distearate or calcium stearate), fatty amine alkoxylate (e.g., Atmer AS-990), polyethyleneimines (e.g., LUPASOL FG or LUPASOL WF), and hindered amine light stabilizers (e.g., CHIMASSORB 944) are some of the commercially used CAs which can be added to the process either separately or as part of the supported catalyst composition [1,65–72]. Same as the catalysts, CAs are periodically injected into the reactor as a solution in liquid hydrocarbons, slurry in mineral oil, or in dry solid form through separate pneumatic conveying lines (typically stainless-steel tubes with a 4.75×10^{-3} m inner diameter) [65–67,72,73]. CAs are hypothesized to either induce a charge polarity within the reactor opposite to that of a dominant bed charge polarity or increase the electrostatic conductivity of the reactor material (i.e., growing PE resin) [4,56,71,72,74].

Despite employing various techniques to eliminate the reactor sheeting, the problem persists and the new generation of catalysts (such as metallocene and other single site catalysts) demand more effective techniques. With the application of CAs, their exact role in controlling the reactor sheeting is not well examined and their selection has been based on trial and error. As such, a comprehensive study to determine the triboelectric effects of different commercially used CAs on PE fluidized bed electrification and the extent of wall fouling is needed.

1-2-2 Summary of Reported Research Works Related to PE Reactor

Numerous works have investigated the occurrence of electrostatic charge build-up in atmospheric and pressurized (up to 2600 kPa) at small and pilot-scale in particular with reference to PE reactors. In the course of 60 minutes fluidization period of PE resin, Giffin et al [41,58] observed that the majority of the wall fouling formed at the first 15 – 20 minutes of the fluidization. The wall fouling was found to decline using a fluidizing gas with a relative humidity greater than 60% in a stainless-steel fluidization column [75]. Song and Mehrani [58] observed that transitioning from the bubbling to the turbulent flow regime, by increasing the fluidizing gas velocity, increases the wall fouling of PE resin approximately 5 times. Their study was carried out in a pilot-scale 0.15 m pressurized (i.e., 2600 kPa) fluidization column. The same authors also observed that increasing the operating pressure from atmospheric to 2600 kPa to augment the extent of wall fouling of PE resin [76]. The effect of particle size distribution was also studied and it was found that increasing

the fraction of smaller size PE resin (212 – 400 μm) in a mixture with larger PE resin (600 – 700 μm) increased the wall fouling magnitude [77,78].

With respect to the underlying mechanism of charge build-up leading to wall fouling formation in PE fluidized beds, the only work found in the open literature is that of Song and Mehrani [59]. In studying PE resin electrostatic charging and reactor sheeting, they proposed a mechanism for reactor wall fouling in fluidized beds with metallic columns. Their work signifies the contribution of induction charging leading to *attractive image force* between the charged PE resin and the column wall, in addition to the *attractive electrostatic forces* between the charged particles on the wall and particles of opposite charge in the bulk of the bed (see **Figure 1-12**). They reported that the thickness of the coating layer depends on the magnitude of the image and electrostatic forces relative to gravity and drag force inside the fluidized bed.

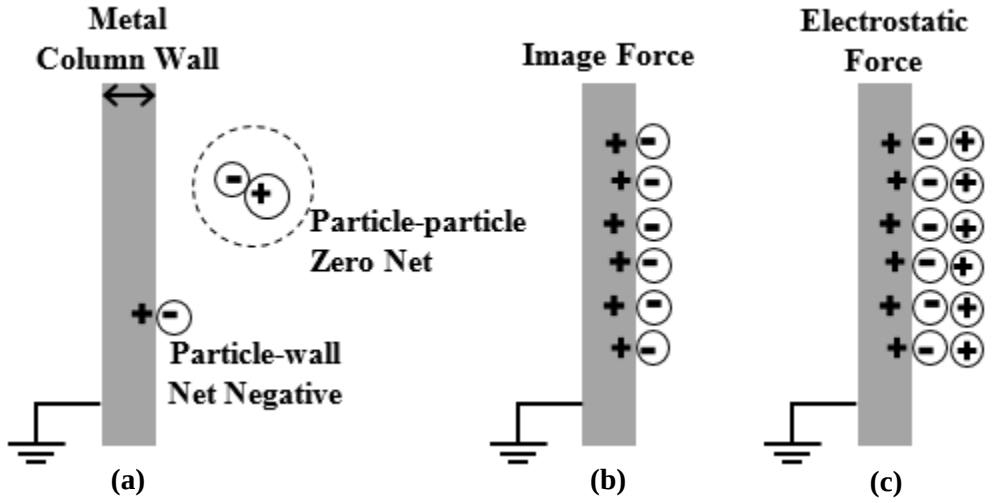

Figure 1-12 The wall fouling mechanism proposed by Song and Mehrani [59]; (a) electrostatic charge transfer and generation as a result of inter-particle and particle-wall contacts, (b) attraction of particles towards the metallic column wall due to image force, (c) attraction of oppositely charged particles towards the fouled layer on the column wall.

The focus of all studies reported in the literature in relation to the electrostatic charging in PE gas-solid fluidized bed reactors has been the charging behaviour of PE resin alone. However, in a commercial PE process, catalyst particles and other solid additives (e.g., co-catalyst and CAs) exist alongside the PE resin. All these particles are of different surface chemistry and size distribution and thus it is expected that they would result in different triboelectrification behaviour when in contact with each other and the PE resin inside the fluidization column. Thus, their role and

contribution to the PE reactor electrification and wall fouling must be determined. This is a critical area that has not received any attention.

1-3 Electrostatics in Pneumatic Conveying

Pneumatic conveying is a process which involves the transportation of dry powdery or granular solids in a gas stream [79]. Pneumatic transport is known for generating electrostatic charge on the conveying solids. Suspended solids acquire a tremendous amount of electrostatic charge as a result of the contact between themselves and especially with the conveying line walls while being transported in the gas phase. In fact, it is believed that among all gas-solid processes, pneumatic conveying systems generate the most charge on the particles [80]. Based on the concentration of the solid particles in the gas stream, pneumatic conveying is categorized as either a dilute phase or a dense phase system. Since the pneumatic conveying of catalyst particles in the PE process falls under the dilute phase category, the focus here will mainly remain on dilute phase systems. Depending on the application, dilute particle flow within pneumatic conveying lines can be performed in either continuous or pulse flow (pulse injection). Several studies have been carried out throughout the years to understand the electrostatic charge generation in continuous dilute pneumatic conveying systems. **Table 1-1** summarizes these works.

Table 1-1 Investigations on the electrostatic charge generation of particles during their pneumatic transport.

#	Year Investigators	Conveying line			Particle			Operating condition	
		Material	ID (cm)	L (m)	Material	d_P (μm)	ρ_P (kg/m^3)	$\dot{m}_s$ (g/s)	U_g (m/s)
1	1969 Cole et al. [81]	Brass	2.22	45	Polystyrene	150 to 450	1057	100	up to 50
		Nylon							
2	1982 Smeltzer et al. [82]	PMMA	2.54	3	Glass beads	75	2495	not specified	up to 39
						150			
3	1989 Gajewski [83]	SS	5	8.8	Polystyrene pearl	400 to 2200	1040	220	1.5 to 15
4	1994 Masuda et al. [84]	SS (SUS304)	0.6	0.8	Fly ash	3.4	2300	0.0003, 0.0036	30
		SS (TiN coated)		0.07	Alumina	3.1	4000	0.0008, 0.0037	30
		SS (Pt coated)		0.07					
5	1998 Masuda et al. [85]	SS	0.6	0.4	Epoxy resin	33	1450		29
		PTFE		0.1					
		Conductive PTFE		0.1					
		Conductive Nylon		0.1					
6	2002 Matsusaka et al. [86]	SS	0.46	0.05	Fly ash	7	2300	0.0006	36 to 77
				0.25					
				0.5					
				1					
				2					
7	2003 Matsusaka et al. [87]	SS (spiral)	0.6	up to 3	Fly ash	4.2	2300	0.0005 kg solid/kg air	20 to 39
					Alumina	3.9	4000		
8	2003 Nifuku and Katoh [88]	Brass	5.3	1	Pulverized coal	38		1.1 to 15.5	10 to 35
		Nylon	0.69	100	Fly ash	20	2300	1.1 to 15.5	7.5 to 13.3
9	2004 Yao et al. [89]	PVC	4		PP	3.35 – 4.1	1400	10.2 to 44.7	11.4 to 21.2
					PP + Glass beads	38	1414		
10	2006 Yao et al. [90]	PVC	4		PVC	3.35 – 4.1	1400	10.2 to 44.4	12.6 to 21.2
11	2006 Watano [91]	SS (SUS 304)	2.8	2	PMMA	100 – 200	1090	16.67	33
12	2007 Matsusaka et al. [92]	SS (SUS 316)	0.6	0.5, 1, 2, 3	Alumina	3.3	4000	0.0005 kg solid/kg air	40
		SS (SUS 304)							
		Al							
		Cu							
		Brass							
13	2008 Matsusaka et al. [93]	SS	0.6	0.5, 1, 2, 3 (spiral, 8 cm R)	Alumina	3.1	4000	0.0005 kg solid/kg air	40
		Copper							
14	2009 Dragan et al. [94]	PVC	3.3	2	ABS-PC	3000		1.67, 3.33	25
15	2009 Thomas et al. [95]	Polyurethane	1	up to 6	Polyester + Si	25	1350	3.3	25
					Polyester + Al				

#	Year Investigators	Conveying line			Particle			Operating condition	
		Material	***ID* (cm)**	***L* (m)**	**Material**	**d_P (µm)**	**ρ_P (kg/m^3)**	**$\dot{m}_s$ (g/s)**	**U_g (m/s)**
16	2010 Ndama et al. [96]	PTFE	1	0.5	Sugar	45	1603	1.8	21.2
		Nylon	1	0.5	PVC	38	1414		
17	2011 Saleh et al. [97]	PTFE	1	0.5	Spherical glass beads	80 to 500	2495	0.6 to 3.1	5.3 to 44.6
		Nylon	1	0.5	Non-spherical glass beads	150 to 500	2495		
18	2017 Schwindt et al. [98]	PMMA	2, 5	1.32	PMMA	0.08 to 250	1180	0.56 to 4.72	4 to 36
		PTFE	3	1.43		250 to 500			
		PVC	3.4	1.43					
19	2019 Choi et al. [99]	SS 316	3.4	1.3	Spherical glass beads	22 to 294	2500		9 to 22

Studies with continuous dilute flow have shown a direct relationship between particles charge-to-mass ratio and particles flow rate [81,82,97,98], conveying gas velocity [88,97,98], and conveying line length [80,86,95]. Changing the conveying line pathway from straight to spiral has also shown a rise in particles' charging efficiency [87,92,93]. Increasing the conveying line inner diameter [100,101], particles moisture content [102] and conveying gas relative humidity [82,88,97] have shown to decline the particles charging tendency. Similar trends have been observed for pneumatic conveying systems with pulse injection with the exception that a reduction in the charge-to-mass ratio was observed by increasing the particles' mass loading [98,101–103]. The mean particle diameter has been reported to be inversely related to their charge-to-mass ratio [82,83,97,99,104–108]; although, a direct relationship was observed for submicron-sized particles [109]. Furthermore, it has been confirmed that the addition of the bends to the conveying pathway in both continuous flow and pulse injection cases results in a significant increase in particles charge-to-mass ratio [89,102,105,110].

The Faraday cage technique has been implemented in the majority of the studies in relation to determining particles' electrostatic charging during pneumatic conveying. Depending on the application, the design of the Faraday cages can be modified. For instance, a through-type Faraday cage (**Figure 1-13)**, is mainly designed to be installed at the exit of pneumatic conveying lines and is equipped with a filter bag located inside the inner vessel to capture the conveyed particles and are open at the end to let the conveying gas to escape.

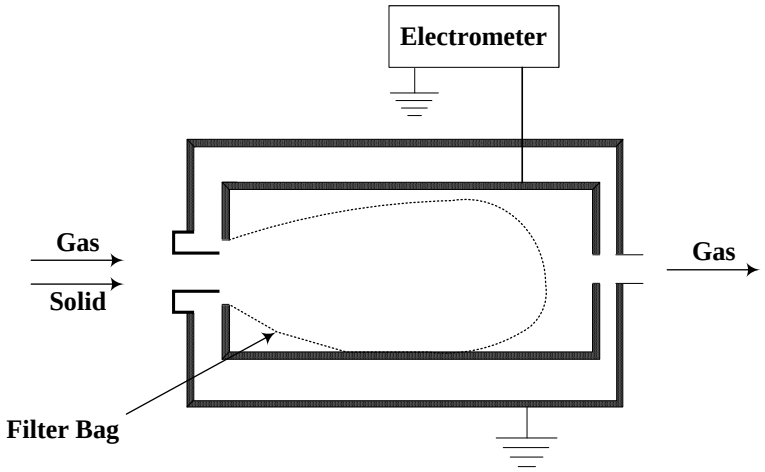

Figure 1-13 Schematic of a Through-type Faraday cage.

Because of the presence of downstream unit operations in any commercial process, implementing a Faraday cage at the conveying line exit is not feasible. Thus, an online technique has been employed. This method involves the measurement of the electric current signal directly from the conveying line that is generated due to particles flow inside the pipe, and translating it into the electrostatic charge using **Equation 1-3**:

$$Q = \int_{t_i}^{t_f} I.dt \qquad \textbf{(Eq. 1-3)}$$

where Q is the electrostatic charge (C), I is the electric current (A), and t is the time (s). t_i and t_f indicate the start and end of the electric current signal, respectively, due to solids flow through the conveying line.

1-3-1 Pneumatic Conveying in Relation to PE Reactors

As mentioned in Section **01-2** in relation to the commercial PE gas-solid fluidized bed reactors, all the solid additives, including the catalyst and the CAs, are periodically conveyed into the reactor through pneumatic injections via long and narrow tubes. Thus, there is a great potential for these additives to become electrostatically charged during the injection process and thus carry an initial charge upon entering the reactor. It is hypothesized that this introduced charge could contribute to the net bed electrification and the wall fouling formation and growth. However, except for one work [111], in which a silica catalyst support and a deactivated metallocene catalyst were injected

into a bed of PE resin through a short tube, no other study has investigated the effect of introduced charge through conveying line neither on the wall fouling nor the fluidized bed electrification. Hence, it important to determine the triboelectric effects of different commercially used catalyst particles and CAs with different surface chemistry and particle size, added through pneumatic injection into a PE fluidized bed, on the bed electrification and extent of wall fouling.

1-4 Thesis Objective

Reactor sheeting and discontinuity resulting from electrostatic charging have been reported as one of the operational challenges in the polyethylene industry and thus necessitating efforts to understand and investigate methods to mitigate/eliminate charge build-up in such reactors. In any gas-phase commercial polyethylene fluidized bed reactor, along with the PE resin, catalyst particles also exist which are periodically conveyed into the reactor. As discussed in section **1-3**, solids conveying via a gas stream could generate a large amount of electrostatic charge on the conveyed particles. Therefore, in any gas-phase PE process with dry catalyst feeding, the catalyst particles are anticipated to be electrostatically charged upon entering the reactor. The combination of the introduced charge to the reactor by the catalyst particles and the generated charge due to catalyst contacts with the PE resin inside the reactor, could then contribute to the net charge accumulation inside the reactor and subsequently the potential of migration and accumulation of the particles on the reactor wall.

Furthermore, same as the catalyst particles, continuity additives that are injected into the PE reactor through dry feeding are also anticipated to become electrostatically charged due to contacts with the conveying tube. However, it is not fully known how this charge would influence the net bed electrification. Additionally, the underlying mechanism by which the CAs control the wall fouling and sheeting is not clear deeming for further investigation.

The ultimate objective of this thesis was to study the role of catalyst particles and CAs on the PE fluidized bed electrification and wall fouling formation. Thus, a systematic study was performed to understand the triboelectrification of both solids not only due to their pneumatic conveying but also due to their contacts with PE resin inside the fluidized bed. The research was then divided into two phases, each with specific objectives.

1) Phase One: Characterization of Solids Charging due to Pneumatic Conveying

The aim of this phase of the research was to determine the electrostatic charging tendency of various types of amorphous silica catalyst support and five commercially available continuity additives (aluminum distearate, calcium stearate, zinc stearate, Chimassorb 944, and AS-990) due to pneumatic conveying. Since a big portion (approximately 60 wt.%) of catalysts that are typically used in the PE process are occupied by the support, the charging behavior of the catalyst support was studied prior to examining a catalyst. The specific objectives of phase one were to:

a) Design and build a pneumatic conveying system containing a conveying line of similar dimension and material to that of the PE process while housing an online charge measurement technique.

b) Gain fundamental knowledge about electrostatic charging behaviour of conveyed solids by first testing single particles. In particular, to investigate the effects of various parameters including particle type and size, as well as other operating conditions including conveying gas velocity, conveying line length and pathway.

c) Study the electrostatic charging of powder flow (amorphous silica catalyst support, and five commercially used continuity additives) through pulse pneumatic injection.

- Study the effects of various operating conditions such as conveying gas velocity, conveying line length and pathway, powders mass loading and their surface moisture.
- In the case that the powders developed tube fouling in the conveyed tube, to determine the effect of the conveying line inner surface fouling on the extent of powders electrostatic charge generation.
- Study the influence of various types of contacts (e.g., sliding, rolling, or hitting) between the conveyed particles and conveying line on the degree of particles electrostatic charging.

2) Phase Two: Solids Pneumatic Injection into a Fluidized Bed

The goal of this phase of the research was to pneumatically convey the powders (i.e., silica catalyst supports and CAs) directly into a fluidized bed of PE resin and to determine their role on the extent of fluidized bed electrification and the degree of adhesion of polyethylene resins to the fluid bed walls. The specific objectives of phase two were to:

a) Study the influence of powders' electrostatic charge gained due to their pneumatic transport on the extent of fluidized bed electrification and wall fouling.
b) Investigate the effects of various parameters including powders' surface chemistry, injection time, and mass loading on the extent of fluidized bed electrification and the degree of wall fouling.
c) Determine the possible underlying mechanisms of CA effectiveness on the PE bed electrification and mitigation of wall fouling.

1-5 Thesis Outline

The thesis is divided into seven chapters from which five chapters are prepared in manuscript form for publication in refereed journals.

The second chapter describes the electrostatic charging of two sizes of PTFE and Nylon particles individually conveyed under various operating conditions through stainless-steel pneumatic conveying line. Effects of operating conditions including conveying gas velocity, conveying line length and pathway were on the particles electrostatic charging were investigated. This chapter is a manuscript published in Powder Technology journal (*M. Taghavivand, B. Elchamaa, A. Sowinski, P. Mehrani, Study of electrostatic charging of single particles during pneumatic conveying, Powder Technol. 355 (2019) 242–250*).

The third chapter presents the electrostatic charging behaviour of an amorphous silica catalyst support during pneumatic conveying. Effects of surface moisture, powder mass loading, conveying gas velocity, conveying line length and pathway on the silica tribocharging were investigated. This chapter is a manuscript published in Powder Technology journal (*M. Taghavivand, B.J. Cho, P. Mehrani, A. Sowinski, Electrostatic charging behaviour of a silica powder during pulse pneumatic conveying, Powder Technol. 366 (2020) 119–129*).

The fourth chapter which was a collaborative work with the Japan National Institute of Occupational Safety and Health (JNIOSH) presents a relationship between the particles' motion pattern resulting in different contact types and the electrostatic charge they gain during pulse pneumatic conveying. This chapter is a manuscript published in the journal of Chemical Engineering Science (*M. Taghavivand, P. Mehrani, A. Sowinski, K. Choi, Electrostatic charging behaviour of polypropylene particles during pulse pneumatic conveying with spiral gas flow*

pattern, Chem. Eng. Sci. 229 (2021) 116081). There are videos attached to this publication that are not attached to this thesis.

The fifth chapter presents the results of pneumatically injecting an amorphous silica catalyst support on the PE fluidized bed wall fouling. Effects of silica mass loading, injection time and silica's electrostatic charge upon entering the fluidized bed were investigated on the degree of bed electrification and wall fouling. This chapter is a manuscript submitted to the journal of Powder Technology for publication (*M. Taghavivand, P. Mehrani, A. Sowinski, Triboelectric effects of a pneumatically injected silica catalyst support on polyethylene fluidized bed wall fouling, Manuscript ID: POWTEC-D-20-03328*).

The sixth chapter discusses the triboelectric effects of five commercially available continuity additives on the PE fluidized bed electrification and wall fouling. Various concentrations of five different continuity additives were added either individually or in a mixed form at different ratios into the PE fluidized bed where their influence on the wall fouling were examined. The effect of surface chemistry of continuity additives was also investigated on both the bed electrification and fluidized bed wall fouling. This chapter is a manuscript prepared to be submitted to the Chemical Engineering Journal.

The final chapter, chapter seven, presents the overall conclusions of this research and recommendations for future work.

Additional supporting information are presented in the appendices.

References

[1] G. Hendrickson, Electrostatics and gas phase fluidized bed polymerization reactor wall sheeting, Chem. Eng. Sci. 61 (2006) 1041–1064.

[2] Y. Hu, D. Wang, J. Liu, J. Gao, A case study of electrostatic accidents in the process of oil-gas storage and transportation, J. Phys. Conf. Ser. 418 (2013) 012037.

[3] M. Ghori, E. Šupuk, B. Conway, Tribo-electrification and Powder Adhesion Studies in the Development of Polymeric Hydrophilic Drug Matrices, Materials (Basel). 8 (2015) 1482–1498.

[4] B.D. Fulks, S.P. Sawin, C.D. Aikman, J.M. Jenkins, Process for reducing sheeting during polymerization of alpha-olefins, US Patent 4532311, 1985.

[5] S. Naik, R. Mukherjee, B. Chaudhuri, Triboelectrification: A review of experimental and mechanistic modeling approaches with a special focus on pharmaceutical powders, Int. J. Pharm. 510 (2016) 375–385.

[6] A. Ohsawa, Statistical analysis of fires and explosions attributed to static electricity over the last 50 years in Japanese industry, J. Phys. Conf. Ser. 301 (2011) 012033.

[7] M. Glor, Ignition hazard due to static electricity in particulate processes, Powder Technol. 135–136 (2003) 223–233.

[8] J.A. Cross, Electrostatics: principles, problems and applications, Adam Hilger, Bristol, 1987.

[9] B.G. Streetman, S.K. Banerjee, Solid state electronic devices, 6th Editio, Pearson Education Inc., 2006.

[10] A. Kahn, Fermi level, work function and vacuum level, Mater. Horiz. 3 (2016) 7–10.

[11] J. Wong, P. Chi, L. Kwok, H. Chan, Electrostatics in pharmaceutical solids, Chem. Eng. Sci. 125 (2015) 225–237.

[12] W.O. Moughrabiah, J.R. Grace, X.T. Bi, Effects of pressure , temperature , and gas velocity on electrostatics in gas - solid fluidized beds, Chem. Eng. Sci. 123 (2009) 320–325.

[13] S. Karner, N. Anne Urbanetz, The impact of electrostatic charge in pharmaceutical powders with specific focus on inhalation-powders, J. Aerosol Sci. 42 (2011) 428–445.

[14] S. Matsusaka, H. Maruyama, T. Matsuyama, M. Ghadiri, Triboelectric charging of powders: A review, Chem. Eng. Sci. 65 (2010) 5781–5807.

[15] T.B. Jones, Fluidization, solids handling, and processing, Elsevier, 1998.

[16] S. Matsusaka, H. Masuda, Electrostatics of particles, Adv. Powder Technol. 14 (2003) 143–166.

[17] L.S. McCarty, G.M. Whitesides, Electrostatic charging due to separation of ions at

interfaces: Contact electrification of ionic electrets, Angew. Chemie - Int. Ed. 47 (2008) 2188–2207.

[18] M.W. Williams, Triboelectric charging of insulating polymers-some new perspectives, AIP Adv. 2 (2012).

[19] A.F. Diaz, R.M. Felix-Navarro, A semi-quantitative tribo-electric series for polymeric materials: the influence of chemical structure and properties, J. Electrostat. 62 (2004) 277–290.

[20] A. Diaz, D. Fenzel-Alexander, D. Wollmann, J.A. Barker, Importance of Dissociated Ions in Contact Charging, Langmuir. 8 (1992) 2698–2706.

[21] A.F. Diaz, J. Guay, Contact charging of organic materials: Ion vs. electron transfer, IBM J. Res. Dev. 37 (1993) 249–260.

[22] A.F. Diaz, Contact electrification of materials: The chemistry of ions on polymer surfaces, J. Adhes. 67 (1998) 111–122.

[23] T.A. Jadwin, A.N. Mutz, B.J. Rubin, Electrographic toner and developer composition, US Patent 3893935, 1975.

[24] D.M. Burness, T.K. Dykstra, T.A. Jadwin, H.G. Ling, Electrographic toner and developer composition containing a 4-AZA-1-Azoniabicyclo(2.2.2) Octane Salt as a charge control agent, US Patent 4079014, 1978.

[25] T.A. Jadwin, Electrographic toner and developer composition containing quaternary ammonium salt charge control agent, US Patent 4323634, 1982.

[26] T.A. Jadwin, R.C. Storey, Electrophotographic dry toner and developer compositions, US Patent 4394430, 1983.

[27] R.P.N. Veregin, M.N.V. McDougall, M.S. Hawkins, C. Vong, V. Skorokhod, H.P. Schreiber, A bidirectional acid-base charging model for triboelectrification: Part II. Experimental verification by inverse gas chromatography and charging of metal oxides, J. Imaging Sci. Technol. 50 (2006) 288–293.

[28] R.P.N. Veregin, M.N.V. McDougall, M.S. Hawkins, C. Vong, V. Skorokhod, H.P.

Schreiber, A bidirectional acid-base charging model for triboelectrification: Part 1. Theory, J. Imaging Sci. Technol. 50 (2006) 282–287.

[29] J.H. Clint, T.S. Dunstan, Acid-base components of solid surfaces and the triboelectric series, Europhys. Lett. 54 (2001) 320–322.

[30] J.A. Medley, Fractional electrification of polar polymers, Nature. 171 (1953) 1077.

[31] A. Auroux, A. Gervasini, Microcalorimetric study of the acidity and basicity of metal oxide surfaces, J. Phys. Chem. 94 (1990) 6371–6379.

[32] A. Gervasini, A. Auroux, Acidity and basicity of metal oxide surfaces II. Determination by catalytic decomposition of isopropanol, J. Catal. 131 (1991) 190–198.

[33] G. Busca, The surface acidity of solid oxides and its characterization by IR spectroscopic methods. An attempt at systematization, Phys. Chem. Chem. Phys. 1 (1999) 723–736.

[34] V. Lee, N.M. James, S.R. Waitukaitis, H.M. Jaeger, Collisional charging of individual submillimeter particles: Using ultrasonic levitation to initiate and track charge transfer, Phys. Rev. Mater. (2018).

[35] P.S. Gil, D.J. Lacks, Humidity transforms immobile surface charges into mobile charges during triboelectric charging, Phys. Chem. Chem. Phys. 21 (2019) 13821–13825.

[36] H.T. Baytekin, B. Baytekin, S. Soh, B.A. Grzybowski, Is water necessary for contact electrification?, Angew. Chemie Int. Ed. 50 (2011) 6766–6770.

[37] H.T. Baytekin, B. Baytekin, J.T. Incorvati, B.A. Grzybowski, Material transfer and polarity reversal in contact charging, Angew. Chemie Int. Ed. 51 (2012) 4843–4847.

[38] D.J. Lacks, T. Shinbrot, Long-standing and unresolved issues in triboelectric charging, Nat. Rev. Chem. 3 (2019) 465–476.

[39] P. Mehrani, Characterization of electrostatic charges in gas-solid fluidized beds, The University of British Columbia, 2005.

[40] C. He, X.T. Bi, J.R. Grace, Simultaneous measurements of particle charge density and bubble properties in gas-solid fluidized beds by dual-tip electrostatic probes, Chem. Eng. Sci. 123 (2015) 11–21.

[41] A. Giffin, P. Mehrani, Comparison of influence of fluidization time on electrostatic charge build-up in the bubbling vs. slugging flow regimes in gas–solid fluidized beds, J. Electrostat. 68 (2010) 492–502.

[42] A. Sowinski, F. Salama, P. Mehrani, New technique for electrostatic charge measurement in gas-solid fluidized beds, J. Electrostat. 67 (2009) 568–573.

[43] T. Xie, K.B. McAuley, J.C.C. Hsu, D.W. Bacon, Gas phase ethylene polymerization: Production processes, polymer properties, and reactor modeling, Ind. Eng. Chem. Res. 33 (1994) 449–479.

[44] G. Jiménez-García, R. Aguilar-López, R. Maya-Yescas, The fluidized-bed catalytic cracking unit building its future environment, Fuel. 90 (2011) 3531–3541.

[45] R. Sivakumar, R. Saravanan, A. Elaya Perumal, S. Iniyan, Fluidized bed drying of some agro products – A review, Renew. Sustain. Energy Rev. 61 (2016) 280–301.

[46] R. Liu, L. Li, W. Yin, D. Xu, H. Zang, Near-infrared spectroscopy monitoring and control of the fluidized bed granulation and coating processes—A review, Int. J. Pharm. 530 (2017) 308–315.

[47] M. Taghavivand, K. Choi, L. Zhang, Investigation on drying kinetics and tribocharging behaviour of pharmaceutical granules in a fluidized bed dryer, Powder Technol. 316 (2017) 171–180.

[48] A. Sowinski, L. Miller, P. Mehrani, Investigation of electrostatic charge distribution in gas-solid fluidized beds, Chem. Eng. Sci. 65 (2010) 2771–2781.

[49] P. Mehrani, H.T. Bi, J.R. Grace, Electrostatic charge generation in gas-solid fluidized beds, J. Electrostat. 63 (2005) 165–173.

[50] P. Mehrani, M. Murtomaa, D.J. Lacks, An overview of advances in understanding electrostatic charge buildup in gas-solid fluidized beds, J. Electrostat. 87 (2017) 64–78.

[51] World polyethylene: Industry study with forecasts for 2018 & 2023, 2014.

[52] J.B.P. Soares, T.F. McKenna, Polyolefin reaction engineering, WILEY-VCH Verlag, 2012.

[53] K.C.H. Tijssen, E.S. (Merijn) Blaakmeer, A.P.M. Kentgens, Solid-state NMR studies of

Ziegler–Natta and metallocene catalysts, Solid State Nucl. Magn. Reson. 68–69 (2015) 37–56.

[54] A. Alizadeh, Study of sorption, heat and mass transfer during condensed mode operation of gas phase ethylene polymerization on supported catalyst, Université Claude Bernard - Lyon I, 2014.

[55] N. Kazemi, S. Brown, L. VanAsseldonk, X. Wang, S. Salmons, Y. Lacombe, Multi reactor solution polymerization, US Patent 9963529 B1, 2018.

[56] Y. Rao, P. Cai, K.J. Cann, F.D. Hussein, W.R. Mariott, P.A. Cao, Supported catalyst with improved flowability, US Patent 10280283, 2019.

[57] D. Song, F. Salama, J. Matta, P. Mehrani, Implementation of Faraday cup electrostatic charge measurement technique in high-pressure gas-solid fluidized beds at pilot-scale, Powder Technol. 290 (2016) 21–26.

[58] D. Song, P. Mehrani, Comparison of electrostatic charge generation in gas-solid fluidized beds in turbulent versus pre-turbulent flow regime, Powder Technol. 319 (2017) 426–433.

[59] D. Song, P. Mehrani, Mechanism of particle build-up on gas-solid fluidization column wall due to electrostatic charge generation, Powder Technol. 316 (2017) 166–170.

[60] A.G. Wonders, G.E. Moore, R.R. Ford, J.D. Daily, K.A. Dooley, J.J. Garcia, Suppression of fines forming in a fluidized bed ethylene polymerization process, WO Patent 97/14721, 1997.

[61] R.B. Painter, B.J. Garner, G.-H. Song, Gas phase fluidized bed polyolefin polymerization process using gas or gas-solids tangential flow, US Patent 5428118, 1995.

[62] S.J. Rhee, L.L. Simpson, Fluidized Bed Polymerization Reactors, US Patent 4933149, 1990.

[63] A.K. Agapiou, C.-I. Kuo, Method for preparing a supported catalyst system and its use in a polymerization process, US Patent 6482903 B1, 2002.

[64] T.F.L. McKenna, Condensed Mode Cooling of Ethylene Polymerization in Fluidized Bed Reactors, Macromol. React. Eng. 13 (2019) 1800026.

[65] C.-I. Kuo, G.G.H. Patel, R.E. Pequeno, B.J. Savatsky, F.D. Hussein, Continuity additive for

polyolefin polymerization processes, US Patent 9221936 B2, 2015.

[66] R.B. Pannell, D.M. Glowczwski, C.-I. Kuo, T.R. Lynn, D.F. Hussein, P.A. Cao, W.R. Mariott, M.D. Awe, Continuity compositions and methods of making and using the same, US Patent 9676885 B2, 2017.

[67] D.F. Hussein, M.E. Muhle, Additive for polyolefin polymerization processes, WO Patent 2010/080870 A2, 2010.

[68] R.O. Hagerty, M.E. Muhle, A.K. Agapiou, C.-T. Kuo, M.G. Goode, D.F. Hussein, R.B. Pannell, J.F. Szul, Method for controlling sheeting in gas phase reactors, US Patent 2005/0148742 A1, 2005.

[69] R.O. Hagerty, M.E. Muhle, A.K. Agapiou, C.-I. Kuo, M.G. Goode, D.F. Hussein, R. Pannell, J.F. Szul, Method for controlling sheeting in gas phase reactors, EP Patent 1699830 B1, 2005.

[70] R.B. Pannell, E.J. Markel, A.K. Agapiou, Method for seed bed treatment before a polymerization reaction, US Patent 8039562 B2, 2011.

[71] M.G. Goode, D.M. Hasenberg, T.J. McNeil, T.E. Spriggs, Method for reducing sheeting during polymerization of alpha-olefins, US Patent 4803251, 1989.

[72] G.-H. Song, A.S. Rhee, G.R. Lowder, Method for reducing sheeting and static charges during polymerization of ethylene polymers, US Patent 5391657, 1995.

[73] K.J. Cann, J.H. Moorhouse, P.A. Khokhani, T.T. Tamargo, K.R. Gross, M.G. Goode, Chromium-based catalyst compositions for olefin polymerization, US Patent 10266618 B2, 2019.

[74] K. Dong, Q. Zhang, Z. Huang, Z. Liao, J. Wang, Y. Yang, Experimental investigation of electrostatic effect on bubble behaviors in gas-solid fluidized bed, AIChE J. 61 (2015) 1160–1171.

[75] A. Giffin, P. Mehrani, Effect of gas relative humidity on reactor wall fouling generated due to bed electrification in gas-solid fluidized beds, Powder Technol. 235 (2013) 368–375.

[76] D. Song, P. Mehrani, Effect of fluidization pressure on electrostatic charge generation of

polyethylene particles, Ind. Eng. Chem. Res. 56 (2017) 14716–14724.

[77] A. Sowinski, A. Mayne, P. Mehrani, Effect of fluidizing particle size on electrostatic charge generation and reactor wall fouling in gas-solid fluidized beds, Chem. Eng. Sci. 71 (2012) 552–563.

[78] Y. Tian, P. Mehrani, Effect of particle size in fluidization of polyethylene particle mixtures on the extent of bed electrification and wall coating, J. Electrostat. 76 (2015) 138–144.

[79] G.E. Klinzing, F. Rizk, R. Marcus, L.S. Leung, Pneumatic Conveying of Solids: A theorical and practical approach, 2010.

[80] P. Bunchatheeravate, J. Curtis, Y. Fujii, S. Matsusaka, Prediction of particle charging in a dilute pneumatic conveying system, AIChE J. 59 (2013) 2308–2316.

[81] B.N. Cole, M.R. Baum, F.R. Mobbs, An investigation of electrostatic charging fffects in high-speed gas-solids pipe flows, Proc. Inst. Mech. Eng. Conf. Proc. 184 (1969) 77–83.

[82] E.E. Smeltzer, M.L. Weaver, G.E. Klinzing, Individual electrostatic particle interaction in pneumatic transport, Powder Technol. 33 (1982) 31–42.

[83] A. Gajewski, Measuring the charging tendency of polysterene particles in pneumatic conveyance, J. Electrostat. 23 (1989) 55–66.

[84] H. Masuda, S. Matsusaka, S. Nagatani, Measurements of powder flow rate in gas-solids pipe flow based on the static electrification of particles, Adv. Powder Technol. 5 (1994) 241–254.

[85] H. Masuda, S. Matsusaka, H. Shimomura, Measurement of mass flow rate of polymer powder based on static electrification of particles, Adv. Powder Technol. 9 (1998) 169–179.

[86] S. Matsusaka, H. Umemoto, M. Nishitani, H. Masuda, Electrostatic charge distribution of particles in gas–solids pipe flow, J. Electrostat. 55 (2002) 81–96.

[87] S. Matsusaka, M. Oki, H. Masuda, Bipolar charge distribution of a mixture of particles with different electrostatic characteristics in gas–solids pipe flow, Powder Technol. 135–136 (2003) 150–155.

[88] M. Nifuku, H. Katoh, A study on the static electrification of powders during pneumatic

transportation and the ignition of dust cloud, Powder Technol. 135–136 (2003) 234–242.

[89] J. Yao, Y. Zhang, C.-H. Wang, S. Matsusaka, H. Masuda, Electrostatics of the Granular Flow in a Pneumatic Conveying System, Ind. Eng. Chem. Res. 43 (2004) 7181–7199.

[90] J. Yao, C.H. Wang, Granular size and shape effect on electrostatics in pneumatic conveying systems, Chem. Eng. Sci. 61 (2006) 3858–3874.

[91] S. Watano, Mechanism and control of electrification in pneumatic conveying of powders, Chem. Eng. Sci. 61 (2006) 2271–2278.

[92] S. Matsusaka, M. Oki, H. Masuda, Control of electrostatic charge on particles by impact charging, Adv. Powder Technol. 18 (2007) 229–244.

[93] S. Matsusaka, H. Fukuda, Y. Sakura, H. Masuda, M. Ghadiri, Analysis of pulsating electric signals generated in gas–solids pipe flow, Chem. Eng. Sci. 63 (2008) 1353–1360.

[94] C. Dragan, A. Samuila, S. Das, D. Iancu, M. Bilici, L. Dascalescu, Factors that influence the tribo-charging of insulating ducts in suction-type dilute-phase pneumatic transport systems, J. Electrostat. 67 (2009) 184–188.

[95] A. Thomas, K. Saleh, P. Guigon, C. Czechowski, Characterisation of electrostatic properties of powder coatings in relation with their industrial application, Powder Technol. 190 (2009) 230–235.

[96] A.T. Ndama, P. Guigon, K. Saleh, A reproducible test to characterise the triboelectric charging of powders during their pneumatic transport, J. Electrostat. 69 (2011) 146–156.

[97] K. Saleh, A. Traore Ndama, P. Guigon, Relevant parameters involved in tribocharging of powders during dilute phase pneumatic transport, Chem. Eng. Res. Des. 89 (2011) 2582–2597.

[98] N. Schwindt, U. von Pidoll, D. Markus, U. Klausmeyer, M. V. Papalexandris, H. Grosshans, Measurement of electrostatic charging during pneumatic conveying of powders, J. Loss Prev. Process Ind. 49 (2017) 461–471.

[99] K. Choi, H. Choi, T. Suzuki, Charging behavior of glass beads using a spiral air type tribocharging apparatus that utilizes a Faraday cup, J. Loss Prev. Process Ind. 65 (2020)

104124.

[100] P. Boschung, M. Glor, Methods for investigating the electrostatic behaviour of powders, J. Electrostat. 8 (1980) 205–219.

[101] H. Grosshans, M. V. Papalexandris, Evaluation of the parameters influencing electrostatic charging of powder in a pipe flow, J. Loss Prev. Process Ind. 43 (2016) 83–91.

[102] M. Taghavivand, B.J. Cho, P. Mehrani, A. Sowinski, Electrostatic charging behaviour of a silica powder during pulse pneumatic conveying, Powder Technol. 366 (2020) 119–129.

[103] S. Watano, S. Saito, T. Suzuki, Numerical simulation of electrostatic charge in powder pneumatic conveying process, Powder Technol. (2003).

[104] F. Chowdhury, A. Sowinski, M. Ray, A. Passalacqua, P. Mehrani, Charge generation and saturation on polymer particles due to single and repeated particle-metal contacts, J. Electrostat. 91 (2018) 9–15.

[105] M. Taghavivand, B. Elchamaa, A. Sowinski, P. Mehrani, Study of electrostatic charging of single particles during pneumatic conveying, Powder Technol. 355 (2019) 242–250.

[106] H. Masuda, T. Komatsu, K. Iinoya, The static electrification of particles in gas-solids pipe flow, AIChE J. 22 (1976) 558–564.

[107] J. Yao, C.-H. Wang, Granular size and shape effect on electrostatics in pneumatic conveying systems, Chem. Eng. Sci. 61 (2006) 3858–3874.

[108] H. Masuda, K. Iinoya, Electrification of particles by impact on inclined metal plates, AIChE J. 24 (1978) 950–956.

[109] S. Alois, J. Merrison, J.J. Iversen, J. Sesterhenn, Quantifying the contact electrification of aerosolized insulating particles, Powder Technol. 332 (2018) 106–113.

[110] C.K. Diu, C.P. Yu, Deposition from charged aerosol flows through a two-dimensional bend, J. Aerosol Sci. 11 (1980) 391–395.

[111] A. Sowinski, P. Mehrani, Impact of addition of a catalyst or its support on reactor wall coating due to electrostatic charging during fluidization of polyethylene, Ind. Eng. Chem. Res. 54 (2015) 3981–3988.

Chapter 2 - Study of Electrostatic Charging of Single Particles During Pneumatic Conveying

Milad Taghavivand, Bilal Elchamaa, Andrew Sowinski, Poupak Mehrani*

Department of Chemical and Biological Engineering, University of Ottawa, 161 Louis Pasteur, Ottawa, ON, K1N 6N5, Canada

* Corresponding author. E-mail: poupak.mehrani@uottawa.ca; Tel: 1-613-562-5800 ext. 6098

The current chapter is a manuscript published in the journal of Powder Technology "Powder Technology, 355, 242–250, 2019"

Abstract

In this study the electrostatic charging behaviour of single particles of different sizes and materials were investigated during pneumatic conveying. The particles used included 3.18 and 0.79 mm PTFE as well as 3.18 mm Nylon particles. Particles were pneumatically conveyed in stainless steel (316 Grade) tubes with 4.57 mm inner diameter. Effects of conveying tube length, conveying gas velocity and pathway of particles (i.e., addition of 90˚ elbows and smooth bends) on particles charge-to-mass ratio were studied. Results showed that the smaller PTFE particles reached the saturation charge in the longest straight tube for all conveying gas velocities tested. Whereas the other two larger particles reached saturation charge only in the longest straight tube and at the lowest gas velocity. For large particles moving in straight tubes, in general, the lowest gas velocity resulted in a higher charge-to-mass ratio. The particles pathway had a large impact on their charging behaviour at high gas velocities, whereas at the lowest gas velocity, the total tube length was more influential on particles charging. Finally, the charge of the particles determined by measuring the current from the conveying line was found to be in good agreement with that measured directly by a Faraday cage.

Keywords: Electrostatics, Pneumatic conveying, Charge measurement

2-1 Introduction

In many gas-solid processes, electrostatic charges are generated by triboelectric charging due to particle-particle and particle-wall contacts during particle handling, transport and processing. Segregation and agglomeration of particles, adhesion of particles to surfaces, and finally explosions caused by electrostatic discharge are generally the problems associated with solids tribocharging. Examples of such complications are observed in gas-solid fluidized beds [1–3] with significant negative impacts reported in industries including petrochemical [4], oil and gas [5], and pharmaceutical [6]. The polyolefin industry, particularly in the gas-phase polyethylene production, has significantly suffered from the operational challenges resulting from fluid bed charging. In this gas-phase process, large amounts of electrostatic charges are generated causing polyethylene and catalyst particles to adhere to the reactor wall, leading to a problem known as "sheeting" [7]. Sheeting is known to be a major operational challenge since the sheets can break off and block the reactor, causing long shut down periods for clean-up. Despite a number of works reported in the literature, the problem of sheeting in polyethylene reactors still persists [4,8–10] due to the lack of comprehensive understanding of the underlying mechanism of electrostatic charge build-up in these reactors. The only work reported on wall fouling mechanism in such systems is that of Song and Mehrani [11]. In studying polyethylene reactor sheeting, they proposed a mechanism for reactor wall fouling in fluidized beds with metallic columns that signifies the contribution of induction charging leading to image force, in addition to the attractive electrostatic forces. In their experimental work, the only source of bed electrification was the charged polyethylene particles; however, in a commercial polyethylene reactor where catalyst particles also exist, their charging and contribution to the net bed electrification must be evaluated. With the exception of one report specifying the approximate charge on conveyed catalyst particles in the polyethylene process [12], no work has been found to investigate the catalyst charging and its contribution to the polyethylene reactor sheeting.

In the polyethylene production process, catalyst particles are pneumatically conveyed into the fluidized bed reactor. In general, pneumatic conveying systems are believed to generate the most electrostatic charge on conveyed particles among all gas-solid processes [13,14]. Therefore, with reference to the polyethylene process, it is anticipated the catalyst particles would be highly charged upon entering the reactor. In relation to solids electrostatic charging in dilute pneumatic

conveying systems, previous studies have found that parameters such as solids loading ratio, conveying line length, mean particle size, conveying gas velocity and relative humidity significantly influence the charging phenomenon. For instance, it has been observed that increasing the solids loading ratio [15–17], conveying tube length [13,18–22], and conveying gas velocity [15,23–25] can increase the generated charge on particles by increasing the number of particle-wall and particle-particle contacts as well as the impact force. In many cases, the particles mean diameter and charge-to-mass ratio were inversely related; however, some reports have found a linear relationship between these two parameters [15]. Relative humidity has been experimentally proven to reduce the charging tendency of materials such as pharmaceutical powders, pulverized coal, glass beads, PMMA and PVC by lowering their volume resistivity [15,17,23,26–29].

It is important to note that all the above-mentioned studies have considered pneumatic conveying as an isolated system; and therefore, did not take into account the influence of electrostatic charges gained by the particles during pneumatic conveying on the performance of unit operations downstream in the process. In real systems, however, the electrostatic charge arising from pneumatic conveyors could have a remarkable impact on downstream units and processes. An example of this would be the influence of catalyst particle charging through conveying lines on polyethylene reactor sheeting. In order to study such influence, it is vital to gain comprehensive knowledge about particle charging in pneumatic conveying. In relation to the polyethylene process, preliminary work is necessary to provide fundamental knowledge about single particle charging prior to study powder (e.g., catalyst) conveying into a fluidized bed. However, no study has been found evaluating the charging behaviour of single particles during pneumatic conveying. In addition, catalyst conveying lines could be of different lengths and configurations with respect to the number of bends and their location in the line. Therefore, understanding the combined effects of tube length and pathway on particles charging is necessary. It is well known that bends can create severe problems in pneumatic conveying systems such as energy loss, erosion of the conveying line, and particles attrition [14,30]. However, bends are indispensable for the normal operation of conveying and therefore their impact on charging needs to be understood. With reference to electrostatic charging, the influence of bends has received minimal attention with only one study found in open literature by Matsusaka et al. [19,20] in which only spiral tubes were tested. Although catalyst conveying lines in the polyethylene process are typically operated at low

gas velocities, the influence of gas velocity on the degree of particles charging must be examined to determine the optimum velocity that minimizes electrostatic charge generation.

The goal of this work was to provide an in-depth study on single particle charging through pneumatic conveying by evaluating parameters including conveying tube length and pathway, as well as conveying gas velocity and particle size. This work was carried out in relation to the polyethylene process and thus the experimental work was conducted with an effort to keep the operating conditions similar to that of the catalyst pneumatic conveying lines in the commercial polyethylene process. This work also provides the basis for the methodology and apparatus for powder testing in future works and thus is the foundation for understanding the impact of catalyst charging through pneumatic conveying on gas-solid fluidized bed performance.

2-2 Materials and Methods

The schematic diagram of the apparatus used in this work is shown in **Figure 2-1**. The apparatus consists of three sections: gas and particle injection; pneumatic conveying line; and electrostatic charge measurement.

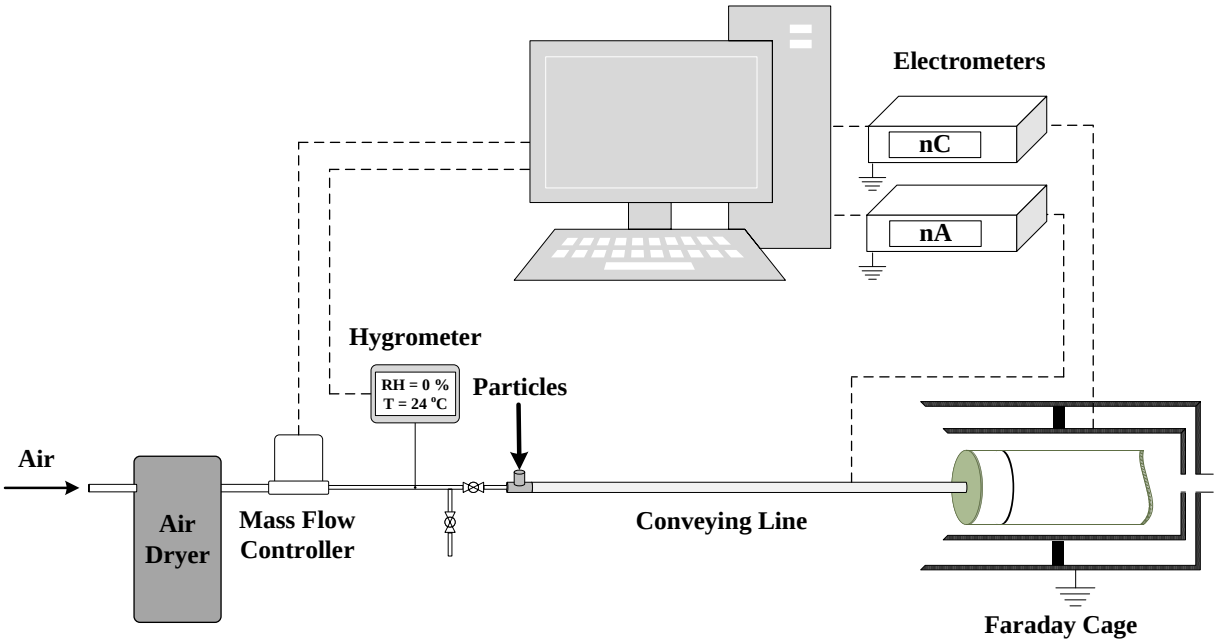

Figure 2-1 Schematic diagram of pneumatic conveying apparatus.

Air was used as the carrier gas and its relative humidity was reduced to approximately zero after passing through an air dryer (Atlas Copco Model CD12). The air flow rate was controlled by a mass flow controller (MKS Model 1559) while a hygrometer (Vaisala Model HMT 338) was used to monitor its temperature and relative humidity. The catalyst pneumatic conveying lines in commercial polyethylene processes are typically stainless steel tubes with an inner diameter of 4.57 mm. Therefore, the conveying line used in this research was of similar material and size. A branch tee was used to provide an inlet for particles into the conveying tube and to serve as a particle holder. It is known that particles' initial charge influences the amount of charge transfer during particle-wall contacts [31–33] and thus in this study, a fan type ionizer (SMC Model IZF10R) was used to neutralize particles before their usage.

Two charge measurement methods were employed in this study. A Faraday cage containing a filter bag (tightly connected to the conveying line with an adaptor to capture the particles) and connected to a digital electrometer (Keithley model 6514), was used to directly measure the particles' electrostatic charge as they exited the conveying line. Additionally, the electric current, I (C/s), from the conveying line was measured by directly connecting a second digital electrometer of the same model with a data collection frequency set at 400 Hz to the conveying line. In this case, the tee and the conveying tube were electrically isolated from the rest of the apparatus. The electrostatic charge measured in this technique from the outer surface of the metallic conveying line must be equal but in opposite polarity of the particle charge measured by the Faraday cage located at the exit of the conveying line. **Equation 2-1** was applied to find the electrostatic charge based on the current measured for a certain time span. This method also verified the conservation of charge in the system.

$$|Q| = \left|\int_0^t I\, dt\right| \qquad \textbf{(Eq. 2-1)}$$

Particles chosen for this study were PTFE (Teflon) and Nylon with work functions of approximately 5.75 eV [34] and 4.3 eV [34], respectively. When contacting the stainless steel conveying tube wall (with a work function of approximately 4.5 eV [11]) PTFE and Nylon particles were expected to become negatively and positively charged, respectively. **Table 2-1** illustrates the operating conditions in which the experiments were carried out.

Table 2-1 Operating conditions of the pneumatic conveying system.

Conveying tube			**Conveying gas**		**Particles**		
Material	***L*** **(m)**	***ID*** **(mm)**	**Gas type**	U_g **(m/s)**	**Type**	ρ_P **(kg/m^3)**	***dp*** **(mm)**
Stainless steel 316/316L	0.8, 1.2, 2, 3	4.57	Dry air	20, 30, 60, 100	PTFE	2200	3.18, 0.79
					Nylon	1150	3.18

The length of catalyst conveying lines in a typical polyethylene plant could be in the range of 3 to 10 m. For this study, the tube lengths of 0.8 to 3 m were tested. Different horizontal configurations for particles pathway were tested as presented in **Figure 2-2**. Particles entrance is indicated by an arrow in every case. The influence of two extreme cases of bends, a sharp 90˚ bend (i.e., a 90˚ elbow) and a smooth long-radius bend with a 1 m radius, on particles charging, was investigated. Smooth long-radius bend was selected due to its common application in commercial processes since it minimizes the risk of attrition and erosion by providing a gradual change in the solids flow direction which will also reduce the risk of blockage [30]. It was expected that the 90˚ elbow (stainless steel union elbow with 6.35 mm outer diameter) would create a larger charge on particles compared to the smooth bend. The effect of bend location on particles' charging was also investigated by considering two cases for the 3 m tube with one 90° elbow; in case A the elbow was located closer to the tube exit and in case B the elbow was located farther from the tube exit.

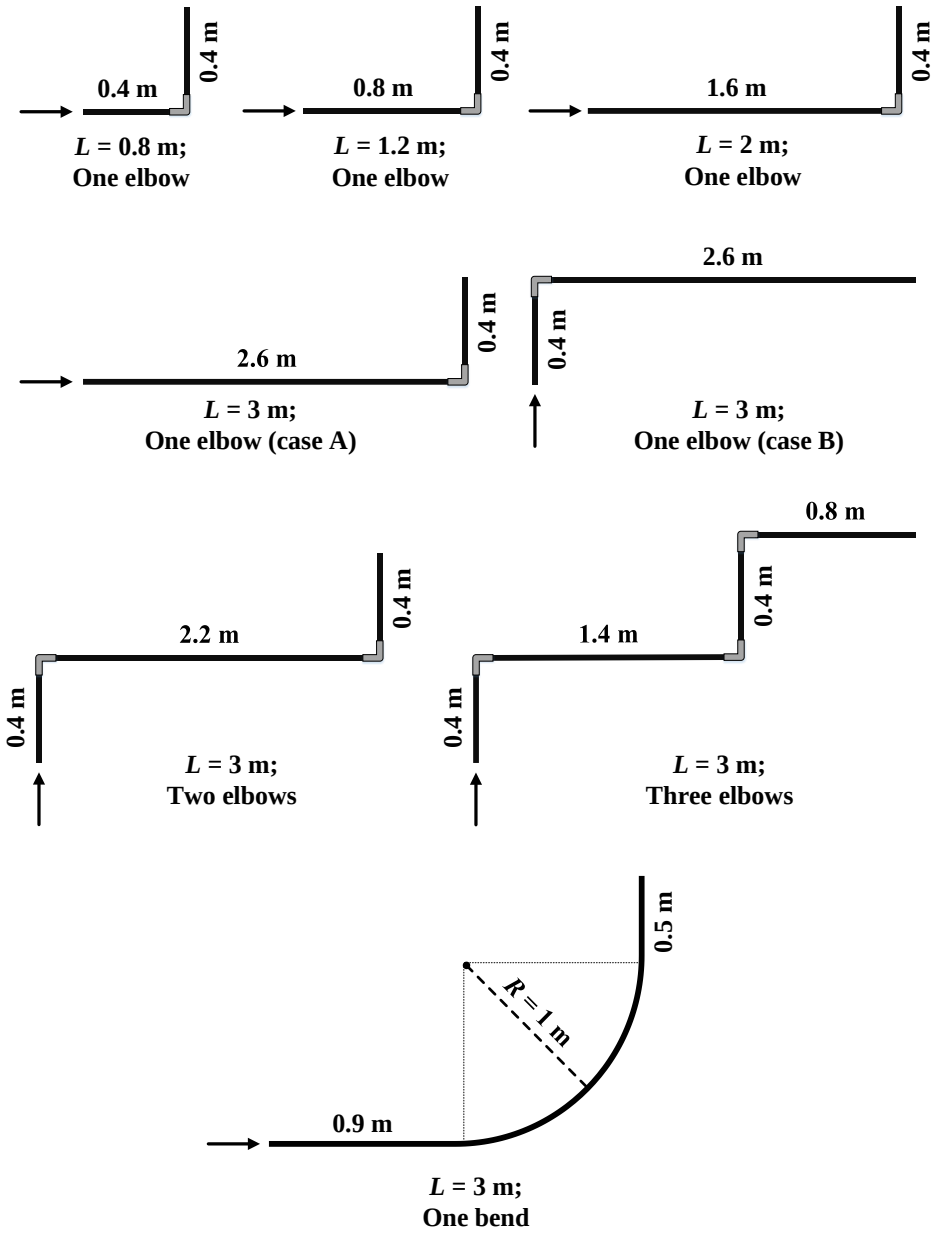

Figure 2-2 Different particle pathways tested.

Experiments were carried out in sets of 16 injections for each condition. Standard error bars presented in the results section are based on a 95% confidence level. After the completion of each set of injections and prior to starting a new set, dry air was passed through the conveying line for approximately half an hour at a high flow rate to remove any moisture or dust residual from the tube inner surface. Particles were all cleaned with water and ethanol to remove all surface contaminations before each set of injections. Washed particles were then kept in a container at 4 ± 1% relative humidity and 23 ± 1˚C. The entire system was controlled by LabVIEW software.

To ensure movement of particles under studied conveying gas velocities, the pick-up velocity of the particles needed to be smaller than the conveying gas velocity. The pick-up velocity was calculated using the equation proposed by Cabrejos and Klinzing [35].

$$\frac{U_{gPU}}{\sqrt{g d_P}} = \left(0.0428 {Re_P}^{0.175}\right)\left(\frac{ID}{d_P}\right)^{0.25}\left(\frac{\rho_P}{\rho_g}\right)^{0.75} \quad \textbf{(Eq. 2-2)}$$

$$Re_P = \frac{\rho_g U_g d_P}{\mu_g} \quad \textbf{(Eq. 2-3)}$$

where U_{gPU} is the pick-up velocity (m/s), d_P is the mean particle diameter (m), Re_P is the particle Reynolds number, ID is the tube inner diameter (m), ρ_P is the particle density (kg/m^3), ρ_g is the gas density (kg/m^3), U_g is the conveying gas velocity (m/s) and μ_g is the gas dynamic viscosity (kg/m/s).

2-3 Results and Discussion

The charging behaviour of PTFE and Nylon particles due to pneumatic conveying was investigated. It was observed that under all operating conditions tested, PTFE particles became negatively charged whereas Nylon particles gained positive charge in contact with the stainless steel conveying tube. Such observation is in agreement with the existing triboelectric series [34].

2-3-1 PTFE Particles

The effect of the tube length on the electrostatic charging behaviour of two sizes of PTFE particles at different conveying gas velocities was first examined (**Figure 2-3**). Results shown in **Figure 2-3a** for the larger PTFE particles indicate that increasing the tube length causes an increase in particles *Q/m*, although no significant difference was found between tube lengths of 1.2 and 2 m. The largest effect was observed when the tube length was extended to 3 m. While keeping the tube length constant but varying the conveying gas velocity, it was found that particles gained a larger *Q/m* at the lowest gas velocity of 20 m/s compared to the higher velocities. It is believed that charge transfer in any particle-wall contact is influenced by particles' impact force, duration of contact, the number of contacts, contact area, and contact frequency [31–33,36]. Comparing the effect of tube length on particles *Q/m* at a certain gas velocity, it can be concluded that while increasing the tube length will not change the impact force and the particle contact frequency

noticeably, it will result in an increase in the particle residence time in the tube and therefore an increase in the number of contacts as well as the available contact area both on the tube and the particle surface. Such an effect will in turn result in an increase in the amount of electrostatic charge transferred between the particle and the tube wall. Here it must be noted that increasing the number of particle-wall contacts alone would not increase the transferred charge and it must be accompanied by a surface area which has not yet experienced a contact. Korevaar et al. [37] defined a parameter called effective surface area which considered two areas on the surface of a particle moving in a conveying duct: a surface that makes contact for the first time and the majority of the charge transfer takes place from this area, and a surface that has already made contact in previous collisions and does not acquire much charge during later contacts. Thus, as a particle moves in a conveying line, its effective surface area for electrostatic charge transfer decreases gradually.

The observed greater particles *Q/m* at the lower gas velocity of 20 m/s can be attributed to the higher residence time of the particles within the conveying line [38]. It should also be noted that during the experiments, the sound produced due to the particle movement inside the conveying tube at this velocity implied that the particle was rolling inside the tube while for other conditions such observation was not made. This in turn is an indication of more particle-wall contacts as well as more effective contact area and eventually more electrostatic charge transfer at such low conveying velocity.

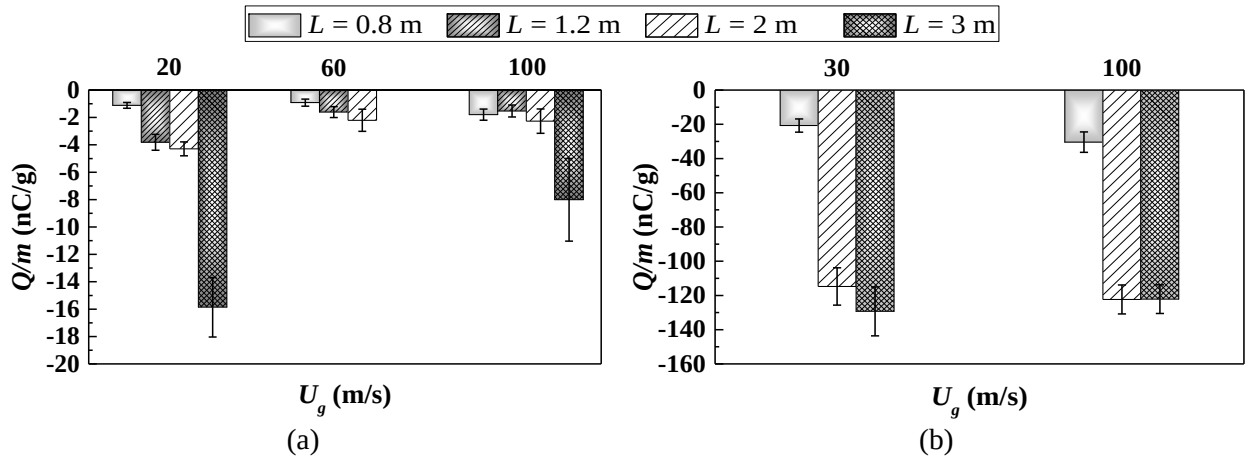

Figure 2-3 Effect of tube length and gas velocity on electrostatic charging behaviour of (a) 3.18 mm and (b) 0.79 mm PTFE particles conveyed through straight conveying tubes.

Effect of particle size on its charging tendency was tested with smaller (0.79 mm) PTFE particles for selected operating conditions (**Figure 2-3b)**. In comparison to the larger PTFE particles, the smaller particles gained a much larger *Q/m* for all conditions tested. Chowdhury et al. [33] observed a similar behaviour for LLDPE particles where decreasing the particle size led to an increase in particles *Q/m*. This is due to a higher specific surface area of smaller compared to larger particles of a same material [39]. Assuming both size particles to be spherical, smaller PTFE particles had a specific surface area approximately four times greater than the larger particles. As can be seen in **Figure 2-3b**, for all tube lengths tested the change in gas velocity had no influence on particles *Q/m*. However, increasing the tube length from 0.8 m to 2 m increased the particles' charge-to-mass ratio by a factor of 5 while the further increase to 3 m had no significant effect. This can be explained by the increase in the number of contacts and available surface area for contact between the particle and the tube wall in longer tubes.

2-3-1-1 Addition of 90˚ Elbows

The effect of the tube pathway was evaluated by addition of 90˚ elbows to the straight tubing of various length (**Figure 2-4**). It is clear that particles *Q/m* increased significantly (by a factor of 6 or 7 times at higher gas velocities) in presence of an elbow. Results also indicate that except for the 20 m/s gas velocity, regardless of the tube total length, particles acquired approximately similar quantity of electrostatic charges under the same gas velocities in the presence of one elbow. Such observation implies that the charge gained by the PTFE particle tested in the presence of an elbow at gas velocities higher than 20 m/s is more dependent on the pathway and gas velocity and in turn the impact force, rather than the tube length. Results at 20 m/s gas velocity show that the increase in particles *Q/m* in the presence of even one elbow became less significant as the tube length reached 3 m. This implies that PTFE particles charging behaviour at this velocity depends more on the tube total length rather than the pathway or the impact force.

Assuming that particles could reach saturation charge by undergoing multiple severe contacts with the tube wall, experiments were also conducted with multiple 90˚ elbows for the 3 m tube. Although a slight increase in *Q/m* was observed in the presence of two elbows but no significant difference was seen when a third elbow was added. In a separate study by Chowdhury et al. [33], the saturation *Q/m* of the same size PTFE particles was found to be -18.03 ± 1.64 nC/g. This is close to the particles' *Q/m* measured in this work (-20.18 ± 1.66 nC/g) in the presence of two and

three elbows. Comparing the particles charging in the 3 m tube at 20 m/s gas velocity with other conditions shown in **Figure 2-4** and **Figure 2-3a**, it is also clear that particles reached close to the saturation charge in the 3 m straight tube, whereas they did not reach this value in shorter straight tubes. Therefore, it can be concluded that providing particles with a high enough residence time by lowering the gas velocity and increasing the tube length, can make them reach the saturation charge regardless of the tube configuration. Thus the present work demonstrates that having the particles conveyed at a low gas velocity in a long straight conveying tube or collided with one 90˚ elbow when accompanied by a high enough impact force is equivalent to almost 480 collisions in a particle shaker that is presented in the work of Chowdhury et al. [33]. This is an important finding signifying that any pneumatic conveying line if exceeds a certain length or contains only one sharp bend could result in generating a large amount of electrostatic charge on the conveyed particles.

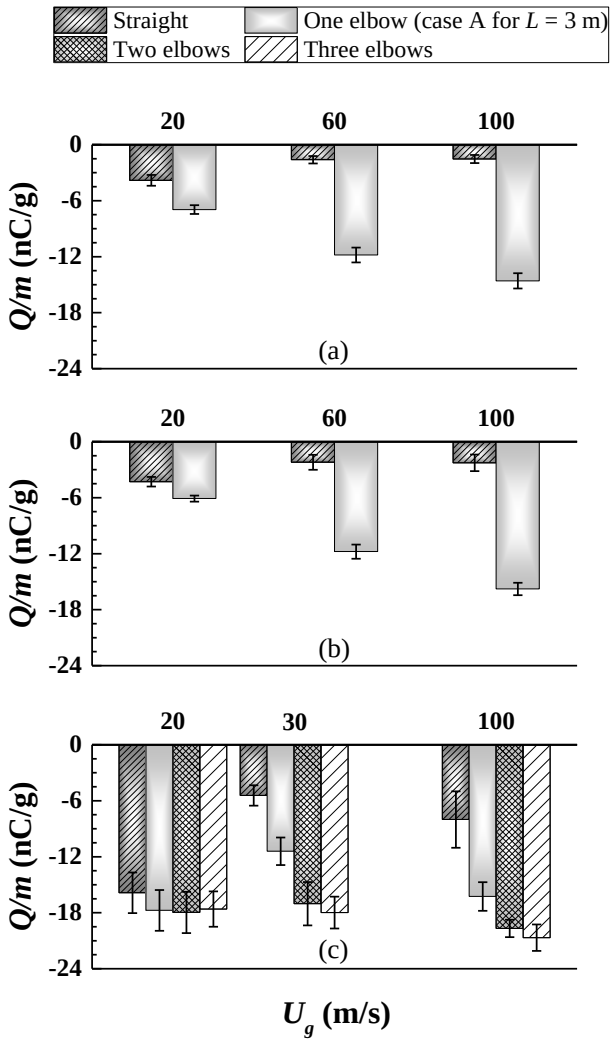

Figure 2-4 Effect of adding 90˚ elbows on charging behaviour of 3.18 mm PTFE particles in (a) 1.2 m, (b) 2 m and (c) 3m conveying tubes. The location of the elbows is indicated in the figure caption.

Similar tests were performed with smaller (0.79 mm) PTFE particles for two tube lengths of 0.8 m and 3 m. Results in **Figure 2-5** show a similar trend in charging tendency for smaller particles to that of the larger PTFE particles. No difference was observed in particles *Q/m* at various gas velocities in the 3 m tube with and without 90˚ elbow(s) suggesting that the particles might have reached the saturation charge. Since the surface area of the larger PTFE particle is 16 times greater than that of the smaller particle, and considering an ideal situation where the entire surface of a particle contacts the tube wall, when the whole area on the surface of larger particle touches the wall, a smaller particle has already contacted the tube wall 16 times. In other words, the possibility of all points on the surface of the smaller particle coming into contact with the tube wall is higher

than that for the larger particle. Therefore, smaller size PTFE particles can reach charge equilibrium faster than the larger particles.

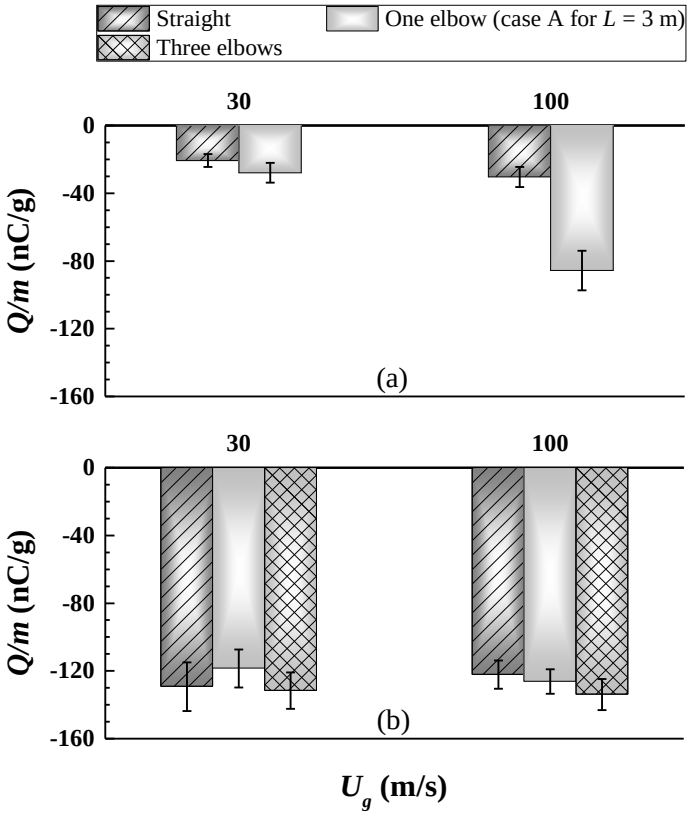

Figure 2-5 Effect of adding a 90˚ elbow on charging behaviour of 0.79 mm PTFE particles in (a) 0.8 m and (b) 3 m conveying tubes. The location of the elbows is indicated in the figure caption.

2-3-1-2 Location of Elbow

With the longer conveying lines of 2 m and 3 m, the influence of location of the 90˚ elbow on charging behaviour of 3.18 mm PTFE particles was also investigated. **Figure 2-6** presents the effect of elbow location on *Q/m* of 3.18 mm PTFE particles in a 3 m tube. Statistically, no significant difference was observed at both gas velocities. However, on average, placing the elbow close to the tube inlet slightly increased the particle *Q/m* at 30 m/s gas velocity in both lengths. The first reason might be related to the higher particle velocity in colliding the elbow when it is located close to the inlet than when it is further away. It is possible that particles lose a portion of their kinetic energy due to the friction when travelling a longer distance before colliding with the elbow and as a result make a less strong contact with the elbow. Other reason could be due to the fact that when the elbow is located close to the tube exit, the residence time of the particles in the

short 0.4 m straight tube after the elbow becomes very small. Such behaviour minimizes the contribution of the short straight tube on charge generation by lowering the number of particle-wall collisions compared to the case where the elbow is placed further away from the tube exit. It is anticipated that when the elbow is placed further from the tube exit the residence time of the particle and hence the number of contacts become higher in the longer straight tube after the elbow, and that in turn will increase the charge of the particle.

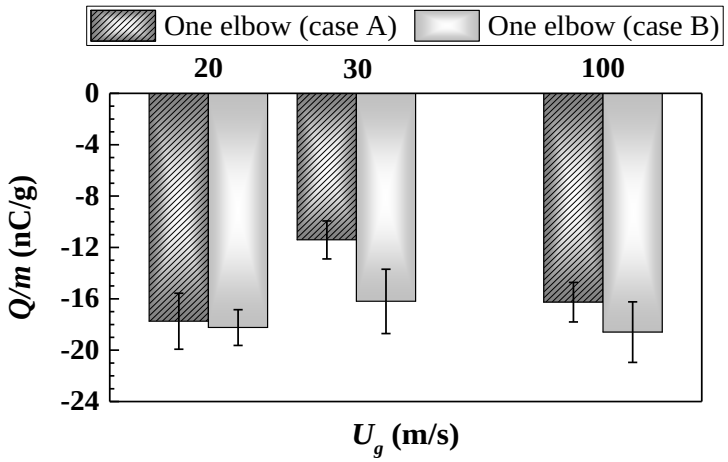

Figure 2-6 Effect of location of the elbow on charging behaviour of 3.18 mm PTFE particles in the 3 m conveying tube. Location of the elbow is stated in figure caption.

2-3-2 Nylon Particles

Tests were also conducted with particles of a same size (3.18 mm) but of a different material of Nylon. The 3 m tube length was selected owing the flexibility that it provides in testing different conditions. Comparison of the results in **Figure 2-4c** and **Figure 2-7** indicates that both type of particles charging behaviour is similar for the operating conditions tested in this work. Both type of particles gained a greater *Q/m* at the lower gas velocity of 20 m/s. The addition of 90˚ elbows to the particles' pathway showed a similar behaviour and changing the elbow location did not show a significant change on Nylon particles charging at both gas velocities. The only difference was observed where the Nylon particles *Q/m* declined when the conveying gas velocity was varied from 30 to 100 m/s. This could be partially due to the fact that Nylon particles are lighter and therefore have smaller residence time within the conveying line especially at higher gas velocities which in turn will result in less particle-wall contacts and less particles charging.

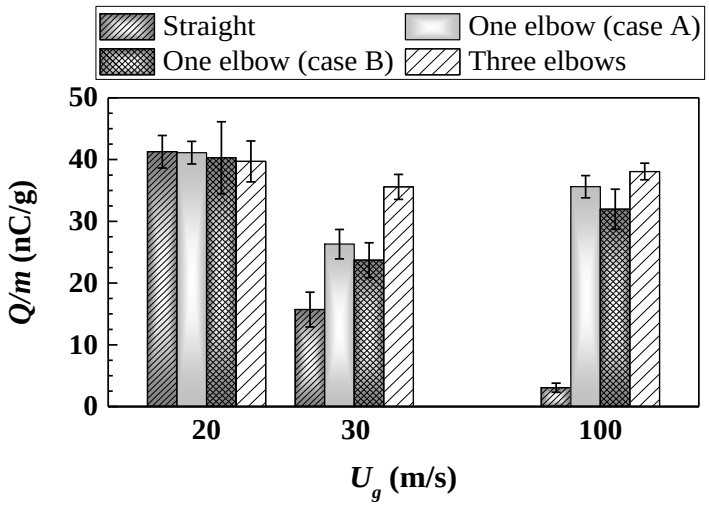

Figure 2-7 Charging behaviour of 3.18 mm Nylon particles under different operating conditions in the 3 m conveying tube.

2-3-3 Comparison of Smooth Bend and 90˚ Elbow

Tests were carried out to compare the charging tendency of particles of same size in a conveying line consisting of a smooth bend (with 1 m radius) and a 90˚ elbow. Results obtained from straight tube of a similar length were also used to provide a better comparative analysis (**Figure 2-8**). It was expected that a smooth bend generates less charge on particles compared to a 90˚ elbow. Results clearly show that smooth bend did not affect the *Q/m* of PTFE particles at 20 m/s gas velocity while it increased the *Q/m* magnitude at 30 m/s gas velocity up to the saturation charge level. Such a behaviour implies that for the PTFE particles there was no difference between smooth bend and elbow in terms of the particle-wall collisions and thus both configurations raised the electrostatic charge on the particles significantly. However, for Nylon particles, a significant decrease was observed in *Q/m* at 100 m/s gas velocity. This could likely be attributed to the fact that the smooth bend reduced the impact force and perhaps number of contacts (in comparison with elbow) between the Nylon particles and the tube wall which subsequently resulted in a reduction in the amount of electrostatic charge transfer. One possible explanation for these observations could be related to the inertia and subsequently to the momentum of these two particles [40]. PTFE particles are almost two times more dense than Nylon particles. This makes PTFE particles to posses two times greater momentum than the Nylon particles upon entering the bend. Higher momentum makes the PTFE particles direction less affected by the gas flow direction. However, the movement direction of Nylon particles, owing to their lighter mass, can be influenced by air flow with less resistance compared to the heavier PTFE particles. Therefore,

Nylon particles can easily get carried away by the air flow compared to PTFE particles. One possible consequence could be a lower residence time for Nylon particles in the bend as well as lesser number of contacts between the tube and Nylon particles [41]. Experimental and simulation works have proven that due to the centrifugal forces particles shift towards the outer wall of the conveying line once reaching a bend [40–44]. Particles with higher momentum will undergo a higher centrifugal force and therefore will experience a stronger impact force when colliding the tube wall, and as explained earlier, higher impact force can lead into higher amount of electrostatic charge transfer. Another plausible occurrence would be that the Nylon particles slide all the way through the bend providing less contact area while PTFE particles provide higher contact area by either rolling or making numerous contacts with the tube wall [42]. Overall, the exact charge transfer mechanism for this case is still unclear and further experimental and numerical works are required to explain this phenomenon.

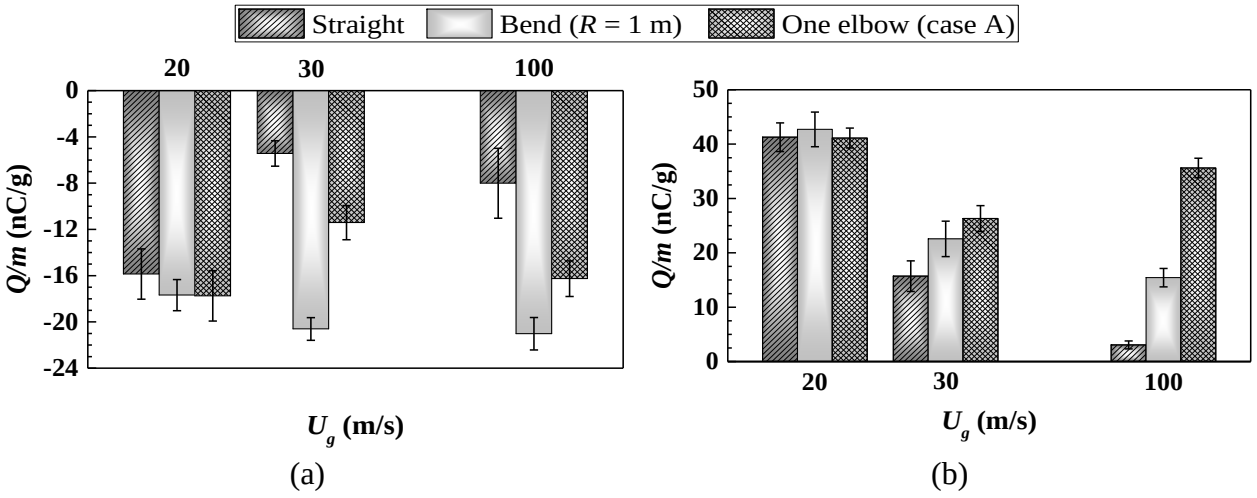

Figure 2-8 Comparing the effect of bend and elbow on charging behavior of 3.18 mm particles in the 3 m conveying tube; (a) PTFE particles, (b) Nylon particles.

2-3-4 Comparison of the Current and the Charge Measurement

In a real process it may not be feasible to implement the Faraday cage technique to measure the charge on the conveying solids. Therefore, current measurement off of the conveying line was applied and examined in this study as a secondary charge measurement technique.

Figure 2-9 presents the absolute values for Q_F (particle charge measured by the Faraday cage) versus Q_I (particle charge calculated from the current measurement) for 3.18 mm PTFE particles in the 3 m tube having different pathway and gas velocities. It is clear that there is a good agreement

between the magnitudes of charge measured from both methods. Similar results were obtained for Nylon and smaller PTFE particles under all conditions. Observing such behaviour under different conditions for all three particles indicates that the charge conservation holds in this system. As a result, the current measurement technique, which provides an online charge measurement, has a potential to be employed in commercial processes to measure the degree of charging of catalyst particles as they are conveying to the reactor.

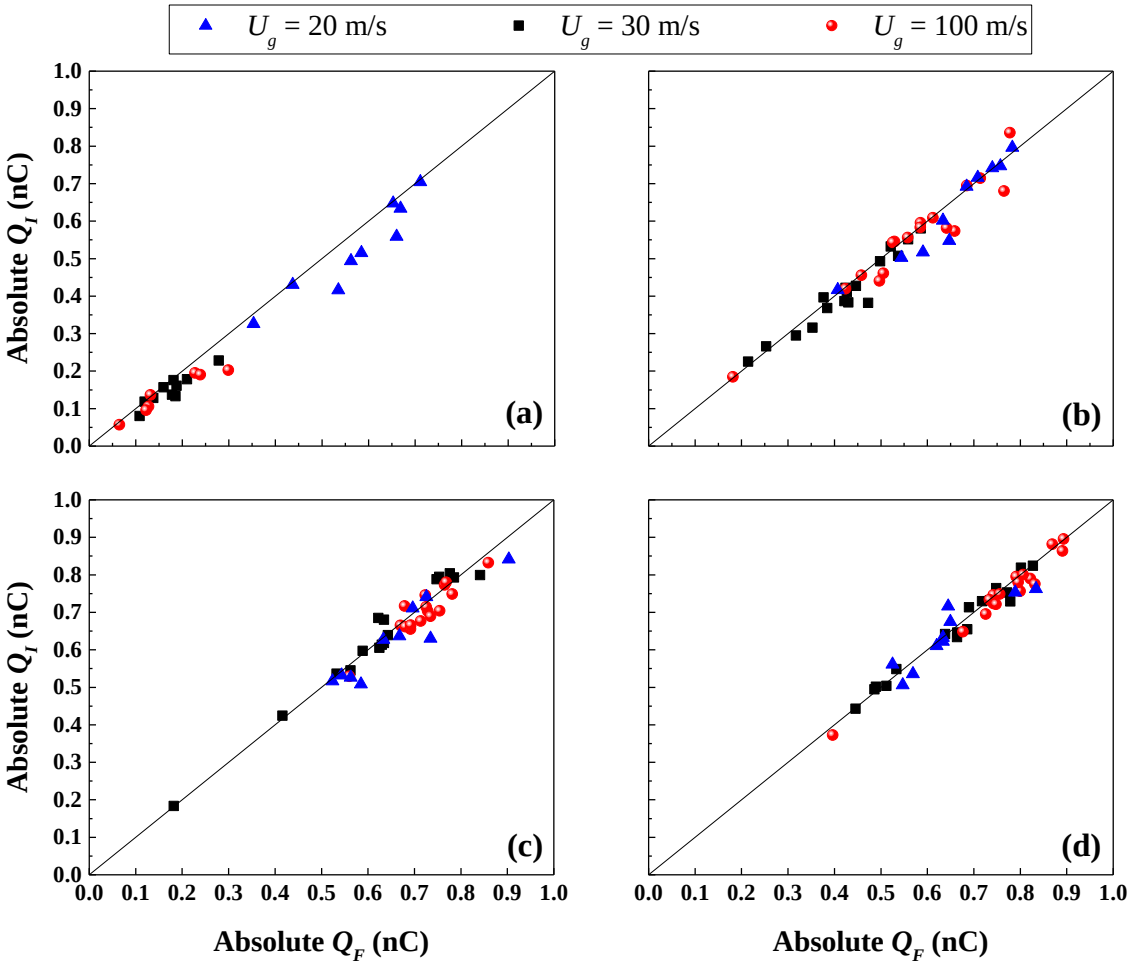

Figure 2-9 Comparison of the 3.18 mm PTFE particle charge measured by a Faraday cage and calculated from current off of the 3 m conveying tube; (a) Straight, (b) One elbow (case A), (c) Two elbows and (d) Three elbows.

2-4 Conclusion

Electrostatic charging behavior of PTFE and Nylon particles of different sizes, pneumatically conveyed in stainless steel 316 tubes of similar size to catalyst lines of polyethylene commercial

process, was studied. Smaller particles, owing to their smaller surface area, reached saturation charge quicker than larger particles in a straight tube. In straight tubes, the influence of the conveying gas velocity on larger particles was mainly observed at the lowest gas velocity (20 m/s) where particles *Q/m* was greatest due to particles higher residence time within the tube at this condition. Results also proved that larger particles charging behaviour at 20 m/s mostly depends on the tube total length rather than the pathway. However, the particle pathway was found to be an important parameter in determining the degree of charge transfer at higher gas velocities. In fact, in some cases particles could reach their saturation charge with only one elbow present. In tubes with elbows and at gas velocities above 20 m/s, increasing the gas velocity increased the charge magnitude of all particles due to the stronger collisions that took place between the particles and tube wall. It was also observed that the location of the elbow had no significant influence on the particles *Q/m*. The charging behaviour of PTFE and Nylon particles of the same size were found to be similar with the exception of the cases that included 90˚ elbow and a smooth bend at higher gas velocities. For Nylon particles it was suspected that particles mass and subsequently their momentum could have influenced the amount of charge transfer in non-straight tubes. Finally, this study also showed that measuring the electric current from the conveying lines can be used as an alternative online electrostatic charge measurement which is of great benefit for commercial operations.

Acknowledgement

Financial support from Univation Technologies, LLC (USA) and The Natural Sciences and Engineering Research Council of Canada (NSERC) is acknowledged with gratitude.

Nomenclature List

d_p	Mean particle diameter, mm
I	Electric current, A or C/s
ID	Tube inner diameter, mm
L	Tube length, m
m	Mass, g
Q	Charge, nC

Q_F	Charge measured by the Faraday cage, nC
Q_I	Charge calculated from current measurement, nC
Re_p	Particle Reynolds number
t	Time, s
U_g	Conveying gas velocity, m/s
U_{gPU}	Pick up velocity, m/s
μ_g	Gas dynamic viscosity, kg/m/s
ρ_g	Gas density, kg/m^3
ρ_P	Particle density, kg/m^3

References

[1] P. Mehrani, H.T. Bi, J.R. Grace, Electrostatic charge generation in gas-solid fluidized beds, J. Electrostat. 63 (2005) 165–173.

[2] A. Sowinski, L. Miller, P. Mehrani, Investigation of electrostatic charge distribution in gas-solid fluidized beds, Chem. Eng. Sci. 65 (2010) 2771–2781.

[3] P. Mehrani, M. Murtomaa, D.J. Lacks, An overview of advances in understanding electrostatic charge buildup in gas-solid fluidized beds, J. Electrostat. 87 (2017) 64–78.

[4] G. Hendrickson, Electrostatics and gas phase fluidized bed polymerization reactor wall sheeting, Chem. Eng. Sci. 61 (2006) 1041–1064.

[5] Y. Hu, D. Wang, J. Liu, J. Gao, A case study of electrostatic accidents in the process of oil-gas storage and transportation, J. Phys. Conf. Ser. 418 (2013) 012037.

[6] M. Ghori, E. Šupuk, B. Conway, Tribo-electrification and Powder Adhesion Studies in the Development of Polymeric Hydrophilic Drug Matrices, Materials (Basel). 8 (2015) 1482–1498.

[7] B.D. Fulks, S.P. Sawin, C.D. Aikman, J.M. Jenkins, Process for reducing sheeting during polymerization of alpha-olefins, US 4532311, 1985.

[8] M.P. Bartilucci, E.R. Davis Jr., B.J. Egan, R.O. Hagerty, P.K. Husby, Method and apparatus

for reducing static charges during polymerization of olefin polymers, US 6905654 B2, 2005.

[9] M.G. Goode, C.C. Williams, F.D. Hussein, T.J. McNeil, K.H. Lee, Static control in olefin polymerization, US 6111034 A, 2000.

[10] C.-I. Kuo, G.G.H. Patel, R.E. Pequeno, B.J. Savatsky, F.D. Hussein, Continuity additive for polyolefin polymerization processes, US 9221936 B2, 2015.

[11] D. Song, P. Mehrani, Mechanism of particle build-up on gas-solid fluidization column wall due to electrostatic charge generation, Powder Technol. 316 (2017) 166–170.

[12] R.G. Rokkam, R.O. Fox, M.E. Muhle, Computational fluid dynamics and electrostatic modeling of polymerization fluidized-bed reactors, Powder Technol. 203 (2010) 109–124.

[13] P. Bunchatheeravate, J. Curtis, Y. Fujii, S. Matsusaka, Prediction of particle charging in a dilute pneumatic conveying system, AIChE J. 59 (2013) 2308–2316.

[14] G.E. Klinzing, A review of pneumatic conveying status, advances and projections, Powder Technol. 333 (2018) 78–90.

[15] K. Saleh, A. Traore Ndama, P. Guigon, Relevant parameters involved in tribocharging of powders during dilute phase pneumatic transport, Chem. Eng. Res. Des. 89 (2011) 2582–2597.

[16] B.N. Cole, M.R. Baum, F.R. Mobbs, An investigation of electrostatic charging fffects in high-speed gas-solids pipe flows, Proc. Inst. Mech. Eng. Conf. Proc. 184 (1969) 77–83.

[17] E.E. Smeltzer, M.L. Weaver, G.E. Klinzing, Individual electrostatic particle interaction in pneumatic transport, Powder Technol. 33 (1982) 31–42.

[18] S. Matsusaka, H. Umemoto, M. Nishitani, H. Masuda, Electrostatic charge distribution of particles in gas–solids pipe flow, J. Electrostat. 55 (2002) 81–96.

[19] S. Matsusaka, M. Oki, H. Masuda, Bipolar charge distribution of a mixture of particles with different electrostatic characteristics in gas–solids pipe flow, Powder Technol. 135–136 (2003) 150–155.

[20] S. Matsusaka, M. Oki, H. Masuda, Control of electrostatic charge on particles by impact charging, Adv. Powder Technol. 18 (2007) 229–244.

[21] S. Matsusaka, H. Fukuda, Y. Sakura, H. Masuda, M. Ghadiri, Analysis of pulsating electric signals generated in gas–solids pipe flow, Chem. Eng. Sci. 63 (2008) 1353–1360.

[22] A. Thomas, K. Saleh, P. Guigon, C. Czechowski, Characterisation of electrostatic properties of powder coatings in relation with their industrial application, Powder Technol. 190 (2009) 230–235.

[23] M. Nifuku, H. Katoh, A study on the static electrification of powders during pneumatic transportation and the ignition of dust cloud, Powder Technol. 135–136 (2003) 234–242.

[24] N. Schwindt, U. von Pidoll, D. Markus, U. Klausmeyer, M. V. Papalexandris, H. Grosshans, Measurement of electrostatic charging during pneumatic conveying of powders, J. Loss Prev. Process Ind. 49 (2017) 461–471.

[25] M. Taghavivand, K. Choi, L. Zhang, Investigation on drying kinetics and tribocharging behaviour of pharmaceutical granules in a fluidized bed dryer, Powder Technol. 316 (2017) 171–180.

[26] K. Choi, M. Taghavivand, L. Zhang, Experimental studies on the effect of moisture content and volume resistivity on electrostatic behaviour of pharmaceutical powders, Int. J. Pharm. 519 (2017) 98–103.

[27] A. Giffin, P. Mehrani, Effect of gas relative humidity on reactor wall fouling generated due to bed electrification in gas-solid fluidized beds, Powder Technol. 235 (2013) 368–375.

[28] L.S. McCarty, G.M. Whitesides, Electrostatic charging due to separation of ions at interfaces: Contact electrification of ionic electrets, Angew. Chemie - Int. Ed. 47 (2008) 2188–2207.

[29] C.H. Park, J.K. Park, H.S. Jeon, B.C. Chun, Triboelectric series and charging properties of plastics using the designed vertical-reciprocation charger, J. Electrostat. 66 (2008) 578–583.

[30] S. Dhodapkar, P. Solt, G. Klinzing, Understanding bends in pneumatic conveying systems, Chem. Eng. 116 (2009) 46–52.

[31] H. Watanabe, M. Ghadiri, T. Matsuyama, Y.L. Ding, K.G. Pitt, H. Maruyama, S. Matsusaka, H. Masuda, Triboelectrification of pharmaceutical powders by particle impact,

Int. J. Pharm. 334 (2007) 149–155.

[32] S. Matsusaka, M. Ghadiri, H. Masuda, Electrification of an elastic sphere by repeated impacts on a metal plate, J. Phys. D. Appl. Phys. 33 (2000) 2311–2319.

[33] F. Chowdhury, A. Sowinski, M. Ray, A. Passalacqua, P. Mehrani, Charge generation and saturation on polymer particles due to single and repeated particle-metal contacts, J. Electrostat. 91 (2018) 9–15.

[34] J.A. Cross, Electrostatics: principles, problems and applications, Adam Hilger, Bristol, 1987.

[35] F.J. Cabrejos, G.E. Klinzing, Pickup and saltation mechanisms of solid particles in horizontal pneumatic transport, Powder Technol. 79 (1994) 173–186.

[36] H. Masuda, S. Matsusaka, S. Nagatani, Measurements of powder flow rate in gas-solids pipe flow based on the static electrification of particles, Adv. Powder Technol. 5 (1994) 241–254.

[37] M.W. Korevaar, J.T. Padding, M.A. Van Der Hoef, J.A.M. Kuipers, Integrated DEM – CFD modeling of the contact charging of pneumatically conveyed powders, Powder Technol. 258 (2014) 144–156.

[38] J. Wu, J. Yao, Y. Zhao, The effects of granular velocity and shape factors on the generation of polymer-metal electrostatic charge, J. Electrostat. 82 (2016).

[39] A.G. Bailey, Electrostatic phenomena during powder handling, Powder Technol. 37 (1984) 71–85.

[40] S. Fokeer, S. Kingman, I. Lowndes, A. Reynolds, Characterisation of the cross sectional particle concentration distribution in horizontal dilute flow conveying—a review, Chem. Eng. Process. Process Intensif. 43 (2004) 677–691.

[41] J.R. Fan, J. Yao, K.F. Cen, Antierosion in a 90° bend by particle impaction, AIChE J. 48 (2002) 1401–1412.

[42] H. Ghafori, M. Sharifi, Numerical and experimental study of an innovative design of elbow in the pipe line of a pneumatic conveying system, Powder Technol. 331 (2018) 171–178.

[43] H. Kruggel-Emden, T. Oschmann, Numerical study of rope formation and dispersion of non-spherical particles during pneumatic conveying in a pipe bend, Powder Technol. 268 (2014) 219–236.

[44] A. Rinoshika, Self-excited pneumatic conveying of granular particles in various horizontal curved 90° bends, Exp. Therm. Fluid Sci. 63 (2015) 9–19.

Chapter 3 - Electrostatic Charging Behaviour of a Silica Powder during Pulse Pneumatic Conveying

Milad Taghavivand, Benjamin J. Cho, Poupak Mehrani, Andrew Sowinski*

Department of Chemical and Biological Engineering, University of Ottawa, 161 Louis Pasteur, Ottawa, ON, K1N 6N5, Canada

* Corresponding author. E-mail: sowinski@uottawa.ca; Tel: 1-613-562-5800 ext. 6288

The current chapter is a manuscript published in the journal of Powder Technology "Powder Technology, 366, 119–129, 2020"

Abstract

The electrostatic charging of a dehydrated and non-dehydrated silica powder used as a catalyst support in polyethylene production was investigated using pulse pneumatic injection. The charge-to-mass ratios (*Q/m*) of powders were studied at varying conveying line lengths and pathways, conveying gas velocities and powder mass loadings. Results showed a direct relationship between the conveying line length and the powders' charging, whereas changing the pathway did not show a significant effect. Increasing the mass loading from 0.1 to 1 g decreased the powders' *Q/m*, while increasing the mass loading from 1 to 2 g showed no influence. Increasing the conveying gas velocity from 15 to 30 m/s increased the *Q/m* of the non-dehydrated powder, whereas no change was observed in the case of the dehydrated powder. Significant tube fouling was observed with the dehydrated powder, while the non-dehydrated powder left a negligible amount of fouling.

Keywords: Pneumatic conveying, Electrostatics, Charge measurement, Silica powder

3-1 Introduction

Electrostatic charge generation is a commonly observed phenomenon in many gas-solid processes due to the continuous inter-particle contacts as well as contacts between the particles and the vessel walls. This phenomenon creates severe operational challenges in gas-solid fluidized bed reactors used in the polyolefin industry. Gas-solid polyethylene fluidized bed reactors are examples where the adhesion of the highly charged polyethylene resins and catalyst particles to the reactor wall results in a problem known as "sheeting" [1]. Sheeting can cause long reactor shut down periods for cleaning and ultimately a significant economic loss [2]. As summarized by Mehrani et al. [3] and Fotovat et al. [4], a number of works have reported on understanding the electrostatic charging mechanisms in relation to polyethylene reactors. Majority of the works reported in literature have mainly studied fluidized beds containing polyethylene resins. This is unlike the commercial polyethylene reactors where catalyst particles also exist and thus their contribution to the bed electrification must be assessed. In commercial polyethylene processes, catalyst particles are typically pneumatically injected into the reactor with consecutive pulses. In general, pneumatic conveying systems are known to generate the largest amount of electrostatic charge among all gas-solid processes [5,6]. Thus, in relation to the polyethylene process, catalyst particles are anticipated to be electrostatically charged upon entering the reactor. Song and Mehrani [7] proposed a mechanism for polyethylene wall coating formation in metallic fluidized beds. They proposed that in such systems, aside from the attractive electrostatic forces within the bed material, the image force caused by induction charging on the fluidized bed wall could also contribute and promote the particles wall coating. Thus, if catalyst particles enter the reactor charged due to the pneumatic conveying, they could contribute to the formation of image forces upon entering the fluidized bed reactor and in turn to the formation of wall fouling.

In general, previous works on solids charging in dilute pneumatic conveying systems with continuous solids flow has shown that solids charge-to-mass ratio is proportional to parameters such as solids mass loading [8–10], conveying gas velocity [8,11,12], conveying line length and pathway [5,13–17], whereas it is inversely proportional to the particles' mean diameter [8,18–20], their moisture content [21] and conveying gas relative humidity [8,10,11]. In relation to the polyethylene process, not only is no work found in open literature reporting on electrostatic charging behaviour of the pneumatically conveyed catalyst particles with pulse injections, but also

the contribution of the catalyst particles' electrostatic charge on the formation and growth of the wall coating has not been studied and reported. In order to study the catalyst particles influence on reactor sheeting, it is vital to first gain a comprehensive knowledge of the charging of these particles during pneumatic conveying. Due to the fact that the majority of the catalyst particle (typically 90 to 99 wt.%) is occupied by its support [22–26], it is probable that the catalyst support shows a dominant effect on catalyst charging tendency [24]. Thus, the goal of this work was to study the charging behaviour of a silica powder, commonly used as a support for chromium-based (e.g., Phillips type), Metallocene and Ziegler-Natta catalysts in polyethylene production, through pneumatic pulse injection.

This work is in continuation of our previous work on charging of single particles in pneumatic conveying [20] with the exception that the apparatus was modified in this work to accommodate powder flow. In commercial polyethylene production plants, catalyst conveying lines could be of different lengths and configurations. This necessitates a comprehensive investigation of the combined effects of tube length and pathway on particles charging. Particles' electrostatic charging behaviour at two different conveying gas velocities was also investigated in this study. As a result, this study evaluates the effect of conveying line length and pathway, as well as conveying gas velocity on the electrostatic charging tendency of a dehydrated versus a non-dehydrated silica powder.

3-2 Materials and Method

The schematic diagram of the apparatus used in this work is shown in **Figure 3-1**. The apparatus consists of three sections: gas and solids injection; pneumatic conveying line; and electrostatic charge measurement.

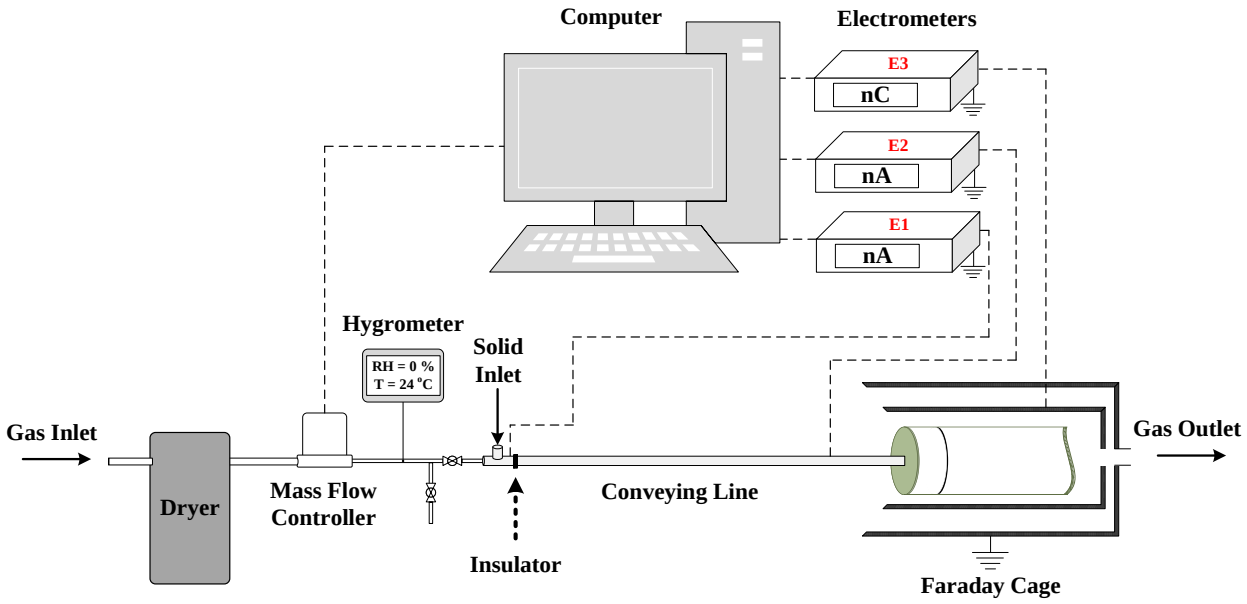

Figure 3-1 Schematic diagram of pneumatic conveying apparatus with electrostatic charge measurement.

Air at 22 ± 1 ˚C was used as the conveying gas and its relative humidity was reduced to approximately zero after passing through a dryer (Atlas Copco Model CD12). A mass flow controller (MKS Model 1559) was used to control the conveying gas flow rate. The temperature and relative humidity of the conveying gas was monitored by a hygrometer (Vaisala Model HMT 338). A stainless steel tube with an inner diameter of 4.57 mm was used as the pneumatic conveying line to replicate the catalyst conveying lines used in commercial polyethylene processes. A stainless steel branch tee was used to provide an inlet for solids into the conveying line and to serve as a solids holder. The two valves located before the branch tee (shown in **Figure 3-1**) were used to activate the injection system by allowing the gas to flow through the conveying line and transport the solids. The gas flow was stopped after 6 s which was adequate for the majority of the solid mass to exit the conveying line. In order to eliminate the effect of the solids' initial charge during the measurements, a fan type ionizer (SMC ModelIZF10R) was used to neutralize the particles before their usage. A double layer filter bag made of Nylon Monofilament (NMO) mesh with a definitive opening size of 1 micron was placed inside a Faraday cage and connected by an insulator piece to the conveying line exit to capture the conveyed solids.

The operating conditions utilized in this study are summarized in **Table 3-1**.

Table 3-1 Summary of operating conditions tested.

Conveying line			**Conveying gas**		**Powder**					
Material	***L*** **(m)**	***ID*** **(mm)**	**Type**	U_g **(m/s)**	**Size (μm)**			**Density (kg/m^3)**		**Mass Loading (g)**
					d_{10}	d_{50}	d_{90}	**Particle**	**Bulk**	
Stainless steel 316/316L	1, 3, 5	4.57	Dry air	15, 30	27	54	90	2170 - 2200	200 - 600	0.1, 1, 2

A porous spherical silica powder – used as a catalyst support – received from industry was tested in this work. To study the effect of conveying gas velocity on solids charging, two gas velocities of 15 and 30 m/s were tested. The former is the typical gas velocity used for catalyst conveying in commercial polyethylene process. In choosing the solids mass loading, the catalyst productivity of 8000 to 10000 g-PE/g-catalyst was considered and thus loadings of 0.1, 1 and 2 g were selected.

In a typical polyethylene plant, catalyst conveying lines length varies approximately between 3 to 10 m. Thus, the conveying line lengths tested in this study were 1, 3 and 5 m. To study the effect of the solids' conveying pathway, three different horizontal configurations were tested as presented in **Figure 3-2**. Case A represents the straight conveying lines, while Case B and Case C represent conveying lines containing one sharp 90˚ elbow and one smooth long-radius (1 m radius) bend, respectively. It should be noted that Case C was only tested for the 3 m conveying line. The smooth long-radius bend was selected due to its wide application in commercial processes as it reduces the risk of powder attrition and conveying line erosion and blockage compared to the sharp bends [27]. The 90˚ elbow was selected as it was expected to generate a larger charge on powders compared to the smooth bend.

Figure 3-2 Different solids conveying pathways tested. Arrows indicate solids entrance in each configuration.

For catalyst synthesis the silica support must be dehydrated otherwise the moisture within the pores of the support will poison and deactivate the catalyst [28–30]. Therefore, samples used in this study were dehydrated following the industry specific procedure by heating the samples to 600°C using an inert Argon gas in a tubular furnace. **Figure 3-3** shows a silica particle surface chemical structure transition due to the dehydration process [31–35]. As can be seen in **Figure 3-3a** prior to the dehydration the surface of the silica particle is composed of various silanol groups (≡Si–OH), some of which are connected to water molecules by hydrogen bonds (red dashed lines represent hydrogen bonds). In an ideal dehydration process **(Figure 3-3b)**, all of the water molecules are removed and silanol groups condense to form siloxane groups (≡Si–O–Si≡) [33]. In this work, the removed moisture content for the powders was in the range of 6 – 8 wt.%. In addition, the particle size distribution (PSD) analysis showed no difference in the size distribution after the dehydration process.

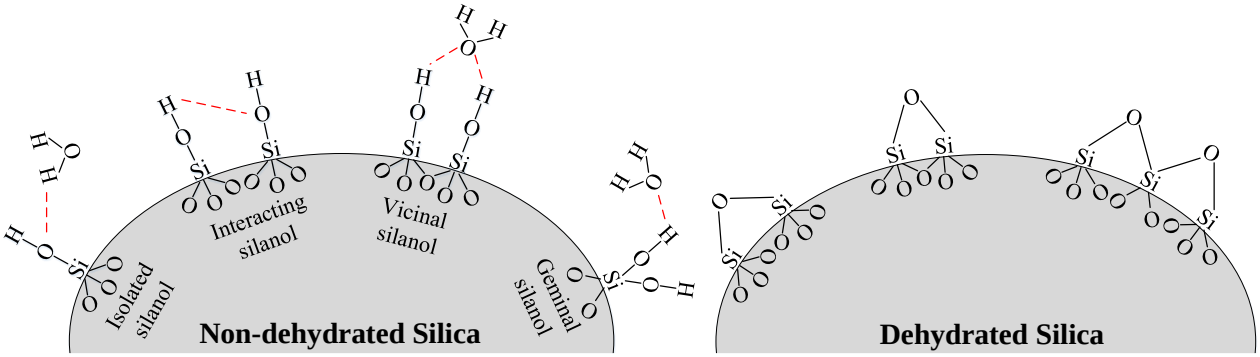

Figure 3-3 Surface chemical structure of a silica powder. (a) Before dehydration, (b) after dehydration.

Experiments were carried out in sets of 5 injections for each operating condition; however, in cases where significant tube fouling occurred 10 injections were performed. Standard error bars presented in the results section are based on a 95% confidence level. To mimic the commercial catalyst injection process, no tube cleaning was performed between the injections of each set. During the experiments it was important to determine whether the injected powders fouled inside the conveying line, and if so, how much electrostatic charge they possess. Therefore, in order to remove any fouled solids after the last injection of each set, the conveying gas velocity was increased to 50 m/s enabling the removal as much of the fouled powder as possible. The removed powder which is referred as “Tube fouling” was collected in the filter bag at the exit of the conveying line and its charge and mass were recorded.

After the completion of each set of injections and prior to starting a new set, the conveying line was scrubbed to remove any excess fouled powder and then washed with water and ethanol. Then, dry air was passed through the conveying line for a minimum of two hours at a high flow rate to dry the tube and to remove any residual moisture from the tube inner surface. A hygrometer was used to monitor the relative humidity of air leaving the conveying tube to confirm the tube is well-dried.

3-2-1 Electrostatic Charge Measurement and Signal Analysis

The charge on the pneumatically conveyed powders was measured using two techniques; direct charge measurement using a Faraday cage and on-line charge measurement via conversion of electric current. In a commercial process, implementing the Faraday cage technique to measure the charge of pneumatically conveyed particles might not be practical. Thus, the on-line charge measurement technique was tested for viability in this work.

Three digital electrometers (Keithley model 6514), as shown in **Figure 3-1**, set at a data collection frequency of 400 Hz were used in this work. **Figure 3-4a** shows an example of the signals measured by the three electrometers from injecting 0.1 g of the non-dehydrated powder in the 5 m straight conveying line at 15 m/s conveying gas velocity. The first electrometer (E1) was connected to the branch tee and used to measure the electric current, I (C/s), generated by the powder leaving the branch tee. The peak detected by E1, numbered as 1 in **Figure 3-4a**, occurs when the powder exits the branch tee. The negatively charged powder, as a result of contacts between the powder and branch tee, leaves an equal magnitude of positive charge on the branch tee. This charge becomes neutralized by the ground source as the powder exits the tee. The second electrometer (E2) was connected to the conveying line and used to measure the electric current flowing from the conveying line as a result of charge transfer between the conveyed powders and the tube wall. It needs to be mentioned that so long as the conveying line is electrically conductive, the point at which E2 is connected to the conveying line does not matter on the current measurement from the conveying line; however, for consistency, the connection point was set at approximately 50 cm from conveying line exit. As can be seen in **Figure 3-4a**, two peaks were detected by E2; peaks 2 and 2′. Peak 2, which occurs immediately after peak 1, happens when the negatively charged powder enters the conveying line and induces the same amount of charge on the conveying tube wall. According to the charge conservation law, the electric current magnitude captured from the

branch tee upon exiting the powder must be equal but in the opposite polarity of the electric current measured from the conveying line upon entering the powder. A negligible difference is expected due to the presence of the insulating piece which can generate extra charge on the powder. While the powder is traveling inside the conveying line, despite the ongoing contacts and charge transfer between the powder and the conveying line, no electric current signal is generated which is due to the fact that the powder and the conveying line are in electrostatic equilibrium. Finally, peak 2′ forms when the powder leaves the conveying line and enters the filter bag inside the Faraday cage. The surface area under peak 2′, represents the final electrostatic charge of the powder as a result of charge transfer between the conveyed powders and the tube wall. **Equation 3-1** was applied to find the electrostatic charge based on the current measured for a certain time span, t (s):

$$Q = \int_{t_i}^{t_f} I \, dt \qquad \textbf{(Eq. 3-1)}$$

t_i (s) and t_f (s) are the times when the current signal peak starts and ends, respectively.

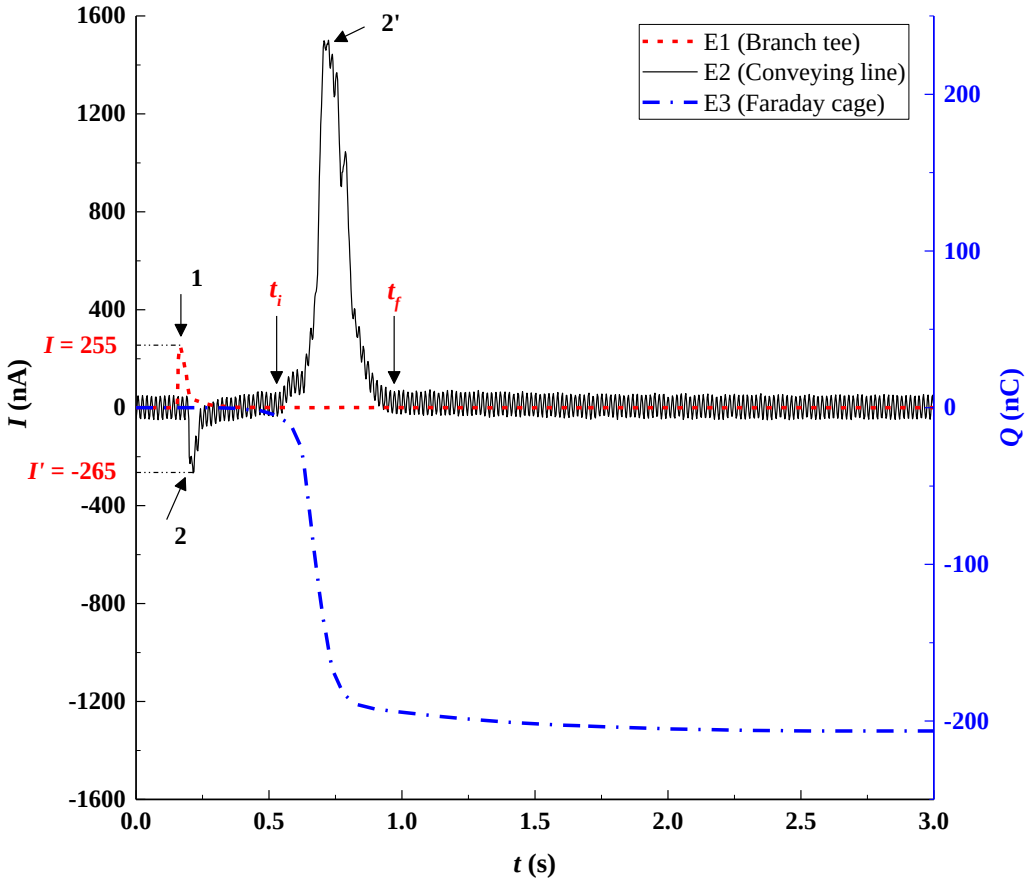

(a)

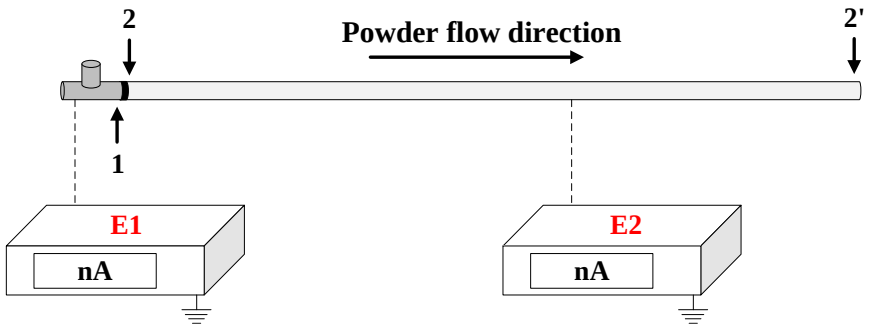

(b)

Figure 3-4 (a) Signals recorded by electrometers from injecting 0.1 g of non-dehydrated powder in the 5 m straight conveying line at U_g = 15 m/s; (b) order of current signals recorded by electrometers.

The third electrometer (E3) was connected to a Faraday cage located at the outlet of the conveying line and measured the electrostatic charge, Q (C), of the powders as they exit the conveying tube.

The electrostatic charge calculated by measuring the electric current from the conveying line must be equal but in opposite polarity of the powders charge measured by the Faraday cage.

3-3 Results and Discussion

The charging behaviour of a silica powder due to pneumatic pulse injection was investigated. Overall, under all tested operating conditions the particles gained negative charge in contact with the stainless steel conveying tube.

3-3-1 Electrostatic Charging of the Non-Dehydrated Powder

The first set of experiments were performed with non-dehydrated powder. For this solid, 5 injections took place for each testing condition. **Figure 3-5** shows the effects of conveying line length, pathway and conveying gas velocity on the solids' electrostatic charging behaviour for two mass loadings.

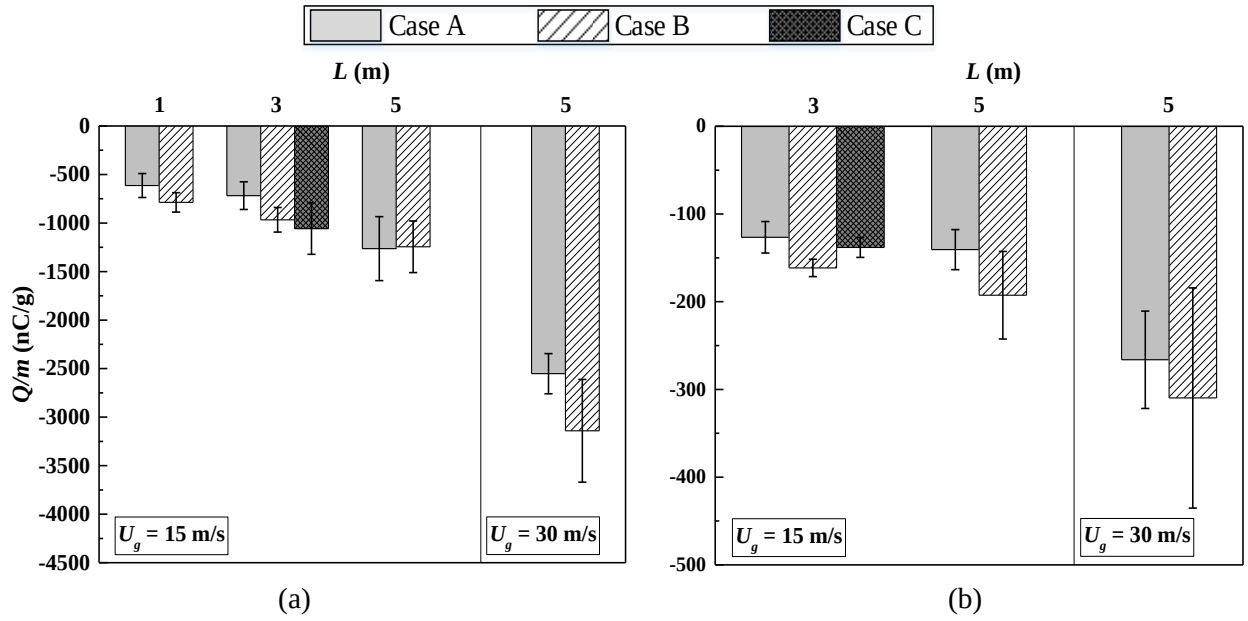

Figure 3-5 Effects of conveying line length, pathway and gas velocity on *Q/m* of non-dehydrated powder. (a) 0.1 g mass loading; and (b) 1 g mass loading.

Results shown in **Figure 3-5** indicate that for the mass loading of 0.1 g, increasing the tube length caused an increase in solids *Q/m*, while no significant difference was observed for the 1 g mass loading. In comparing the effect of solids conveying pathway, although on average the presence of a bend (either 90º elbow or smooth bend) increased the solids *Q/m*, it can be concluded that

(based on the standard error bars) the conveying pathway did not show a statistically significant influence on solids charging. On the other hand, increasing the gas velocity from 15 to 30 m/s, which was only studied in the 5 m conveying line, resulted in an increase in solids *Q/m*.

Despite the fact that increasing the mass loading from 0.1 to 1 g slightly increased the solids *Q*, the corresponding *Q/m* significantly declined at both gas velocities and under similar experimental conditions. This contradicts other works [8–10] where increasing the mass loading has shown to increase the solids charge-to-mass ratio. This is because the conveying systems used in other works were based on the continuous dilute flow of powder whereas a pulse injection was carried out in this work. As illustrated in **Figure 3-6**, in a pulse injection all of the loaded powder injected at once making the solids travel in concentrated plume(s) (i.e., single elongated plum or multiple small plums). Thus, as the solids mass loading increases, the concentration of powder at the center of the plume becomes higher. This means that not all of the individual particles within the plume(s) will contact the conveying tube wall and become charged. Grosshans and Papalexandris [36] and Watano et al. [37] have reported similar finding in their works. In another study, Ceresiat et al. [38] showed that in a pneumatic conveying system, the charged particles tend to concentrate near the wall region while the less charged particles concentrate in the centre of the conveying line. This also confirms why the solids *Q/m* drops at higher mass loadings. **Figure 3-7** shows that further increasing the solids mass loading to 2 g in the 5 m conveying line at 15 m/s gas velocity resulted in a larger drop in the solids *Q/m*. Also, from **Figure 3-7** it is clear that changing the conveying pathway did not significantly affect the solids *Q/m* significantly at each mass loading.

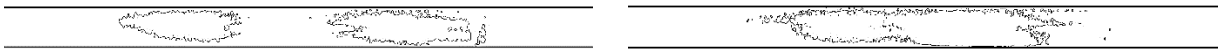

(a) (b)

Figure 3-6 Schematic of powder flow pattern in a pulse injection. (a) Two concentrated plumes; and (b) one concentrated plume. *The schematics constructed based on images taken of the powder flow through a small glass tube (4 cm in length) added to the conveying line*.

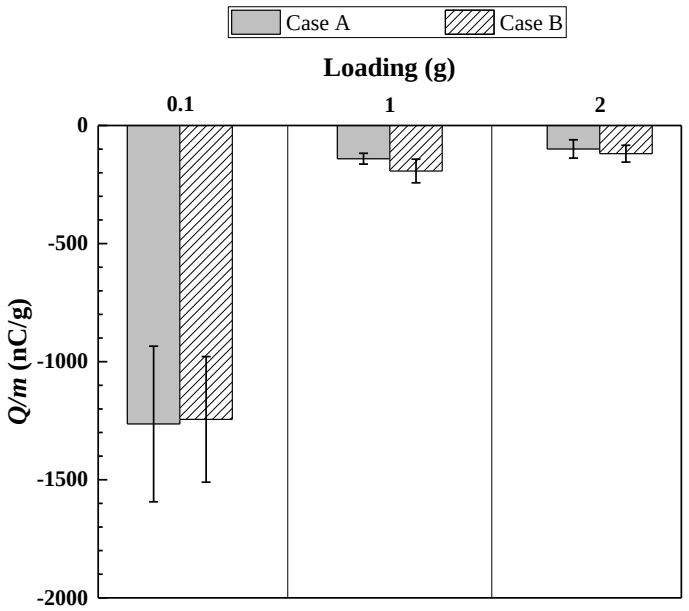

Figure 3-7 Effect of mass loading on solids *Q/m* tested with non-dehydrated powder in the 5 m conveying line at U_g = 15 m/s.

Although no mass loss was detected for each of the 5 consecutive injections, notable fouling was observed close to the exit of the conveying line. However, it needs to be mentioned that inside the tube was not observable to detect any possible fouling. An example of the tube exit fouling is shown in **Figure 3-8**. The solids accumulation might be due to the high concentration of electric field generated around the exit point of the conveying line inside the filter bag. As can be seen in **Figure 3-8**, comparing the effect of conveying gas velocity on the extent of tube outlet fouling indicates that the fouling at 15 m/s gas velocity was greater than that at 30 m/s gas velocity. This is due to the drag force exerted by the gas flow on the particles being dominant over the electrostatic attractive forces between the particles and the tube wall.

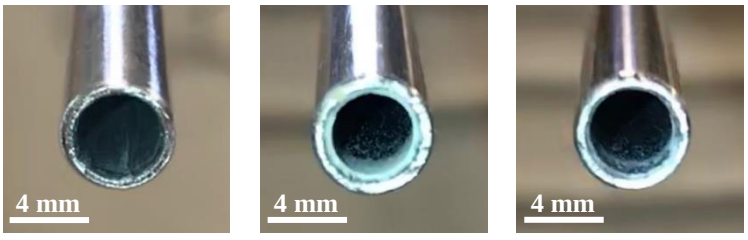

(a) (b) (c)

Figure 3-8 Effect of conveying gas velocity on the degree of tube fouling. Results are shown for 5 m straight conveying line after 5 consecutive injections of 0.1 g non-dehydrated powder. (a) Clean tube prior to injection; (b) tube outlet after injection at U_g = 15 m/s; (c) tube outlet after injection at U_g = 30 m/s.

An effort was made to collect any accumulated particles on the conveying tube inner wall to measure their mass and net charge. This was achieved by passing gas through the conveying line

at a much higher velocity of 50 m/s. Even though the mass of the collected particles was not measurable, its charge measured by the Faraday cage was 25 to 180% greater than that for the powder injected at each pulse. Such an observation confirmed that the fouled particles were extremely charged. **Figure 3-9a** shows an example of the fouling formed in the 5 m straight tube after 5 consecutive injections of 1 g of solids at 15 m/s gas velocity and compared with the same tube after passing the gas at 50 m/s (**Figure 3-9b**). **Figure 3-9d** shows the corresponding charge of the collected fouling which is approximately 60% greater than the charge of powder measured in the 5th injection as shown in **Figure 3-9c**.

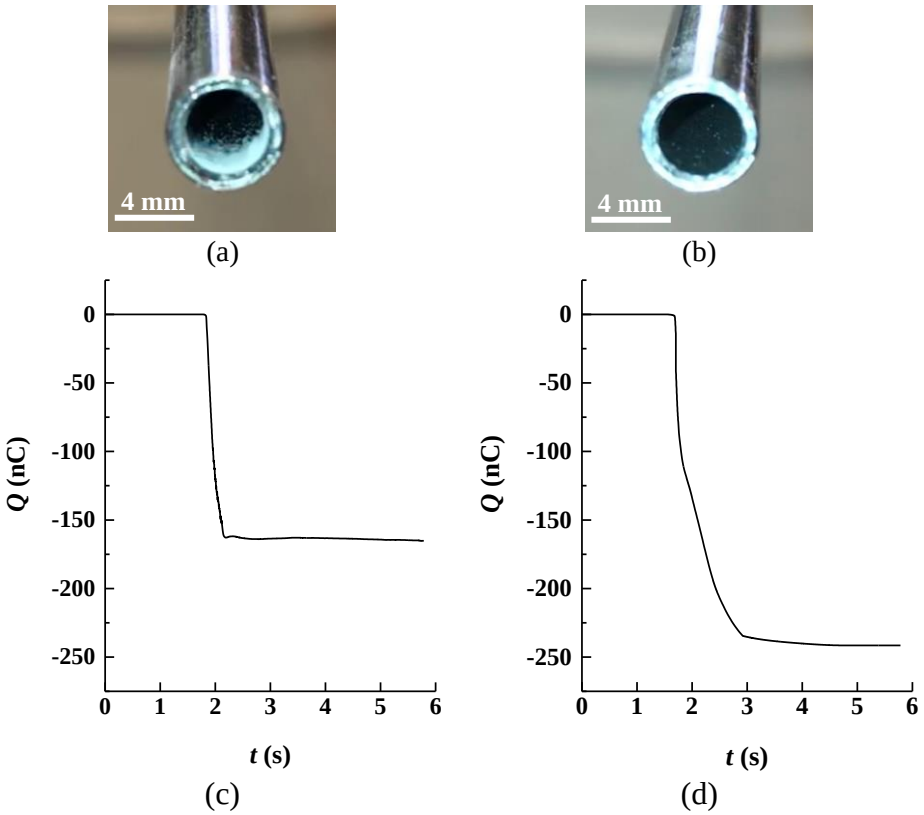

Figure 3-9 Fouling in 5 m straight tube after 5 consecutive injections of 1 g non-dehydrated powder at U_g = 15 m/s. (a) Tube outlet after 5 consecutive injections; (b) tube outlet after passing gas at 50 m/s; (c) charge of the injected powder for the 5th injection measured by Faraday cage; and (d) charge of the fouled solids collected.

3-3-2 Electrostatic Charging of the Dehydrated Powder

Results obtained from non-dehydrated powder implied that conveying pathway was not an influential factor on solids *Q/m*, whereas a direct relationship was found between the conveying line length and the solids *Q/m*. As well, it was observed that (despite a slight difference) the solids *Q/m* for mass loadings of 1 and 2 g were similar. Therefore, the experiments on dehydrated powder

were limited to a few operating conditions including the 5 m straight tube with solids mass loadings of 0.1 and 1 g, and gas velocities of 15 and 30 m/s.

Upon the 1st injection of the dehydrated powder significant mass loss (60-70% for 0.1 g loading and 30-40% for 1 g loading) was observed for both solid mass loadings tested. This is unlike the non-dehydrated power behaviour. This finding led to conducting multiple consecutive injections to better understand the occurrence of tube fouling for this powder.

Figure 3-10a presents the results for two repeated runs when 0.1 g of dehydrated powder was injected 10 consecutive times at 15 m/s gas velocity. It can be seen that the mass loss caused by tube fouling was significant during the first few injections for both trials. This could be a crucial problem in achieving a stable powder flow rate in industries including polyethylene production. From this figure it is also clear that the mass loss began to decline as the injections proceeded and leveled off after the 7th injection while reaching <20% of the injected mass (red dashed line indicates 80% recovery). Results in **Figure 3-10a** also show that the solids *Q/m* was extremely high during the first few injections when the mass loss was significant. However, the *Q/m* magnitude gradually declined and reached a steady level towards the last injections. An explanation for this decrease would be the switching of the dominant contact mechanism during the pneumatic conveying. In the first few injections, the dominant contact is between the powder and the stainless steel tube wall; whereas, towards the last injections when the tube fouling develops and the tube becomes coated with a layer of the powder, the particle-wall contact loses its dominant effect and the powder obtains less charge.

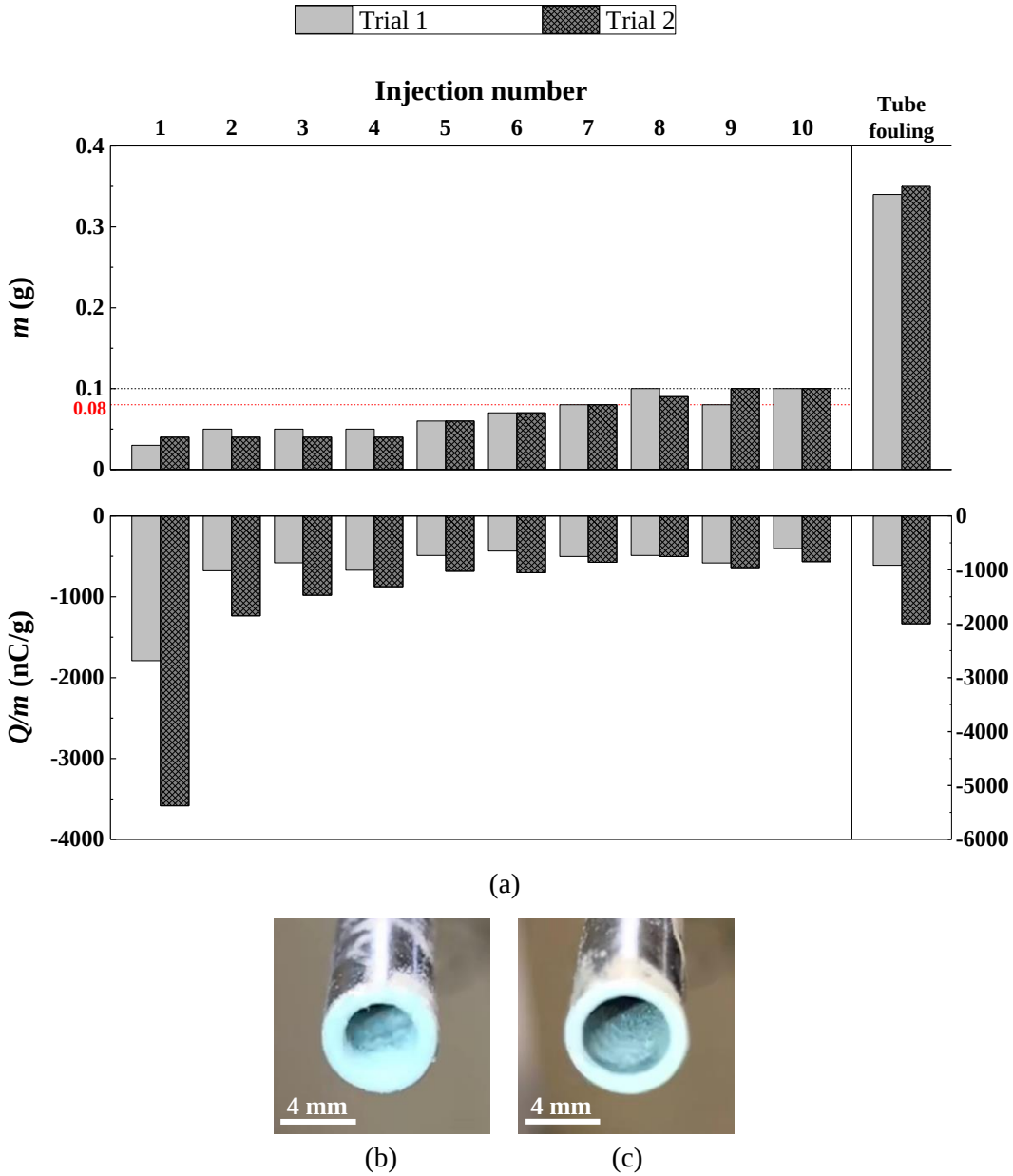

Figure 3-10 (a) Dynamic change of collected mass from injection of 0.1 g of dehydrated powder in the 5 m straight tube at U_g = 15 m/s and the corresponding Q/m; (b) tube outlet after the 10th injection; (c) tube outlet after passing gas at 50 m/s.

In addition, a relatively thick layer of powder was observed at the exit of the conveying line at the end of the 10th injection (**Figure 3-10b)**. Such observation can be contributed to the high charge of dehydrated powder which results in a high attractive electrostatic force between the tube wall and the charged powder. Once the last injection took place and the fouling reached an equilibrium (**Figure 3-10b**), a gas flow of 50 m/s was passed through the conveying line, as also performed on the non-dehydrated powder, to remove the fouled solids and to collect them in the filter bag for

their mass and charge measurements. The collected solids mass and *Q/m* are presented on the right side of the graph in **Figure 3-10a**. Comparing the images taken from the tube outlet after the 10th injection and after passing the gas at 50 m/s (**Figure 3-10b** and **Figure 3-10c)**, it is clear that the 50 m/s gas velocity was not sufficient to completely remove the fouled solids from the tube wall. This implies that the dehydrated powder became significantly charged, such that the electrostatic attractive force formed between the solids and the tube wall overcomes the drag force exerted on the powder by gas flow and therefore a thin dust-like layer still remains inside the tube.

Figure 3-11 illustrates the charging behaviour of dehydrated powder at different mass loadings and gas velocities. To better compare the results, only 5 out of 10 injections are presented in **Figure 3-11a**; but the mass shown as "Tube fouling" corresponds to after 10 injections. Comparing the effect of gas velocity on the tube fouling, it is clear that 15 m/s gas velocity resulted in a larger amount of tube fouling; the majority of the injected powder was recovered at the 30 m/s gas velocity. From **Figure 3-11a** and **Figure 3-11c** it can be seen that the tube fouling at the 15 m/s gas velocity is almost similar (between 0.3 to 0.4 g) for 0.1 and 1 g of the mass loadings. Also, it is clear that the majority of the tube fouling in the 1 g loading forms after the first injection and continuing the injections does not significantly contribute to the fouling. Therefore, a conclusion can be drawn that there is a maximum of 0.3 - 0.4 g tube fouling for a 5 m straight tube at 15 m/s conveying gas velocity. Same as for the non-dehydrated powder, increasing the mass loading resulted in a decrease in the solids *Q/m*. However, unlike the non-dehydrated powder, an insignificant difference was observed in the solids *Q/m* by changing the gas velocity. One probable reason could be related to the strong attractive electrostatic forces between charged particles and the tube wall, which results in the majority of the highly charged particles to adhere to the tube and stay within the conveying line rather than exiting. Therefore, even if the powder becomes more charged at the 30 m/s gas velocity, the highly charged particles always stay inside the tube as a fouling layer. Another possible explanation would be related to the powder dispersion and fouling formation inside the tube during the injections. Since the dehydrated powder, unlike the non-dehydrated solids, forms an extensive fouling layer (especially during the first injections) at both gas velocities, it is possible that particle-wall contacts become less dominant compared to the particle-particle contacts and thus both gas velocities result in a similar contact mechanism leading to a similar magnitude of charge on the powder.

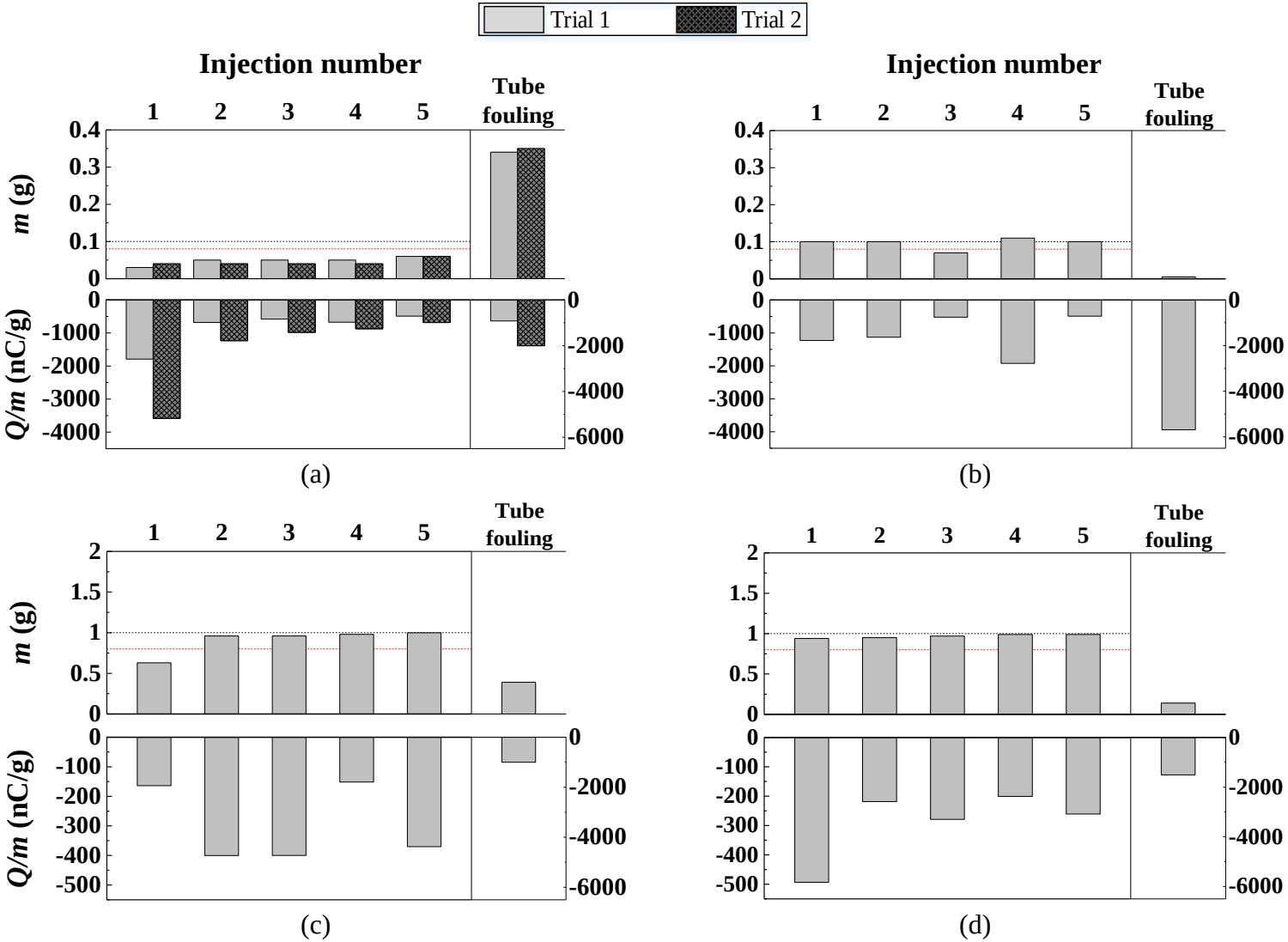

Figure 3-11 Effects of solids mass loading and conveying gas velocity on *Q/m* of the deyhdrated powder in the 5m straight tube. (a) 0.1 g mass loading, U_g = 15 m/s; (b) 0.1 g mass loading, U_g = 30 m/s; (c) 1 g mass loading, U_g = 15 m/s; (d) 1 g mass loading, U_g = 30 m/s.

3-3-3 Bipolar Charging

During the experiments, and specifically for the dehydrated powder, fluctuations in the current and charge signals were observed for all conditions. Fluctuations became severe as the injections progressed and the tube fouling grew. An example of signals containing fluctuations is presented in **Figure 3-12**. **Figure 3-12a** presents a case in which no significant tube fouling was observed and thus no fluctuations in either of the signals occurred. Whereas **Figure 3-12b** is for a case where significant tube fouling and signal fluctuations were observed. By looking at the current and charge signals in **Figure 3-12b**, it can be clearly seen that whenever the polarity of the current signal changes from positive to negative, a peak with a positive polarity forms in the charge signal measured by the Faraday cage. Such behaviour was detected seven times in the case shown in **Figure 3-12b**. This means that a small portion of the powder at each injection gains positive charge by contacting the fouled powder inside the tube and by developing the fouling a larger portion of the powder gets positive charge. This could also be one of the reasons for observing no difference in charge magnitude of dehydrated powder between two gas velocities. The formed fouled layer in case of injecting dehydrated powder does not allow the net charge magnitude of the powder increases after reaching a certain value.

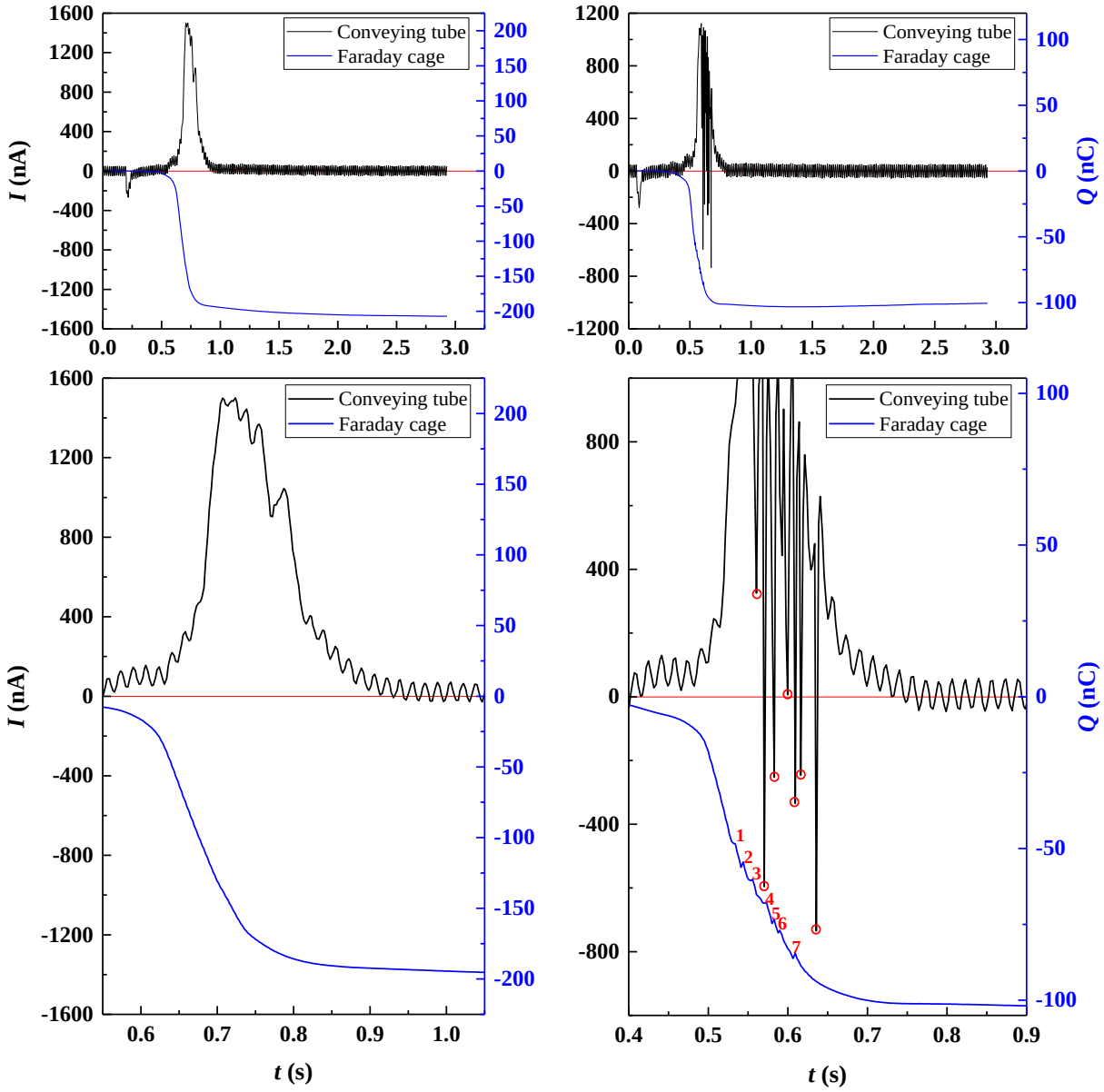

Figure 3-12 Signal fluctuations and bipolar charging effect. (a) Bipolar charging was not detected; (b) bipolar charging was detected.

3-3-4 Comparison of the Charge from the Faraday Cage and the Current Measurement

Figure 3-13 presents the absolute values for solids charge measured by the Faraday cage (Q_F) versus the charge calculated from the current measurement (Q_I). There is a good agreement between the magnitudes of charge determined from both methods, with less than ±10% difference between the measurements. In addition, observing such behaviour under various operating conditions indicates that the charge conservation holds in this system. As a result, the current measurement technique, which provides an online charge measurement, has a potential to be

employed in commercial processes to measure the degree of charging of catalyst powders as they pneumatically convey to the reactor.

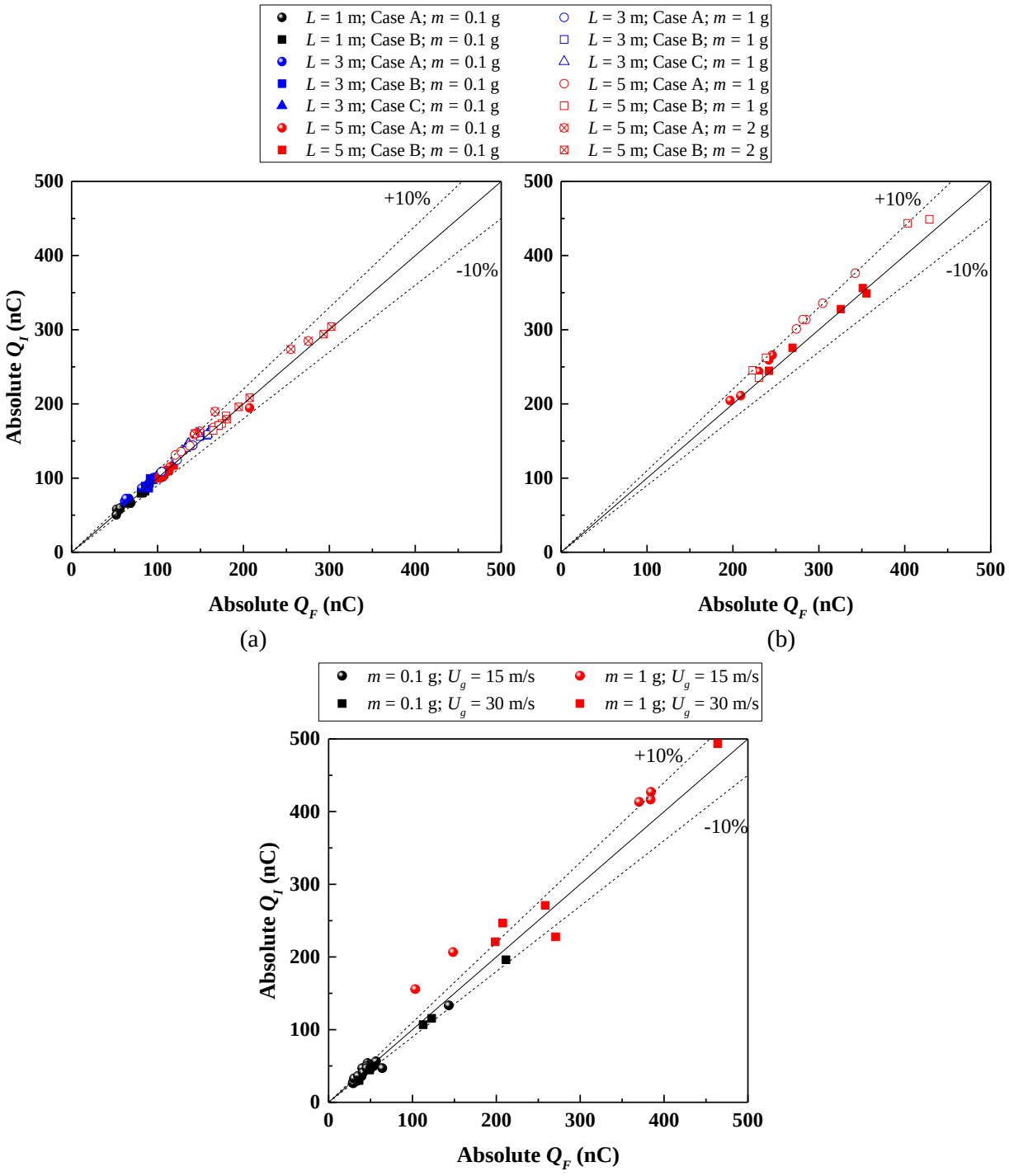

Figure 3-13 Comparison of solids charge measured using a Faraday cage with that calculated from the current signal measured off the conveying tube. (a) Non-dehydrated powder, U_g = 15 m/s; (b) non-hydrated powder, U_g = 30 m/s; (c) dehydrated powder, U_g = 15 and 30 m/s.

3-4 Conclusion

The electrostatic charging behavior of a silica powder (non-dehydrated and dehydrated) used as a catalyst support in commercial polyethylene processes was investigated through a pulse pneumatic injection. The solids were tested in a 4.57 mm stainless steel 316 tube, having a similar diameter to that of the catalyst lines in polyethylene commercial processes. To replicate a commercial process as well as to investigate the tendency of the powders in forming tube fouling, no tube cleaning was performed between the injections of each set. Conveying line length was found to have a direct relation to the extent of the solids charging. On average, changing the solids pathway from a straight tube to a tube with a bend increased the amount of charge transfer between the solids and the tube wall, but no statistically significant change was observed in the particles net *Q/m*. It was observed that increasing the solids mass loading had an inverse effect on the solids *Q/m*. Changing the gas velocity was found to have a direct relationship with the non-dehydrated solids *Q/m*. In addition, not a significant tube fouling was detected during injection of the non-dehydrated powders.

Results proved that dehydrating the solids significantly affected their charging behaviour as well as the degree of tube fouling. The specific charge of the dehydrated powder was significantly larger compared to that of the non-dehydrated powder, especially during the first couple of injections, though it dropped to a magnitude closer to that of the non-dehydrated powder by continuing the injections. Significant tube fouling was also found during the dehydrated powder conveying, with the fouled powder having a high charge. Unlike the non-dehydrated powder, gas velocity had no significant influence on the dehydrated powder charging. Fluctuations were observed for both the current and charge signals during the injection of the dehydrated powder which was attributed to the bi-polar charging of the particles caused by the formation of tube fouling. This study also showed that measuring the electric current off the conveying lines could be used as an alternative online electrostatic charge measurement technique which is of great benefit for commercial operations.

Acknowledgement

Financial support from Univation Technologies, LLC (USA) and The Natural Sciences and Engineering Research Council of Canada (NSERC) is acknowledged with gratitude.

Nomenclature List

d_p	Mean particle diameter, mm
I	Electric current, A or C/s
ID	Tube inner diameter, mm
L	Tube length, m
m	Mass, g
Q	Charge, C
Q_F	Charge measured by the Faraday cage, C
Q_I	Charge calculated from current measurement, C
t	Time, s
U_g	Conveying gas velocity, m/s
ρ_P	Particle density, kg/m^3

References

[1] B.D. Fulks, S.P. Sawin, C.D. Aikman, J.M. Jenkins, Process for reducing sheeting during polymerization of alpha-olefins, US Patent 4532311, 1985.

[2] R.O. Hagerty, M.E. Muhle, A.K. Agapiou, C.-T.I. Kuo, M.G. Goode, F.D. Hussein, R.B. Pannell, J.F. Szul, Method for controlling sheeting in gas phase reactors, US Patent 7985811 B2, 2011.

[3] P. Mehrani, M. Murtomaa, D.J. Lacks, An overview of advances in understanding electrostatic charge buildup in gas-solid fluidized beds, J. Electrostat. 87 (2017) 64–78.

[4] F. Fotovat, X.T. Bi, J.R. Grace, Electrostatics in gas-solid fluidized beds: A review, Chem. Eng. Sci. 173 (2017) 303–334.

[5] P. Bunchatheeravate, J. Curtis, Y. Fujii, S. Matsusaka, Prediction of particle charging in a dilute pneumatic conveying system, AIChE J. 59 (2013) 2308–2316.

[6] G.E. Klinzing, A review of pneumatic conveying status, advances and projections, Powder Technol. 333 (2018) 78–90.

[7] D. Song, P. Mehrani, Mechanism of particle build-up on gas-solid fluidization column wall due to electrostatic charge generation, Powder Technol. 316 (2017) 166–170.

[8] K. Saleh, A. Traore Ndama, P. Guigon, Relevant parameters involved in tribocharging of powders during dilute phase pneumatic transport, Chem. Eng. Res. Des. 89 (2011) 2582–2597.

[9] B.N. Cole, M.R. Baum, F.R. Mobbs, An investigation of electrostatic charging fffects in high-speed gas-solids pipe flows, Proc. Inst. Mech. Eng. Conf. Proc. 184 (1969) 77–83.

[10] E.E. Smeltzer, M.L. Weaver, G.E. Klinzing, Individual electrostatic particle interaction in pneumatic transport, Powder Technol. 33 (1982) 31–42.

[11] M. Nifuku, H. Katoh, A study on the static electrification of powders during pneumatic transportation and the ignition of dust cloud, Powder Technol. 135–136 (2003) 234–242.

[12] N. Schwindt, U. von Pidoll, D. Markus, U. Klausmeyer, M. V. Papalexandris, H. Grosshans, Measurement of electrostatic charging during pneumatic conveying of powders, J. Loss Prev. Process Ind. 49 (2017) 461–471.

[13] S. Matsusaka, H. Umemoto, M. Nishitani, H. Masuda, Electrostatic charge distribution of particles in gas–solids pipe flow, J. Electrostat. 55 (2002) 81–96.

[14] S. Matsusaka, M. Oki, H. Masuda, Bipolar charge distribution of a mixture of particles with different electrostatic characteristics in gas–solids pipe flow, Powder Technol. 135–136 (2003) 150–155.

[15] S. Matsusaka, M. Oki, H. Masuda, Control of electrostatic charge on particles by impact charging, Adv. Powder Technol. 18 (2007) 229–244.

[16] S. Matsusaka, H. Fukuda, Y. Sakura, H. Masuda, M. Ghadiri, Analysis of pulsating electric signals generated in gas–solids pipe flow, Chem. Eng. Sci. 63 (2008) 1353–1360.

[17] A. Thomas, K. Saleh, P. Guigon, C. Czechowski, Characterisation of electrostatic properties of powder coatings in relation with their industrial application, Powder Technol. 190 (2009) 230–235.

[18] H. Masuda, T. Komatsu, K. Iinoya, The static electrification of particles in gas-solids pipe

flow, AIChE J. 22 (1976) 558–564.

[19] H. Masuda, K. Iinoya, Electrification of particles by impact on inclined metal plates, AIChE J. 24 (1978) 950–956.

[20] M. Taghavivand, B. Elchamaa, A. Sowinski, P. Mehrani, Study of electrostatic charging of single particles during pneumatic conveying, Powder Technol. 355 (2019) 242–250.

[21] K. Choi, M. Taghavivand, L. Zhang, Experimental studies on the effect of moisture content and volume resistivity on electrostatic behaviour of pharmaceutical powders, Int. J. Pharm. 519 (2017) 98–103.

[22] Y. Rao, P. Cai, K.J. Cann, F.D. Hussein, W.R. Mariott, P.A. Cao, Supported catalyst with improved flowability, US Patent 10280283, 2019.

[23] K.J. Cann, J.H. Moorhouse, P.A. Khokhani, T.T. Tamargo, K.R. Gross, M.G. Goode, Chromium-based catalyst compositions for olefin polymerization, US Patent 10266618 B2, 2019.

[24] A. Sowinski, P. Mehrani, Impact of addition of a catalyst or its support on reactor wall coating due to electrostatic charging during fluidization of polyethylene, Ind. Eng. Chem. Res. 54 (2015) 3981–3988.

[25] H.C. Welborn Jr., Supported polymerization catalyst, US 4808561, 1989.

[26] R. Hoff, ed., Handbook of transition metal polymerization catalysts, Second Edi, John Wiley & Sons, Inc., 2018.

[27] S. Dhodapkar, P. Solt, G. Klinzing, Understanding bends in pneumatic conveying systems, Chem. Eng. 116 (2009) 46–52.

[28] J.H. Moorhouse, K.J. Cann, M.G. Goode, R.S. Eisinger, Modified chromium-based catalysts and polymerization processes for using the same, US Patent 9303103 B2, 2016.

[29] T. Xie, K.B. McAuley, J.C.C. Hsu, D.W. Bacon, Gas phase ethylene polymerization: Production processes, polymer properties, and reactor modeling, Ind. Eng. Chem. Res. 33 (1994) 449–479.

[30] C. Jenny, P. Maddox, Supported polyolefin catalysts, Curr. Opin. Solid State Mater. Sci.

(1998).

[31] T.J. Pullukat, R.E. Hoff, Silica-based Ziegler–Natta catalysts: A patent review, Catal. Rev. 41 (1999) 389–428.

[32] C.K. Buehler, A.P. Masino, Olefin polymerization using silica supported catalyst, US Patent 5232998A, 1993.

[33] A. Comas-Vives, Amorphous SiO2 surface models: energetics of the dehydroxylation process, strain, ab initio atomistic thermodynamics and IR spectroscopic signatures, Phys. Chem. Chem. Phys. 18 (2016) 7475–7482.

[34] A.M. Schrader, J.I. Monroe, R. Sheil, H.A. Dobbs, T.J. Keller, Y. Li, S. Jain, M.S. Shell, J.N. Israelachvili, S. Han, Surface chemical heterogeneity modulates silica surface hydration., Proc. Natl. Acad. Sci. U. S. A. 115 (2018) 2890–2895.

[35] C. Rosales-Landeros, C.E. Barrera-Díaz, B. Bilyeu, V.V. Guerrero, F.U. Núñez, A review on Cr(VI) adsorption using inorganic materials, Am. J. Anal. Chem. 04 (2013) 8–16.

[36] H. Grosshans, M. V. Papalexandris, Evaluation of the parameters influencing electrostatic charging of powder in a pipe flow, J. Loss Prev. Process Ind. 43 (2016) 83–91.

[37] S. Watano, S. Saito, T. Suzuki, Numerical simulation of electrostatic charge in powder pneumatic conveying process, Powder Technol. (2003).

[38] L. Ceresiat, H. Grosshans, M. V. Papalexandris, Powder electrification during pneumatic transport: The role of the particle properties and flow rates, J. Loss Prev. Process Ind. 58 (2019) 60–69.

Chapter 4 - Electrostatic Charging Behaviour of Polypropylene Particles during Pulse Pneumatic Conveying with Spiral Gas Flow Pattern

Milad Taghavivand [a], Poupak Mehrani [a], Andrew Sowinski [a], Kwangseok Choi [b,*]

[a] Department of Chemical and Biological Engineering, University of Ottawa, 161 Louis Pasteur, Ottawa, ON, K1N 6N5, Canada

[b] National Institute of Occupational Safety and Health, 1-4-6 Umezono Kiyose, Tokyo 204-0024, Japan

* Corresponding author. E-mail: choiks@s.jniosh.johas.go.jp; Tel: 81-424-91-4512 ext. 630

The current chapter is a manuscript published in the journal of Chemical Engineering Science "Chemical Engineering Science, 229, 116081, 2021"

Abstract

The electrostatic charging behaviour of 5-µm and 1500-µm polypropylene particles were studied during pulse pneumatic conveying with a spiral air flow. The conveying line was made of stainless steel with a total length of 1.3 m and inner diameter of 0.035 m. Effects of conveying gas velocity as well as particles mass loading were studied on particles charge-to-mass (*Q/m*) ratio. A high-speed camera set at 5000 frames per second (fps) capturing speed was used to record the particles movement pattern within the conveying line. Results clearly indicated a relationship between the particles motion pattern and their electrostatic charging behaviour. A direct relationship was observed between the conveying gas velocity and particles *Q/m*, whereas in general, particles *Q/m* magnitude was found to be inversely related with the mass loading. The *Q/m* of larger particles was found to be greater than that for the smaller particles. Additionally, charge measurements were performed and compared between a cyclone-type Faraday cage and a through-type Faraday cage with a filter bag inside. It was observed that the charge measured by these Faraday cages could differ drastically depending on particles size. The back pressure created inside the filter bag was suspected to be a significant contributor for such as observation.

Keywords: Electrostatics, Pneumatic conveying, Cyclone-type Faraday cage, Through-type Faraday cage, Particles motion pattern

4-1 Introduction

Electrostatic charge generation is an unavoidable phenomenon that occurs in many processes which involve liquids (e.g., flow of hydrocarbons in the pipelines) or solids (e.g., sieving, mixing, gas-solid fluidization and pneumatic conveying) [1–6]. Among different types of processes that involve solid particulates, pneumatic conveying has a wide range of applications (e.g., agricultural, pharmaceutical, petrochemical, food and etc.) mainly due to its simplicity in routing along with the low maintenance cost [7–9]. However, pneumatic conveying systems are believed to generate the most electrostatic charge on the conveyed particles among all solid-involving processes [5,10,11]. Since conveying lines are usually accompanied by other unit operations downstream the process (e.g., fluidized bed reactors in polyolefin production, or silos) it is thus vital to study particles electrostatic charge obtained during conveying. The particles' degree of charging could potentially influence the operation of the downstream equipment.

Depending on the application, particle flow within pneumatic conveying lines can be performed in either continuous or pulse flow (pulse injection). Studies with continuous dilute flow have shown a direct relationship between particles charge-to-mass ratio and particles flow rate [12–15], conveying gas velocity [13,14,16], and conveying line length [11,17,18]. Changing the conveying line pathway from straight to spiral has also shown a rise in particles charging efficiency [19–21]. Increasing the conveying line inner diameter [22,23], particles moisture content [24] and conveying gas relative humidity [13,15,16] have shown to decline the particles charging tendency. Similar trends have been observed for pneumatic conveying systems with pulse injection with the exception that a reduction in charge-to-mass ratio was observed by increasing the particles mass loading [14,23–25]. The mean particle diameter has been reported to be inversely related to their charge-to-mass ratio [13,15,26–32]; although, a direct relationship was observed for submicron sized particles [33]. Furthermore, it has been confirmed that the addition of the bends to the conveying pathway in both continuous flow and pulse injection cases results in a significant increase in particles charge-to-mass ratio [24,27,34,35].

Due to the wide application of pneumatic conveying systems as well as their great contribution with respect to the electrostatic charge generation, further quantitative research on understanding particle charging behaviour under various conditions would be beneficial. As such, the overall goal of this work was to provide a clear understanding of the charging behaviour of particles in relation

to their flow pattern within the conveying line (i.e., the types of contacts between the particles and the conveying tube wall). This unique aspect was achieved by adding transparent sections to the conveying line and obtaining real time images of the conveyed solids while measuring their electrostatic charge. In addition, this study was conducted using spiral gas flow pattern to promote the contacts between particles and conveying tube wall. Finally, since having a reliable charge measurement device is of great importance to both industrial and academic sectors, this work provided a comparison between three charge measurement methods. They included two types of Faraday cages (a cyclone-type and a conventional through-type housing a filter bag) and direct measurement of charge from the conveying line. In this work, the charging behaviour of solids in two sizes were evaluated by varying the conveying gas velocity and solids mass loading during pulse pneumatic conveying.

4-2 Materials and Method

The schematic diagram of the pneumatic conveying apparatus used in this work is illustrated in **Figure 4-1**. A stainless steel tube with an inner diameter of 0.035 m and total length of 1.3 m was used as the conveying line. In order to visualize the particles' flow pattern inside the conveying line, a 0.13 m in length transparent Plexiglass tube with an inner diameter similar to that of the conveying line was placed at location A, 0.39 m downstream of the entrance of the particles feeder (as shown in red in **Figure 4-1**). A high-speed camera (Photron model FASTCAM Mini UX100) set at 5000 fps with an imaging quality of 1280×1000 was used to record the particles movement at location A. A square (0.08 by 0.08 m) LED light was placed behind the Plexiglass tube to better visualize the particles movement.

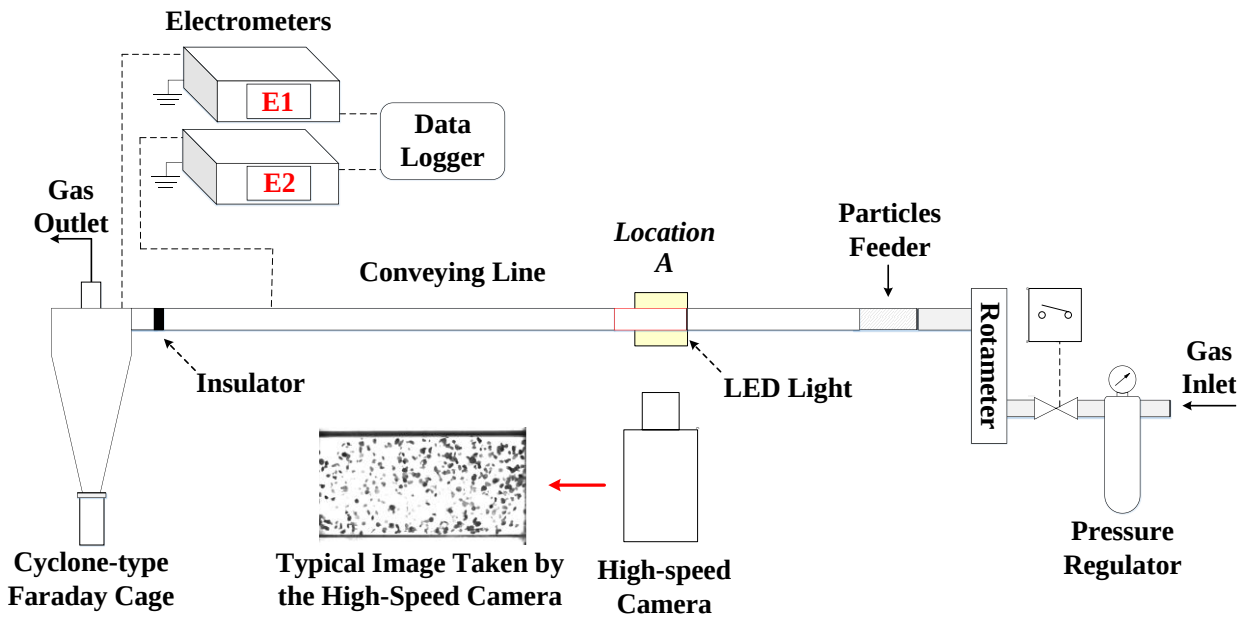

Figure 4-1 Schematic diagram of pneumatic conveying apparatus with a cyclone-type Faraday cage for electrostatic charge measurement.

In order to create a spiral gas flow and subsequently spiral particle flow pattern inside the conveying line, a particle feeder was designed and fabricated as shown in **Figure 4-2a.** The feeder consisted of a stainless steel cylinder, 0.035 m in diameter and 0.1 m in length. The feeder had a removable top allowing the solids loading. As illustrated in **Figure 4-2b**, the entrance of the feeder was a disk with eight holes 6 mm in diameter drilled with a 60˚ slant relative to the circular cross section allowing the particles to collide the conveying line with a contact angle of 30˚. This disk also contained two conical pieces with a base diameter of 0.014 m and height of 0.005 m attached to its center on both sides. The conical pieces enhanced the spiral pattern of the gas flow. To eliminate effects of any external noise on electrostatic charge measurement, the particle feeder and the conveying line were placed inside an electrically grounded stainless steel box.

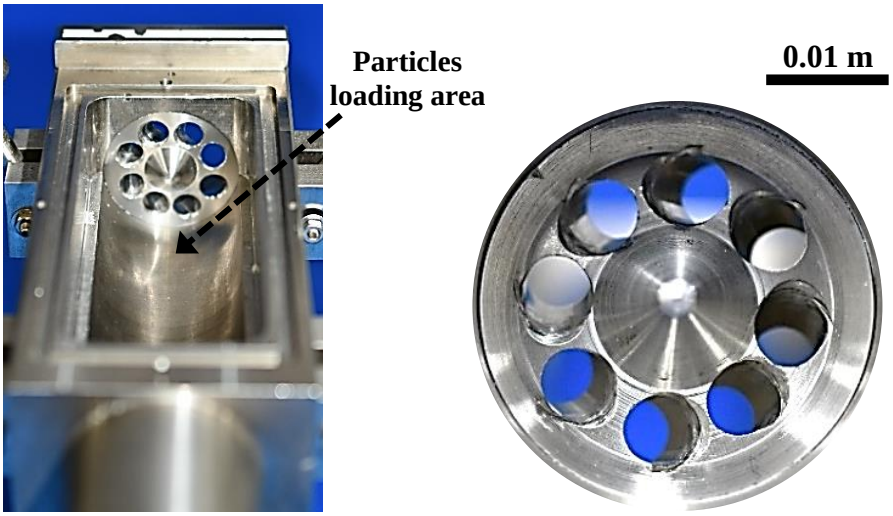

(a) (b)

Figure 4-2 Images of the particles' feeder. (a) Inside view of the feeder displaying the front view of the spiral flow generator as well as the particles loading area; and (b) back view of the spiral flow generator.

To measure the electrostatic charge of the conveyed particles, two types of Faraday cages were used and compared in this work. A custom designed stainless steel cyclone-type Faraday cage (detailed schematic shown in **Figure 4-3a**) connected to a digital Keithley model 6514 electrometer (E1) was connected to the conveying line exit to both capture the conveyed particles and measure their charge, Q (C). The Cyclone-type Faraday cage was electrically isolated from the conveying line by an insulator piece made of Teflon. To confirm the charge conservation, another digital Keithley model 6517A electrometer (E2) set on charge (Q) mode was directly connected to the conveying line. While the particles are traveling inside the conveying line, due to the electrostatic equilibrium between the particles and the conveying line, no charge signal will be detected despite the ongoing contacts and charge transfer. However, as the particles exit the conveying line a charge (Q) signal will be detected by E2. As such, the charge measured by E2 must be equal, but of an opposite polarity, to the charge measured by E1. Both electrometers had a data collection frequency of 100 Hz. The plexiglass tube at location A was replaced with a stainless steel tube of the same inner diameter and length during the electrostatic charge measurement. In order to provide a comparison between different electrostatic charge measuring devices, the cyclone-type Faraday cage was replaced with a conventional through-type Faraday cage made of stainless steel housing a filter bag to capture the particles (**Figure 4-3b**). The filter bag was made of polyester which is a typical material used in industry to capture the dust and fine particulates and had a capturing efficiency of 99.99 % for particles of 0.2 – 0.3 µm. Both the

cyclone-type and the through-type Faraday cages were electrically isolated to eliminate the effect of any external noise.

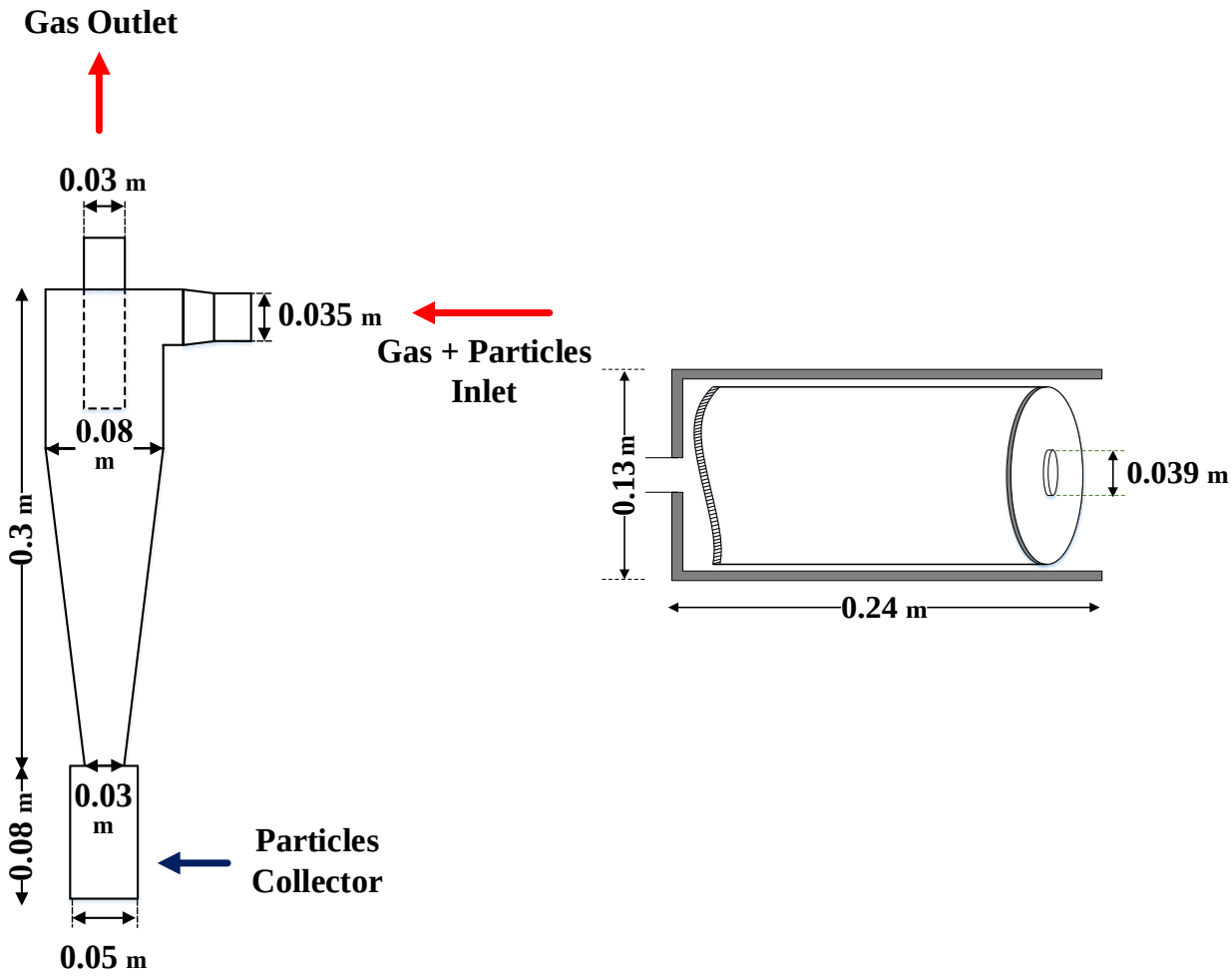

Figure 4-3 Schematics of (a) cyclone-type Faraday cage; and (b) through-type Faraday cage with a filter bag.

Air from a gas cylinder at zero relative humidity was used as the conveying gas. The conveying gas flow rate and subsequently the velocity was controlled and adjusted by an air pressure regulator connected to a rotameter (Tokyo Keiso model F07-110354). A normally closed solenoid valve connected to a manual switch was used to start and stop the conveying gas flow. The gas flow was kept on for 6 – 7 seconds which was adequate for the loaded particles to exit the conveying line. To study the effect of conveying gas velocity (U_g) on particles electrostatic charging, three gas velocities of 9, 15 and 25 m/s were tested.

Conveying particles were polypropylene (PP) of two different sizes with properties summarized in **Table 4-1.** In order to better understand the extent of the electrostatic charging of the particles, their charge prior to conveying (i.e., initial charge) was measured by a Faraday cage. Along with varying the conveying gas velocity, the solids mass loadings (m_L) were varied from 1 and 2 g. For the 5 µm particles, due to fouling formation inside the conveying line, experiments were carried out in sets of five consecutive injections for each condition and each condition was repeated two times. Further detailed procedure can be found elsewhere [24]. After the completion of each injection set and prior to starting a new set, the conveying line was scrubbed and vacuumed to remove any excess fouling. For the 1500 µm particles since no fouling occurred within the conveying line, only one injection was carried out for each condition and each condition was repeated three times. To prevent particles from adsorbing moisture, they were kept in a closed container inside a desiccator cabinet. All experiments were conducted at room temperature (21 ºC) with 35% relative humidity.

Table 4-1 Particle properties used in this work.

Particle type	**Particle Size (µm)**			**Particle Density (kg/m^3)**	**Initial *Q/m* (nC/g)**
	d_{10}	d_{50}	d_{90}		
Polypropylene (PP)	2	5	10	946	-0.03 ± 0.01
	1100	1500	1900		-0.01 ± 0.01

4-3 Results and Discussion

For all operating conditions tested, considering the initial charge of the solids as shown in **Table 4-1**, polypropylene particles acquired negative charge when conveyed in the stainless steel tube. This was expected due to the difference in the two materials' work functions. The work functions were measured by Riken Keiki models AC-2 and AC-3 for stainless steel and PP particles and were found to be 5.29 ± 0.61 and 6.44 ± 0.06 eV, respectively. In this study due to the nature of the injection (i.e., pulse injection) particles traveled in a plume along the conveying line. However, the dispersion of the particles within the plume and their flow pattern within the tube varied between the two particle sizes.

4-3-1 5-μm PP Particles

Snapshots of the particles flow pattern captured by the high-speed camera at location A are shown in **Figure 4-4**. For all the conditions tested, particles were moving in a spiral motion while majority of them were sliding along the tube wall. As well, it was observed that majority of the particles were moving in the form of clusters with their sizes varying (as large as 3.5 mm in diameter) depending on the U_g. Examples of clusters are identified in red in **Figure 4-4a** at t = 5.6 ms. Smaller clusters observed at 15 and especially 25 m/s gas velocities; but instead, particles were smeared over the transparent Plexiglass tube due to an increase in the centripetal force. In addition, concentrated zones were detected alongside the transparent tube. Examples are identified in red in **Figure 4-4b** at t = 4.4 & t = 5.6 ms. These zones became more concentrated as the solids mass loading increased. As expected, with the increase in conveying gas velocity the particles' residence time in the transparent section declined resulting in the plume length to be shorter and the particles' concentration to be higher. However, imaging results indicated that increasing the solids mass loading did not significantly affect the particles' residence time for both conveying gas velocities.

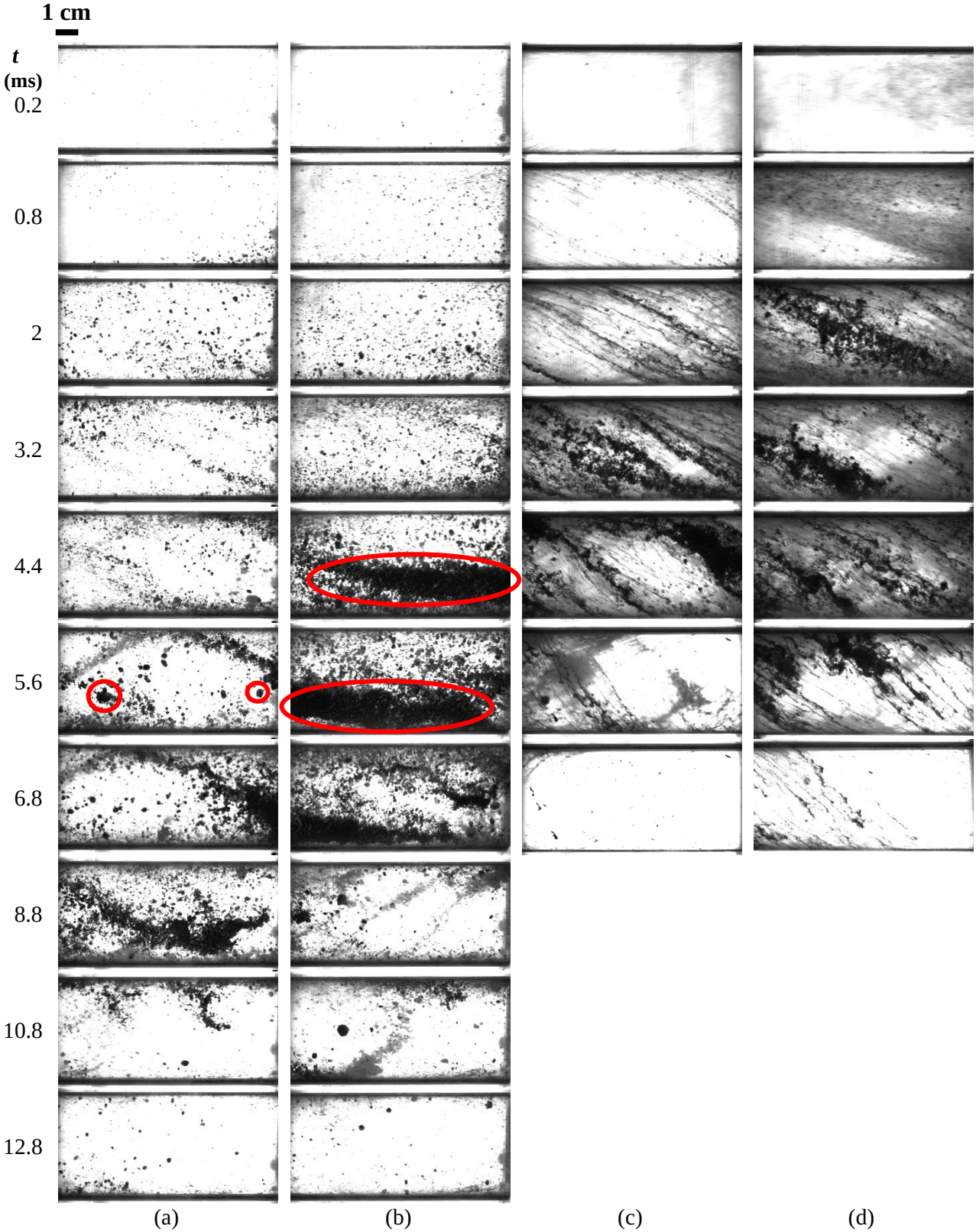

Figure 4-4 Snapshots of the 5-μm PP particles flow pattern captured by the high speed camera at location A for two solids mass loadings and conveying gas velocities. Images captured for a 0.08 m in length and 0.035 m in inner diameter of the Plexiglass tube. (a) m_L = 1 g, U_g = 9 m/s; (b) m_L = 2 g, U_g = 9 m/s; (c) m_L = 1 g, U_g = 25 m/s; and (d) m_L = 2 g, U_g = 25 m/s. The corresponding videos are provided in the supplementary information (Videos 1 – 4).

Figure 4-5 shows the influence of increasing solids mass loading and conveying gas velocity on the recovered particle masses (*m*) after each injection and their charge-to-mass ratios (*Q/m)*. This figure also compares the results between the cyclone-type and the conventional through-type Faraday cage.

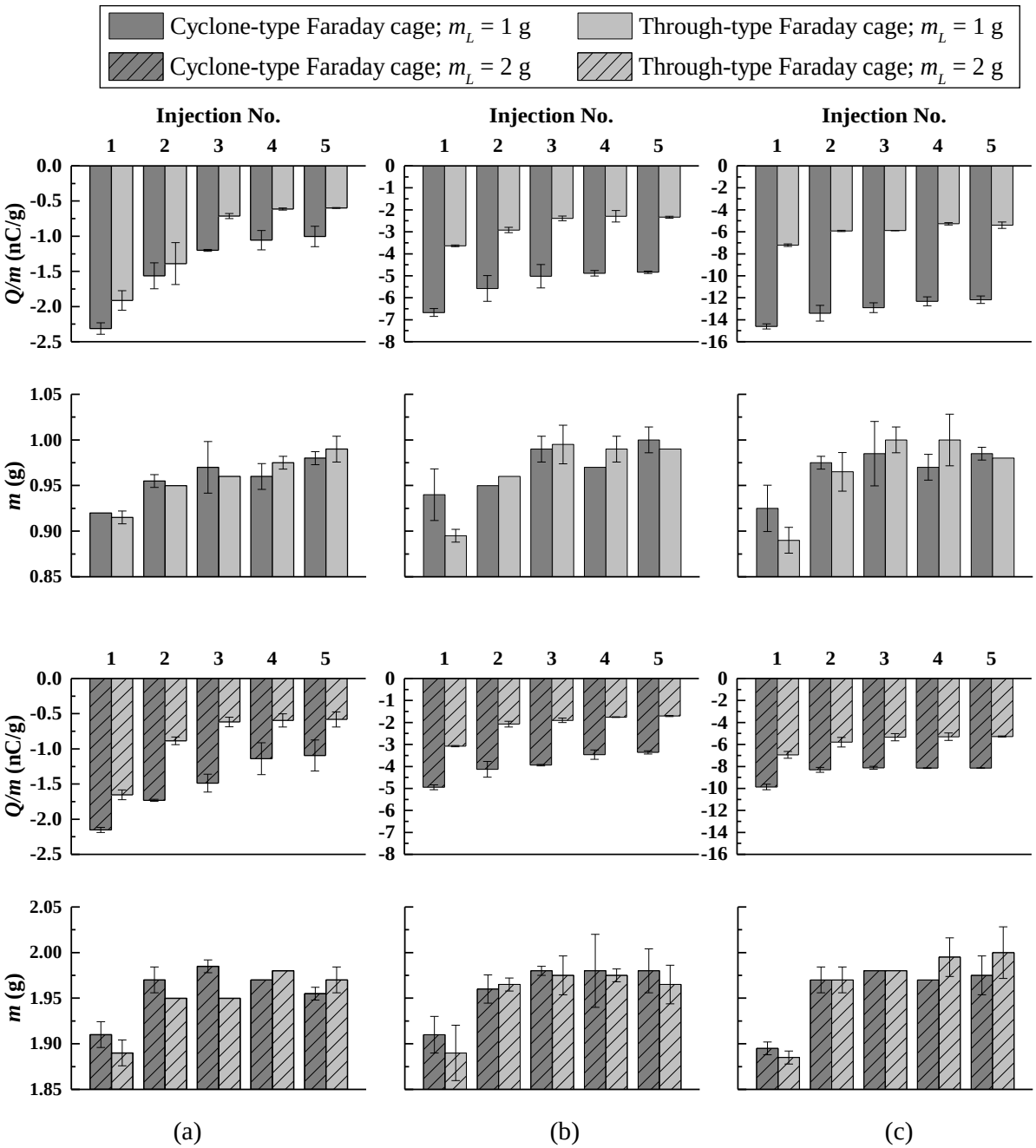

Figure 4-5 Conveyed 5-μm PP particles recovered masses and *Q/m* for m_L = 1 & 2 g. (a) U_g = 9 m/s; (b) U_g = 15 m/s; (c) U_g = 25 m/s.

For both mass loadings, on average, approximately 92 – 93 wt.% and 94 – 95 wt.% of the initial injected masses were recovered after the first injection that is a clear indication of particle build up on the tube wall. For all the cases, the recovered masses eventually reached 98 – 100 wt.% with subsequent injections. **Figure 4-6** illustrates that at all the gas velocities tested a thin dust like layer formed inside the conveying line for 1 g mass loading when the cyclone-type Faraday cage was used. Images were taken upon completion of the fifth injection for all the cases. Similar fouling was observed for the 2 g solids mass loading. The number of injections required to achieve a mass recovery of 98 – 100 wt.% depended on the conveying gas velocity and solids mass loading. Almost 5 injections were required at the lowest gas velocity when the mass loading was 1 g whereas at the highest gas velocity this value could be reached in the third injection. For the 2 g mass loading; however, 98 – 100 wt.% recovery was reached at the second injection for all the conditions.

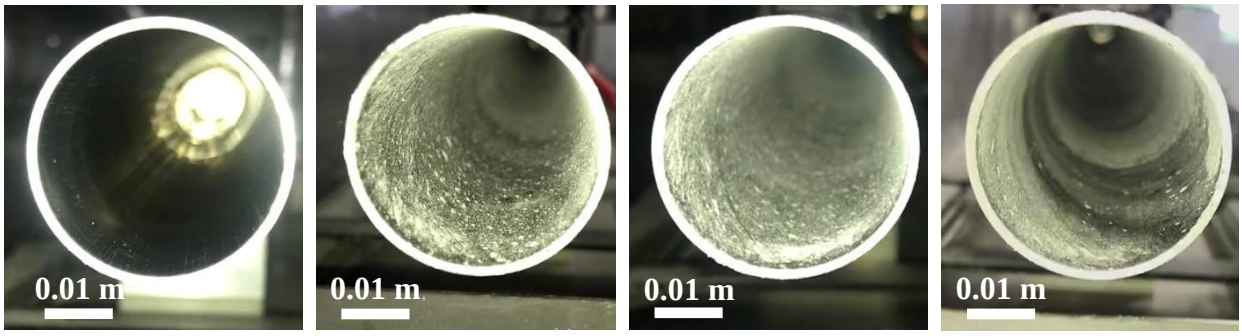

(a) (b) (c) (d)

Figure 4-6 Images of conveying tube outlet indicating formation of fouling for 5-µm PP particles at m_L = 1 g. (a) Clean tube prior to injection; (b) after the 5th injection at U_g = 9 m/s; (c) after the 5th injection at U_g = 15 m/s; and (d) after the 5th injection at U_g = 25 m/s.

Results in **Figure *4-5*** also show that the first injection of each condition resulted in the largest degree of charge transfer, which decreased gradually and reached a steady value as more injections carried out. As discussed in our previous work [24] such behaviour is attributed to the formation of a fouling layer inside the conveying line. Particles build up on the tube wall would switch the contact mechanism from dominantly being particle-metal wall in the first injection to the combination of particle-metal wall and particle-wall fouling as injections proceed.

Results in **Figure 4-5** clearly indicate that for both mass loadings, the particles became electrostatically charged (with respect to their minimal initial charge) due to their pneumatic conveying and their degree of charging per mass was directly proportional to the conveying gas

velocity. Although the particles' residence time decreased by increasing the gas velocity, the contact force between the particles and the conveying line must have increased and in turn resulted in a higher electrostatic charge transfer. In addition, images shown in **Figure *4-4*** imply that for both mass loadings clusters were observed more frequently at the lower conveying gas velocity. This implies a lower possibility of contact and subsequently less charge transfer between the tube wall and the individual particles within the clusters.

While keeping the conveying gas velocity constant at 9 m/s, increasing the particles' mass loading did not significantly influence their *Q/m.* At this condition, since the plume length was relatively long, doubling the mass loading still allowed the particles to experience wall contacts, resulting in almost doubling the net *Q* (i.e., keeping particles *Q/m* constant). However, the number of particles experiencing the wall contact did not increase proportionally when the mass loading doubled at higher gas velocities and thus the particles' *Q/m* reduced. Although it is not clear from snapshots presented in **Figure 4-4**, analyzing the video images clearly showed that since at these gas velocities the plume length was short the majority of the particles were sliding on top of each other and thus not contacting the conveying tube wall. In addition, it was seen that the particles that were moving against the wall were sliding rather that rolling or bouncing and thus had less available effective contact area, which in turn could result in less charge generation on their surface. This observation was in agreement with other findings [14,23–25] including our previous work [24].

An important observation was made for all conditions tested that the measured *Q/m* by the cyclone-type Faraday cage was found to be significantly larger (e.g., approximately 140 – 150% larger for m_L = 1 g) than that measured by the through-type Faraday cage. This was suspected to be due to the backpressure created by the filter bag preventing some of the particles from exiting the conveying line. This is specifically clear in the first injection of all the cases tested where the recovered mass in presence of filter bag was less than that when the cyclone was used. Although such conclusion cannot be made for the subsequent injections since the recovered masses were almost equal, it is anticipated that a negligible amount of dust like particles which also possess a notable amount of charge (as proven in our previous work [24]) still remained inside the conveying line when the filter bag was used. This in turn results in a lower *Q* read by the electrometers.

Finally, **Figure 4-7** compares *Q* signals measured by the two Faraday cages (E1) and from the conveying line (E2), at 25 m/s conveying gas velocity for the 1 g solids mass loading. A good

agreement between the measured absolute charge magnitude was obtained under all tested operating conditions. Such finding indicates that the charge conservation holds in this system and the charge measurement directly conducted from the conveying line could reliably be used as an online measurement technique.

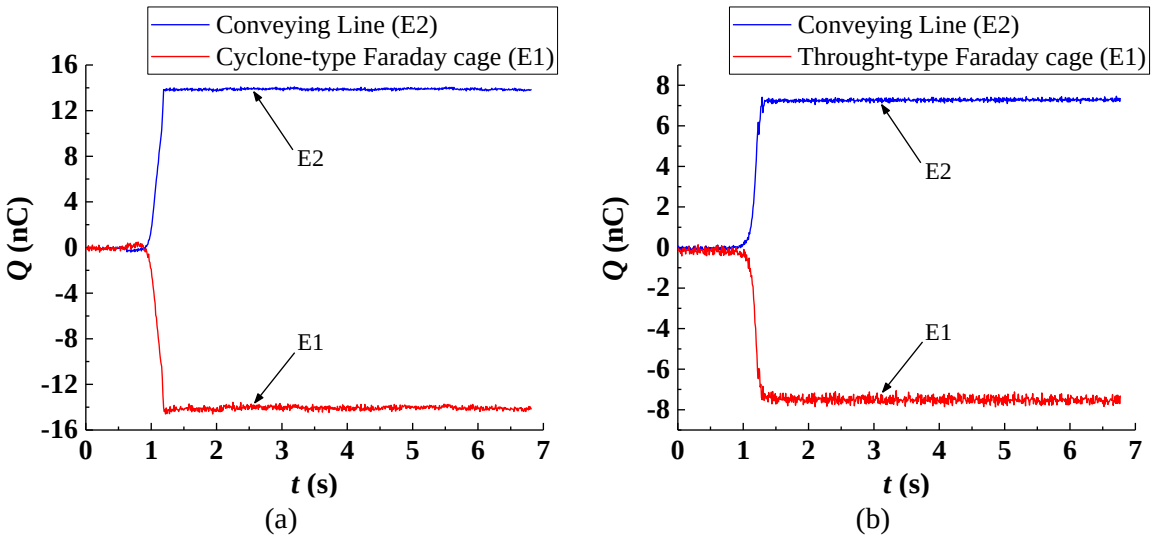

Figure 4-7 Comparison of charge signals recorded by E1 and E2 from injecting 1 g of 5-µm PP particles at U_g = 25 m/s. (a) Cyclone-type Faraday cage; (b) Through-type Faraday cage.

4-3-2 1500-µm PP Particles

Figure 4-8 presents snapshots of the 1500-µm particles flow pattern captured by the high-speed camera. Similar to the 5-µm particles, for all the tested conditions, particles were observed to move in a spiral motion. Analysis of the video images however showed that unlike the 5-µm particles that were mostly sliding along the conveying tube wall, majority of the 1500-µm particles were rolling and/or bouncing along the wall. The dense zones, which were clearly observed for the 5-µm particles, were not as dense for the 1500-µm case. Same as for the small size particles, the particles residence time declined as the conveying gas velocity increased. As well, it was observed that increasing the solids mass loading while keeping the gas velocity constant, did not influence the particles' residence time. Comparing **Figure 4-4** and **Figure 4-8** also reveals that under the same experimental condition (i.e., same m_L and U_g), it took longer for larger particles to transport alongside the tube. This could be attributed to the greater mass of the larger particles which leads the gravitational force to counteracts the drag force.

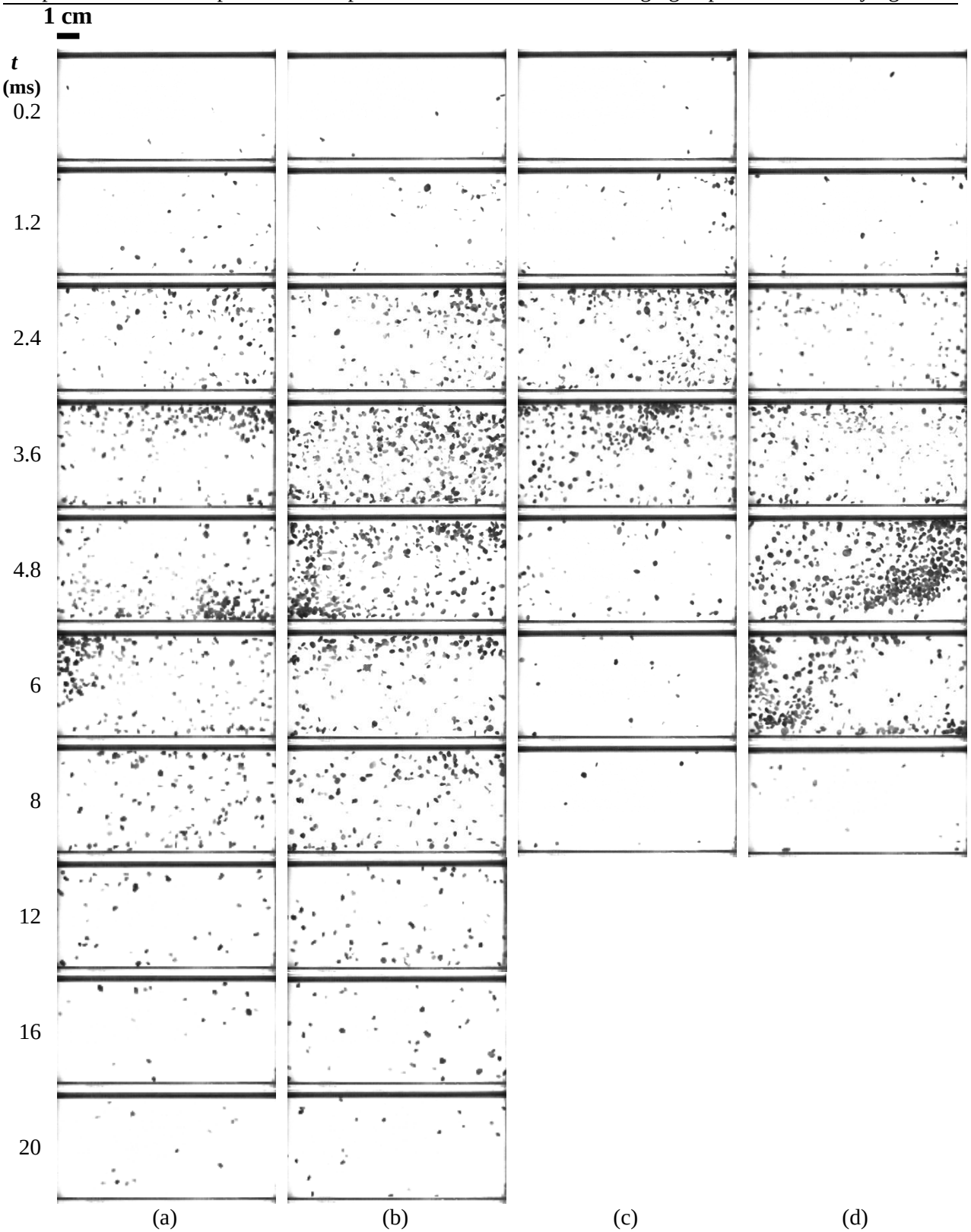

Figure 4-8 Snapshots of the 1500-μm PP particles flow pattern captured by the high speed camera at location A for two solids mass loadings and conveying gas velocities. Images captured for a 0.08 m in length and 0.035 m in inner diameter of the Plexiglass tube. (a) m_L = 1 g, U_g = 9 m/s; (b) m_L = 2 g, U_g = 9 m/s; (c) m_L = 1g, U_g = 25 m/s; and (d) m_L = 2 g, U_g = 25 m/s. The corresponding videos are provided in the supplementary information (Videos 5 – 8).

Due to the large size of these particles, no fouling was observed inside the conveying line and almost 100 wt.% of the initial injected particles mass was recovered at the first injection. As can be seen in **Figure 4-9**, direct relationship was observed between the particles' *Q/m* and the conveying gas velocity. Analysis of the videos clearly indicated that at higher gas velocities, particles were colliding the conveying line wall with a greater momentum which would have resulted in a greater degree of charging. As well, increasing the mass loading from 1 g to 2 g resulted in a decrease in the *Q/m* of the particles.

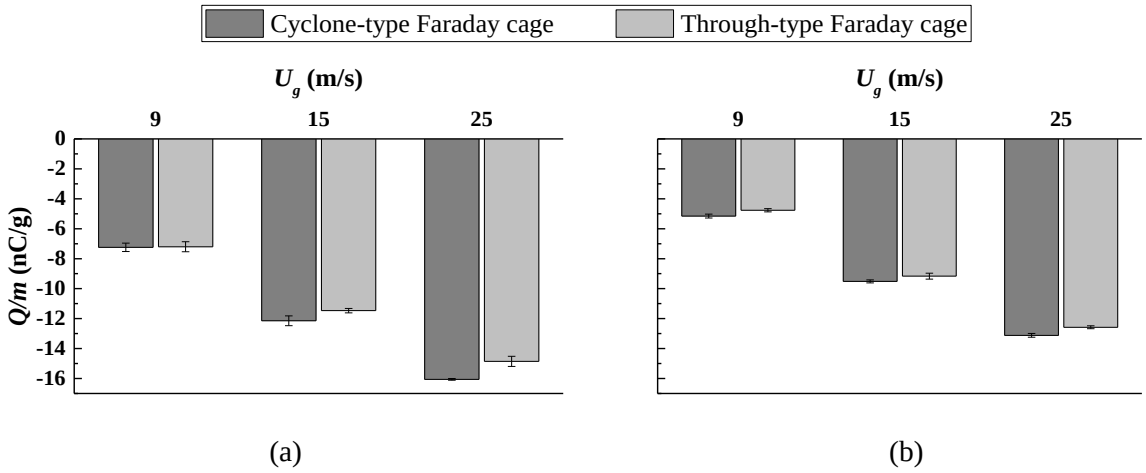

(a) (b)

Figure 4-9 Effects of U_g on conveyed 1500-µm PP particles *Q/m*. (a) m_L = 1 g; (b) m_L = 2 g.

Comparing the results obtained by using the cyclone-type Faraday cage and the through-type showed that both methods resulted in an approximately equal magnitudes of the *Q/m*. This implies that the backpressure created by the filter bag that was a suspected reason for the differences found for the 5-µm particles, did not affect the charge measurements significantly when 1500-µm particles were used.

4-4 Conclusion

The electrostatic charging behaviour of polypropylene particles of two different sizes were investigated through a pulse pneumatic conveying with a spiral air flow pattern. Analysis of the videos taken by a high-speed camera provided a clear picture of the particles' motion and collision patterns with the conveying line wall. Such an observation was found to be of great importance in better understanding the degree of electrostatic charging of particles at various operating conditions.

Analysis of the videos clearly showed that the 5-μm particles smeared over and slid against the conveying line wall while the 1500-μm particles mostly rolled and/or bounced off the walls. In addition, 5-μm particles tended to form clusters and concentrated zones, in turn providing less available effective contact area than that of the larger particles (that neither formed clusters nor concentrated zones). Hence, the *Q/m* was greater for the larger particles than that for the smaller particles. The dust like highly charged particles that remained inside the conveying line as fouling for the case of 5-μm particles might have also contributed in the observed smaller *Q/m* magnitude

For both particle sizes, image analysis confirmed that increasing the conveying gas velocity increased the contact force between the particles and the conveying line which in turn elevated the electrostatic charge gained by the particles. In addition, mass loading of the solids, in general, was found to be inversely related to the *Q/m* magnitude. Both particle sizes were observed to move in a more concentrated form and on top of each other when the mass loading increased, resulting in less available effective contact area.

In this work it can be concluded that the electrostatic charge measured by two types of Faraday cages (cyclone-type and through-type) could be significantly different depending on the particles size. The backpressure created in the filter bag of the through-type Faraday cage was suspected to contribute to such a difference. This suggests that attention must be paid when selecting a charge measurement device for systems dealing with fine particulates. The good agreement between the particles charge read directly from the conveying line and that of the Faraday cages implies that such technique can be reliably utilized as an online measurement method.

Acknowledgment

Financial support from the Faculty of Engineering at the University of Ottawa and The Natural Sciences and Engineering Research Council of Canada (NSERC) is acknowledged with gratitude. As well, authors would like to express their gratitude to the assistance received from Dr. Yoshiyuki Nakajima, and Mr. Shuji Fujiwara from the Riken Keiki Company in Tokyo, Japan. Authors would also like to thank Mr. Yuki Osada from Kasuga Denki Company for his help during the experimental work.

References

[1] K.S. Choi, M. Yamaguma, A. Ohsawa, Electrostatic charges during liquid leakage, J. Loss Prev. Process Ind. 23 (2010) 294–299.

[2] K.S. Choi, M. Yamaguma, A. Ohsawa, Experimental study on selectrostatic hazards in sprayed liquid, Jpn. J. Appl. Phys. 46 (2007) 7861–7864.

[3] M.R. Giles, Electrostatic hazards in liquids and relevance to process chemistry, Org. Process Res. Dev. 7 (2003) 1048–1050.

[4] M. Glor, Ignition source static electricity: Incident investigation, J. Electrostat. 67 (2009) 242–246.

[5] J. Wong, P. Chi, L. Kwok, H. Chan, Electrostatics in pharmaceutical solids, Chem. Eng. Sci. 125 (2015) 225–237.

[6] K. Choi, M. Omar, X. Bi, J.R. Grace, Experimental study on electrostatic charging of polymer powders in mixing processes, J. Loss Prev. Process Ind. 23 (2010) 594–600.

[7] G.E. Klinzing, F. Rizk, R. Marcus, L.S. Leung, Pneumatic Conveying of Solids: A theorical and practical approach, 2010.

[8] S. Dhodapkar, P. Solt, G. Klinzing, Understanding bends in pneumatic conveying systems, Chem. Eng. 116 (2009) 46–52.

[9] A.K. Olaleye, O. Shardt, G.M. Walker, H.E.A. Van den Akker, Pneumatic conveying of cohesive dairy powder: Experiments and CFD-DEM simulations, Powder Technol. 357 (2019) 193–213.

[10] G.E. Klinzing, A review of pneumatic conveying status, advances and projections, Powder Technol. 333 (2018) 78–90.

[11] P. Bunchatheeravate, J. Curtis, Y. Fujii, S. Matsusaka, Prediction of particle charging in a dilute pneumatic conveying system, AIChE J. 59 (2013) 2308–2316.

[12] B.N. Cole, M.R. Baum, F.R. Mobbs, An investigation of electrostatic charging fffects in high-speed gas-solids pipe flows, Proc. Inst. Mech. Eng. Conf. Proc. 184 (1969) 77–83.

[13] K. Saleh, A. Traore Ndama, P. Guigon, Relevant parameters involved in tribocharging of powders during dilute phase pneumatic transport, Chem. Eng. Res. Des. 89 (2011) 2582–2597.

[14] N. Schwindt, U. von Pidoll, D. Markus, U. Klausmeyer, M. V. Papalexandris, H. Grosshans, Measurement of electrostatic charging during pneumatic conveying of powders, J. Loss Prev. Process Ind. 49 (2017) 461–471.

[15] E.E. Smeltzer, M.L. Weaver, G.E. Klinzing, Individual electrostatic particle interaction in pneumatic transport, Powder Technol. 33 (1982) 31–42.

[16] M. Nifuku, H. Katoh, A study on the static electrification of powders during pneumatic transportation and the ignition of dust cloud, Powder Technol. 135–136 (2003) 234–242.

[17] S. Matsusaka, H. Umemoto, M. Nishitani, H. Masuda, Electrostatic charge distribution of particles in gas–solids pipe flow, J. Electrostat. 55 (2002) 81–96.

[18] A. Thomas, K. Saleh, P. Guigon, C. Czechowski, Characterisation of electrostatic properties of powder coatings in relation with their industrial application, Powder Technol. 190 (2009) 230–235.

[19] S. Matsusaka, H. Fukuda, Y. Sakura, H. Masuda, M. Ghadiri, Analysis of pulsating electric signals generated in gas–solids pipe flow, Chem. Eng. Sci. 63 (2008) 1353–1360.

[20] S. Matsusaka, M. Oki, H. Masuda, Control of electrostatic charge on particles by impact charging, Adv. Powder Technol. 18 (2007) 229–244.

[21] S. Matsusaka, M. Oki, H. Masuda, Bipolar charge distribution of a mixture of particles with different electrostatic characteristics in gas–solids pipe flow, Powder Technol. 135–136 (2003) 150–155.

[22] P. Boschung, M. Glor, Methods for investigating the electrostatic behaviour of powders, J. Electrostat. 8 (1980) 205–219.

[23] H. Grosshans, M. V. Papalexandris, Evaluation of the parameters influencing electrostatic charging of powder in a pipe flow, J. Loss Prev. Process Ind. 43 (2016) 83–91.

[24] M. Taghavivand, B.J. Cho, P. Mehrani, A. Sowinski, Electrostatic charging behaviour of a

silica powder during pulse pneumatic conveying, Powder Technol. 366 (2020) 119–129.

[25] S. Watano, S. Saito, T. Suzuki, Numerical simulation of electrostatic charge in powder pneumatic conveying process, Powder Technol. (2003).

[26] F. Chowdhury, A. Sowinski, M. Ray, A. Passalacqua, P. Mehrani, Charge generation and saturation on polymer particles due to single and repeated particle-metal contacts, J. Electrostat. 91 (2018) 9–15.

[27] M. Taghavivand, B. Elchamaa, A. Sowinski, P. Mehrani, Study of electrostatic charging of single particles during pneumatic conveying, Powder Technol. 355 (2019) 242–250.

[28] H. Masuda, T. Komatsu, K. Iinoya, The static electrification of particles in gas-solids pipe flow, AIChE J. 22 (1976) 558–564.

[29] A. Gajewski, Measuring the charging tendency of polysterene particles in pneumatic conveyance, J. Electrostat. 23 (1989) 55–66.

[30] J. Yao, C.-H. Wang, Granular size and shape effect on electrostatics in pneumatic conveying systems, Chem. Eng. Sci. 61 (2006) 3858–3874.

[31] K. Choi, H. Choi, T. Suzuki, Charging behavior of glass beads using a spiral air type tribocharging apparatus that utilizes a Faraday cup, J. Loss Prev. Process Ind. 65 (2020) 104124.

[32] H. Masuda, K. Iinoya, Electrification of particles by impact on inclined metal plates, AIChE J. 24 (1978) 950–956.

[33] S. Alois, J. Merrison, J.J. Iversen, J. Sesterhenn, Quantifying the contact electrification of aerosolized insulating particles, Powder Technol. 332 (2018) 106–113.

[34] C.K. Diu, C.P. Yu, Deposition from charged aerosol flows through a two-dimensional bend, J. Aerosol Sci. 11 (1980) 391–395.

[35] J. Yao, Y. Zhang, C.-H. Wang, S. Matsusaka, H. Masuda, Electrostatics of the Granular Flow in a Pneumatic Conveying System, Ind. Eng. Chem. Res. 43 (2004) 7181–7199.

Chapter 5 - Triboelectric Effects of a Pneumatically Injected Silica Catalyst Support on the Polyethylene Fluidized Bed Wall Fouling

Milad Taghavivand, Poupak Mehrani, Andrew Sowinski*

Department of Chemical and Biological Engineering, University of Ottawa, 161 Louis Pasteur, Ottawa, ON, K1N 6N5, Canada

* Corresponding author. E-mail: sowinski@uottawa.ca; Tel: 1-613-562-5800 ext. 6288

The current chapter is a manuscript submitted to the journal of Powder Technology "Publication under review, Manuscript ID: POWTEC-D-20-03328"

Abstract

In commercial ethylene gas-phase polymerization, small loads of catalyst particles periodically fed into the reactor. This necessitates studying their contribution on the fluidized bed reactor electrification and sheeting. Prior to testing catalysts utilized in commercial processes, this work focused to investigate the role of a typical amorphous silica catalyst support used in ethylene polymerization on the polyethylene fluidized bed electrification and wall fouling. A 5 m in length and 0.00475 m in inner diameter stainless-steel pneumatic conveying line with was used to convey 0.1 and 1 g of silica at various fluidization times of 0, 15 and 30 minutes into a 1-kg bed of polyethylene fluidized in a 0.1 m diameter stainless-steel atmospheric column. Overall, a reduction was observed in the wall fouling. This was attributed to the silica's negative charge upon entering the bed, silica/polyethylene particle number ratio, and silica's capability to induce negative charge within the bed.

Keywords: Ethylene gas-phase polymerization, Fluidized bed, Sheeting, Electrostatics, Silica catalyst support

5-1 Introduction

Electrostatic charge generation due to continuous interparticle and particle-vessel wall contacts, which occurs during particle handling, transport (e.g., pneumatic conveying) and processing (e.g., gas-solid fluidized beds), is a phenomenon that can result in severe problems such as particle-wall adhesion, electrostatic discharge, as well as particle segregation and agglomeration. Gas-solid polyethylene (PE) fluidized bed reactors are examples where the highly electrostatically charged PE resin and catalyst particles adhere to the reactor wall, resulting in poor removal of the heat of the exothermic polymerization reaction in the wall regions. This in turn results in melting of the fouled polyethylene particles and forming sheets that can grow and break off of the reactor wall, causing reactor shut down periods and ultimately a significant economic loss [1].

The majority of the works studying electrostatic charge generation in relation to PE fluidized bed reactors, have only considered PE resin charging [2]. Whereas, in the commercial PE reactors, catalyst particles as well as other solid additives (e.g., continuity additives) and reactants (e.g., co-catalyst) also exist which necessitates studying their contribution on the degree of fluidized bed electrification. In commercial PE processes, catalyst particles are periodically injected into the reactor in either slurry or dry solid form. However, problems such as uneven distribution of catalyst particles inside the reactor after the injection, the need for an additional slurry making equipment and procedure, as well as possible impacts on catalyst activity are associated with slurry feeding [3]. In the dry feeding systems, catalyst particles are pneumatically conveyed into the reactor through narrow and long tubes (typically stainless steel tubes with a 4.75×10^{-3} m in inner diameter). It is important to realize that in general, pneumatic conveying systems are known to generate the largest amount of electrostatic charge among all gas-solid processes [4]. Thus, in relation to the polyethylene process, catalyst particles are anticipated to be electrostatically charged upon entering the reactor. Reports have emphasized on the influence of the electrostatic charge introduced into the reactor by flow of the charged catalyst on the sheeting growth [5,6]. In an earlier work [7], we had concluded that the attractive image forces formed due to the induction charging between the fluidized bed wall and pneumatically injected charged catalyst particles, attractive electrostatic forces between the fouled particles and newly injected catalyst, as well as repulsive electrostatic forces between the catalyst particles and PE resins of a same polarity are

suspected to contribute in the formation/promotion of reactor wall fouling. However, no experimental results are available to evaluate and to either prove or disprove this hypothesis.

Due to the fact that a major portion of the catalyst particles is occupied by their support [3,8,9], it is probable that the catalyst support shows a dominant effect on the catalyst charging tendency in the PE process. One of the common supports used for chromium-based (e.g., Phillips type), Ziegler-Natta and Metallocene catalysts in ethylene polymerization is dehydrated amorphous silica which in our earlier works was shown to become significantly electrostatically charged during pneumatic conveying [10]. As such, the aim of this work was to study the effect of pneumatically injecting charged silica powder at different stages of fluidization (prior to and after fluidization onset) and at two mass loadings (0.1 and 1 g) on the degree of a PE fluidized bed wall fouling.

5-2 Materials and Methods

Fig. 1 shows the schematic diagram of the atmospheric gas-solid fluidization system along with the horizontal solids conveying line used in this work. Details of the fluidization column and its compartments can be found elsewhere [11,12]. The fluidization column consisted of a 0.1 m in diameter and 1.3 m in height stainless steel column connected to two Faraday cages, one at the top and one at the bottom. Both Faraday cages were connected to Keithley 6514 digital electrometers and were electrically isolated from the grounded fluidization column. The top Faraday cage was a through-type and housed a filter bag to contain the entrained particles (referred to as “Fines”) for their mass, cumulative net charge, and size distribution measurements. A modified knife gate valve was used as a removable distributor plate (perforated type). As a result, the distributer plate could be opened and closed easily, allowing the collection of the bulk particles (referred to as “Dropped”) without any particle handling, in the bottom Faraday cage at the end of the fluidization run for their mass, net charge, and size distribution measurement. The fluidizing gas was dry air with approximately 0% relative humidity at 22 ± 1˚C. The fluidization was carried out for 60 minutes at a fluidizing gas velocity set at 1.5 times minimum fluidization velocity (U_{mf}) to represent the bubbling flow regime.

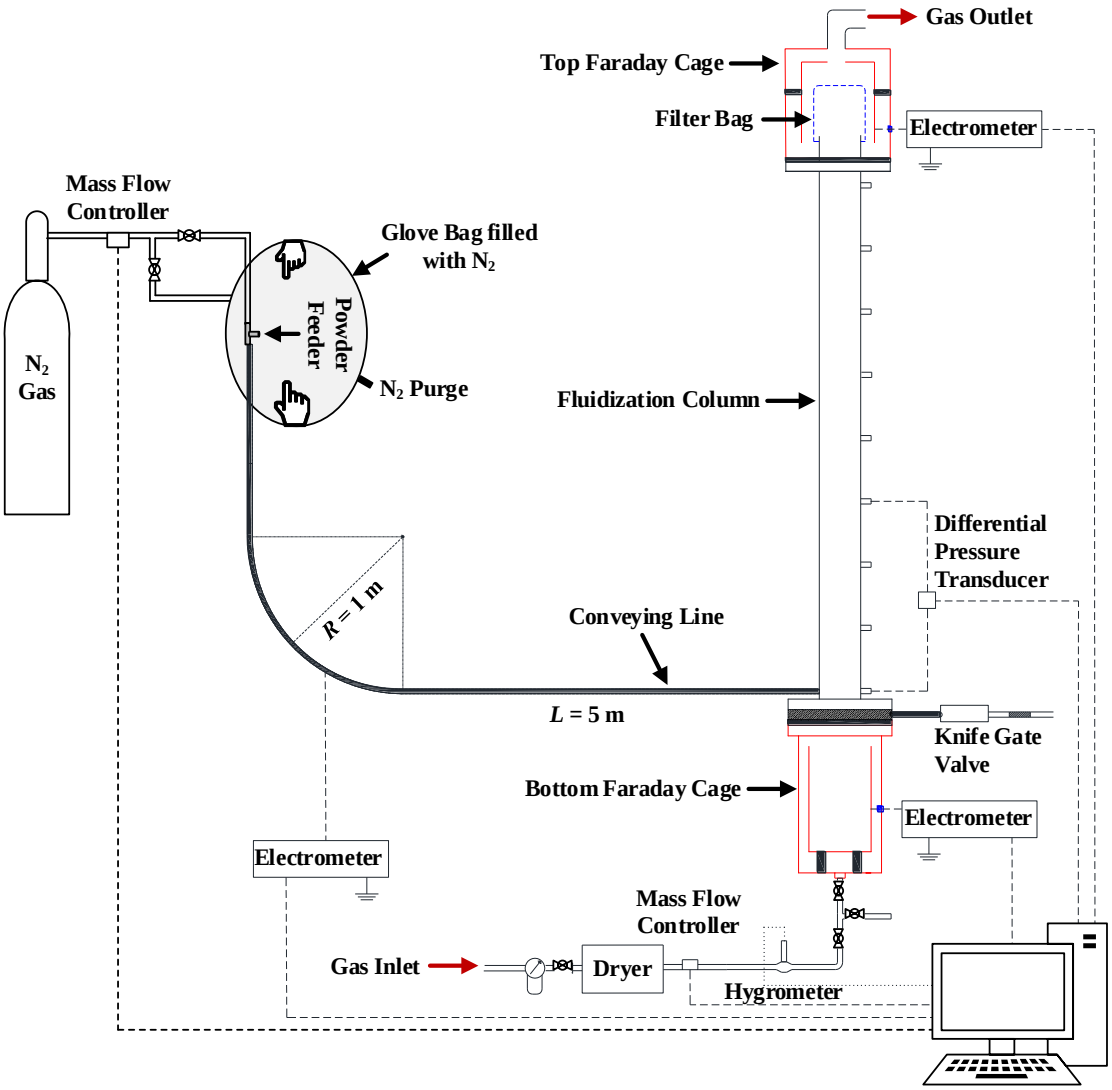

Figure 5-1 Schematic diagram of the fluidization system along with the horizontal conveying line directly connected to the fluidized bed.

A stainless steel tube with an inner diameter of 4.75 x 10^{-3} m and a length of 5 m with a smooth 1 m in radius bend was used as the pneumatic conveying line to replicate a typical commercial catalyst conveying line used in PE processes. The conveying line was connected to the fluidization column at approximately 0.025 m above the distributor plate. As shown in **Figure 5-1**, the conveying line was directly connected to a Keithley 6514 digital electrometer to measure the electric current signal generated due to the powder flow. The details of such measurement can be found in our earlier work [10]. To minimize the effect of the atmospheric moisture on the conveyed powder, the powder feeder was placed in a glove bag filled up with dry nitrogen. The conveying

gas was dry nitrogen with a velocity set at 15 m/s which is a typical velocity used for catalyst injection in PE production.

The fluidizing particles were LLDPE resin directly received from a commercial plant having a wide size distribution (35 to 1300 μm) with a volume-based mean diameter of 590 μm, a particle density of 915 kg/m^3 and a bulk density of 424 kg/m^3. The conveyed powder was dehydrated amorphous silica which was the support of the catalyst used for producing the same PE resin and had a volume-based mean diameter of 43 μm, a particle density of 2200 kg/m^3 and an average bulk density of 400 kg/m^3. A Malvern Mastersizer 2000 was used to measure the particle size distribution. The volume resistivity of both the PE resin and the silica powder were measured to be greater than 10^{13} Ω.m indicating the electrically insulative nature of both powders. The measurement details for volume resistivity can be found elsewhere [13]. Silica powder was dehydrated in-house at 600˚C for 90 minutes. At the time of experiments, no measurement was performed to analyze the moisture content (amount of adsorbed water and silanol groups) on the dehydrated silica powder; however, FTIR analysis was performed later and confirmed the lower concentration of the adsorbed water and hydroxyl groups on the surface of the dehydrated silica powder compared to the non-dehydrated sample. The mass loading of the silica powder per injection was determined based on the catalyst productivity of 10,000 g-PE/g-catalyst. Since the mass of the fluidizing polyethylene in this work was set at 1 kg, the proportional mass of the silica powder was calculated to be 0.1 g. However, higher amount of silica powder (i.e., 1 g) was also examined to better analyze its contribution within the PE fluidized bed.

5-2-1 Experiment Design

To gain a comprehensive understanding of the influence of injection of silica on the extent of wall fouling inside the fluidized bed, a number of fluidization experiments were designed with a summary presented in **Table 5-1**.

First it was essential to obtain reference points of the extent of wall fouling of PE resin fluidized alone (referred to as “PE”). As such, in category A, fluidization runs of t_F = 15, 30 and 60 minutes

of PE resin were performed. These runs also provided important information on the fluidization time needed for wall fouling to grow and reach a steady level.

Category B experiments included single injection of silica with two mass loadings (m_L) of 0.1 or 1 g. The single injections were conducted at various fluidization times of t_{inj} = 0 min (i.e., prior to start of fluidization), as well as t_{inj} = 15 and 30 min into the fluidization period. Comparing the injection at the fluidization onset, where no fouling has formed on the wall, and injections at t_{inj} = 15 and 30 min, where wall fouling has already formed, provides valuable information on the effect of silica in promoting/demoting the wall fouling.

Category C experiments included injection of a total of 1 g of silica in 10 consecutive injections of 0.1 g per injection at t_{inj} = 15 min into the fluidization period. As concluded in our previous works, increasing the solids mass loading in a pulse pneumatic conveying, results in a reduction in the *Q/m* of conveyed particles [10,14]. Preliminary testing in this work also confirmed that silica powder acquired approximately 6 times lower *Q/m* for the 1 g mass loading compared to that of the 0.1 g mass loading. Such a difference in silica's *Q/m* as it enters the fluidized bed could be of importance since it could significantly influence the degree of fluidized bed electrification.

Table 5-1 Summary of the experimental design.

Category	**Experiment type**	**Silica mass loading (m_L) per injection (g)**	**Time of injection (t_{inj}) into the fluid bed (min)**	**Number of injections outside the fluidized bed**	**Fluidization period (t_F) (min)**
A	PE	–	–	–	15, 30, 60
B	PE – Silica	0.1, 1.0	0, 15, 30	• **m_L = 0.1 g** 10 injections followed by the 11th injection into the bed.	60
C	PE – Silica	0.1 (10 x 0.1 g)	15	• **m_L = 1.0 g** 5 injections followed by the 6th injection into the bed.	

5-2-2 Procedure to Pneumatically Inject the Silica Powder into the Fluidized Bed

In injecting the silica powder into the fluidized bed, it was essential to ensure a predetermined amount of the silica powder entered the bed. As well, it was of great importance to know how much charge the silica powder possessed upon entering the bed after being pneumatically

conveyed. The charge of the silica was found by converting the electrical current signal measured from the conveying tube. It had already become evident from our previous works that the silica had a tendency to foul inside the conveying tube [10]. However, multiple consecutive injections had shown a reduction on the extent of the powder loss due to fouling. Thus, in this work to ensure that a certain mass of the silica entered the fluidized bed, the experiments were split into two segments.

5-2-2-1 Pneumatic Conveying

Prior to connecting the conveying line to the fluidization column, consecutive injections of a predetermined mass of silica was carried out into a cyclone-type Faraday cage as shown in **Figure 5-2** until the mass of fouling in the conveying line reached saturation.

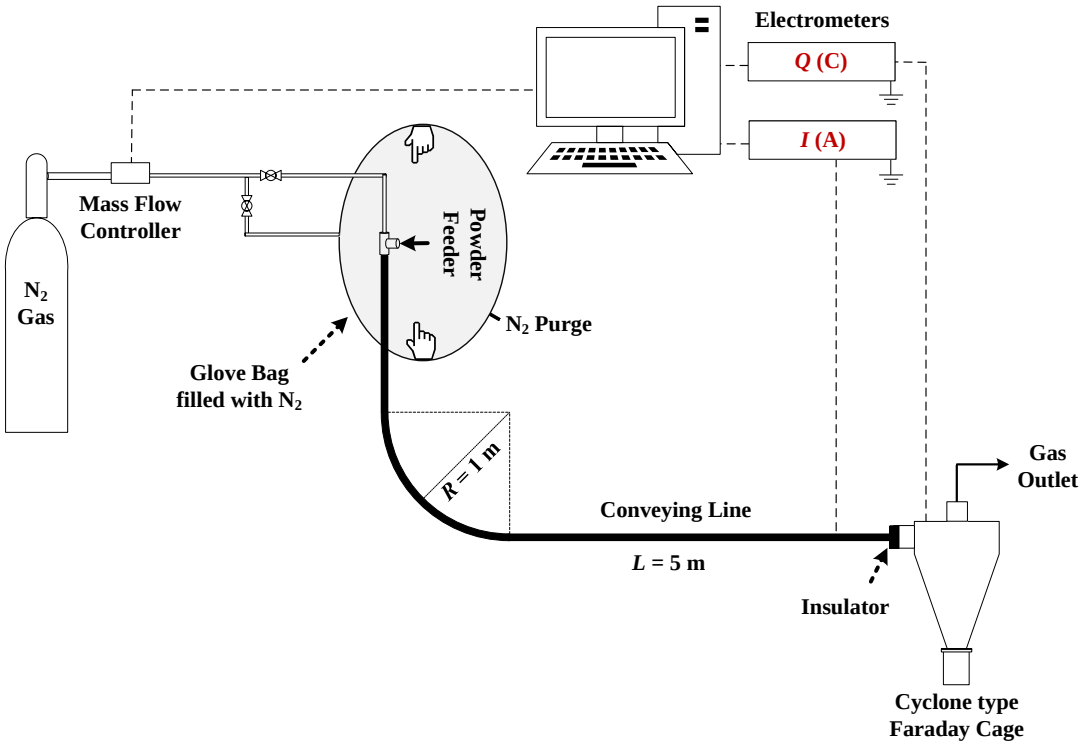

Figure 5-2 Schematic diagram of horizontal pneumatic conveying apparatus connected to a cyclone-type Faraday cage.

The number of the consecutive injections, n, varied depending on the silica powder m_L per each injection (details can be found in our previous work [10]). For instance, for a silica mass loading of 0.1 g, ten injections were required to achieve approximately 98-100 wt.% recovery of the

injected mass; whereas, five injections were found to be sufficient to ensure same percentage of the mass recovery for 1 g silica mass loading.

5-2-2-2 Fluidization

Once the conveying line fouling reached the saturation level at the n^{th} injection outside the fluidized bed (i.e., ten and five injections for m_L = 0.1 and 1 g, respectively), the conveying line was disconnected from the cyclone Faraday cage and connected to the fluidized bed to carry out the second segment of the experiment which was to perform the $(n + 1)^{th}$ injection into the fluidized bed followed by the fluidization of the mixture of PE and silica (referred to as "PE – silica"). At first, the conveying line was placed all the way inside the fluidization column so that the conveying line exit was blocked by the column wall. This was done to prevent the conveying line blockage while the PE resin was being loaded into the column. Once this step completed, the conveying line was retracted slowly to the centre of the column.

If the injection time was at t_{inj} = 0 min, the fluidizing gas velocity was increased incrementally to $1.1U_{mf}$ at which the silica was injected using nitrogen at 15 m/s gas velocity. Then the conveying line was completely retracted and made flush to the column wall, after which the fluidizing gas velocity was incrementally increased to $1.5U_{mf}$ and the fluidization was proceeded for 60 minutes. In cases where the injection time was at t_{inj} = 15 or 30 min, the conveying line was made flush to the column wall and the fluidizing gas was gradually increased to $1.5U_{mf}$ and the fluidization was carried out for 15 or 30 minutes. During this period, the conveying gas at 15 m/s was passed through the conveying line to prevent any tube blockage. It needs to be mentioned that the conveying gas flow rate was 15% of the fluidizing gas flow rate and therefore had minimal effect on the fluidization of PE resin. After 15 or 30 minutes of fluidization, the conveying line was gradually pushed towards the center of the bed and both the fluidizing and conveying gases were stopped. The silica powder was then loaded into the conveying feeder and the injection was performed similar to that of the t_{inj} = 0 min. The conveying gas was then stopped, the conveying line was retracted and made flush to the column wall and the fluidization was proceeded for 45 or 30 minutes.

For all the tested conditions, upon the completion of the fluidization experiments and after collecting the "Fines" and "Dropped" particles, a layer of fouling was observed extending to top of the column (referred to as "Wall Fouling"). As shown in **Figure 5-3**, the "Wall Fouling"

consisted of two sections including a relatively thick layer formed from the distributor plate to the expanded bed height (referred to as "Wall"), and a thinner layer formed above the expanded bed height (referred to as "Freeboard"). It was found that the "Wall" particles had different polarities depending on their location and as a result, three sublayers were identified for this layer. The particles covering the wall up to the static bed height were referred to as "Wall – Bottom" while those covering the wall from the static bed height up to the expanded bed height were referred to as "Wall – Top". The third sublayer consisted of particles in the very first layer of coating on the wall (referred to as "Wall – Inner"). Particles within each layer were removed from the wall and collected in the bottom Faraday cage by using compressed building air passed through a narrow tube inserted from the top of the column. The mass, charge, and size distribution of particles collected from all regions of the beds were measured.

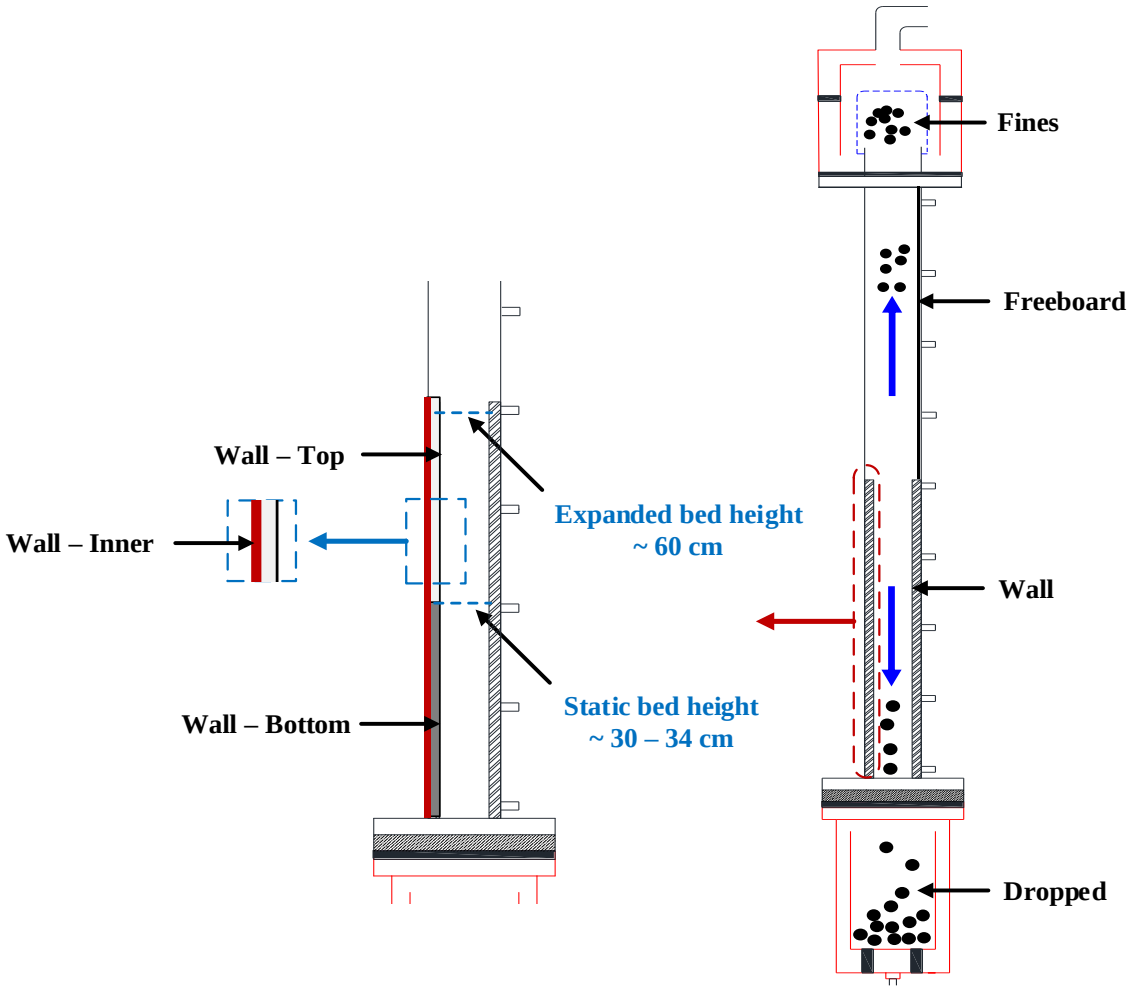

Figure 5-3 Different regions of the fluidization column with respect to particles location.

All experiments were repeated at least two times to ensure the reproducibility of results. In each trial, the initial charge of the polyethylene particles as well as the silica particles were measured in a bench-scale Faraday cage.

5-3 Results and Discussion

Prior to the fluidization of particles used in this work, namely polyethylene resin and dehydrated silica powder, their initial specific charge (*Q/m*) were measured to be -0.01 ± 0.03 and -16.6 ± 0.2 μC/kg, respectively.

To investigate the influence of silica catalyst support on the extent of wall fouling formation during its fluidization with the PE resin, it was essential to first establish a reference case by fluidizing the PE resin alone at various fluidization periods. **Figure 5-4** enables a qualitative comparison of the extent wall fouling by providing images of the inner column wall taken from the bottom of the fluidization column upon completion of the fluidization period and after collecting the "Dropped" particles. The quantitative analysis of the results obtained for the same runs are presented in **Figure 5-5** and **Figure *5-6***. Based on the images in **Figure 5-4** and the total mass of particles that fouled on the wall and shown in **Figure 5-5**, it is evident that 15 minutes of fluidization was sufficient to form a substantial layer of wall fouling. Overall results in **Figure 5-5** and **Figure 5-6** show that all of the measured parameters did not differ significantly after 15 minutes of fluidization with the exception of the mass of the "Fines" which, as expected, kept increasing as the fluidization time increased up to 30 minutes, after which no significant change was observed.

(a) (b) (c)

Figure 5-4 Images of wall fouling for the "PE" fluidization runs taken from the bottom of the fluidized bed. (a) t_F = 15 min; (b) t_F =30 min; (c) t_F = 60 min. The red arrows represent the 0.3 m static bed height.

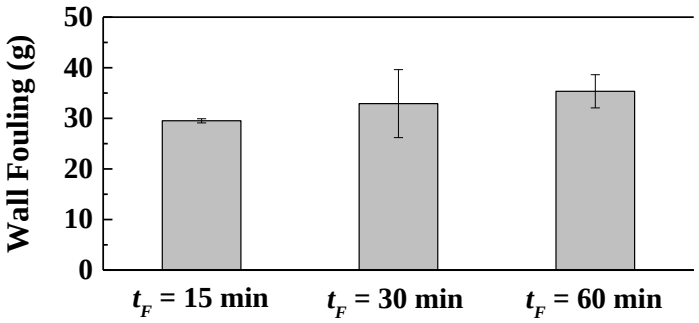

Figure 5-5 Effect of various fluidization periods on the wall fouling magnitude for the "PE" fluidization runs.

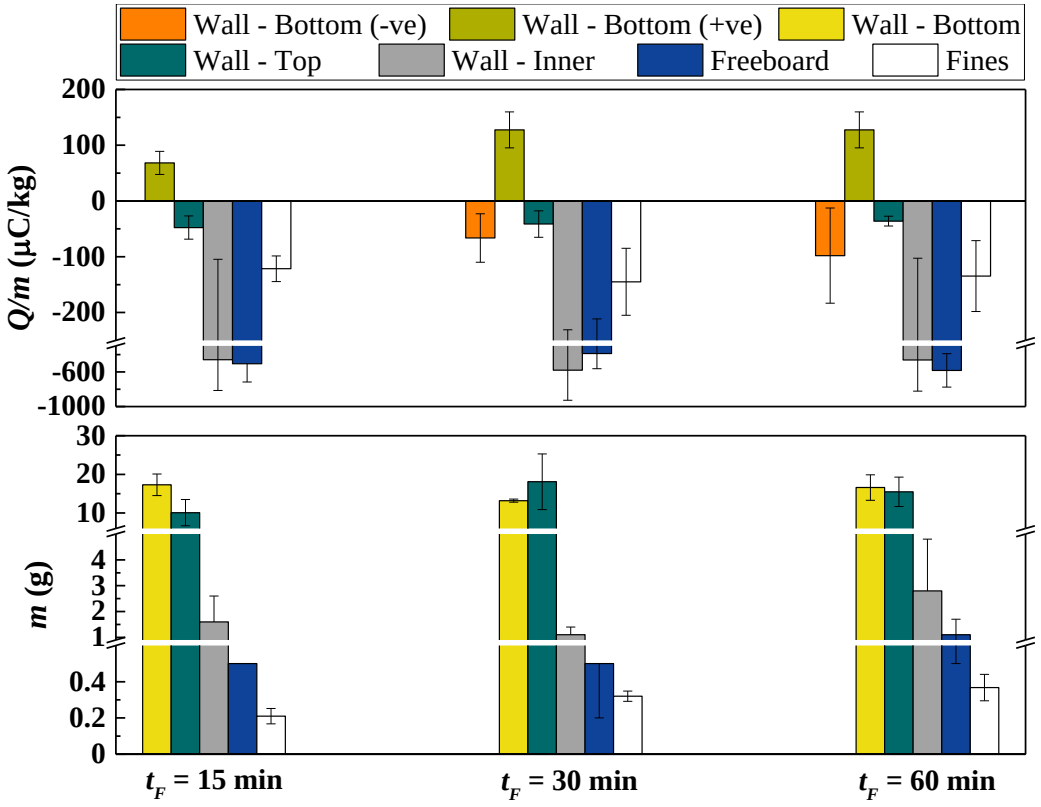

Figure 5-6 Effect of various fluidization times on the *Q/m* and mass of the "Wall – Bottom", "Wall – Top", "Wall – Inner", "Freeboard", and "Fines".

Comparison of the *Q/m* results from all regions of the bed clearly implied the presence of bipolar charging with larger particles in the "Dropped" and "Wall – Bottom" carrying a net positive charge while those in the "Wall – inner", "Wall – Top", "Freeboard", and "Fines" that were smaller, carrying a net negative charge. By comparing the effective work function of the PE with that of the stainless steel, it is clear that PE must become negatively charged [7] which describes the negative charge polarity gained by particles within the "Wall – Inner" layer that were in close

contact with the column wall. On the other hand, particle-particle contacts within the bulk of the bed consisting of various particles sizes could result in small and large particles becoming negatively and positively charged, respectively. Volume-based mean diameter of particles collected from various regions of the bed are presented in **Figure 5-7** and shows that the d_{50} decreases from the bottom to the top of the fluidization column. The fluidizing gas velocity in this work was 0.22 m/s which was sufficient to entrain particles smaller than approximately 100 µm from the bed which supports the results of "Fines" in **Figure 5-7**. This then explains the net negative charge found for the "Wall – Top", "Freeboard" and "Fines" regions of the bed comparing to that of the net positive that was found in "Wall – Bottom" and "Dropped" which would have been the result of particles segregation within the fluidized bed. Results in **Figure 5-6** show that the "Fines" region mostly contained particles with a lower *Q/m* compared to the particles in the "Freeboard" and this is due to the fact that particles with a higher charge were attracted by the column in the freeboard area preventing them from being entrained.

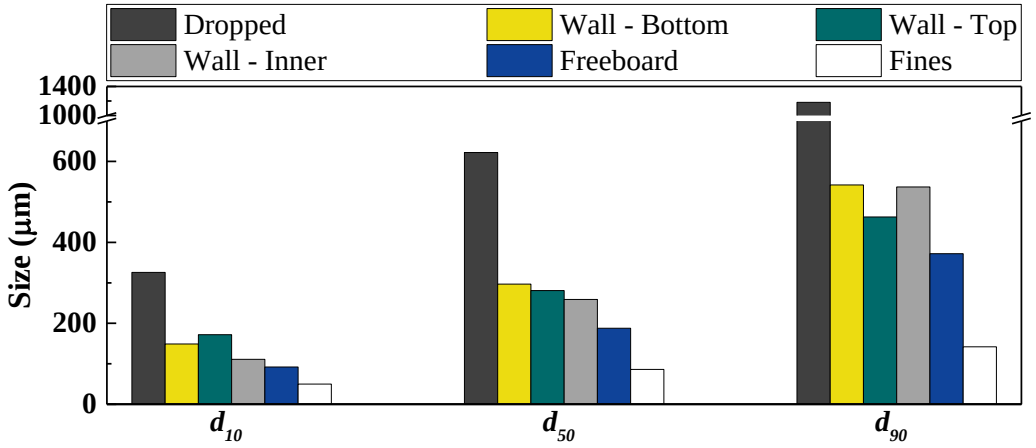

Figure 5-7 Particle size in different regions of the bed for "PE" fluidization runs.

Existence of positively charged particles in the "Wall – Bottom" layer as seen in **Figure *5-6*** is related to the attractive electrostatic forces between the negatively charged inner layer and positively charged bulk particles [7]. As well, the repulsive electrostatic forces between the positively charged bulk particles promotes the migration of positively charged PE particles towards the wall. Results also confirmed that the "Wall – Bottom" and the "Wall – Top" layers constitute the majority of the total wall fouling. As such, these two layers are considered to be of great importance with respect to the total wall fouling and require in depth analysis such as size distribution, mass, and charge measurements. By comparing the particle size distribution of these

two layers as presented in **Figure 5-7** to their absolute charge magnitudes shown in **Figure 5-6**, a qualitative relationship can be drawn. While "Wall – Bottom" layer possesses a higher absolute charge magnitude, it had wider particles size distribution. This indicates that up to the expanded bed height, where particles are moving vigorously, particles attached to the wall must have a large *Q/m* to overcome the drag and gravity forces even for the larger sized particles. Such a large *Q/m* which is higher for the "Wall – Bottom", results in attracting particles of wider sizes towards the wall. Same explanation applies to the "Wall – Inner" layer where particles of a high *Q/m* and a wide size distribution were found.

5-3-1 Category B: "PE – Silica" Single Injection

As mentioned earlier, it was essential to first know the electrostatic charge of the silica powder upon entering the fluidized bed through the conveying line. Measurement of current signal from the conveying line resulted in net specific charges of -6781 ± 519 and -1130 ± 232 μC/kg for mass loading of 0.1 and 1 g, respectively.

To determine as whether the silica particles had been well distributed within the different regions of the bed upon their injection into the column, SEM images were taken from the collected samples as shown in **Figure 5-8**. The particles in white color are silica with those idenfied in red in the "Wall – Top" and "Wall – Bottom" at m_L = 0.1 g and injection time of t_{inj} = 0 min. SEM images confirmed that the silica particles had spread to various regions of the bed as they were found entrapped in the defects of the PE resin in the "Dropped" region, adhered on the PE resin surface specifically within the "Dropped", "Wall – Top" and "Wall – Bottom" regions, and appeared as individual particles mostly in "Fines".

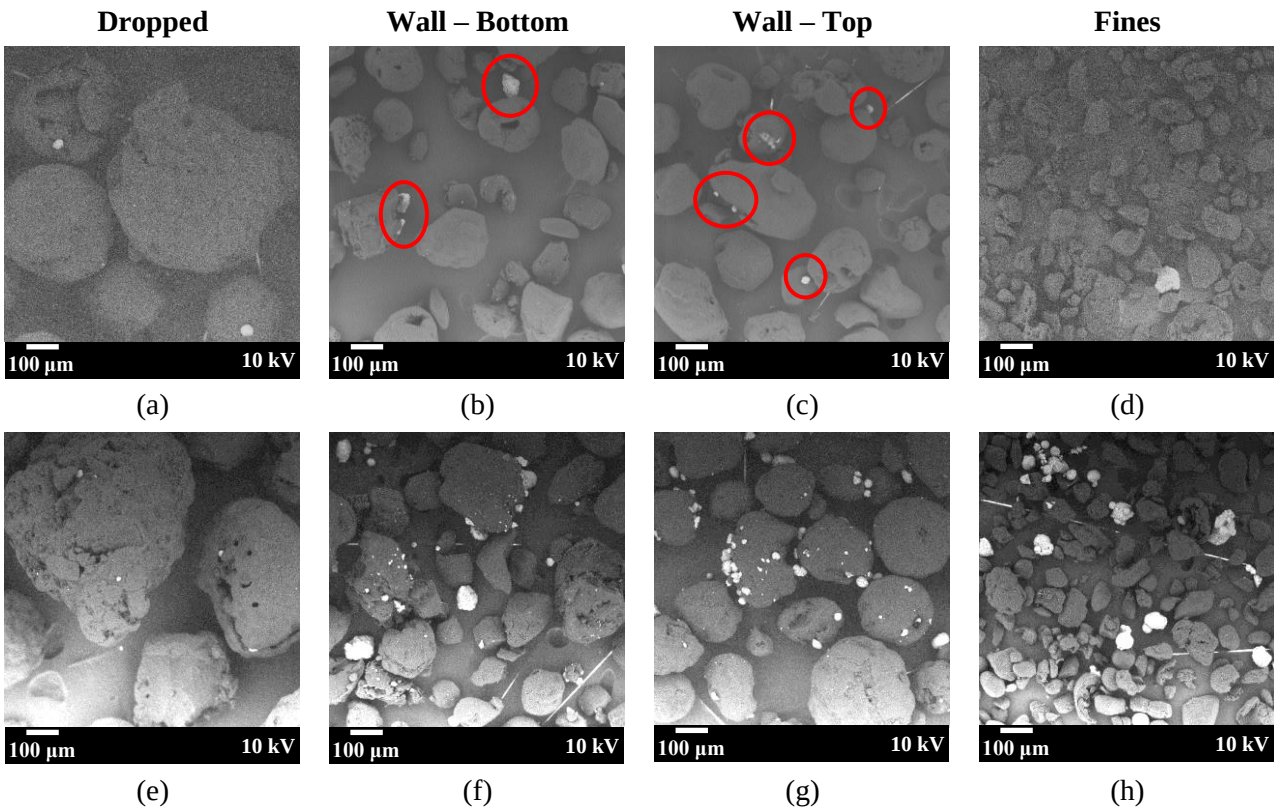

Figure 5-8 SEM images taken from different bed regions showcasing the silica powder distribution. The white color particles are silica. (a) – (d) m_L = 0.1 g, t_{inj} = 0 min; (e) – (h) m_L =1 g, t_{inj} = 0 min.

As for the degree of wall fouling, a qualitative comparison was first made with images taken from the inner column wall upon removal of the "Dropped" particles (**Figure 5-9)**. A reduction in the wall fouling can be observed in the images for the higher silica mas loading (m_L = 1 g).

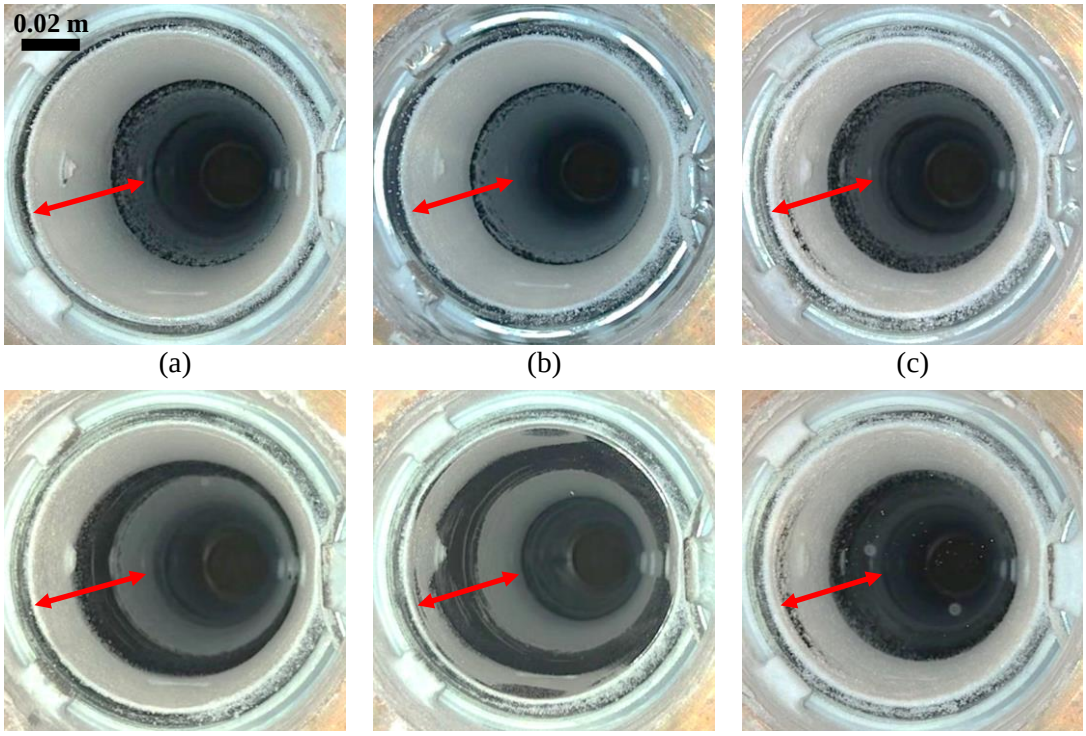

Figure 5-9 Images of wall fouling for the Category B "PE – Silica" runs taken from the bottom of the fluidized bed. (a) m_L = 0.1 g, t_{inj} = 0 min; (b) m_L = 0.1 g, t_{inj} = 15 min; (c) m_L = 0.1 g, t_{inj} = 30 min; (d) m_L = 1 g, t_{inj} = 0 min; (e) m_L = 1 g, t_{inj} = 15 min; (f) m_L = 1 g, t_{inj} = 30 min. The red arrows represent the 0.3 m static bed height.

5-3-1-1 Effect of Silica Powder and Its Mass Loading

The total wall fouling results are shown in **Fig. 10a** and it can be seen that the presence of silica at the mass loading of 0.1 g did not have a significant effect whereas the wall fouling declined for the 1 g mass loading. An important observation was made by comparing **Figure 5-10a** and **Figure 5-10b** where a decline in the wall fouling magnitude corresponded to a decline in "Dropped" net *Q/m*, and vise versa. Such a relationship implies that the decline in the net *Q/m* of the bulk of the bed results in a reduction in the repulsive electrostatic forces between the positively charged particles in the bulk. Similarly, a reduction would be expected in the attractive electrostatic forces between the negatively charged particles on the wall layers and the positively charged bulk particles. In addition, the image force between the column wall and the particles in the bulk must be declined. All these cases will demote the extent of wall fouling.

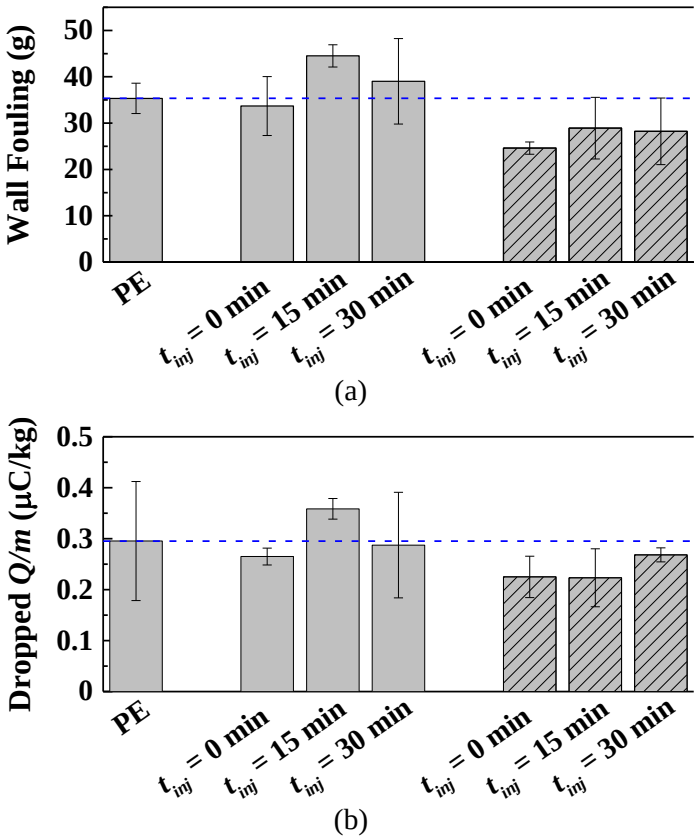

Figure 5-10 Effect of injection of silica powder at two mass loadings of m_L = 0.1 and 1 g (shown with striped pattern) at various times (t_{inj} = 0, 15 and 30 min) on (a) wall fouling magnitude and (b) *Q/m* of the "Dropped". The blue dashed lines correspond to the average t_F = 60 min "PE" run.

One reason behind the drop in the bulk particles net *Q/m* would be that the addition of the negatively charged silica powder results in a reduction in the net positivity of the "Dropped" particles. With respect to the generated charge polarity within the bed after injecting the silica and to better explain the charge polarity that the silica develops in contact with the PE resin, a bench-scale experiment was designed where 0.1 g of the silica powder was shaken in a cylindrical cup made of LDPE with 0.05 m in height and 0.025 m in inner diameter. The cup was shaken using a shaker (Lab-Line Model 4628) at a speed of 300 rpm for a 2-minute period, which was found to be sufficient for the powder to reach the equilibrium charge. Results showed that the silica powder developed a negative charge in contact with the PE cup. This implies that, within the fluidized bed the silica powder would hold on to its negative charge and most likely would become further negatively charged by contacting the stainless steel column wall as well as the PE resin. On the other hand, the positively charged PE resin (which are mostly localized in the bottom of the bed) would develop more positive charge and the negatively charged PE resin would experience a

reduction in the charge magnitude or even a switch in the charge polarity. However, the increase in the positivity of the PE resin might not be detectable (especially at silica m_L = 1 g) due to their shape and size which either entrap or attract the silica in which case despite an ongoing charge transfer between the PE and silica, the net generated charge will be zero. In fact, for the silica mass loading of 1 g due to a higher silica to PE particle number ratio of 3/1 (1/3 at the silica mass loadings of 0.1) a reduction in the positive charge magnitude of the bulk would be expected. As such, a higher silica to PE particle number ratio could be another reason for declining the net *Q/m* of the "Dropped" and consequently a reduction in the wall fouling.

From the results shown in **Figure 5-10a** and **Figure 5-10b** it is also clear that injecting 0.1 g of the silica powder at t_{inj} = 0 min, on average, resulted in a slight decline on the total wall fouling and the "Dropped" *Q/m* compared to the "PE" run. Keeping the injection time at t_{inj} = 0 min and increasing the mass loading to 1 g, however, resulted in a noticeable decline in both the wall fouling magnitude and the "Dropped" *Q/m*. Upon injecting the silica at t_{inj} = 0 min there is a possibility that a portion of the highly charged silica powder gets attracted to the column wall prior to formation of the innermost "Wall – Inner" layer by the PE resin. The formed silica layer on the wall, in turn, could prevent PE resins from contacting the wall and that in turn would decrease the fouling of the PE resin on the column wall.

Figure 5-11 presents the results for particles net specific charge found in various regions of the bed for silica injection at different fluidization times. Evaluation of the *Q/m* of the "Wall – Bottom" shows that injecting the silica first reduced the occurrence of the positively charged layer and second, decreased the *Q/m* magnitude of the positively charged particles in this layer. Such an observation could be an indication of the effect of silica in reducing the positive charges. Considering the *Q/m* of the negatively charged "Wall – Bottom", "Wall – Top" and "Wall – Inner" layers, it can be noticed that the *Q/m* of these layers are in a same range and do not statistically differ from that of the "PE", despite the changes in their masses. Thus, it can be interpreted that in order for particles to form a layer on the wall, they must possess a certain level of *Q/m* regardless of the mass sitting on the wall. In addition, it can be clearly observed that a high or low *Q/m* magnitude on the wall layers (especially "Wall – Bottom" and "Wall – Top") does not necessarily correlate to a high or low mass on the wall. For example, the *Q/m* of the various wall layers for m_L = 0.1 g and t_{inj} = 15 min is similar to that of the m_L = 1 g and t_{inj} = 0 min, whereas the total wall fouling for the former condition is approximately 80% higher than that for the latter condition. In

relation to a commercial ethylene gas-phase reaction, this could be an important finding with respect to the sheeting occurrence where measuring only the electrostatic charge of the reactor wall might not be sufficient for detecting the sheeting.

An overall increase in the mass of "Fines" when the silica powder was injected can be observed in **Figure 5-11**. Obviously, the increase in the entrained mass is partially due to addition of the silica powder, a portion of which would entrain. A decrease in the d_{50} of the "Fines" for the silica mass loading of 1 g ($\bar{d}_{50}$ of 78 and 91 μm for m_L = 1 and 0.1 g, respectively) is an indication of the silica entrainment. With respect to the *Q/m* of the "Fines", it is evident that although more particles entrained specifically at the silica mass loading of 1 g, their corresponding charge did not increase proportionally. In another words, the entrained particles carried either a net of less negative, zero, or positive charge. The reduction in the "Fines" *Q/m* and increase in their mass can be explained by the fact that the entrained PE resin and those within the "Freeboard" layer would have on average a less negative *Q/m* due to the contact charge transfer they experienced with silica. The lower negative charge on the PE resin within the "Freeboard" layer would result in a lower image force, making the particles prone to be carried away by the fluidizing gas.

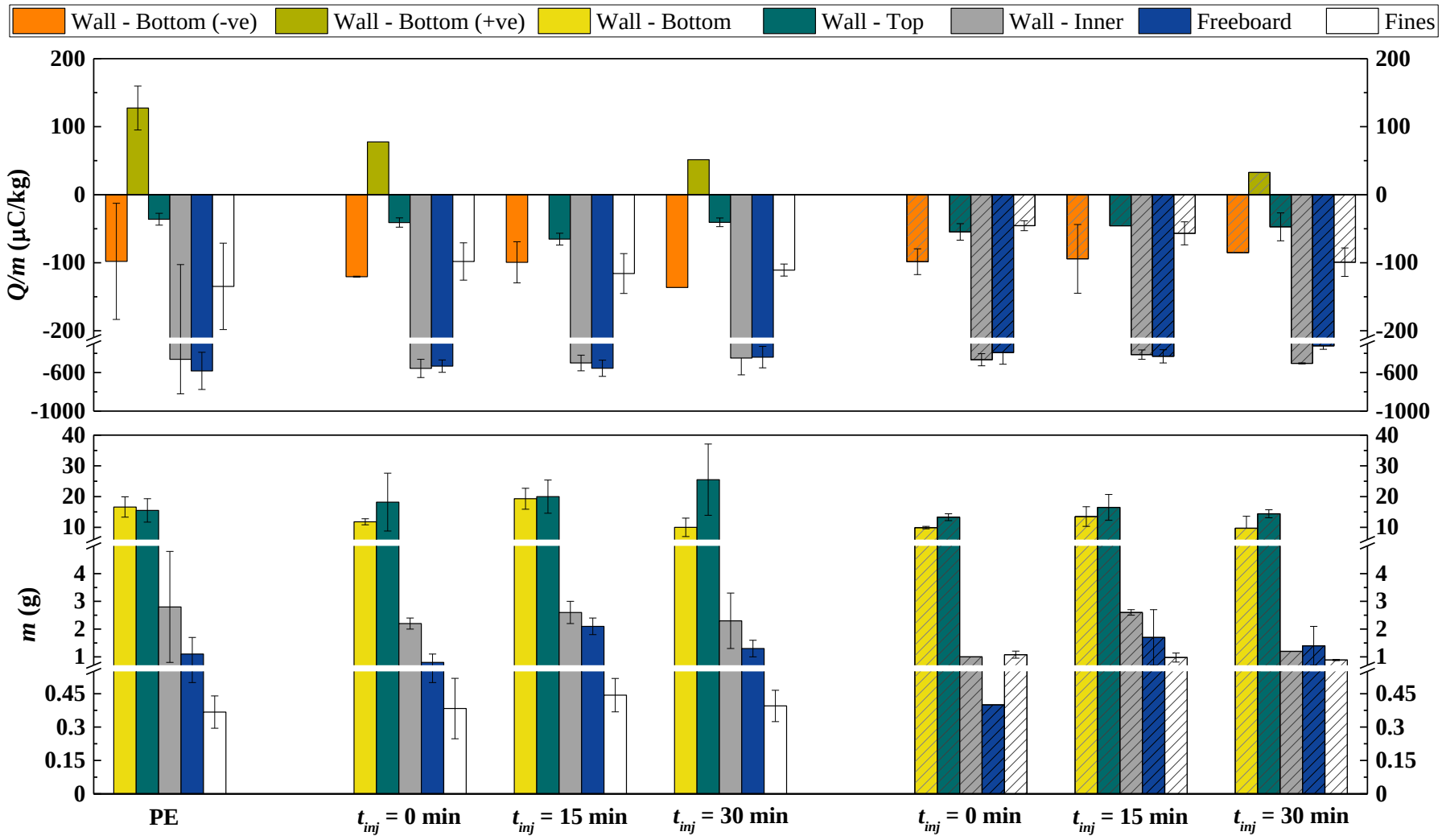

Figure 5-11 Effect of injection of silica powder at two mass loadings of m_L = 0.1 and 1 g (shown with striped pattern) at various times (t_{inj} = 0, 15 and 30 min) on the *Q/m* and mass of the "Wall – Bottom", "Wall – Top", "Wall – Inner", "Freeboard" and "Fines.

5-3-1-2 Effect of Injection Time

Changing the injection time to t_{inj} = 15 or 30 min, on average, resulted in an increase in the wall fouling magnitude and the "Dropped" net *Q/m* for the silica mass loading of 0.1 g. Even though a portion of the injected silica could coat the PE resin in the bulk and decrease its *Q/m*, a portion of the negatively charged silica powder could also migrate towards the positively charged PE resin sitting on the wall and those in turn, would attract more of the positively charged PE resins from the bulk. Such migrations and layering effects promote the wall fouling formation by increasing the net positive charge in the bulk. For the case of the silica m_L of 1 g, performing injection at t_{inj} = 15 or 30 min resulted in a slight increase in the wall fouling and *Q/m* of the "Dropped" in comparison to the injection at t_{inj} = 0 min. However, a larger silica to PE particle number ratio at m_L = 1 g overcame the layering effect and thus the wall fouling did not grow further.

5-3-2 Category C: 10 Consecutive Injections of 0.1 g

Increasing the wall fouling at t_{inj} = 15 min and silica m_L = 0.1 g was attributed to the silica powder's high *Q/m* upon entering the bed, whereas the decline in the wall fouling at the same injection time but at a higher silica mass loading of 1 g was related to the higher silica to PE particle number ratio. Thus, to better evaluate the effect of silica powder's specific charge versus its mass loading, an experiment was designed in which a total of 1 g silica was injected into the bed through 10 consecutive injections of 0.1 g. This way, a total of 1 g of the silica would still be added to the bed however with a *Q/m* equal to that of the 0.1 g mass loading. The results are presented in **Figure 5-12** alongside the results for the 60 minutes "PE" run as well as the results for the t_{inj} = 15 min and silica m_L = 0.1 and 1 g from the Category B experiments. No difference was observed between the two cases where 1 g of the silica was added at once or added through ten consecutive injections. Such an observation suggests that in determining the final wall fouling magnitude, the charge brought into the bed by the silica powder is not as influential as the number of the silica particles and the contact charge transfer that occurs inside the fluidized bed.

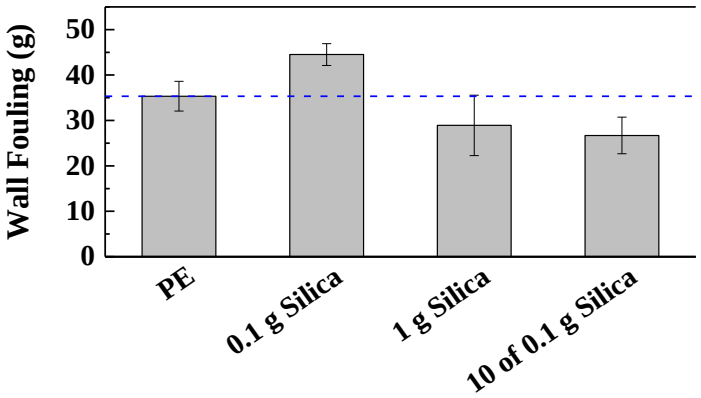

(a)

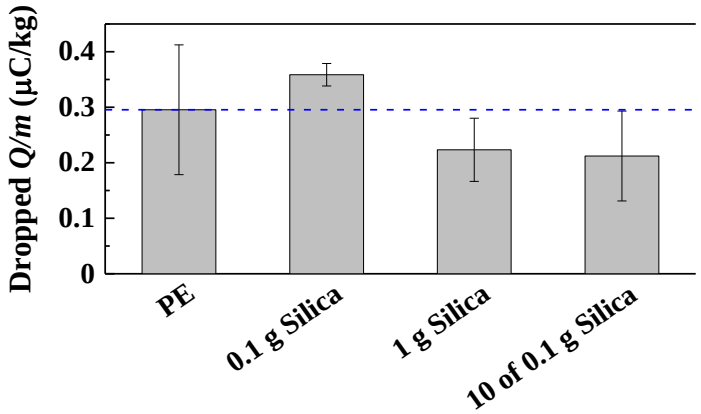

(b)

Figure 5-12 Effect of injection of silica powder at m_L = 0.1 g, 1 g and 10 injections of 0.1 g at t_{inj} = 15 min on (a) wall fouling magnitude and (b) *Q/m* of the "Dropped". The blue dashed lines correspond to the average t_F = 60 min "PE" run.

The *Q/m* of different regions of the bed for the Category C experiment are summarized in **Fig. 13** and are compared to other experiment of Category B at t_{inj} = 15 min. No significant difference was observed between the two cases where 1 g of the silica was added at once or added through ten consecutive injections. Mass of particles on layers as well as their size distribution were also found to be similar between these two cases.

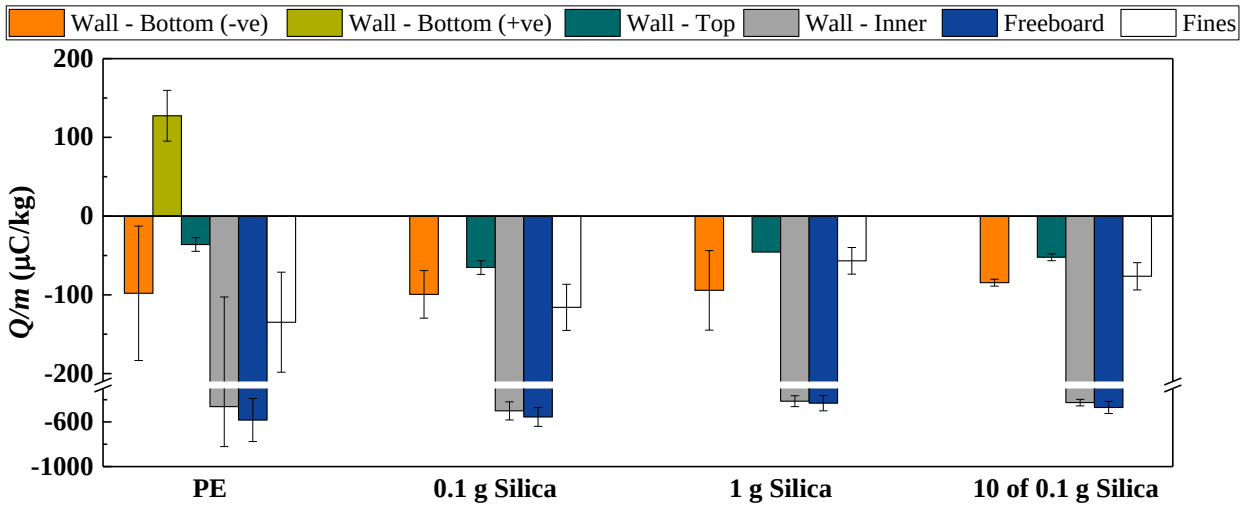

Figure 5-13 Effect of injection of silica powder at m_L = 0.1 g, 1 g and 10 injections of 0.1 g at t_{inj} = 15 min on *Q/m* of "Wall – Bottom", "Wall – Top", "Wall – Inner", "Freeboard" and "Fines".

5-3-3 Charging Mechanism of Silica

To better understand the charging mechanisms in this work, the nature of the involving materials must be identified. It is well known that solid materials, based on their electrical conductivity, are divided into three categories of conductor, semiconductor, and insulator. The materials used in this work include stainless steel (as the conveying line and fluidizing column) which is electronically conductive, PE and silica both of which are insulators. Identifying the charging mechanism for a conductive material involved in a contact charging is quite straightforward and is believed to be dominantly electron transfer. For insulator materials, however, a number of mechanisms have been proposed. Surface acidity/basicity (i.e., pK_a/pK_b), affinity to adsorb H^+/OH^- (i.e., proton/hydroxide affinity) or possessing electron donating/withdrawing functional groups (amide or halide, respectively) are some of the criteria that are proposed throughout the years alongside the electron transfer to explain the charge transfer mechanism for insulators [15–25].

The two involved solid materials in the pneumatic conveying system are the silica powder and the stainless steel tube wall. Due to the axial movement of the silica powder within the conveying line, the dominant contact inside the tube is expected to be particle – wall (although bipolar charging was observed arising due to contacts between the silica particles [10]). With a volume resistivity of above 10^{13} Ω.m, a high band gap of approximately 9 eV [26], a high electronegativity of 4.26 [27], and an acidic nature [21,22,28,29], silica is categorized as an insulator with a tendency of attracting electrons and becoming negatively charged. As such, in contact with the stainless steel,

electron transfer from the stainless steel to the silica powder is expected to be the dominant charging mechanism. Within the fluidized bed the silica experiences contacts with the stainless steel column wall and the PE resins. The possibility of silica – silica contact is very low due to its low concentration within the bed. Same as in the conveying line, the silica will develop a negative charge within the bed by contacting the stainless steel column. Respecting the contacts between the silica and PE resin, it is expected that the silica, owing to its high electronegativity as well as its acidic nature which could result in adsorbing OH^- from the environment and attracting electrons from the PE resin, becomes charged negatively.

With respect to the charging mechanism of PE resin arising from particle – particle contact, it is still a topic of debate and no definite mechanism has been proposed so far. Although mechanisms such as transfer of mobile H^+/OH^- resulting from existence of moisture patches on the surface [25] or material transfer in the form of small patches [30,31] have been proposed to describe the charging of polymeric materials including PE, the most probable mechanism, which also goes inline with the simulation works [32,33], seems to be the electron transfer which is possibly arising due to the PE surface defects and roughness [17,18,34].

Inducing a net of negative charge by adding silica into the PE fluidized bed in this work is in agreement with observations made in commercial ethylene polymerization reactors [35]. Using silica as a charge control agent (i.e., continuity additive) is a conventional method to control the electrostatic charge during ethylene polymerization catalyzed by Ziegler-Natta catalyst [5,35]. Silica was reported to tackle the bed positive voltage by inducing a negative voltage and bringing the bed voltage close to zero.

5-4 Conclusion

The influence of the injection of a dehydrated silica powder (i.e., catalyst support), pneumatically conveyed using a conveying line of similar material and diameter to that used in the polyethylene commercial processes, on the degree of the PE fluidized bed wall fouling was investigated. The charge of the silica powder upon entering the fluidized bed was successfully measured by recording the electric current signal from the conveying line. Overall, pneumatic conveying resulted in silica to become highly negatively charged with the particles Q/m to be six times greater for the 0.1 g mass loading comparting to that of the 1 g mass loading.

With injection of silica into the PE fluidized bed, various injection times were tested. Statistically, injection time was not found to be of a significant importance neither in changing the wall fouling magnitude nor the bed net charge. Silica mass loading showed a noticeable impact on both the wall fouling and the bed net charge. Higher silica mass loading reduced the wall fouling magnitude. In addition, it was shown that keeping the silica mass loading at 1 g and increasing the charge magnitude had no influence on the degree of wall fouling.

Overall, it was found that the silica powder induced a net of negative charge inside the fluidized bed, part of which was attributed to the charge acquired through the pneumatic conveying and silica to PE particle number ratio and the rest was related to the nature of the silica powder and its willingness to develop a negative charge polarity contacting the PE resin. This observation was in line with those made in commercial polyethylene fluidized bed reactors where silica injection was reported to induce a negative charge. The induced negative charge by the silica powder reduced the bulk net positive charge and that in turn reduced the wall fouling magnitude.

Acknowledgement

Financial support from Univation Technologies, LLC (USA) and The Natural Sciences and Engineering Research Council of Canada (NSERC) is acknowledged with gratitude.

Nomenclature

d_p	Mean particle diameter, µm
L	Tube length, m
m	Mass, g
m_L	Mass loading, g
Q	Charge, C
Q/m	Specific charge, µC/kg
t	Time, min
t_F	Fluidization time, min
t_{inj}	Injection time, min
U_{mf}	Minimum fluidization velocity, m/s

LDPE	Low density polyethylene
LLDPE	Linear low density polyethylene
PE	Polyethylene

References

[1] R.O. Hagerty, M.E. Muhle, A.K. Agapiou, C.-T.I. Kuo, M.G. Goode, F.D. Hussein, R.B. Pannell, J.F. Szul, Method for controlling sheeting in gas phase reactors, US Patent 7985811 B2, 2011.

[2] P. Mehrani, M. Murtomaa, D.J. Lacks, An overview of advances in understanding electrostatic charge buildup in gas-solid fluidized beds, J. Electrostat. 87 (2017) 64–78.

[3] Y. Rao, P. Cai, K.J. Cann, F.D. Hussein, W.R. Mariott, P.A. Cao, Supported catalyst with improved flowability, US Patent 10280283, 2019.

[4] G.E. Klinzing, A review of pneumatic conveying status, advances and projections, Powder Technol. 333 (2018) 78–90.

[5] Y. Yamaguchi, S. Suga, M. Morikawa, K. Kubo, M. Watanabe, Y. Sano, Method for producing polyolefin, US Patent 5385991, 1995.

[6] G. Hendrickson, Electrostatics and gas phase fluidized bed polymerization reactor wall sheeting, Chem. Eng. Sci. 61 (2006) 1041–1064.

[7] D. Song, P. Mehrani, Mechanism of particle build-up on gas-solid fluidization column wall due to electrostatic charge generation, Powder Technol. 316 (2017) 166–170.

[8] K.J. Cann, J.H. Moorhouse, P.A. Khokhani, T.T. Tamargo, K.R. Gross, M.G. Goode, Chromium-based catalyst compositions for olefin polymerization, US Patent 10266618 B2, 2019.

[9] R. Hoff, ed., Handbook of transition metal polymerization catalysts, Second Edi, John Wiley & Sons, Inc., 2018.

[10] M. Taghavivand, B.J. Cho, P. Mehrani, A. Sowinski, Electrostatic charging behaviour of a silica powder during pulse pneumatic conveying, Powder Technol. 366 (2020) 119–129.

[11] A. Sowinski, F. Salama, P. Mehrani, New technique for electrostatic charge measurement in gas-solid fluidized beds, J. Electrostat. 67 (2009) 568–573.

[12] A. Sowinski, L. Miller, P. Mehrani, Investigation of electrostatic charge distribution in gas-solid fluidized beds, Chem. Eng. Sci. 65 (2010) 2771–2781.

[13] K. Choi, M. Taghavivand, L. Zhang, Experimental studies on the effect of moisture content and volume resistivity on electrostatic behaviour of pharmaceutical powders, Int. J. Pharm. 519 (2017) 98–103.

[14] M. Taghavivand, P. Mehrani, A. Sowinski, K. Choi, Electrostatic charging behaviour of polypropylene particles during pulse pneumatic conveying with spiral gas flow pattern, Chem. Eng. Sci. 229 (2021) 116081.

[15] K.-E. Byun, Y. Cho, M. Seol, S. Kim, S.-W. Kim, H.-J. Shin, S. Park, S. Hwang, Control of triboelectrification by engineering surface dipole and surface electronic state, ACS Appl. Mater. Interfaces. 8 (2016) 18519–18525.

[16] C. Xu, Y. Zi, A.C. Wang, H. Zou, Y. Dai, X. He, P. Wang, Y.C. Wang, P. Feng, D. Li, Z.L. Wang, On the electron-transfer mechanism in the contact-electrification effect, Adv. Mater. 30 (2018) 1706790.

[17] S. Pan, Z. Zhang, Triboelectric effect: A new perspective on electron transfer process, J. Appl. Phys. 122 (2017).

[18] Z.L. Wang, A.C. Wang, On the origin of contact-electrification, Mater. Today. 30 (2019) 34–51.

[19] M.W. Williams, Triboelectric charging of insulating polymers-some new perspectives, AIP Adv. 2 (2012).

[20] J.H. Clint, T.S. Dunstan, Acid-base components of solid surfaces and the triboelectric series, Europhys. Lett. 54 (2001) 320–322.

[21] R.P.N. Veregin, M.N.V. McDougall, M.S. Hawkins, C. Vong, V. Skorokhod, H.P. Schreiber, A bidirectional acid-base charging model for triboelectrification: Part 1. Theory, J. Imaging Sci. Technol. 50 (2006) 282–287.

[22] R.P.N. Veregin, M.N.V. McDougall, M.S. Hawkins, C. Vong, V. Skorokhod, H.P. Schreiber, A bidirectional acid-base charging model for triboelectrification: Part II. Experimental verification by inverse gas chromatography and charging of metal oxides, J. Imaging Sci. Technol. 50 (2006) 288–293.

[23] J.A. Medley, Fractional electrification of polar polymers, Nature. 171 (1953) 1077.

[24] D.J. Lacks, T. Shinbrot, Long-standing and unresolved issues in triboelectric charging, Nat. Rev. Chem. 3 (2019) 465–476.

[25] P.S. Gil, D.J. Lacks, Humidity transforms immobile surface charges into mobile charges during triboelectric charging, Phys. Chem. Chem. Phys. 21 (2019) 13821–13825.

[26] E. Tea, J. Huang, C. Hin, First principles study of band line up at defective metal-oxide interface: oxygen point defects at Al/SiO2 interface, J. Phys. D. Appl. Phys. 49 (2016) 095304.

[27] G.D. Considine, ed., Van Nostrand's encyclopedia of chemistry, 5th ed., John Wiley, 2005.

[28] A. Auroux, A. Gervasini, Microcalorimetric study of the acidity and basicity of metal oxide surfaces, J. Phys. Chem. 94 (1990) 6371–6379.

[29] A. Gervasini, A. Auroux, Acidity and basicity of metal oxide surfaces II. Determination by catalytic decomposition of isopropanol, J. Catal. 131 (1991) 190–198.

[30] H.T. Baytekin, B. Baytekin, J.T. Incorvati, B.A. Grzybowski, Material transfer and polarity reversal in contact charging, Angew. Chemie Int. Ed. 51 (2012) 4843–4847.

[31] H.T. Baytekin, A.Z. Patashinski, M. Branicki, B. Baytekin, S. Soh, B.A. Grzybowski, The mosaic of surface charge in contact electrification, Science (80-.). 333 (2011) 308 LP – 312.

[32] M. Ray, F. Chowdhury, A. Sowinski, P. Mehrani, A. Passalacqua, Eulerian modeling of charge transport in bi-disperse particulate flows due to triboelectrification, Phys. Fluids. 32 (2020).

[33] M. Ray, F. Chowdhury, A. Sowinski, P. Mehrani, A. Passalacqua, An Euler-Euler model for mono-dispersed gas-particle flows incorporating electrostatic charging due to particle-

wall and particle-particle collisions, Chem. Eng. Sci. 197 (2019) 327–344.

[34] J.C. Angus, I. Greber, Tribo-electric charging of dielectric solids of identical composition, J. Appl. Phys. 123 (2018).

[35] G.-H. Song, A.S. Rhee, G.R. Lowder, Method for reducing sheeting and static charges during polymerization of ethylene polymers, US Patent 5391657, 1995.

Chapter 6 - Triboelectric Effects of Continuity Additives on Polyethylene Fluidized Bed Wall Fouling

Milad Taghavivand, Andrew Sowinski, Poupak Mehrani*

Department of Chemical and Biological Engineering, University of Ottawa, 161 Louis Pasteur, Ottawa, ON, K1N 6N5, Canada

* Corresponding author. E-mail: poupak.mehrani@uottawa.ca; Tel: 1-613-562-5800 ext. 6098

The current chapter is a manuscript submitted to the journal of Chemical Engineering Science "Publication under review, Manuscript ID: CES-D-21-00355"

Abstract

In commercial ethylene gas-phase polymerization reactors, low concentrations of continuity additives (CAs) are periodically fed into the reactor to tackle reactor sheeting. In dry feeding of CAs, they are added into the reactor through pneumatic conveying lines either separately or doped on the catalyst support along with other catalyst elements. This work focused to investigate the role of five commercially available materials reported to act as CA in the open literature naming aluminum distearate, 2-2' (octadecylimino) bisethanol (known as AS-990), calcium stearate, zinc stearate, and CHIMASSORB 944 on the extent of polyethylene fluidized bed wall fouling. A pneumatic conveying line of similar material (stainless-steel) and diameter (4.75×10^{-3} m) to those used in a commercial process, was used to convey various loads of the powders into a 1-kg bed of polyethylene. Fluidization was carried out in a 0.1 m diameter stainless-steel atmospheric fluidized bed. Results showed a direct relationship between the bulk of the bed net specific charge magnitude and the extent of wall fouling. The bed bulk charge and the wall fouling magnitude were observed to be varied by the type and concentration of the CAs, emphasizing the importance of their surface chemistry on mitigating wall fouling. An optimum CA-to-silica ratio was proposed at which the wall fouling reached a minimum.

Keywords: Ethylene gas-phase polymerization, Fluidized bed, Sheeting, Electrostatics, Continuity additives, Pneumatic conveying

6-1 Introduction

Electrostatic charge generation due to continuous particle-particle and particle-vessel wall contacts, which occurs during particle handling, transport (e.g., pneumatic conveying) and processing (e.g., gas-solid fluidized beds), is a phenomenon that can result in severe problems such as particle-wall adhesion, electrostatic discharge, as well as particle segregation and agglomeration. Sheeting formation on the reactor walls during ethylene gas-phase polymerization is a problem which is attributed to electrostatic charging of the polyethylene (PE) resin and catalyst particles, resulting in their adhesion to the reactor wall. The exothermic nature of the polymerization reaction coupled with a poor reaction heat removal from the wall regions, result in melting of the fouled polyethylene resins and forming sheets that can grow and break off of the reactor wall, causing discontinuity in production and ultimately a significant economic loss [1].

Sheeting and reactor shut down (discontinuity) in ethylene gas-phase polymerization has been reported with different types of catalytic systems being Ziegler-Natta, chromium-based (e.g., Philips or chromocene), or single site (e.g., metallocene) [2–10]. Various techniques have been developed throughout the years to overcome the reactor discontinuity with some of them focusing on modifying the catalyst preparation [11]. Operating the reactor at condensed mode is a method that is being used to stabilize the system and to mitigate the sheeting occurrence during ethylene gas-phase polymerization. In this method, the gas feed stream contains an inert condensing agent (ICA) such as iso-pentane or n-hexane which is liquified just below the dew point to enhance the reaction heat removal upon its evaporation inside the reactor [10,12,13]. Although, operating in the condensed mode has shown promising results with respect to controlling the reactor sheeting as well as increasing the PE production rate in the Ziegler-Natta catalytic system, it has appeared to be less influential in the metallocene catalytic system [10,13,14]. In addition, installation of a vent recovery system to collect the ICA and recycling it back to the reactor along with the difficulties in purging the PE resin, are some challenges involved in this method which would make a demand for an alternative method in helping to stabilize the process in regard to sheeting [15,16].

Treating the reactor inner wall prior to polymerization by chromium containing compounds is another technique employed to reduce the electrostatic charge build up and subsequently sheeting formation in commercial reactors [2]. Although this technique is reported to be effective for

Ziegler-Natta catalytic systems, with the new generation of catalysts the sheeting still persists. Suppression of the fines by introducing a hydrocarbon, redesigning the fluidized bed reactor (e.g., redesigning the distributor plate and reactor expanded zone), and using sound waves are other techniques that have been used to attempt mitigating the reactor sheeting [17–20]

Addition of continuity additives (CA), formerly referred to as antistatic agents, is another method employed in controlling polyethylene reactor sheeting. CAs are hypothesized to either induce a charge polarity within the reactor opposite to that of a dominant bed charge polarity, or increase the electrostatic conductivity of the reactor material (i.e., growing PE resin) [2,4,5,21,22]. These additives have been added to the reactor either separately or as part of the supported catalyst composition. Besides the product quality as well as the environmental and health considerations, the most important factor in choosing the continuity additives is that they must not reduce the catalyst activity by poisoning the catalyst active sites [4,10,22–24]. Inorganic metal oxides such as MgO, Al_2O_3, SiO_2 and TiO_2 are examples of CAs used in Ziegler-Natta catalytic system [5,24]. Very low concentrations of water, alcohols, ketones, oxygen and nitric oxide have also been shown to reduce the electrostatic charge build up in a Ziegler-Natta catalytic system [4]. As for the metallocene and in general most of the single site catalysts, metal carboxylate salts (e.g., aluminum distearate or calcium stearate), fatty amine alkoxylate (e.g., KEMAMINE AS-990), polyethyleneimines (e.g., LUPASOL FG or LUPASOL WF), and hindered amine light stabilizers (e.g., CHIMASSORB 944) are some of the publicly disclosed CAs [8–11,23–25]. Although most of the CAs such as metal carboxylate salts may negatively impact the catalyst activity, some other types such as fatty amine alkoxylate or polyethyleneimines, have interestingly been reported to enhance the catalyst activity by scavenging catalyst poisons such as oxygen [10,23].

In commercial PE processes, CAs are periodically injected into the reactor as a solution in liquid hydrocarbons (e.g., n-hexane), slurry in mineral oil (e.g., HYDROBRITE 380), aromatic hydrocarbons or aliphatic hydrocarbons, or in dry solid form [5,6,9,10,23]. In the dry feeding systems, CAs are pneumatically injected into the reactor through long narrow tubes (typically stainless steel tubes with a 4.75×10^{-3} m in inner diameter). It has been shown that in general, pneumatic conveying systems can generate the largest amount of electrostatic charge among all gas-solid processes [26]. Therefore, in relation to the polyethylene process, CAs and all other pneumatically injected solid additives are anticipated to be electrostatically charged upon entering

the reactor. However, their exact role on controlling the reactor sheeting is not well understood. As such, the aim of this work was to carry out a systematic study to determine the triboelectric effects of different commercially available continuity additives, added in their solid form through pneumatic injection into a PE fluidized bed, on the bed electrification and extent of wall fouling.

6-2 Materials and Methods

The schematic diagram of the atmospheric gas-solid fluidization system used in this work along with a horizontal solid conveying line is shown in **Figure 6-1**. Details of the fluidization column and its compartments can be found elsewhere [27,28]. The stainless steel fluidization column, 0.1 m in diameter and 1.3 m in height, was connected to two Faraday cages, one at the top and one at the bottom. Both Faraday cages were connected to Keithley 6514 digital electrometers (with a measurement accuracy of "± (Value*1% + 50 pC)") and were electrically isolated from the grounded fluidization column. The top Faraday cage was a through-type and housed a filter bag to contain the entrained particles (referred to as *Fines*) for their charge-to-mass ratio (*Q/m*) and size distribution measurements. A modified knife gate valve was used as a removable perforated distributor plate. As a result, the distributer plate could be opened and closed easily, allowing the collection of the bulk particles (referred to as *Dropped*) in the bottom Faraday cage at the end of the fluidization run without any particle handling. The fluidizing gas was dry air with approximately 0% relative humidity at 22 ± 1˚C. The fluidization was carried out for 60 minutes at a fluidizing gas velocity set at 1.5 times minimum fluidization velocity (U_{mf}) to represent the bubbling flow regime.

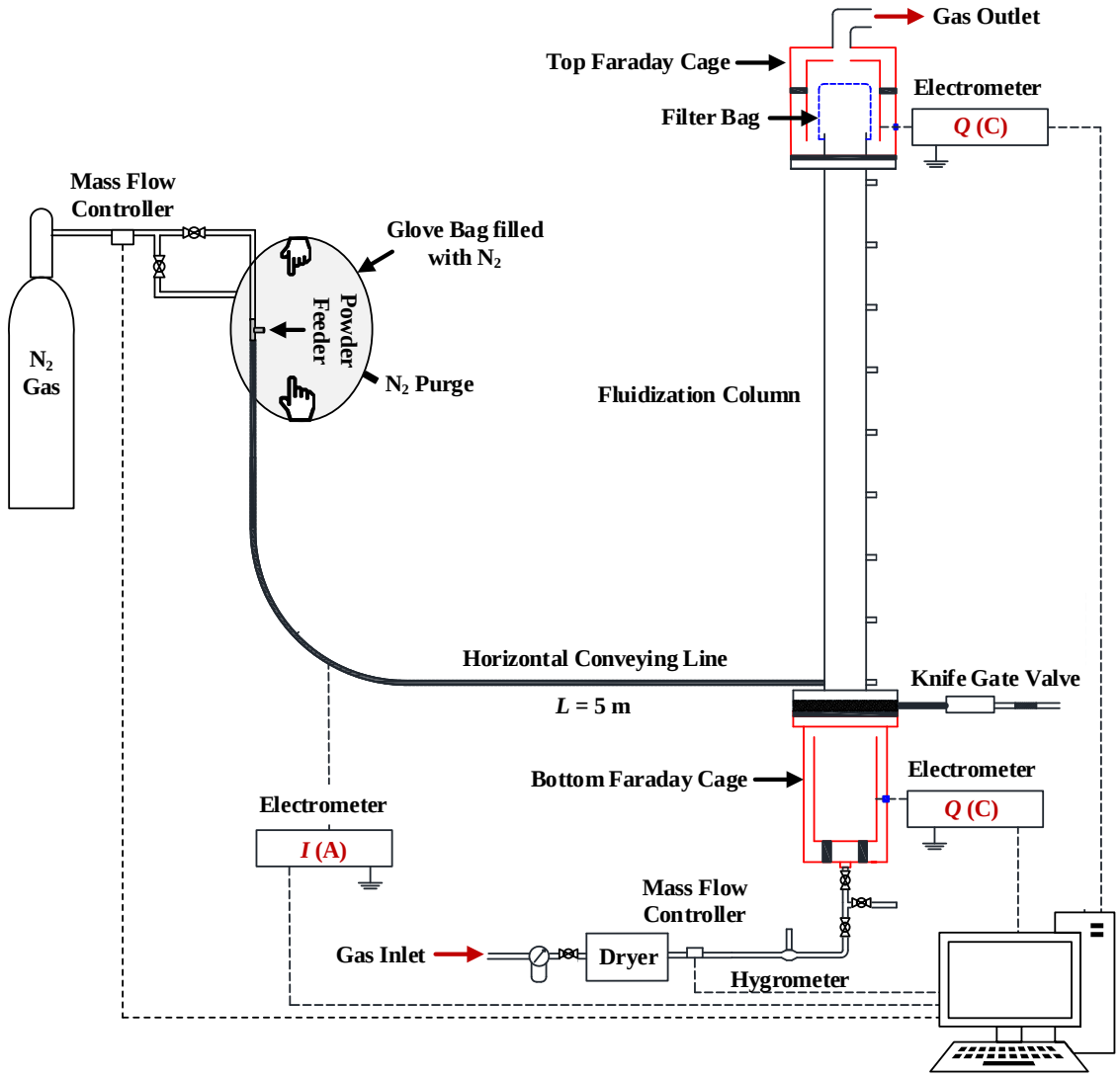

Figure 6-1 Schematic diagram of the fluidization system along with the horizontal conveying line directly connected to the fluidized bed.

To imitate a typical commercial catalyst conveying line used in PE processes, a stainless steel tube with an inner diameter of 4.75×10^{-3} m was used as the pneumatic conveying line. The conveying line was 5 m in length and contained one smooth (1 m in radius) bend and was connected to the fluidization column at approximately 0.025 m above the distributor plate. To determine the charge of the conveyed powder, as shown in **Figure 6-1**, the conveying line was directly connected to a Keithley 6514 digital electrometer with a measurement accuracy of "± (Value*0.1% + 5 pA)" to measure the electric current signal which was then converted to the powder charge. The details of such measurement can be found in our earlier work [29]. To minimize the effect of the atmospheric

moisture on the conveyed powder, the powder feeder was placed in a glove bag filled up with dry nitrogen. The conveying gas was dry nitrogen with a velocity set at 15 m/s which is within a suggested range of carrier gas velocity used for catalyst injection in PE production process [30].

The fluidizing particles, which were directly received from a commercial plant, were LLDPE resin with a volume-based mean diameter of 590 μm and a bulk density of 424 kg/m^3. Five types of CAs that are typically used in industrial processes were tested in this work as summarized in **Table 6-1**. As mentioned earlier, CAs can be added into the reactor either separately or as part of the catalyst (i.e., doped on the catalyst support alongside the co-catalyst, catalyst activator, and active catalyst site). Both cases were examined in this work. The mass of the fluidizing PE was 1 kg and the concentrations of the CAs added to the PE bed were in the range of 1 to 500 ppmw which is the typical concentration of the CAs in a commercial process. In addition, amorphous silica was examined in its dehydrated and non-dehydrated forms. Amorphous silica is a typical catalyst support used in ethylene polymerization which must be dehydrated at a temperature equal or above 600˚C for approximately 4 to 6 hours to remove the surface moisture as well as hydroxide groups. Moisture and hydroxide groups have been reported to adversely affect the catalyst productivity [10]. A Malvern Mastersizer 2000 was used to measure the particle size distributions. The volume resistivity of the PE resin, the CAs, and the silica were measured to be greater than 10^{13} Ω.m indicating the electrically insulative nature of the powders. The measurement details for volume resistivity can be found elsewhere [31].

Table 6-1 List of powders tested in this work.

Particles Category	Type	Acronym	Concentrations in mixtures	Size (µm)		
				dp_{10}	dp_{50}	dp_{90}
Amorphous Silica (catalyst support)	Davison 955	Si	–	10	45	95
Continuity Additive (CA)	2,2'-(octadecyl imino) bisethanol (known as AS-990)	A	–	4	78	200
	Aluminum Distearate	B	–	4	20	50
	Calcium Stearate	C	–	2	7	20
	CHIMASSORB 944 FDL	D	–	30	150	460
	Zinc Stearate	E	–	180	540	1015
CA doped on Si	A	Si – 1% A	99 wt.% Si 1 wt.% A	10	45	95
	B	Si – 3% B	97 wt.% Si 3 wt.% B			
	A & B	Si – 1% A – 3% B	96 wt.% Si 1 wt.% A 3 wt.% B			

6-2-1 Experimental Design

A number of fluidization experiments were designed with a summary presented in **Table 6-2**. Prior to performing any experiment with CAs or silica, a reference point of the extent of wall fouling of PE resin fluidized alone was obtained, called *Category I* . *Category II* experiments were performed with the dehydrated amorphous silica. Two silica mass loadings of 0.1 and 1 g were examined to represent a high and low catalyst productivity of 10000 and 1000 g-PE/g-catalyst, respectively. Additional tests were also performed with a non-dehydrated silica, referred to as $Si_{non\text{-}dehydrated}$, to provide a comparison between a silica surface with and without hydroxide groups. *Category III* experiments included injection of CAs into the PE bed. The mass loading (m_L) of the CAs was set at 0.1 g to represent a concentration of 100 ppmw within the bed; however, where 0.1 g was not sufficient to observe a change, higher mass loadings of up to 1 g were examined. Typically, higher amount of CAs has been reported to inversely affect the catalyst activity [1,10] and therefore mass loadings of greater than 1 g were not tested. *Category IV* included experiments with samples of CAs doped on silica, as well as adding silica and CAs separately into the bed where mass loadings of 0.1 to 1 g were examined. All the powders were added into the fluidized bed through pneumatic

injection; however, some tests were performed where powders were added into the bed using a spatula.

Table 6-2 Summary of the experimental design.

Category	**Experiment type**		**Tested additive**	**Mass loading (m_L) (g)**
I	PE		–	–
II	PE & Si		Si	0.1, 1
			$Si_{non\text{-}dehydrated}$	1
III	PE & CA		A	0.1
			B	
			C	
			D	0.1, 0.5
			E	0.1, 0.5, 1
			C + (33 to 80%) B	0.15, 0.3, 0.5
IV	PE & Si & CA	CA doped on Si	Si – 1% A	0.1, 1
			Si – 3% B	
			Si – 1% A – 3% B	
		CA & Si added separately	Si + (1 to 33%) B	0.1, 0.15, 1
			Si + 25% A + 25% B	0.2

6-2-2 Procedure to Pneumatically Inject the Powder into the Fluidized Bed

Two important aspects of this work were (a) to ensure a predetermined amount of each additive entered the bed through pneumatic injection; and (b) to be able to measure the additives charge upon entering the bed via pneumatic conveying line. The electrical current signal measured off of the conveying tube upon additives flow, was employed to calculate their charge. Our previous works had shown that powders tend to foul inside the conveying lines during the pulse pneumatic injection resulting in a loss in the mass of the powder exiting the conveying line [29,32]. However, multiple consecutive injections had shown a reduction in the extent of the powder loss. Thus, in this work to ensure that a certain mass of each additive entered the fluidized bed, the experiments were split into two segments.

6-2-2-1 Pneumatic Conveying

Prior to connecting the conveying line to the fluidization column, consecutive injections of a predetermined mass of additives were carried out into a cyclone-type Faraday cage as shown in

Figure 6-2 until the mass of fouling in the conveying line reached saturation. Depending on the additive type and mass loading, the number of the consecutive injections, *n*, varied (details can be found in our previous work [29]).

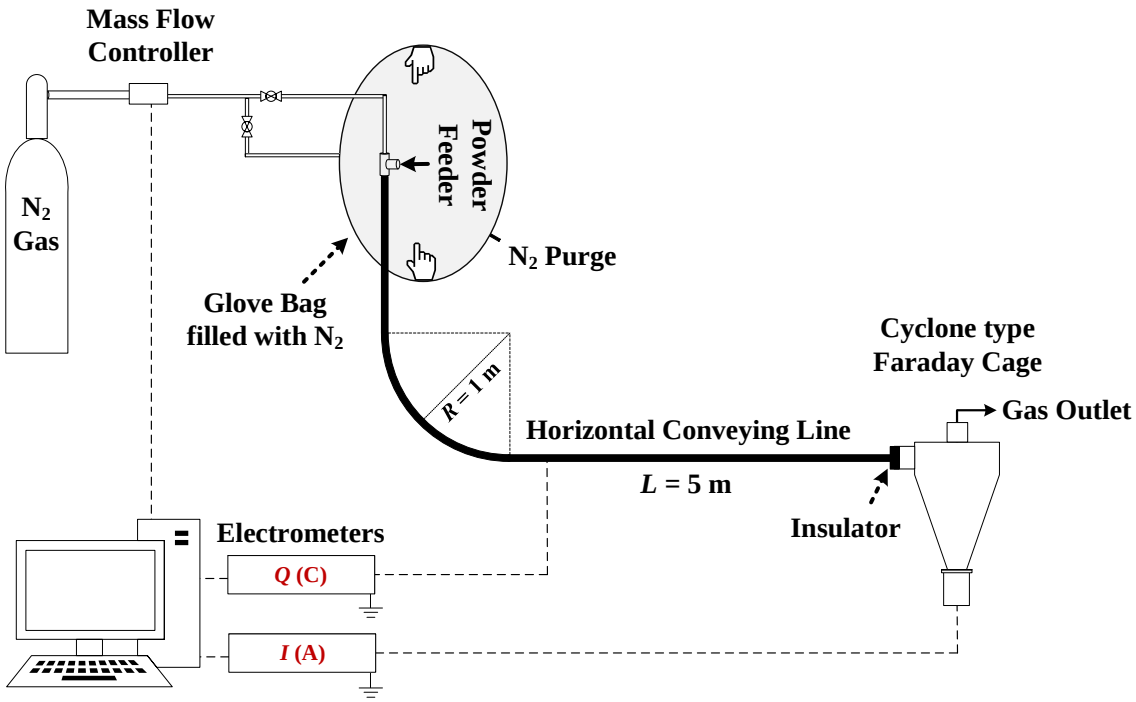

Figure 6-2 Schematic diagram of horizontal pneumatic conveying apparatus connected to a cyclone-type Faraday cage.

6-2-2-2 Fluidization

Once the conveying line fouling reached the saturation level at the n^{th} injection outside the fluidized bed, the conveying line was disconnected from the cyclone Faraday cage and connected to the fluidized bed to carry out the second segment of the experiment which was to perform the $(n + 1)^{th}$ injection into the center of fluidized bed followed by the fluidization of the mixture of PE and the powder. After injecting the powder at the center of the fluidization column, the conveying tube was retracted and made flush to the column wall and the fluidization period was commenced. In the cases where the powders were added by spatula, at first a portion of the PE resin was loaded into the column just enough to reach a height equal to that of the pneumatic injection port (i.e.,

0.025 m above the distributor plate). Then the powder was added by a spatula via this port. The remaining PE resin was then loaded into the column and fluidization period was commenced.

For all the tested conditions, upon the completion of the fluidization experiments and after collecting the *Fines* and *Dropped* particles, a layer of fouling was observed extending to top of the column (referred to as *Wall Fouling*). As shown in **Figure 6-3**, the *Wall Fouling* consisted of two sections including a relatively thick layer formed from the distributor plate to the expanded bed height (referred to as *Wall*), and a thinner layer formed above the expanded bed height (referred to as *Freeboard*). It was found that the *Wall* particles had different polarities depending on their location and as a result, three sublayers were identified for this layer. The particles covering the wall up to the static bed height were referred to as *Wall – Bottom* while those covering the wall from the static bed height up to the expanded bed height were referred to as *Wall – Top*. The third sublayer consisted of particles in the very first layer of coating on the wall (referred to as *Wall – Inner*). Particles within each layer were removed from the wall and collected in the bottom Faraday cage by using compressed building air passed through a narrow tube inserted from the top of the column. The mass, charge, and size distribution of particles collected from all regions of the beds were measured.

All experiments were repeated at least two times to ensure the reproducibility of results. In each trial, the initial charge of the polyethylene particles as well as the silica particles were measured in a bench-scale Faraday cage.

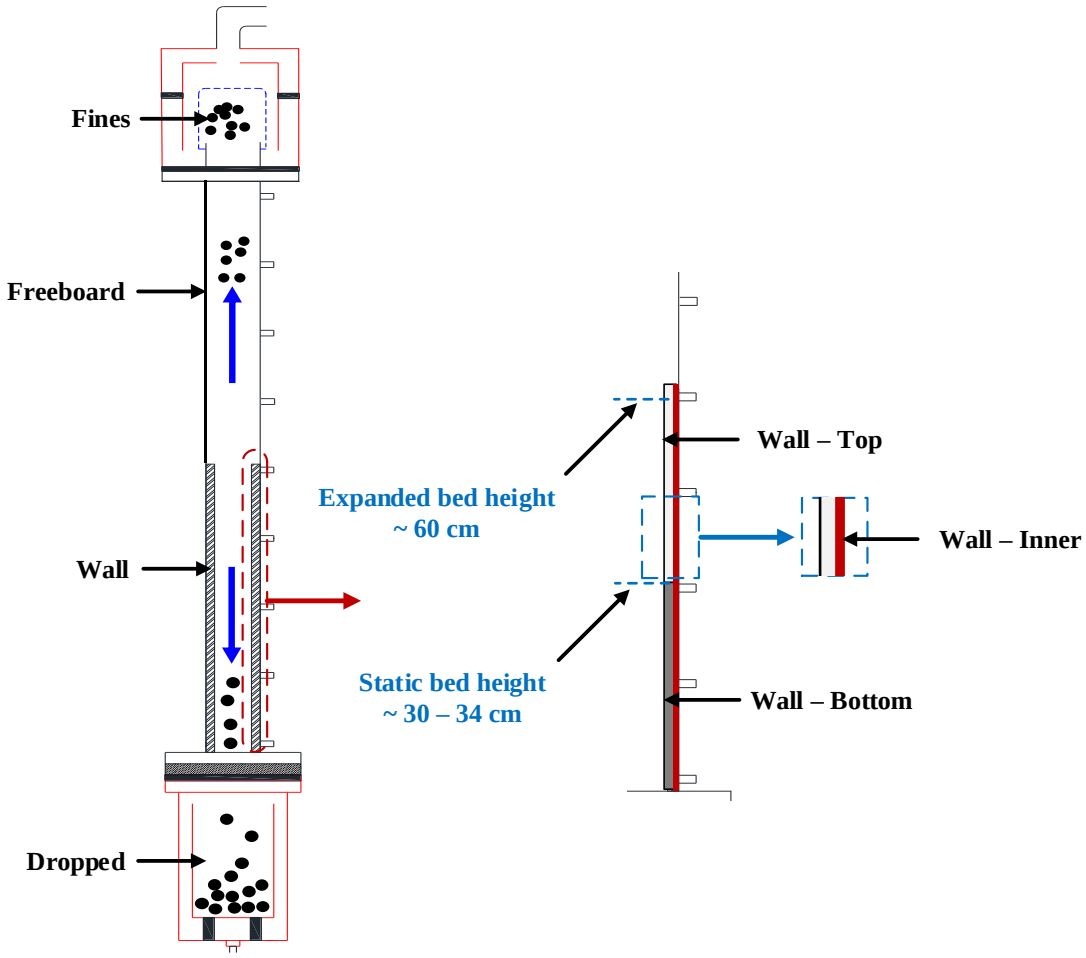

Figure 6-3 Different regions of the fluidization column with respect to particles location.

6-3 Results and Discussion

To investigate the influence of the CAs and silica catalyst support on the extent of wall fouling formation during their fluidization with the PE resin, it was essential to first establish a reference case by fluidizing the PE resin alone. Initial *Q/m* of the resin was -0.01 ± 0.03 μC/kg while that of *Dropped* was found to be 0.3 ± 0.12 μC/kg. **Figure 6-4a** enables a qualitative observation of the extent of the wall fouling which was measured to be a total of 35.34 ± 3.3 g from which *Wall – Bottom* and *Wall – Top* regions accounted for its 97-98 wt.%. As for the *Fines*, although their mass was very small in comparison to the other regions, they provided a valuable information with

respect to bipolar charging. In addition, monitoring the *Fines* charge polarity provides a predictive tool in relation to the charge of the *Dropped* particles which will be discussed later in the manuscript. **Figure 6-4b** and **Figure 6-4c** provide a quantitative analysis of these three regions *Q/m* and mass.

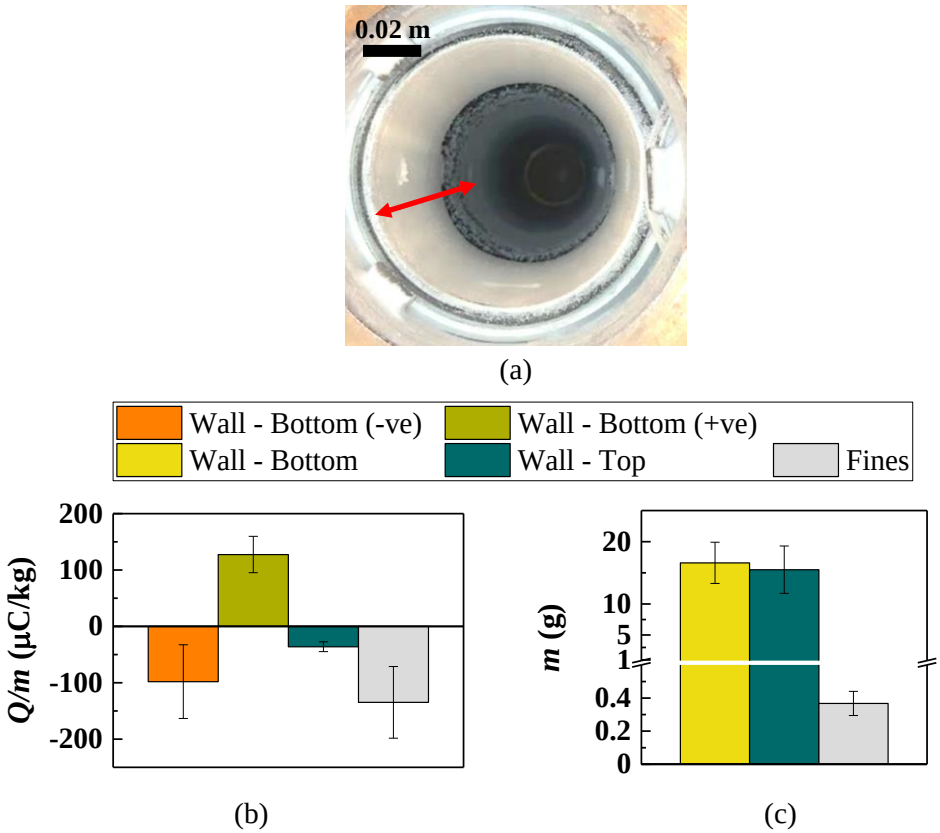

Figure 6-4 (a) Image of wall fouling taken from the bottom of the fluidized bed for PE run (the red arrow represents the 0.3 m static bed height); (b) *Q/m* of the *Wall – Bottom*, *Wall – Top* and *Fines*; (c) mass of the particles in the *Wall – Bottom*, *Wall – Top* and *Fines*.

The comparison of the *Q/m* of the *Dropped* with those in **Figure 6-4b** implied the presence of bipolar charging. As can be seen in **Figure 6-4b**, the *Wall – Bottom* particles at times charged positively (referred to as *Wall – Bottom (+ve)*) or negatively (referred to as *Wall – Bottom (–ve)*); however, the mass of this layer was consistent for all the experiments (**Figure 6-4c**). The *Wall – Inner* and *Freeboard* layers were observed to carry a net of negative charge, which can be explained by higher effective work function for PE compared to stainless steel column wall [33]. However, particle-particle contacts within the bulk of the bed consisting of various particles sizes could result in small (e.g., *Fines*) and large particles (e.g., *Dropped*) becoming negatively and positively charged, respectively. Existence of positively charged particles in the *Wall – Bottom* at

times is related to the attractive electrostatic forces between the negatively charged inner layers and positively charged bulk particles [33]. As well, the repulsive electrostatic forces between the positively charged bulk particles promotes the migration of positively charged PE particles towards the wall. Such layering mechanism and particle migration from the bulk to the wall is applicable for all the experiments of *Categories I – IV*.

6-3-1 Categories II (PE & Si) & III (PE & CA)

Initial *Q/m* of all the powders measured prior to their conveying are reported in **Figure 6-5a** and **Figure 6-5b**. As mentioned earlier, it was essential to ensure a predetermined mass of powders enter the fluidized bed through the conveying line. It was found that except for C and Si both at m_L = 0.1 g, which required ten injections, five injections were sufficient for other cases prior to connecting the conveying line to the fluidized bed. The *Q/m* of the CAs and Si upon entering the fluidized bed through the conveying line, which was measured by reading the current signal from the conveying line, are presented in **Figure 6-5c** and **Figure 6-5d**, respectively. Considering the powders particle size range, *Q/m*, and the number of injections required for tube fouling mass to reach saturation, it becomes clear that for powders with a dp_{90} smaller than 100 μm the tendency in leaving a significant tube fouling increased as the powder either got smaller or acquired a relatively high electrostatic charge. Powder C with the lowest dp_{50} and Si with the highest *Q/m* are two examples both of which required ten injections at m_L = 0.1 g. In addition, from **Figure 6-5d** it is clear that $Si_{non\text{-}dehydrated}$ acquires less *Q/m* in comparison to the dehydrated Si. Such a difference, which was also observed in our previous work [29], is due to the presence of moisture and hydroxide groups on the surface of $Si_{non\text{-}dehydrated}$ and will be discussed later in the manuscript.

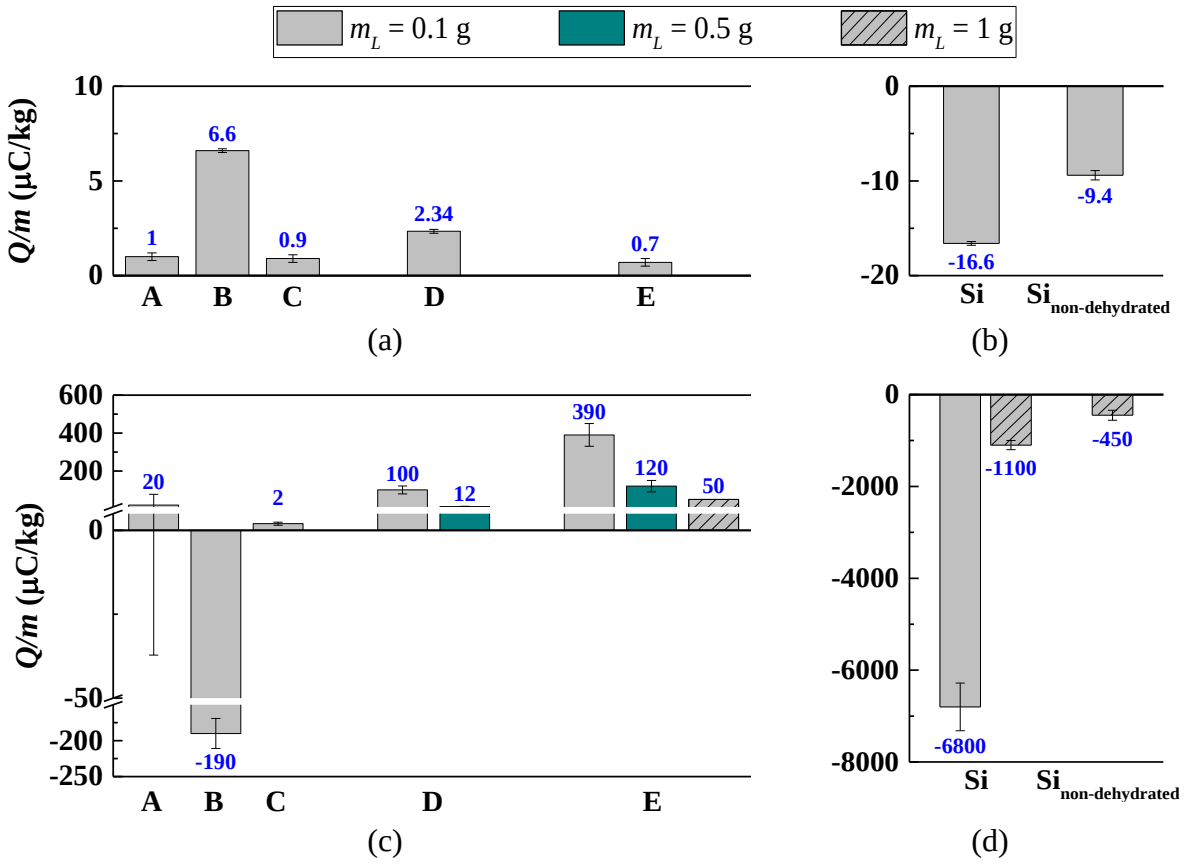

Figure 6-5 (a) Initial *Q/m* of the continuity additives; (b) initial *Q/m* of the dehydrated and non-dehydrated amorphous silica; (c) *Q/m* of the continuity additives upon being injected into the fluidized bed (i.e., 6th or 11th injection); (d) *Q/m* of the dehydrated and non-dehydrated amorphous silica upon being injected into the fluidized bed (i.e., 6th or 11th injection).

6-3-1-1 Effect of CAs and Si and Their Mass Loadings

As shown in **Figure 6-6**, a qualitative comparison on the degree of wall fouling was first made with images taken from the inner column wall upon collecting the *Dropped* particles. Images clearly indicate that some of the powders such as E and $Si_{non\text{-}dehydrated}$ resulted in a noticeable change in the wall fouling magnitude.

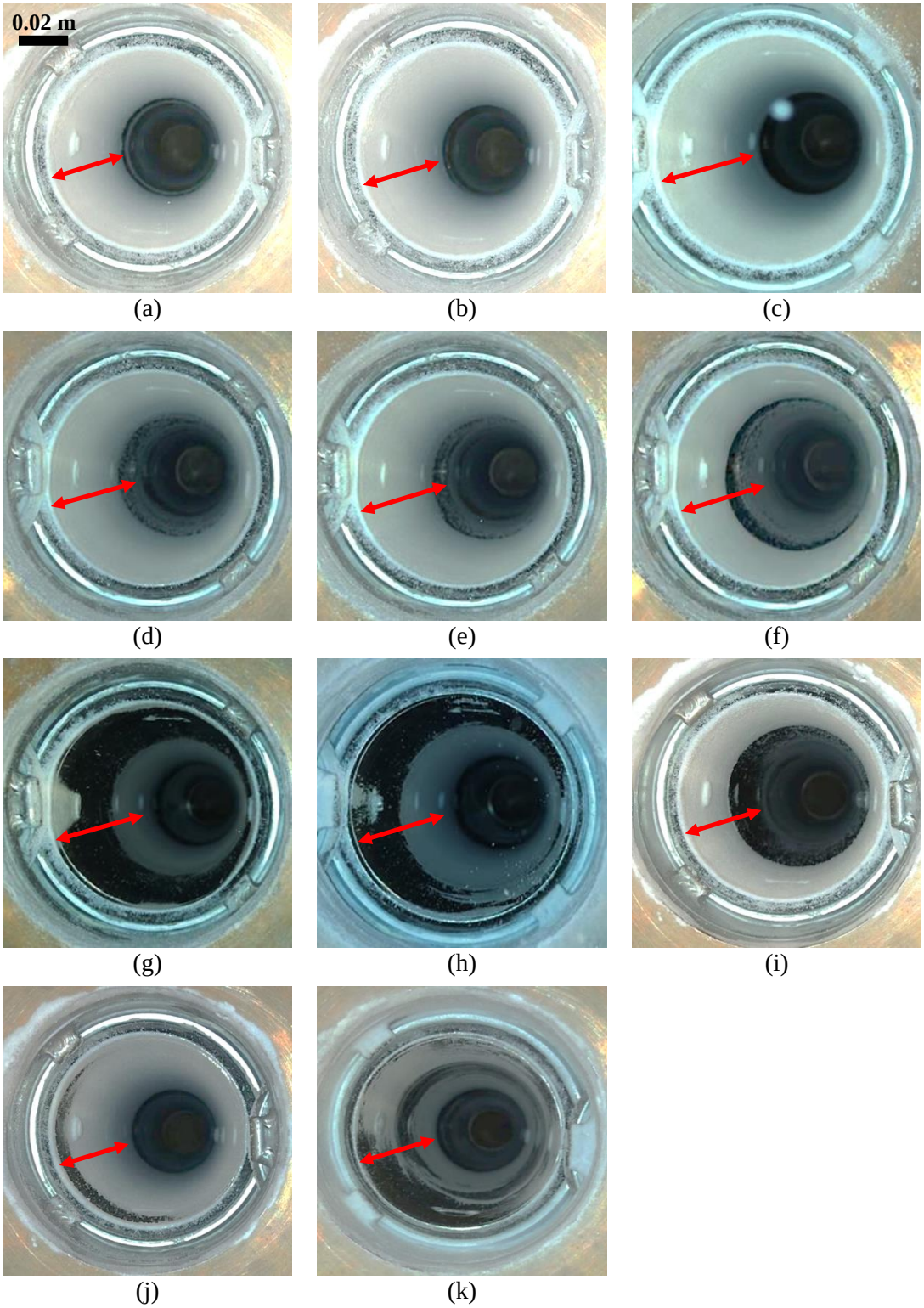

Figure 6-6 Images of wall fouling for the *Category II* (Si) and *III* (CAs) runs taken from the bottom of the fluidized bed. (a) A, m_L = 0.1 g; (b) B, m_L = 0.1 g; (c) C, m_L = 0.1 g; (d) D, m_L = 0.1 g; (e) D, m_L = 0.5 g; (f) E, m_L = 0.1 g; (g) E, m_L = 0.5 g; (h) E, m_L = 1 g; (i) Si, m_L = 0.1 g; (j) Si, m_L = 1 g; (k) $Si_{non\text{-}dehydrated}$, m_L = 1 g. The red arrows represent the 0.3 m static bed height.

The quantitative results of the total wall fouling are presented in **Figure 6-7a** and it can be seen that 0.1 g of powders A, B and C increased the wall fouling, with C approximately doubling the fouling magnitude. On the other hand, 0.1 g of powders D and E did not change the amount of fouling, as such, higher mass loadings were tested. Increasing the m_L of powder D to 0.5 g, still, did not change the amount of wall fouling, whereas 0.5 g of E reduced the fouling. However further increasing the mass of E to 1.0 g had no additional influence. As for the Si, a slight reduction in the wall fouling was observed at m_L = 0.1 g, whereas the wall fouling increased at higher mass loading of 1 g. On the contrast, 1 g of the $Si_{non\text{-}dehydrate}$ reduced the wall fouling noticeably.

A significantly important observation was made by comparing **Figure 6-7a** and **Figure 6-7b** where a direct relationship was found between the total wall fouling and the *Dropped* particles absolute *Q/m*. Such a relationship implies that the decline in the absolute *Q/m* of the bulk of the bed results in a reduction in the repulsive electrostatic forces between the particles of a same charge polarity in the bulk. Similarly, a reduction would be expected in the attractive electrostatic forces between the negatively charged particles in the wall layers and the positively charged bulk particles. In addition, the image force between the column wall and the particles in the bulk must have been declined. All these cases will demote the progression of the wall layering effect and subsequently the extent of the fouling. The opposite of this is also possible where an increase in the absolute *Q/m* of the *Dropped* would result in an increase in the repulsive electrostatic forces within the bulk particles and that in turn pushes more particles towards the column wall. This effect coupled with an increased image force would promote the wall layering effect and subsequently the extent of the fouling.

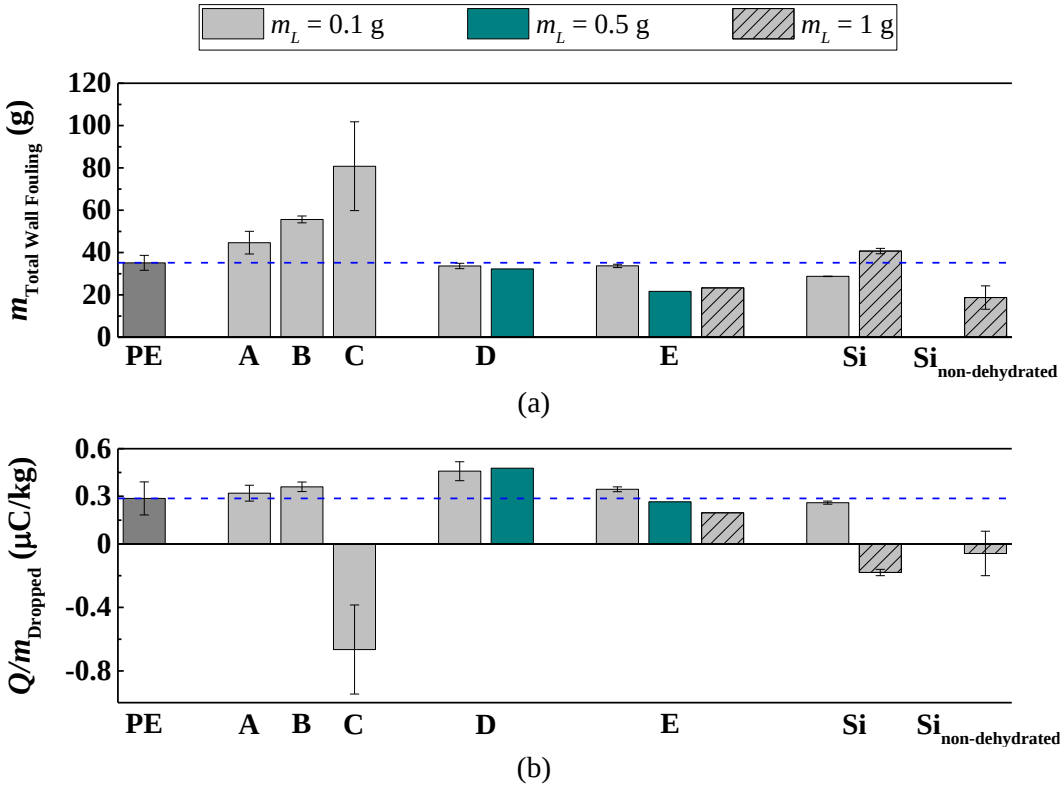

Figure 6-7 Effect of injection of m_L = 0.1 – 1 g CAs and Si on (a) total wall fouling magnitude and (b) *Q/m* of the *Dropped*. The blue dashed lines correspond to the average of results from the PE alone run (*Category I*).

Analyzing the *Dropped* particles charge polarity and magnitude (**Figure 6-7b**) in presence of CAs and Si suggests that the injected powders can be divided into three categories; they either increase the positivity of the *Dropped* by promoting positive charge polarity, decrease the positivity of the *Dropped* particles by promoting negative charge polarity within the bed, or do not influence the bed charge polarity significantly. Such an observation implies that the surface nature (i.e., surface chemistry) of the powders is of great importance in promoting a certain polarity within the fluidized bed. Of course, mass of the powders as well as their physical properties such as bulk density and size, which will eventually affect their number ratio to PE resin, are also important parameters. For example, silica to PE particle number ratio is 1/3 at silica m_L = 0.1 g, whereas it is 3/1 at silica m_L = 1 g at which a switch in *Dropped* charge polarity occurs. As such, powders A, B and C owing to their small sizes and low bulk densities (their bulk densities were not found from literature; however, their morphology suggested a lower bulk density compared to that of 400 m^3/kg for Si) are expected to show even stronger impact compared to Si. This expectation is in line with the results observed in **Figure 6-7a** where powders A, B and C showed a higher impact on the amount of wall fouling compared to other powders.

Based on the ability of the powders used in this study in promoting certain charge polarity, **Table 6-3** was prepared which categorizes the powders into positive or negative charge inducers. Within the studied fluidized bed, positive charge inducer powders shift the *Dropped* particles charge towards larger magnitudes and thus promote both the layering effect and particle migration towards the wall resulting in an increase in the wall fouling. Negative charge inducers counterbalance the positive charge of the bed bulk by shifting it close to zero and therefore mitigate the extend of the wall fouling. However strong negative charge inducers such as Powder C increase the charge magnitude on the negative side so much so that the electrostatic forces become strong again and that in turn results in promoting the wall fouling.

Table 6-3 Powders strength in inducing certain charge polarity within the PE fluidized bed.

Induced polarity	Negative ←						→ Positive
Powder	C	Si	$Si_{non\text{-}dehydrated}$	E	D	A	B

Prior to the experiments, it was hypothesized that the magnitude of the wall fouling and dominant charge polarity within the bulk of the bed would depend on the charge magnitude and polarity of the powders upon entering the fluidized bed through the pneumatic injection line. In fact, it was suspected that higher charge magnitude brought by powders into the fluidized bed promotes the wall fouling owing to a greater image and electrostatic forces formed between them and column wall as well as the fouled PE resin, respectively. However, comparing the powders *Q/m* upon entering the fluidized bed (**Figure 6-5c** and **Figure 6-5d)** with the wall fouling results in **Figure 6-7a** reveals a very weak or almost no relationship. This observation is quite clear for example with Si which although entered the fluidized bed with a significantly large *Q/m* (average of -6800 μC/kg), did not influence the extent of PE wall fouling as much as powder C that had an initial specific charge of +2 μC/kg. To further investigate this observation, three sets of experiments were performed where 0.1 g of powders B, C and Si were added into the bed via spatula so that a minimum possible charge (i.e., initial *Q/m*) would be introduced into the bed. The results of these experiments are presented in **Figure 6-8**. It is clear that both methods resulted in a similar wall fouling and *Dropped Q/m*. Thus, a conclusion can be made that the wall fouling does not necessarily depend on the charge magnitude or polarity introduced via injection line but rather

mostly depends on the generated charge within the bed after addition of powders which again confirms the importance of powders' surface chemistry.

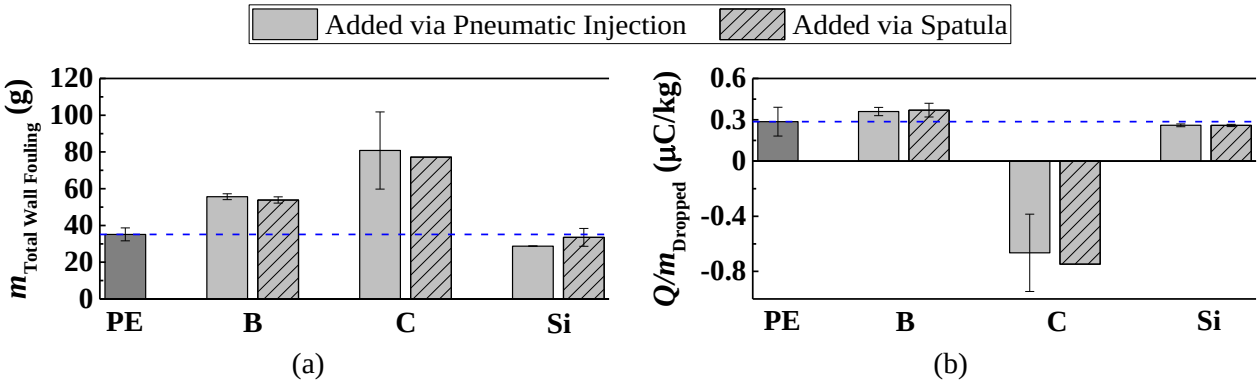

Figure 6-8 Effect of powder addition procedure (i.e., via pneumatic injection or spatula) on the (a) total wall fouling; and (b) *Q/m* of the *Dropped*. The blue dashed lines correspond to the average results from PE run.

The results obtained thus far suggested that the degree of wall fouling could be mitigated by manipulating the specific charge of *Dropped* region (i.e., reducing it to zero). To evaluate this hypothesis tests were designed aiming to vary the *Q/m* of the *Dropped*. By knowing that some of the CAs induced a negative polarity (e.g., powder C) inside the fluid bed while others induced a positive polarity (e.g., powder B), tests were carried out by injecting a mixture of two powders at varying concentrations. In these experiments 0.1 g of C was injected via pneumatic conveying line and different amounts of B were added via spatula. **Figure 6-9a** and **Figure 6-9b** agree with the hypothesis. A significant drop in the *Dropped Q/m* and the amount of wall fouling was observed for the mixture of C + 67% B which implies the induced positive and negative charges in the bulk of the bed have counterbalanced each other at a right concentration of each powder. Qualitative analysis of these three runs is provided in **Figure 6-9c–e**.

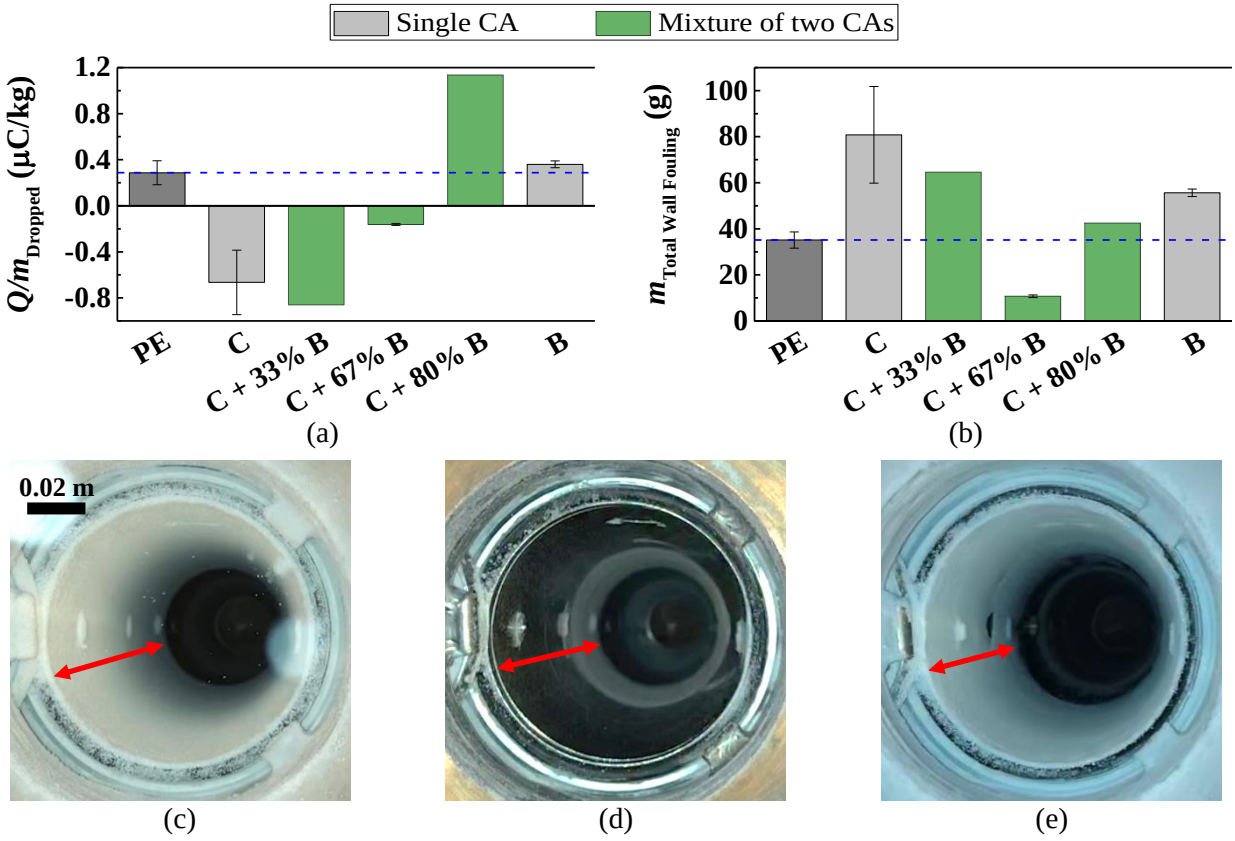

Figure 6-9 Effect of adding a mixture of two continuity additives (C and B) at different ratios on (a) total wall fouling; (b) *Q/m* of the *Dropped*. Images of wall fouling taken from the bottom of the fluidized bed for (c) C + 33% B, (d) C + 67% B and (e) C + 80% B. The red arrows represent the 0.3 m static bed height. The blue dashed lines correspond to the average results from PE run.

The distribution of the CAs and Si within the fluid bed was investigated by performing Scanning Electron Microscopy (SEM) analysis on samples collected from different regions of the bed for all the runs conducted in this work. Si at both mass loadings of 0.1 and 1 g was detected within the three regions of *Dropped*, *Wall – Bottom* and *Fines*. As for the runs with CAs, SEM imaging could not detect the CAs among the PE resin due to the similarities in their morphology and chemical structure (i.e., both having hydrocarbon chains). Low concentration of metal elements in CAs was another reason that made it difficult for them to be detected. As such, Energy Dispersive X-ray (EDX) analysis was used. For instance, for the C + 67% B samples presence of B was confirmed in *Wall – Bottom* and *Fines* regions by detecting traces of aluminum. In conclusion, SEM – EDX analysis confirmed that injected powders were distributed to various regions of the bed and were found entrapped in the defects of the PE resin in the *Dropped* region, adhered on the PE resin surface specifically within the *Dropped*, *Wall – Top* and *Wall – Bottom* regions, and appeared as individual particles mostly in *Fines*.

Since the degree of particles charging and the fouling was found to be influenced by the addition of the CAs and Si, it was important to evaluate the particles charge distribution within the wall layer and fines. As can be seen in **Figure 6-10**, presence of positive and/or negative charge inducers, depending on their type and concentrations, influenced the polarity of the *Wall – Bottom* and *Wall – Top* layers by making them dominantly positive or negative, respectively. As for the $Si_{non\text{-}dehydrated}$, although the *Wall – Top* became negative a variation was observed in the charge polarity of the *Wall – Bottom*. The reason for this variation which had also been observed in the *Dropped* region (**Figure 6-7b**) will be discussed later in the manuscript.

Considering the *Q/m* magnitude and mass of the particles on the *Wall – Bottom* and the *Wall – Top*, it can be noticed that a greater *Q/m* magnitude does not necessarily correspond to a larger wall fouling or vise versa. An example would be the case of C + 67% B for which the *Q/m* of both wall layers were greater than that for powder C despite the fact that it had the least wall fouling. Two important points can be highlighted based on this observation. First, in order for particles to form a layer on the wall they must possess a certain level of *Q/m* so that electrostatic and image forces become dominant making the particles to migrate to the wall region. In other words, lower mass on the wall does not correspond to particles having smaller *Q/m*. Second, is the possibility of bipolarly charged particles existing within the wall layer which could potentially decrease the layer net *Q/m*. An experiment was carried out in support of detecting bipolarly charged particles where 0.1 g of powder B was injected into the bed and a charged particle separator, as described in our previous works [34] and shown in **Figure 6-11a**, was used to collect the wall particles to measure the particles charge distribution. For this experiment, the *Wall* layer dislodging was divided into four segments of equal height. Bipolar charging was clearly observed for this experiment where same size particles gain charges with opposite polarities (**Figure 6-11b**). This is a significant finding in relation to commercial ethylene gas-phase fluidized beds where measuring only the electrostatic charge close to the reactor wall via ball probes will not be an indication of the sheeting formation or its extent.

Analysing the *Q/m* of the *Fines* in **Figure 6-10** and comparing it to **Figure 6-7b** reveals an inverse relationship between the powders induced charge polarity in the *Dropped* and the charge polarity of *Fines*. For example, powders A, B or D which promoted the positivity of *Dropped*, resulted in promoting the negativity of the *Fines*. Such an observation, again, is a clear indication of bipolar charging within the bed. Except for the case of C + 67% B and runs with m_L = 1 g, for which an

increase in the *Fines* mass was observed, other cases did not differ significantly with respect to the entrained mass compared to that of the PE run. Obviously, the increase in the entrained mass is partially due to addition of the powders, a portion of which would entrain. Although powders D and E are not expected to entrain due to their larger sizes. Another contributing reason, especially for C + 67% B, would be entraining those PE resins which have gone through a contact with the injected powders and have partially lost their surface charge.

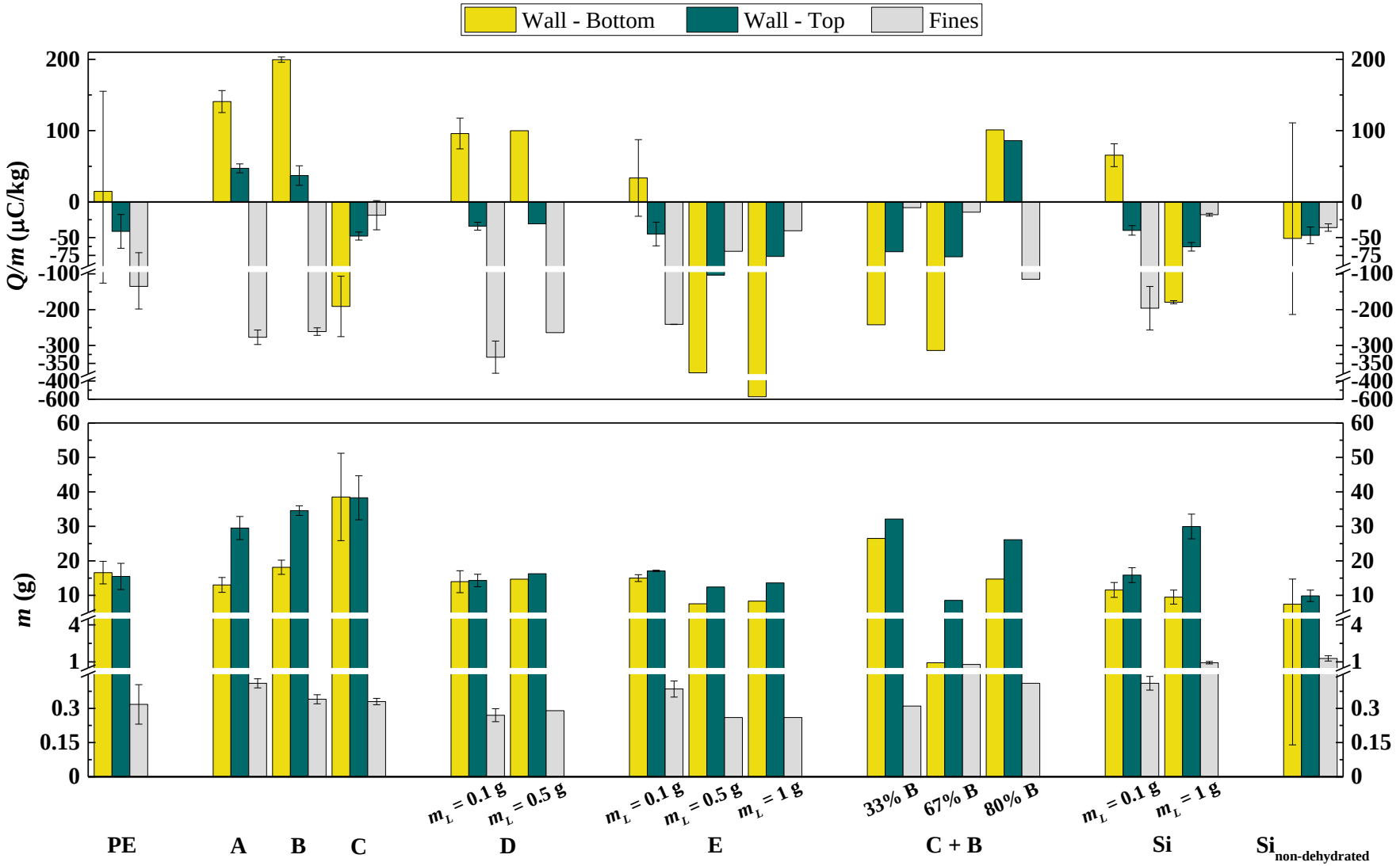

Figure 6-10 Effect of injection of CAs and Si at m_L = 0.1 to 1 g on the *Q/m* and mass of the *Wall – Bottom*, *Wall – Top* and *Fines*.

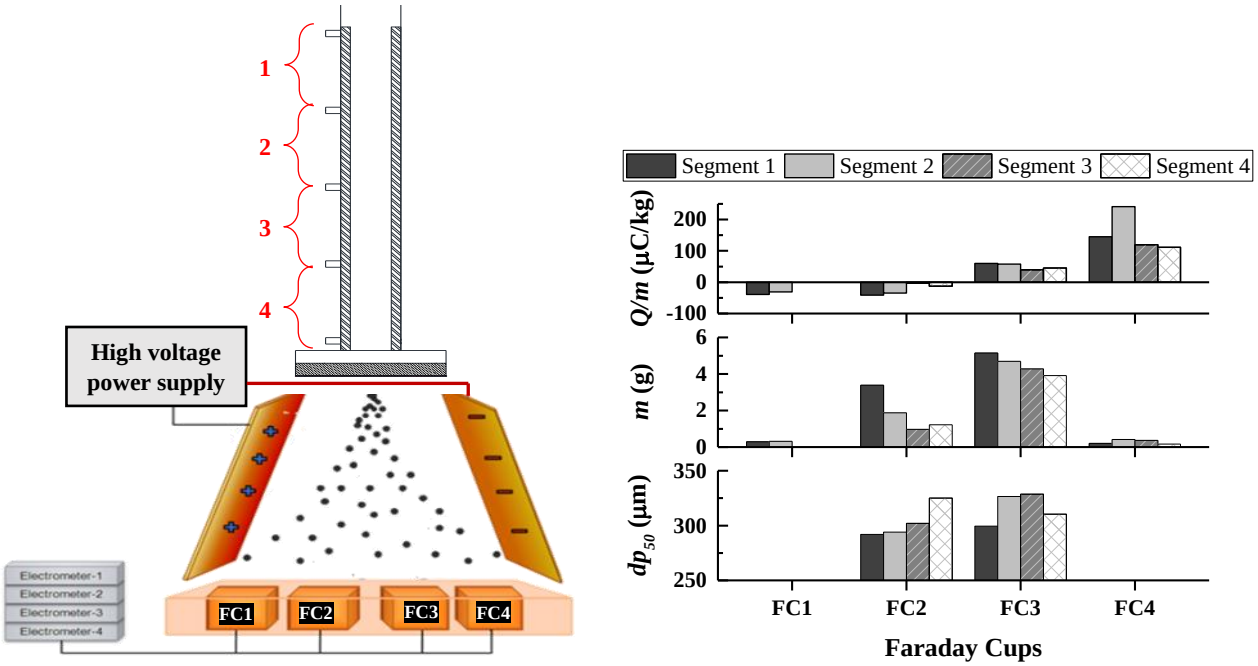

(a) (b)

Figure 6-11 Evaluation of bipolar charging for the case of 0.1 g of B added to the PE bed. (a) Schematic of the wall particles collection using the charged particle separator apparatus; and (b) specific charge, mass, and size distribution of wall particles. FC1 to 4 are referred to Faraday cages 1 to 4 as seen in (a).

The knowledge developed thus far implies that the generated charge polarity within the bed after addition of the CAs and Si strongly depends on the powders surface nature and contacts occurring inside the bed between these powders and the PE resin. To assist in better explaining the charge polarity that the powders develop in contact with the PE, a bench-scale experiment was designed where 0.1 g of the powders B, C and Si were shaken individually in a cylindrical cup made of LDPE (0.05 m in height and 0.025 m in inner diameter). Powders B and C were specifically chosen since they showed stronger impact compared to other CAs. Si was selected due its presence in almost every catalyst type. The cup was shaken using a shaker (Lab-Line Model 4628) at a speed of 300 rpm for 2 minutes. The shaken powders were then poured into a bench-scale Faraday cage to measure their *Q/m*. Each condition was repeated three to four times. Results presented in **Figure 6-12** show that Si acquired negative charge while powder C became positively charged in contact with PE cup wall. Out of four trials for powder B, two became negatively charged and two became positively charged. Fouling was observed inside the cup ranging from 20, 30 to 80 wt.% for Si, B and C, respectively. It is worth mentioning that for both B and C, the fouled particles were observed to carry a charge polarity opposite to those recovered in the Faraday cage.

In relation to the fluidized bed, the amount of fouling within the PE cup could be an indication of the powders capability in coating the PE resin and thus dominating their own charge polarity. For example, B and C, owing to their small size, can either adhere on the PE surface or entrap on the defects of PE resin thereby dominating their own charge acquired due to contact with PE. The non-adhered portion, which could at times be of an opposite polarity, could then entrain from the column alongside the PE fines and influence the charge polarity of *Fines* by driving it towards a polarity opposite to that of the bulk. Obviously D and E with their large size were not expected to entrain, even at higher mass loadings, and influence the mass of *Fines* (as can be seen in **Figure 6-10**); whereas they are mostly expected to remain un-attached to the PE particles inside the bulk of the bed or entrap within the particles accumulated in the wall layers. Thus, larger size particles are expected to have less influence in affecting the mass and *Q/m* of various bed regions.

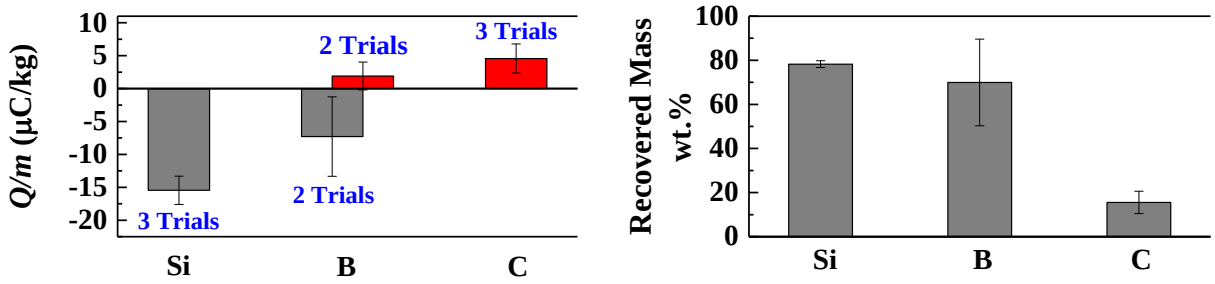

Figure 6-12 (a) *Q/m* and (b) recovered mass of Si, B and C after being shaken in a LDPE cup for 2 minutes.

6-3-1-2 Effect of Injection Time

Another complementary test that was performed was injecting B 30 minutes into the fluidization period (t_{inj} = 30 min). This test was performed to simulate the CAs injection in a commercial process where they are being added into the reactor periodically. This experiment also provided a comparison between injecting B at t_{inj} = 0 min in which no fouling had formed on the column wall and injecting at t_{inj} = 30 min in which the wall fouling had already formed. To provide a reference point on the amount of fouled mass on the wall after 30 minutes, a test with pure PE resin was also performed for the same duration. As shown in **Figure 6-13**, after 30 minutes of fluidizing pure PE the wall fouling was measured to be equal to that of the 60 minutes run. Changing the injection time to t_{inj} = 30 min, statistically, was observed to have no influence on the final wall fouling. Other parameters such as *Q/m* and mass of *Dropped*, *Wall – Bottom*, *Wall – Top* and *Fines* also remained unchanged.

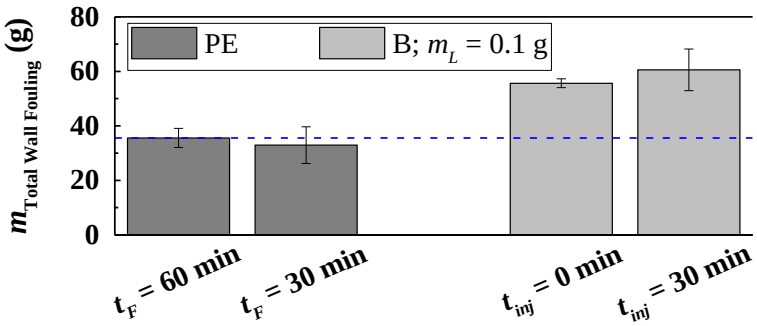

Figure 6-13 Effect of PE fluidization time (i.e., for 30 and 60 minutes) and 0.1 g of B injection time (i.e., at 0 and 30 minutes into fluidization period) on the wall fouling magnitude.

6-3-2 Categories IV

Thus far, the investigated conditions have only considered presence of either CA(s) or silica within the fluidized bed. However, in a commercial reactor, both of these powders are present; silica as the catalyst support and CA either doped on the silica or added separately. Thus, to be even more similar to the industrial condition, *Category IV* experiments were designed and performed by adding both Si and CA into the PE fluidized bed. These experiments were carried out in two mass loadings of 0.1 and 1 g using powders A and B. Two set of experiments were performed where in one the CAs were doped on Si and in second Si and CAs were added separately into the fluidized bed (Si via pneumatic conveying and CAs via spatula). The samples of CA doped on silica, namely Si – 1% A, Si – 3% B, and Si – 1% A – 3% B, had an initial *Q/m* of -14.6 ± 0.4, -14.7 ± 0.1 and -11.2 ± 0.2 μC/kg, respectively. The number of pneumatic conveying injections prior to connecting the conveying line to the fluidized bed were ten and five for 0.1 and 1 g mass loadings, respectively. The *Q/m* of these sample upon entering the fluidized bed are presented in **Figure 6-14**. Increasing the amount of CA in the samples was observed to slightly reduce the sample *Q/m* magnitude.

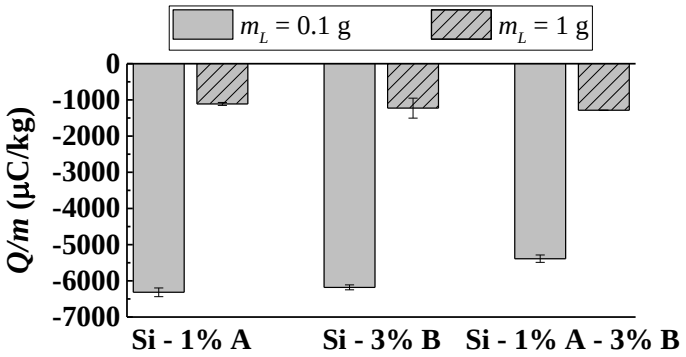

Figure 6-14 *Q/m* of the samples upon entering the fluidized bed (i.e., 6th or 11th injections for m_L of 1 and 0.1 g) for CAs doped on silica.

The fluidizing results for mass loadings of 0.1 g are presented in **Figure 6-15a** and **Figure 6-15b**. For comparison purpose, results of 0.1 g of same powders injected individually are also provided in **Figure 6-15**. For the second set of these experiments, additional tests were also performed by keeping the Si mass loading constant at 0.1 g and varying the concentration of CAs. This was done to investigate effects of different ratios of Si and CAs on the bed electrification. Analyzing the results shows an expected trend whereby increasing the concentration of a positive charge inducer powder in the system gradually overcomes the effect induced by Si as being a negative charge inducer. A slight reduction in both the wall fouling and the *Dropped Q/m* magnitude was detected for the case Si – 1% A. For the case where a constant ratio of Si to B was added into the fluidized bed in two different ways (i.e., Si – 3% B and Si + 3% B) no difference was observed in neither the wall fouling nor the *Dropped Q/m*. However, results obtained from the second set of experiments suggest that adding the CA separately and allowing it to move freely within the bed could result in a stronger impact compared to the case where CA is fixed on the silica.

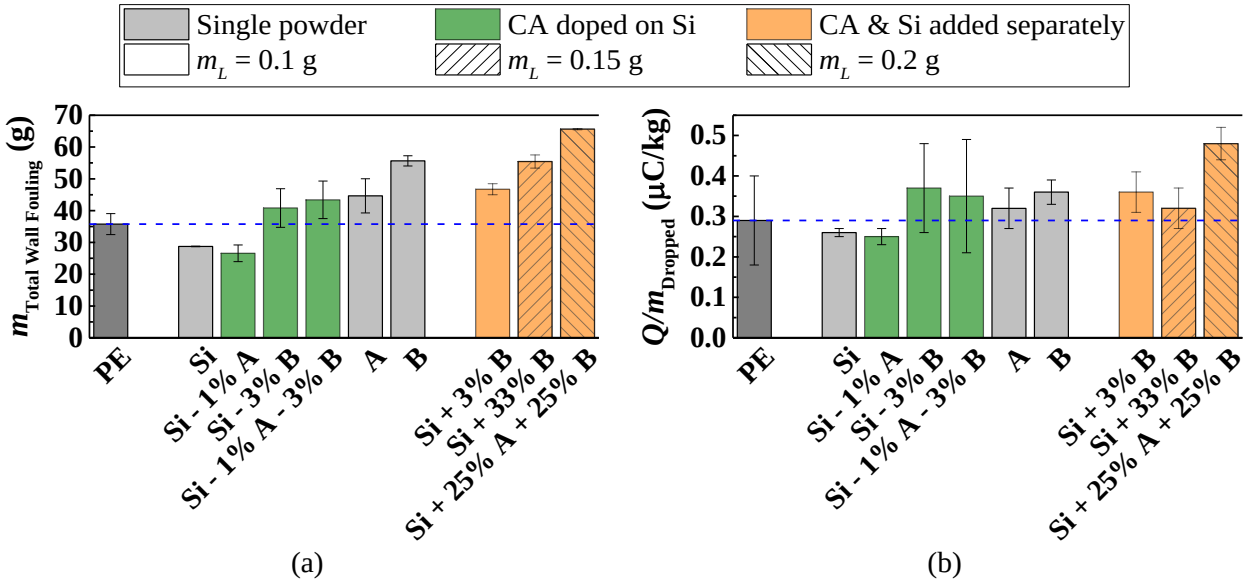

Figure 6-15 Effect of injection of powders belonged to *Category IV* at m_L = 0.1 – 0.2 g on (a) total wall fouling and (b) *Q/m* of the *Dropped*. The blue dashed lines correspond to the average results from PE run.

Mass loading of 1 g was also examined with the results provided in **Figure 6-16** for the two sets of experiments. Same as for the m_L = 0.1 g, higher concentrations of A and B dominated the Si effect and not only did increase the wall fouling but also switched the *Dropped* charge from being negative for Si to positive. A significant reduction in the wall fouling was observed for the case of Si – 1% A suggesting an optimum ratio so that CA and Si counteract and decrease the *Dropped* net charge and thus the wall fouling. The corresponding image of this condition is shown in **Figure 6-16c**. The other experiment was conducted by separately adding Si + 1% B for which the wall fouling further dropped compared to Si – 1% A and became approximately 12 g. The corresponding image of Si + 1% B is shown in **Figure 6-16d**.

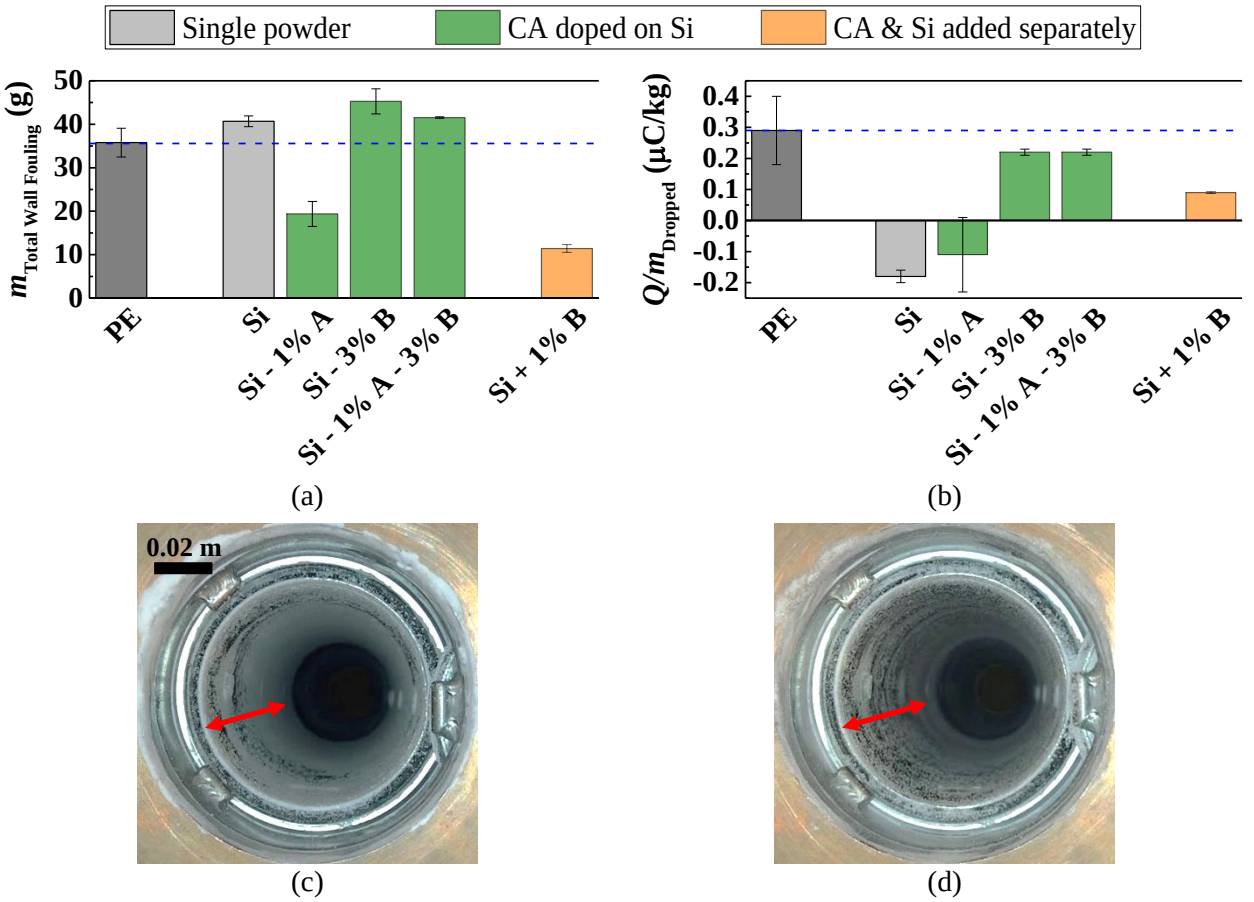

Figure 6-16 Effect of injection of powders belonged to *Category IV* at m_L = 1 g on the (a) total wall fouling and (b) *Q/m* of the *Dropped*. The blue dashed lines correspond to the average results from PE run. Images of wall fouling taken from the bottom of the fluidized bed for (c) Si – 1% A, (d) Si + 1% B. The red arrows represent the 0.3 m static bed height.

The trend for the net *Q/m* and mass of the particles in various regions of the bed for *Category IV* runs were found to be in line with the explanation provided earlier. A clear trend was observed between the wall polarity and CA concentration, whereby increasing the amount of A and/or B dominated a positive charge polarity on the *Wall – Bottom* and *Wall – Top* layers. As for the *Fines*, an increase was observed in their mass which was mostly attributed to a higher mass loading injected to the bed.

6-3-3 Summary

A very important conclusion that can be drawn based on all the experiments would be that in a commercial reactor, the required concentration of CAs within the reactor must be carefully determined for them to be influential in mitigating the sheeting formation. Results in this study have made it clear that adding too much of any CA might not only fail to control/reduce

electrostatic charge build up and sheeting within the reactor but also could worsen the situation. Also, attention must be paid to avoid adding CAs that promote a charge polarity similar to that of the catalyst.

Figure 6-17 which summarizes all the tested conditions in this work clearly shows that reducing the *Dropped Q/m* deviation from zero significantly reduces the total wall fouling. Considering *Category IV* experiments, where both the amorphous silica support and CA were added to the PE fluidized bed, to be the closest condition to a commercial process, the optimum ratio of the CA to silica at which the wall fouling reached a minimum value was suggested to be 1 to 99 with the continuity additive having a concentration of 10 ppmw in the fluidized bed.

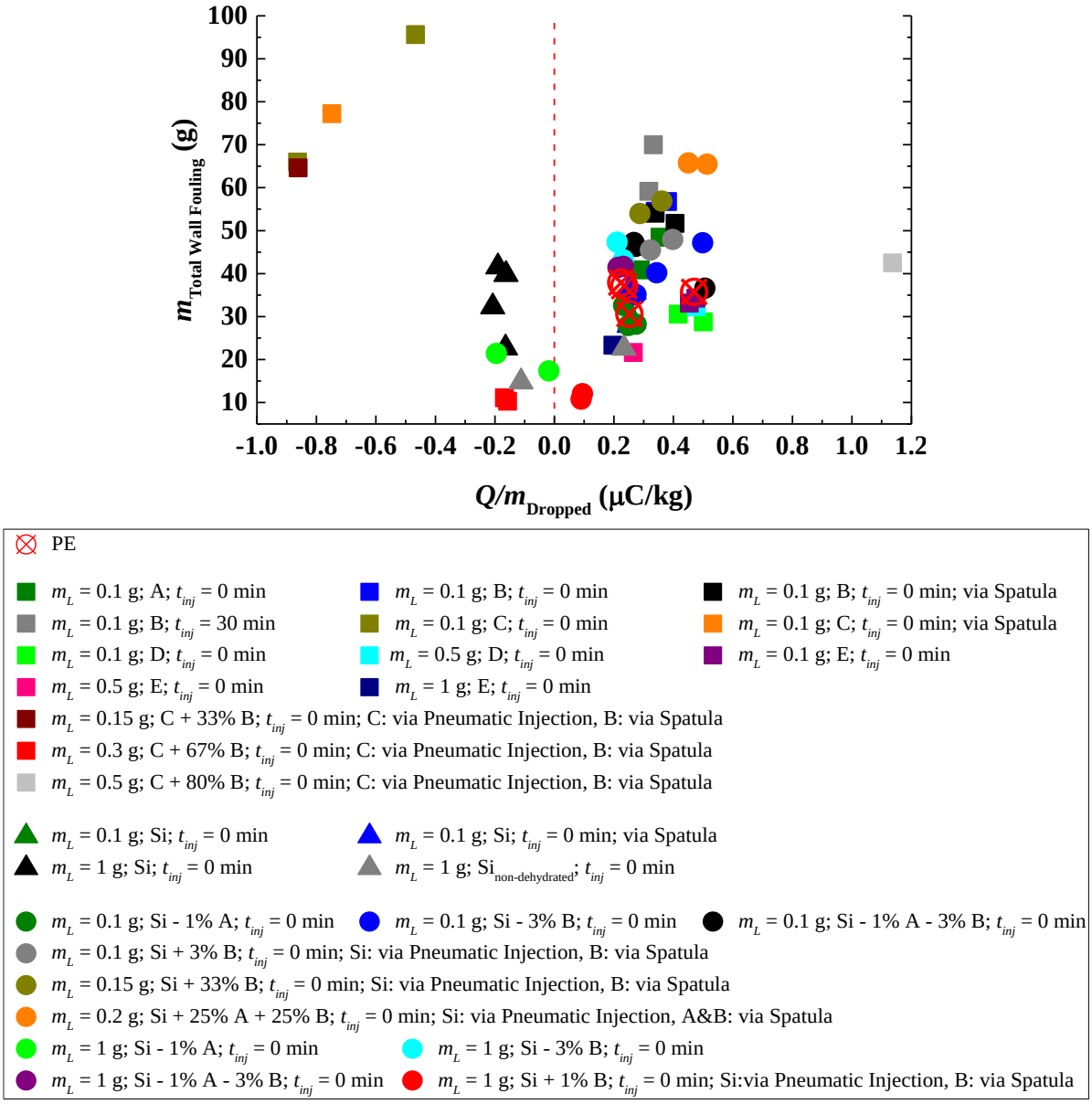

Figure 6-17 Summary of the results showcasing the relationship between the *Dropped Q/m* magnitude and the total wall fouling.

6-3-3-1 Charging Mechanism

As mentioned earlier, understanding the surface chemistry of the materials involved in this work are of great importance in explaining the dominant charging mechanisms. It is well known that solid materials, based on their electrical conductivity, are divided into three categories: conductors, semiconductors, and insulators. The materials used in this work include stainless steel (as the conveying line and fluidizing column) which is electronically conductive as well as PE and other tested powders all of which are insulators. Identifying the charging mechanism for a conductive

material involved in contact charging is quite straightforward and is believed to be dominantly by electron transfer. For insulator materials, however, a number of mechanisms have been proposed. Ionic nature, surface acidity/basicity (i.e., pK_a/pK_b), affinity to adsorb H^+/OH^- (i.e., proton/hydroxide affinity), possessing electron donating/withdrawing functional groups (amide or halide, respectively) or simply material transfer in form of small patches are criteria that are proposed throughout the years alongside electron transfer [35,36,45–52,37–44]. There is an overlap in some cases between these criteria.

Ion transfer is a charge transfer mechanism proposed for contacts between the ionic insulators. It has been observed that insulator surfaces which are covalently functionalized with ionic compounds develop a charge of a similar polarity to that of the covalently bonded side of the ionic compound after contact [38–43]. As for the non-ionic solids, acidity/basicity of the solids' surface or their proton affinity (PA) were proposed as one of the driving forces for charge transfer [43–47]. Solids with an acidic surface (such as SiO_2, TiO_2 or sulfonated polystyrene) are typically regarded as materials with a high work function with a tendency to develop a negative charge by attracting electron pairs or adsorbing OH^- ions (i.e., Lewis definition), or losing H^+ ions (i.e., Bronsted definition) [45–47,53–55]. In contrast, solids with a basic surface (such as MgO, Al_2O_3, or De-acidite FF) would develop a positive charge by losing electron pairs or adsorbing H^+ ions (i.e., Lewis definition), or losing OH^- (i.e., Bronsted definition) [45–47,53–55]. Transferring H^+/OH^- is one specific case for ion transfer charging mechanism.

Another proposed charging mechanism for non-ionic solids is transferring of mobile H^+/OH^- ions resulted from the moisture present either in the environment or as separated patches adsorbed on the surface of the solids (even those with a high hydrophobic nature) [42,50,56]. However, in a separate study, charge transfer was proven to be independent of the moisture presence; although moisture was observed to promote the transferred charge magnitude [57].

The seven different types of powders were tested in this work are summarized in **Table 6-4** with their surface properties, chemical structure, and developed charge polarity within the pneumatic conveying line and bulk of the fluidized bed. It must be mentioned that due to the axial movement of the powders within the conveying line, the dominant contact inside the tube is expected to be particle–wall. Within the fluidized bed, the possibility of these particles contacting each other is considered to be very low due to their low concentrations. As such, the dominant contacts they

experience within the fluidized bed are expected to be with PE resin and stainless steel column wall.

As can be noted from **Table 6-4**, both A and D became positively charged within the pneumatic conveying line and promoted the positive charge polarity within the bulk of the bed. This could be due to existence of an electron donating amine group which essentially lowers the effective work function of these two powders in comparison with PE and stainless steel. Both Si and $Si_{non\text{-}dehydrated}$ were observed to be negative charge drivers in both systems with $Si_{non\text{-}dehydrated}$ having a weaker impact. With a high band gap of approximately 9 eV [58], a high electronegativity of 4.26 [59], and an acidic nature [45,46,53,54], silica is an insulator with a tendency of attracting negative charge. Respecting the contacts between the silica and PE resin, it is expected that the silica, owing to its high electronegativity as well as its acidic nature, attracts electrons from the PE resin or adsorbs OH^- from the environment or PE resin surface and becomes negatively charged. Presence of hydroxide groups on the non-dehydrated silica surface is expected to reduce the acidity of the surface and that in turn could result in observing less charging within the conveying line and less influence within the fluidized bed from this powder [60]. Adsorbed moisture on the silica surface is also expected to reduce the tendency of silica to become highly negatively charged which agrees with what observed in this study.

Table 6-4 Summary of properties of powders used in this work.

Surface characteristic	Chemical structure	Developed charge polarity within	
		Pneumatic conveying	Fluidized bed
Non-ionic	**A** 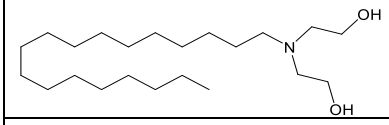	+	+
	D 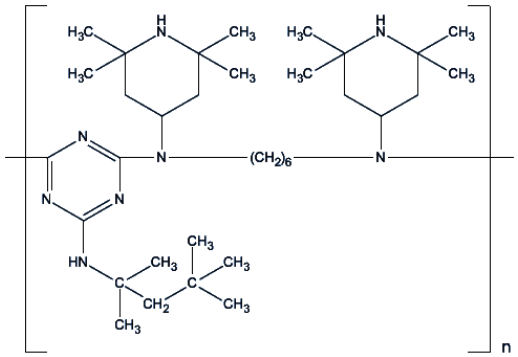	+	+
	Si 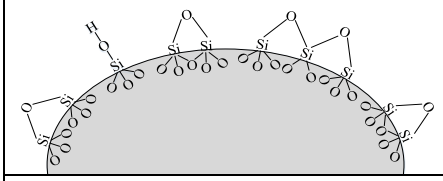	−	−
	$Si_{non\text{-}dehydrated}$ 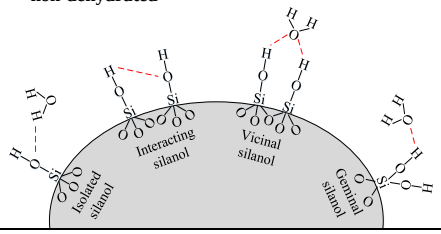	−	−
Ionic	**B** 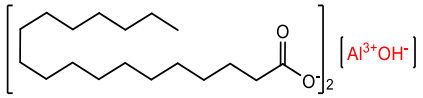	−	+
	C 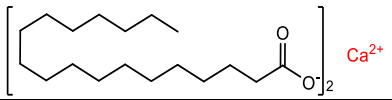	+	−
	E 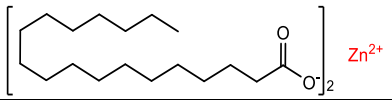	+	−

As for the ionic compounds, C and E behaved similar with respect to the developed charge polarity, whereas B behaved oppositely. Such difference is expected to be due to the $[Al^{3+}–OH^{-}]^{2+}$ group

which could give rise to the acidic nature of the compound. From **Table 4**, it can also be noticed that the charge that the ionic powders B, C and E developed during pneumatic conveying and within the fluidized bed were of opposite polarities. In addition, from the bench-scale shake test experiments (shown in **Fig. 12**) it was observed that B and C developed bipolar charging upon contacting the LDPE cup. All these findings suggest for ion transfer to be a contributing charge transfer mechanism here. To investigate the ion transfer mechanism, samples of B, C and E were collected after the shake test as well as pneumatic conveying and were analyzed under X-ray Photoelectron Spectroscopy (XPS). Although no meaningful difference was observed in atomic concentrations of elements (specifically metal cationic head) before and after the experiments; yet ion transfer in the form of H^+/OH^- is expected to contribute to the charging mechanism within the conveying line. XPS analysis was not performed for the samples collected from fluidized bed due to uneven distribution of powders making the results analysis unreliable. However, EDX analysis on the samples collected from C + 67% B run detected a very small trace of aluminum (lower than what should be for aluminum distearate) on the surface of some of the PE resins. Although the detected aluminum could be related to the presence of aluminum-containing activators on the catalyst surface, it is critical to still consider material and/or ion transfer as a possible charge transfer mechanism. Therefore, ion/material transfer is proposed for the ionic compounds which results in a significant bipolar charging.

6-4 Conclusions

Reactor fouling/sheeting in ethylene gas-phase polymerization fluidized beds has been a challenge for decades with the development of advanced catalyst systems despite the mitigation techniques of CAs'. Thus, the main objective of this work was to carry out a comprehensive experimental program to determine the exact role of some of the most common CAs mentioned in public sources. The ultimate goal is to propose an approach to control and possibly reduce the fouling at least in a cold flow system. This work concludes that the degree of wall fouling directly relates to the net specific charge of particles in the bulk of the fluidized bed, and thus managing to reduce this net charge will lessen the formation and progression of the wall fouling. Adding a very small amount of continuity additives (as low as 1 ppmw) was observed to have a potential to significantly alter the dominant charge polarity and magnitude within the bulk of the bed and in turn mitigating the amount of wall fouling.

Such an observation clearly emphasizes the significance of having knowledge of the solids surface chemistry involved in the process and its utilization as a predictive tool in determining the charging mechanism of the continuity additives in contact with the PE resin inside the rector. Knowing the charging mechanism enables the prediction of the dominant charge polarity within the reactor resulting in effectively controlling the reactor sheeting.

Additionally, the *Dropped Q/m* and the extent of wall fouling were found to be independent of the continuity additives charge upon entering the fluidized bed. This again implies the significance of surface nature of the added powders over the charge that they carry.

Size of the continuity additives and their freedom of movement were also other parameters which found to be affecting the results. Larger particle size and being doped on the silica showed a lesser impact with respect to altering the bed bulk net charge polarity and magnitude compared to smaller size particles and when they were added separately to the bed.

Electron transfer was proposed to be the dominant charge transfer mechanism for Si as well as A and D both within the conveying line and within the fluidized bed upon contacting the PE resin. However, for the ionic compounds (i.e., B, C, and E) ion transfer was proposed as a dominant contributing charge transfer mechanism upon contacting the PE resin and the stainless steel wall.

Acknowledgment

Financial support from Univation Technologies, LLC (USA) and The Natural Sciences and Engineering Research Council of Canada (NSERC) is acknowledged with gratitude.

References

[1] R.O. Hagerty, M.E. Muhle, A.K. Agapiou, C.-T.I. Kuo, M.G. Goode, F.D. Hussein, R.B. Pannell, J.F. Szul, Method for controlling sheeting in gas phase reactors, US Patent 7985811 B2, 2011.

[2] B.D. Fulks, S.P. Sawin, C.D. Aikman, J.M. Jenkins, Process for reducing sheeting during polymerization of alpha-olefins, US Patent 4532311, 1985.

[3] J.R. Chirillo, K.C. Kimbrough II, P.E. McHattie, Method for reducing sheeting during polymerization of alpha-olefins, US Patent 4855370, 1989.

[4] M.G. Goode, D.M. Hasenberg, T.J. McNeil, T.E. Spriggs, Method for reducing sheeting during polymerization of alpha-olefins, US Patent 4803251, 1989.

[5] G.-H. Song, A.S. Rhee, G.R. Lowder, Method for reducing sheeting and static charges during polymerization of ethylene polymers, US Patent 5391657, 1995.

[6] K.J. Cann, J.H. Moorhouse, P.A. Khokhani, T.T. Tamargo, K.R. Gross, M.G. Goode, Chromium-based catalyst compositions for olefin polymerization, US Patent 10266618 B2, 2019.

[7] L.H. Kiu, D.F. Hussein, C.C. Williams, Process for controlling static in polymerizations utilizing metallocene catalysts, EP Patent 0811638 A2, 1997.

[8] R.O. Hagerty, M.E. Muhle, A.K. Agapiou, C.-T. Kuo, M.G. Goode, D.F. Hussein, R.B. Pannell, J.F. Szul, Method for controlling sheeting in gas phase reactors, US Patent 2005/0148742 A1, 2005.

[9] R.B. Pannell, D.M. Glowczwski, C.-I. Kuo, T.R. Lynn, D.F. Hussein, P.A. Cao, W.R. Mariott, M.D. Awe, Continuity compositions and methods of making and using the same, US Patent 9676885 B2, 2017.

[10] D.F. Hussein, M.E. Muhle, Additive for polyolefin polymerization processes, WO Patent 2010/080870 A2, 2010.

[11] R.O. Hagerty, M.E. Muhle, A.K. Agapiou, C.-I. Kuo, M.G. Goode, D.F. Hussein, R. Pannell, J.F. Szul, Method for controlling sheeting in gas phase reactors, EP Patent 1699830 B1, 2005.

[12] M. Namkajorn, A. Alizadeh, E. Somsook, T.F.L. McKenna, Condensed-mode cooling for ethylene polymerization: The influence of inert condensing agent on the polymerization rate, Macromol. Chem. Phys. 215 (2014) 873–878.

[13] T.F.L. McKenna, Condensed Mode Cooling of Ethylene Polymerization in Fluidized Bed Reactors, Macromol. React. Eng. 13 (2019) 1800026.

[14] A. Alizadeh, M. Namkajorn, E. Somsook, T.F.L. McKenna, Condensed Mode Cooling for Ethylene Polymerization: Part I. The Effect of Different Induced Condensing Agents on

Polymerization Rate, Macromol. Chem. Phys. 216 (2015) 903–913.

[15] Y. Banat, Improved gas phase olefins polymerization process operating in condensing mode, WO Patent 2017/114930 A1, 2017.

[16] D.A. Wright, J.R. Parrish, J.L. Swecker, M.G. Goode, Methods and systems for catalyst delivery, US Patent 9023958 B2, 2015.

[17] A.G. Wonders, G.E. Moore, R.R. Ford, J.D. Daily, K.A. Dooley, J.J. Garcia, Suppression of fines forming in a fluidized bed ethylene polymerization process, WO Patent 97/14721, 1997.

[18] R.B. Painter, B.J. Garner, G.-H. Song, Gas phase fluidized bed polyolefin polymerization process using gas or gas-solids tangential flow, US Patent 5428118, 1995.

[19] S.J. Rhee, L.L. Simpson, Fluidized Bed Polymerization Reactors, US Patent 4933149, 1990.

[20] A.K. Agapiou, C.-I. Kuo, Method for preparing a supported catalyst system and its use in a polymerization process, US Patent 6482903 B1, 2002.

[21] K. Dong, Q. Zhang, Z. Huang, Z. Liao, J. Wang, Y. Yang, Experimental investigation of electrostatic effect on bubble behaviors in gas-solid fluidized bed, AIChE J. 61 (2015) 1160–1171.

[22] Y. Rao, P. Cai, K.J. Cann, F.D. Hussein, W.R. Mariott, P.A. Cao, Supported catalyst with improved flowability, US Patent 10280283, 2019.

[23] C.-I. Kuo, G.G.H. Patel, R.E. Pequeno, B.J. Savatsky, F.D. Hussein, Continuity additive for polyolefin polymerization processes, US Patent 9221936 B2, 2015.

[24] G. Hendrickson, Electrostatics and gas phase fluidized bed polymerization reactor wall sheeting, Chem. Eng. Sci. 61 (2006) 1041–1064.

[25] R.B. Pannell, E.J. Markel, A.K. Agapiou, Method for seed bed treatment before a polymerization reaction, US Patent 8039562 B2, 2011.

[26] G.E. Klinzing, A review of pneumatic conveying status, advances and projections, Powder Technol. 333 (2018) 78–90.

[27] A. Sowinski, F. Salama, P. Mehrani, New technique for electrostatic charge measurement in gas-solid fluidized beds, J. Electrostat. 67 (2009) 568–573.

[28] A. Sowinski, L. Miller, P. Mehrani, Investigation of electrostatic charge distribution in gas-solid fluidized beds, Chem. Eng. Sci. 65 (2010) 2771–2781.

[29] M. Taghavivand, B.J. Cho, P. Mehrani, A. Sowinski, Electrostatic charging behaviour of a silica powder during pulse pneumatic conveying, Powder Technol. 366 (2020) 119–129.

[30] A.R. Miller, Fluid bed polymerization catalyst injection system, US Patent 3790036, 1974.

[31] K. Choi, M. Taghavivand, L. Zhang, Experimental studies on the effect of moisture content and volume resistivity on electrostatic behaviour of pharmaceutical powders, Int. J. Pharm. 519 (2017) 98–103.

[32] M. Taghavivand, P. Mehrani, A. Sowinski, K. Choi, Electrostatic charging behaviour of polypropylene particles during pulse pneumatic conveying with spiral gas flow pattern, Chem. Eng. Sci. 229 (2021) 116081.

[33] D. Song, P. Mehrani, Mechanism of particle build-up on gas-solid fluidization column wall due to electrostatic charge generation, Powder Technol. 316 (2017) 166–170.

[34] F. Salama, A. Sowinski, K. Atieh, P. Mehrani, Investigation of electrostatic charge distribution within the reactor wall fouling and bulk regions of a gas-solid fluidized bed, J. Electrostat. 71 (2013) 21–27.

[35] K.-E. Byun, Y. Cho, M. Seol, S. Kim, S.-W. Kim, H.-J. Shin, S. Park, S. Hwang, Control of triboelectrification by engineering surface dipole and surface electronic state, ACS Appl. Mater. Interfaces. 8 (2016) 18519–18525.

[36] C. Xu, Y. Zi, A.C. Wang, H. Zou, Y. Dai, X. He, P. Wang, Y.C. Wang, P. Feng, D. Li, Z.L. Wang, On the electron-transfer mechanism in the contact-electrification effect, Adv. Mater. 30 (2018) 1706790.

[37] Z.L. Wang, A.C. Wang, On the origin of contact-electrification, Mater. Today. 30 (2019) 34–51.

[38] A. Diaz, D. Fenzel-Alexander, D. Wollmann, J.A. Barker, Importance of Dissociated Ions

in Contact Charging, Langmuir. 8 (1992) 2698–2706.

[39] A.F. Diaz, J. Guay, Contact charging of organic materials: Ion vs. electron transfer, IBM J. Res. Dev. 37 (1993) 249–260.

[40] A.F. Diaz, Contact electrification of materials: The chemistry of ions on polymer surfaces, J. Adhes. 67 (1998) 111–122.

[41] A.F. Diaz, R.M. Felix-Navarro, A semi-quantitative tribo-electric series for polymeric materials: the influence of chemical structure and properties, J. Electrostat. 62 (2004) 277–290.

[42] L.S. McCarty, G.M. Whitesides, Electrostatic charging due to separation of ions at interfaces: Contact electrification of ionic electrets, Angew. Chemie - Int. Ed. 47 (2008) 2188–2207.

[43] M.W. Williams, Triboelectric charging of insulating polymers-some new perspectives, AIP Adv. 2 (2012).

[44] J.H. Clint, T.S. Dunstan, Acid-base components of solid surfaces and the triboelectric series, Europhys. Lett. 54 (2001) 320–322.

[45] R.P.N. Veregin, M.N.V. McDougall, M.S. Hawkins, C. Vong, V. Skorokhod, H.P. Schreiber, A bidirectional acid-base charging model for triboelectrification: Part 1. Theory, J. Imaging Sci. Technol. 50 (2006) 282–287.

[46] R.P.N. Veregin, M.N.V. McDougall, M.S. Hawkins, C. Vong, V. Skorokhod, H.P. Schreiber, A bidirectional acid-base charging model for triboelectrification: Part II. Experimental verification by inverse gas chromatography and charging of metal oxides, J. Imaging Sci. Technol. 50 (2006) 288–293.

[47] J.A. Medley, Fractional electrification of polar polymers, Nature. 171 (1953) 1077.

[48] D.J. Lacks, T. Shinbrot, Long-standing and unresolved issues in triboelectric charging, Nat. Rev. Chem. 3 (2019) 465–476.

[49] H.T. Baytekin, B. Baytekin, J.T. Incorvati, B.A. Grzybowski, Material transfer and polarity reversal in contact charging, Angew. Chemie Int. Ed. 51 (2012) 4843–4847.

[50] P.S. Gil, D.J. Lacks, Humidity transforms immobile surface charges into mobile charges during triboelectric charging, Phys. Chem. Chem. Phys. 21 (2019) 13821–13825.

[51] H.T. Baytekin, A.Z. Patashinski, M. Branicki, B. Baytekin, S. Soh, B.A. Grzybowski, The mosaic of surface charge in contact electrification, Science (80-.). 333 (2011) 308 LP – 312.

[52] S. Pan, Z. Zhang, Triboelectric effect: A new perspective on electron transfer process, J. Appl. Phys. 122 (2017).

[53] A. Auroux, A. Gervasini, Microcalorimetric study of the acidity and basicity of metal oxide surfaces, J. Phys. Chem. 94 (1990) 6371–6379.

[54] A. Gervasini, A. Auroux, Acidity and basicity of metal oxide surfaces II. Determination by catalytic decomposition of isopropanol, J. Catal. 131 (1991) 190–198.

[55] G. Busca, The surface acidity of solid oxides and its characterization by IR spectroscopic methods. An attempt at systematization, Phys. Chem. Chem. Phys. 1 (1999) 723–736.

[56] V. Lee, N.M. James, S.R. Waitukaitis, H.M. Jaeger, Collisional charging of individual submillimeter particles: Using ultrasonic levitation to initiate and track charge transfer, Phys. Rev. Mater. (2018).

[57] H.T. Baytekin, B. Baytekin, S. Soh, B.A. Grzybowski, Is water necessary for contact electrification?, Angew. Chemie Int. Ed. 50 (2011) 6766–6770.

[58] E. Tea, J. Huang, C. Hin, First principles study of band line up at defective metal-oxide interface: oxygen point defects at Al/SiO_2 interface, J. Phys. D. Appl. Phys. 49 (2016) 095304.

[59] G.D. Considine, ed., Van Nostrand's encyclopedia of chemistry, 5th ed., John Wiley, 2005.

[60] K. Leung, I.M.B. Nielsen, L.J. Criscenti, Elucidating the bimodal acid−base behavior of the water−silica interface from first principles, J. Am. Chem. Soc. 131 (2009) 18358–18365.

Chapter 7 - Conclusions and Recommendations

Sheeting formation due to electrostatic charge generation in polyethylene gas-phase fluidized bed reactors results in operational challenges that necessitates control/mitigation strategies. A comprehensive knowledge of the potential sources of electrostatic charge generation and interactions of all the materials involved (i.e., catalyst, polyethylene resin, co-catalyst, continuity additives, co-monomers and chain control molecules) is thus essential. Over the past two decades, numerous works have investigated the electrostatic phenomenon in polyethylene reactors. However, the majority of those works have focused on understanding the charging behaviour of PE resin alone and very minimum attention has been given to understand the influence of other compounds such as catalysts or CAs neither on the degree of bed electrification nor on the wall fouling/sheeting formation. To mimic a condition similar to that of the PE commercial reactors where catalysts and CAs are present alongside the PE resin, this thesis aimed to provide an in-depth understanding of the role of a typical catalyst support (amorphous silica) and five commercially available CAs (aluminum distearate, calcium stearate, zinc stearate, AS-990, and Chimassorb 944) on the PE fluidized bed electrification and wall fouling formation. A systematic study was performed to understand the triboelectrification of both solids not only due to their pneumatic conveying but also due to their contacts with PE resin inside a fluidized bed.

During the first phase of this thesis, the electrostatic charging behaviour of various solids due to their pneumatic conveying was evaluated. A pneumatic conveying apparatus was first designed and built that consisted of a 316 stainless-steel conveying line with an inner diameter of 4.75×10^{-3} m which is similar to typical catalysts and CAs dry feeding systems in commercial PE processes. Measuring the electric current directly from the conveying line to determine the conveyed particles electrostatic charge was examined and proven to be a reliable online alternative technique to the conventional Faraday cage method. This system was first tested for studying single particles pneumatic conveying and gaining basic knowledge of influential parameters such as conveying line geometry (conveying line lengths and pathway) and operating condition including conveying gas velocity on particles' electrostatic charging behaviour. Next the experiments were extended to evaluate the electrostatic charging behaviour of powder flow during pneumatic conveying whereby effects of parameters such as conveying line length and pathway, as well as conveying gas velocity were studied.

Pneumatic conveying of single PTFE and Nylon particles of various sizes showed that smaller particles, owing to their smaller surface area, reached saturation charge quicker than larger particles. Conveying line pathway was proven to significantly affect the particles charging behaviour. Presence of only one elbow/bend was sufficient to allow particles reaching the saturation charge due to experiencing a larger contact force with the conveying line. A direct relationship was observed between the particles' residence time inside the conveying line and the generated charge which was attributed to the larger number of contacts between the particle and the conveying tube walls. Therefore, increasing the conveying line length from 0.8 to 3 m and lowering the conveying gas velocity to just above the particles' pick-up velocity were observed to increase the particles' acquired charge. In general, increasing the conveying gas velocity from 20 to 100 m/s was observed to increase the degree of particles charging.

The electrostatic charging behavior of an amorphous silica catalyst support (non-dehydrated and dehydrated) was investigated through a pulse pneumatic injection. Increasing the conveying line length and addition of a bend or an elbow were both found to increase the extent of the silica charging. The *Q/m* of the conveyed silica was observed to be directly related to the conveying gas velocity while inversely proportional to solids mass loading. Dehydrating the silica resulted in a significant increase in the particles *Q/m* and that in turn resulted in a notable fouling inside the conveying tube. The mass of tube fouling gradually reached a steady level by performing consecutive pulse injections. In addition, as the tube fouling grew a reduction was observed in the solids' *Q/m* which was attributed to a shift in contacts nature from being dominantly particle-metallic tube wall to the combination of particle-tube wall and particle-particle.

Based on the knowledge developed on the parameters influencing the powder charging due to pneumatic conveying, a 5 m in length conveying line containing one large radius bend and a conveying gas velocity of 15 m/s were selected as the operating conditions for testing amorphous silica catalyst support and various CAs. The triboelectrification of five commercially used CAs with three being ionic (aluminum distearate, calcium stearate and zinc stearate) and two being non-ionic (AS-990 and Chimassorb 944) were examined through pulse injection. In addition, electrostatic charging on silica powder doped with various concentrations of aluminum distearate and/or AS-990 were studied. The *Q/m* of CAs were measured to be significantly lower than that

for the silica and silica doped with CAs due to pneumatic conveying. Significant tube fouling was observed for calcium stearate with a dp_{50} of 7 μm and silica doped with CAs.

After gaining a comprehensive understanding on the triboelectrification of the tested powders during pneumatic conveying, the conveying line apparatus was connected to a pilot-scale atmospheric gas-solid fluidized bed (0.1 m in diameter and 1.3 m in height). This study for the first time enabled the direct investigation of the influence of injecting charged powders through pneumatic conveying on the extent of fluidized bed fouling. To provide a comparative analysis on the effect of introduced charge by powders' injection, two methods were employed to load the powders into the fluidized bed; first, via pneumatic injection whereby a certain level of charge developed on the powders' when entering the bed and second, via spatula whereby powders were introduced into the bed with a minimum possible charge. Powders' initial charge upon entering the fluidized bed was confirmed to have minimal influence on the extent of the wall fouling and the bed electrification.

A major finding from this thesis was that the degree of wall fouling was directly related to the net specific charge magnitude of the particles in the bulk of the fluidized bed. Reducing the bed bulk specific charge magnitude was found to lessen the formation and progression of the wall fouling.

Depending on the powders type, they either promoted positive charge (aluminum distearate and AS-990) or negative charge (calcium stearate and silica) inside the PE fluidized bed. Some of the powders, especially those with larger particle sizes such as zinc stearate, were found to have a slightest influence on the bed charging. Thus, it was concluded that the surface chemistry of the powders entering the fluidized bed are of significant importance in determining the bed dominant charge polarity and thus the potential of wall fouling formation and progression. In relation to the CAs, their particle size and freedom of movement were also found to be affecting the results. Larger particle sizes or when doped on the silica catalyst support showed a lesser impact with respect to altering the bed bulk net charge polarity and magnitude compared to smaller size particles and when they were added separately to the bed.

Electron transfer was proposed to be the dominant charge transfer mechanism for silica and non-ionic CAs within the conveying line and the fluidized bed upon contacting the PE resin. Conversely, for the ionic CAs ion transfer was proposed as a dominant contributing charge transfer mechanism upon contacting the PE resin and the stainless-steel wall.

In a separate work conducted in collaboration with the Japan National Institute of Occupational Safety and Health (JNIOSH) the electrostatic charging behaviour of polypropylene powder was investigated with a goal of understanding the types of contacts (i.e., hitting, rolling, or sliding) on the generated charge on particles. The pneumatic conveying apparatus consisted of a stainless-steel tube with an inner diameter of 0.035 m and a 5000 frame-per-second high speed camera to capture the particle flow motion. Three convey gas velocities were examined. It was found that particles which were sliding against the tube wall generated a lesser amount of charge in comparison to the particles which were rolling. It was also confirmed that the particles which hit the conveying line, on average, developed a greater charge magnitude that those rolled or slide against the tube wall. A direct relationship was found between the impact force and the particles acquired electrostatic charge.

Overall, this thesis concludes that the knowledge of surface chemistry of the catalyst and CAs involved in the ethylene gas-phase polymerization process is essential in determining their charge transfer mechanisms inside the reactor. Knowing the charging mechanism enables the prediction of the dominant charge polarity within the reactor resulting in effectively balancing the net charge inside the reactor and in turn minimizing the formation of sheeting.

7-1 Recommendations for Future Work

Knowledge was gained through this work with respect to the relationship between the surface chemistry of silica catalyst support and continuity additives and the extent of the bed electrification and subsequently wall fouling. However, there are still unknowns which require further in-depth investigation. Thus, the following recommendations are proposed for the future work:

a) Three ionic CAs were tested in this work. CAs with smaller particles sizes (aluminum distearate and calcium stearate) within a range of 20-µm were observed to significantly affect both the bed electrification and the wall fouling, whereas the CA with a larger particles size (zinc stearate with a dp_{50} of 540 µm) was not. It is recommended to test zinc stearate with a smaller particles size (within a 20-µm range) to determine the effect of CAs particle sizes on the bed electrification.

b) This work investigated the triboelectric effects of a common catalyst support (i.e., amorphous silica) on the PE fluidized bed. Knowing that charge transfer is a surface related

phenomenon and that in a heterogenous catalyst, the support gets covered by various types of elements such as continuity additives, flow enhancers, co-catalysts, and active catalyst sites, which themselves consist of various elements, it is recommended to perform experiments where these elements are individually doped on the amorphous silica support.

c) The ultimate goal will be to study triboelectric effect of a deactivated catalyst followed by an active catalyst which would represent a real system.

d) In this research, all the experiments were conducted at ambient temperature, 25°C. and atmospheric pressure. However, commercial polyethylene reactors operate at higher temperatures (75 – 110°C) and elevated pressures in the range of 2600 kPa. Thus, it is recommended to investigate the triboelectric effects of catalyst and CAs at an operating condition close to the commercial process.

e) In a commercial PE gas-phase process, both the catalyst and CAs can be added into the reactor either in dry solid form, slurry, or in a solution. Considering that this thesis focused on the dry feeding method, it is recommended to examine slurry and solution feeding methods on the fluidized bed wall fouling. It is suggested to perform this testing at an elevated temperature to ensure solvent/slurry liquid fast evaporation.

Appendix A - Gas-Solid Fluidized Bed

As shown in **Figure A-1**, Geldart categorized solid particles based on their fluidization quality, size and density into four types (A, B, C and D) [1].

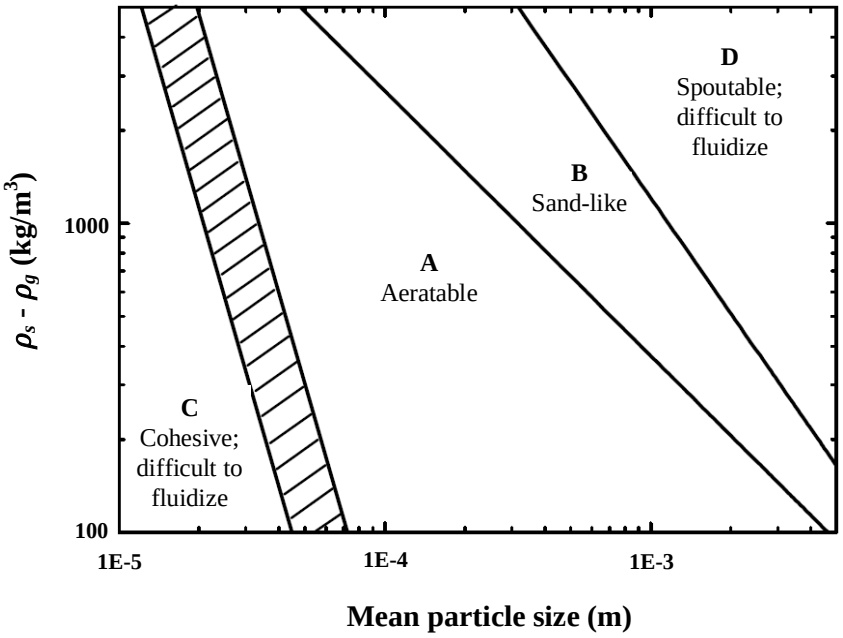

Figure A-1 The Geldart chart for the classification of particles [1].

Particles that belong to group C are fine and ultrafine particles which are difficult to fluidize due to large cohesive forces between them. Group A particles are aeratable and easily fluidized in their dry form. Group B particles are sand-like particles and same as group A are easy to fluidize. Larger and denser particles are categorized as group D particles, which exhibit poor fluidization quality.

Depending on the type of particles being fluidized and the bed dimensions, different types of flow regimes may be observed. As the gas passes through the bed of particles at a velocity referred to as the minimum fluidization velocity (U_{mf}), the drag and buoyant forces equal the gravity force, and thus the pressure drop across the bed remains constant by further increasing the gas flow [2]. The value of minimum fluidization velocity is a function of several operating parameters, among which the particle physical properties such as size, shape and density are considered the most important [3]. With further increasing the gas flow rate, bubbling flow regime is achieved where the excess gas passes through the column in the form of bubbles. The velocity at which bubbles start to form is noted as the minimum bubbling velocity (U_{mb}) [4,5]. In beds with large height-to-diameter ratios, a slugging regime is expected to occur [2]. In this regime, the size of gas bubbles reaches 60% of the internal diameter of the fluidized bed [2]. The next regime is called turbulent fluidization where the high shear forces resulting from the fast moving gas cause bubbles to become

distorted and eventually disappear [2]. Entrainment is expected to occur in this regime [3]. Further increasing the gas velocity leads to more entrainment and the fast fluidization regime appears. Finally, at large gas velocities, all of the solid particles will be suspended in the fluidizing gas and move upward [2]. This regime is known as pneumatic transport.

Appendix B - Polyethylene Catalyst

The production of polyethylene with desired properties (e.g., molecular weight distribution or density) highly relies on the type of the catalyst, H_2 concentration (used as a chain terminator which has a reverse relation with the PE molecular weight distribution), as well as the type and concentration of the co-monomers (effective in determining the branching and PE density) used in its synthesis process. Ziegler-Natta and metallocene catalysts are two of the most commonly used catalysts in PE production. Ziegler-Natta catalysts have many variations but are generally $TiCl_4$ supported on SiO_2 or $MgCl_2$, combined with a variety of electron donors and co-catalysts [6]. In operations, a trialkyl aluminum (typically triethyl aluminum) is used as a co-catalyst. **Figure B-1** shows the chemical formula of $TiCl_4$ along with its co-catalyst.

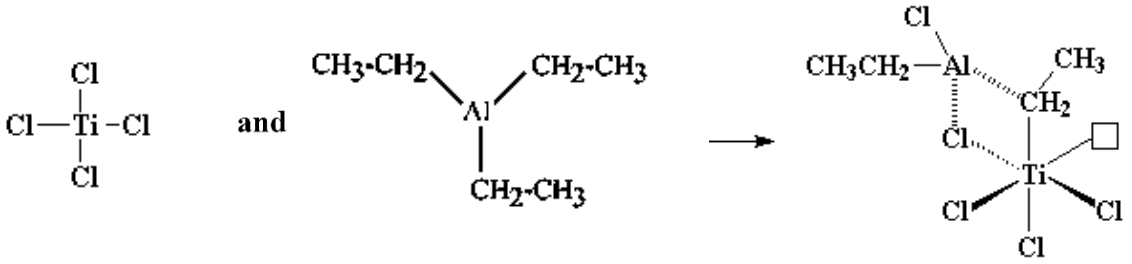

Titanium tetrachloride **Triethyl aluminium** **Ziegler-Natta catalyst**

Figure B-1 Schematic of ethylene polymerization using Ziegler-Natta catalyst [7].

Metallocene catalysts are "sandwich" compounds of the type $B(L_1L_2)MX_2$, where a transition metal, M (most commonly zirconium or titanium), is sandwiched between two ligands, L_1 and L_2 (cyclopentadienyl, indenyl, Euorenyl, etc.), and bonded to two substituents, X (very commonly Cl or methyl) [8]. The ligands can be connected by a bridge, B (e.g., silyl). **Figure B-2a** represents a typical structure of a metallocene catalyst. **Figure B-2b** shows the activation and polymerization mechanism of a zirconium metallocene catalyst with its co-catalyst (methyl aluminoxane). Three typical methods of supporting a metallocene catalyst on a silica surface are presented in **Figure B-3**. The metallocene catalysts are becoming more favorable catalysts in polyethylene production due to their high activities, narrow molecular weight distributions, and easy implementation in existing Ziegler-Natta processes [6,10].

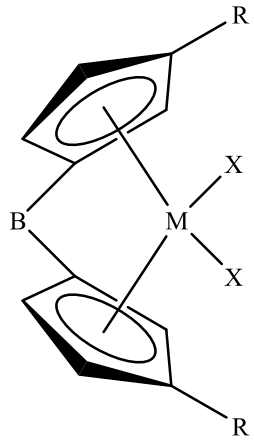

R	Methyl, n-propyl, n-butyl
B	Could be absent depending on the catalyst type.
M	Zirconium, Titanium, Hafnium
X	Cl, Methyl

(a)

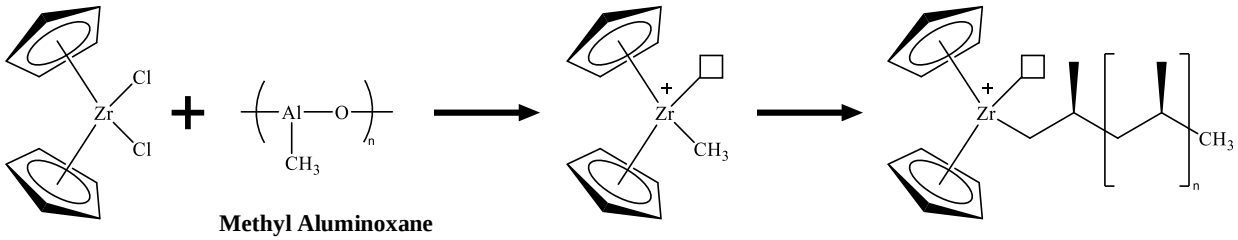

Methyl Aluminoxane (MAO)

(b)

Figure B-2 (a) A typical chemical structure of a metallocene catalyst; (b) schematic of ethylene polymerization using zirconium based metallocene catalyst [9].

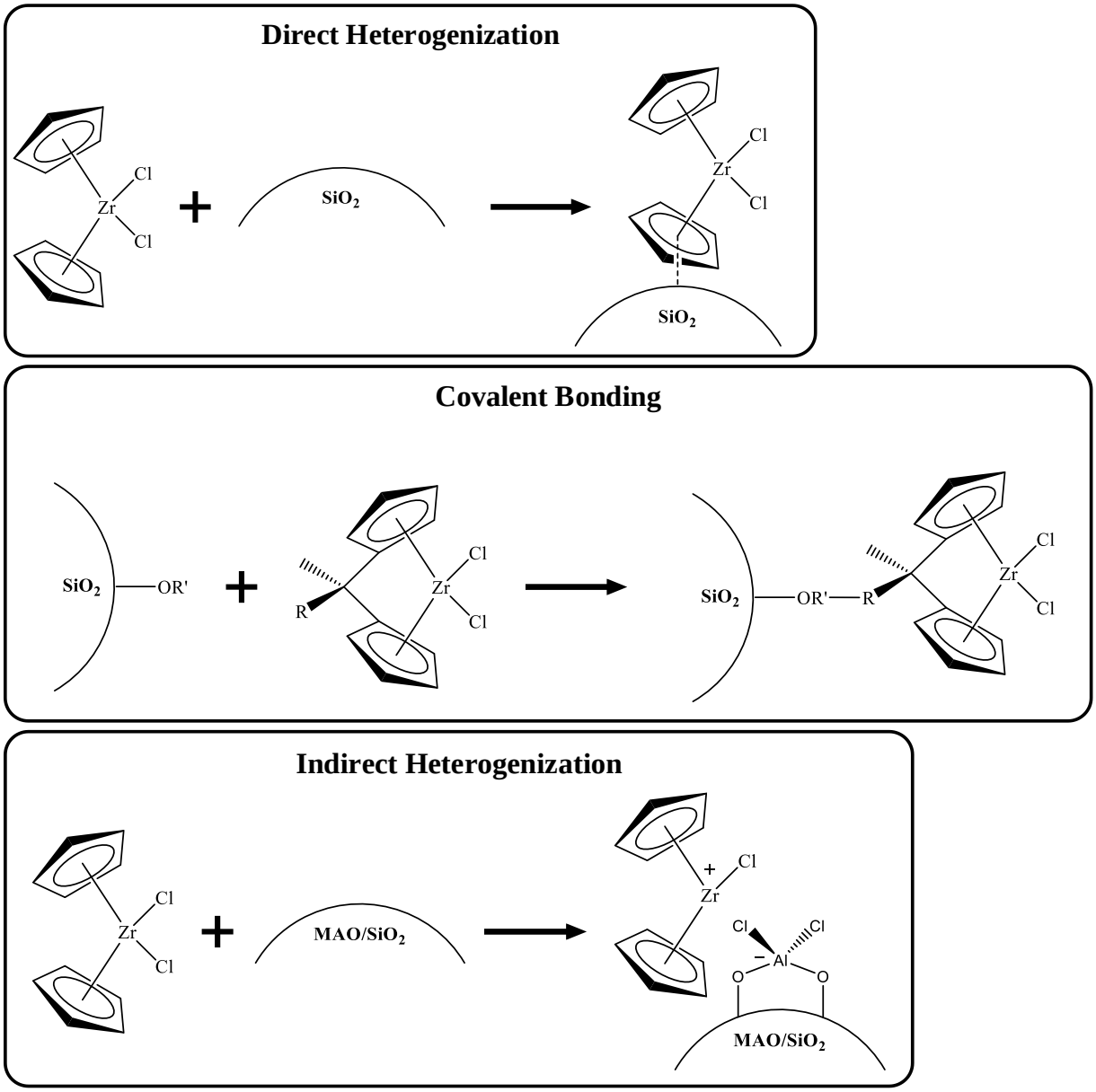

Figure B-3 Supporting methods of a metallocene catalyst on silica surface [9].

Appendix C - Relationship between Fines and Dropped *Q/m*

Aside from the direct relationship between the total wall fouling and the *Q/m* magnitude of the *Dropped* particles presented in **Chapter 6**, an inverse relationship was observed between the *Q/m* polarity of the *Fines* and *Dropped* particles. Such relationship which is illustrated in **Figure C-1** and was discussed in detail in **Chapter 6** is attributed to the presence of bipolar charging between the larger and smaller size particles within the bulk and entrainment regions of the bed, respectively.

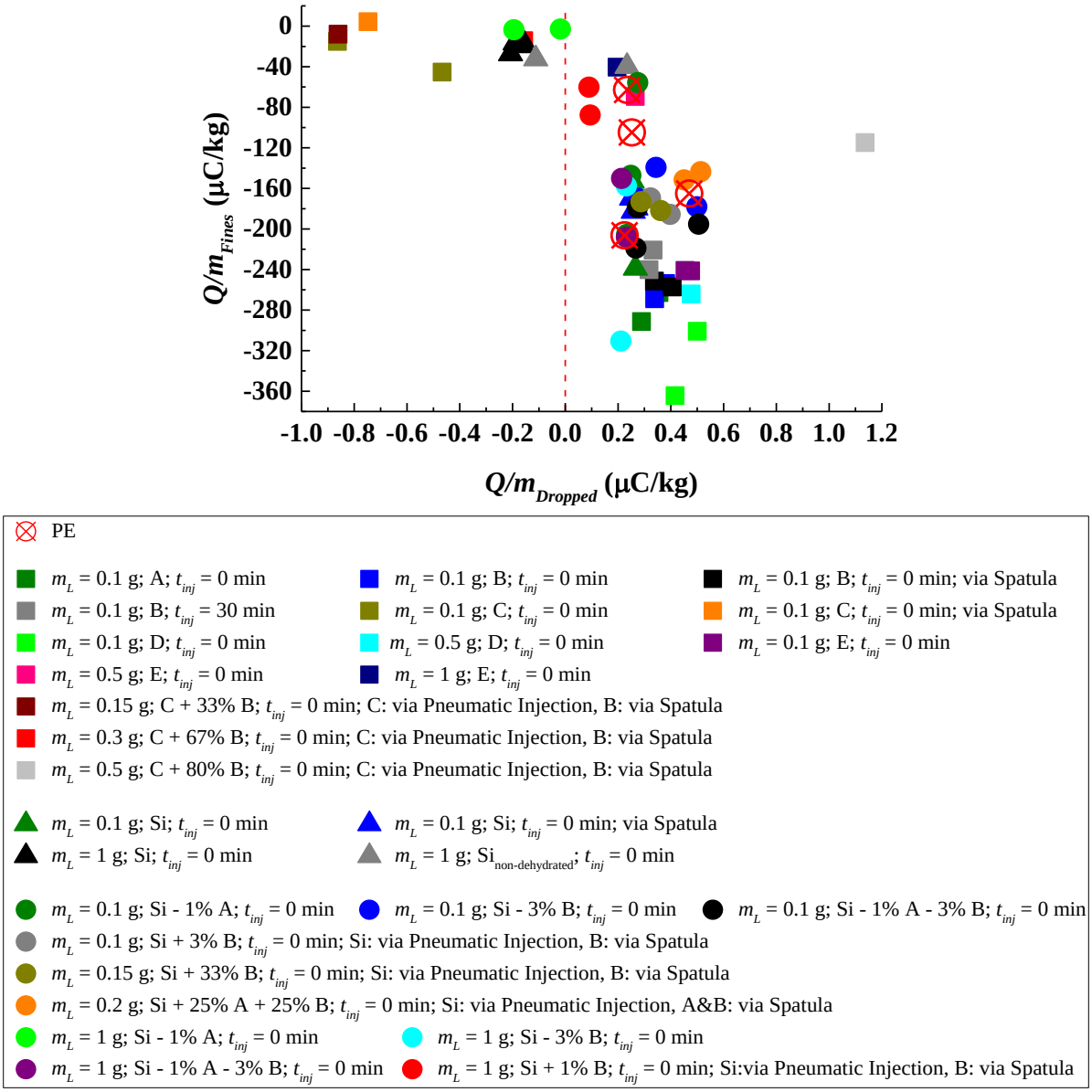

Figure C-1 Summary of the results showcasing the relationship between the *Q/m* of the *Fines* and *Dropped*.

Appendix D - Experimental Apparatus

This section presents the pneumatic conveying and atmospheric gas-solid fluidization system.

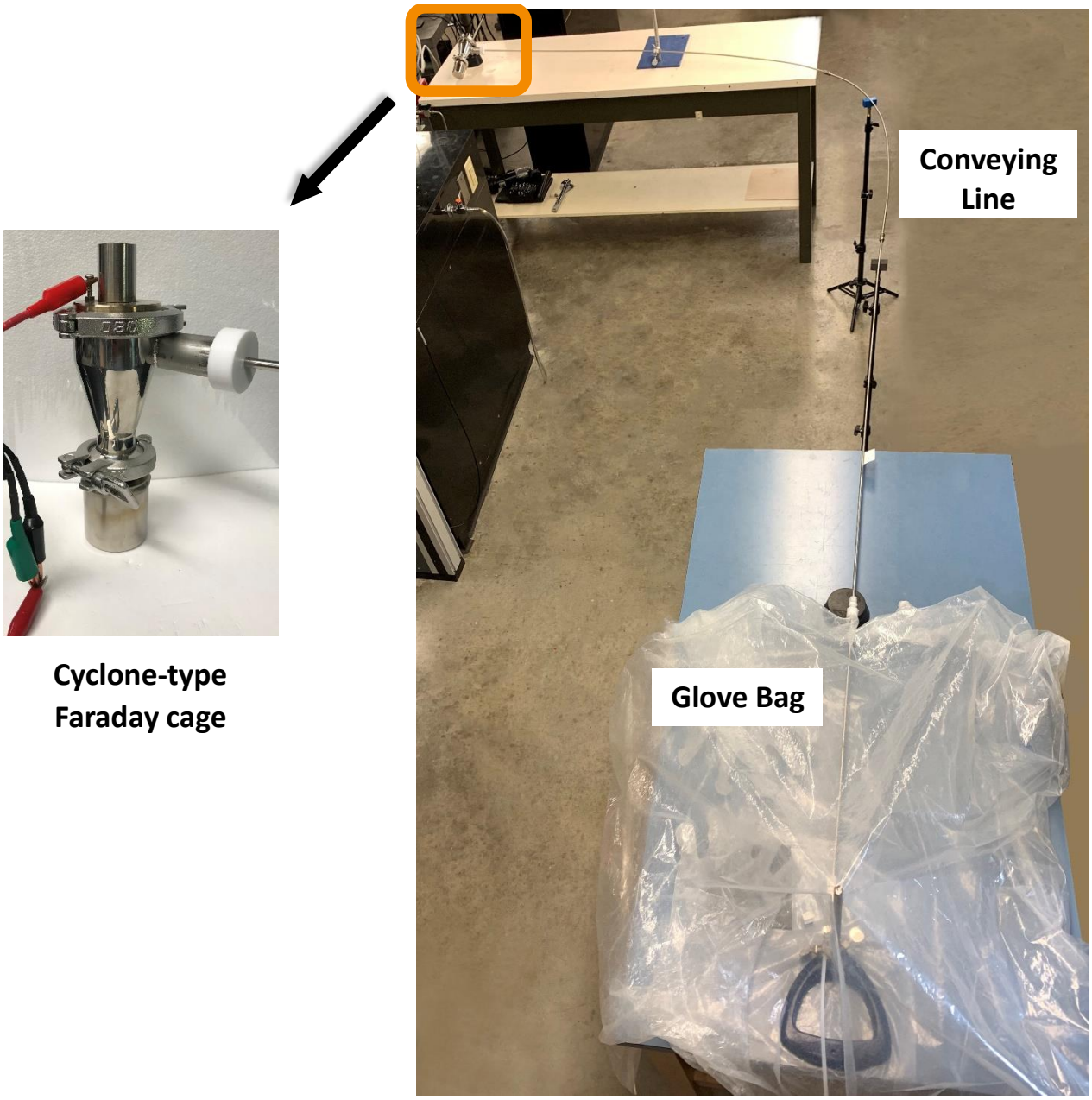

Figure D-1 Pneumatic conveying apparatus including a 5 m pneumatic conveying line, a glove bag, and a cyclone-type faraday cage.

Figure D-2 Gas-solid atmospheric fluidization system connected to the pneumatic conveying line.

Appendix E - Health and Safety

Numerous types of particles with various size distributions (ranging from approximately 2 µm to 1900 µm) were used in this thesis. As such, it is recommended to take the following safety steps when handling the particles.

Table E-1 Recommended personal protective equipment for handling of the particles in this thesis.

Particle Type	**Particle Size Range**	**Personal protective equipment (PPE)**
PTFE	3.18 and 0.79 mm	Safety glasses and lab coat
Nylon	3.18 mm	Safety glasses and lab coat
Polyethylene	35 – 1300 µm	Safety glasses, N95 mask, gloves, and lab coat
Polypropylene	2 – 10 µm 1100 – 1900 µm	Safety glasses, N95 mask, gloves, and lab coat
Amorphous silica	27 – 90 µm	Safety glasses, N95 mask, gloves, and lab coat
Aluminum Distearate	35 – 1300 µm	Safety glasses, N95 mask, gloves, and lab coat
Calcium Stearate	2 – 20 µm	Safety glasses, N95 mask, gloves, and lab coat
2-2' (octadecylimino)bisethanol (known as AS-990)	4 – 200 µm	Safety glasses, N95 mask, gloves, and lab coat
Zinc Stearate	180 – 1015 µm	Safety glasses, N95 mask, gloves, and lab coat
Chimassorb 944 fdl	30 – 460 µm	Safety glasses, N95 mask, gloves, and lab coat

Solids Disposal:

- Amorphous silica is a designated material. Although the used amount of the silica for the experiments is within the safe concentration, it is highly recommended to dispose samples containing silica in a solid waste container provided by the Office of Health and Safety Management.
- Solids Handling: To reduce the risk of small size particles suspension in the open air, all additives must be handled inside a fume hood or glove box.
- A vacuum cleaner containing a Hepa filter must be used to clean the working area; however, upon changing the vacuum bag attention must be paid to contain it in a plastic garbage bag to reduce the risk of having particles suspended in the open air.

Appendix References

[1] D. Geldart, Types of gas fluidization, Powder Technol. 7 (1973) 285–292.

[2] D. Kunii, O. Levenspiel, Fluidization engineering, Elsevier, 1991.

[3] G. Chaplin, Monitoring fluidized bed dryer hydrodynamics using pressure fluctuations and electrical capacitance tomography, University of Saskatchewan, 2005.

[4] D. Kunii, O. Levenspiel, Fluidization engineering, Elsevier, 1991.

[5] C.L. Law, A.S. Mujumdar, Fluidized bed dryers, in: A.S. Mujumdar (Ed.), Handb. Ind. Dry., Fourth Edi, CRC Press, 2014: pp. 161–189.

[6] T. Xie, K.B. McAuley, J.C.C. Hsu, D.W. Bacon, Gas phase ethylene polymerization: Production processes, polymer properties, and reactor modeling, Ind. Eng. Chem. Res. 33 (1994) 449–479.

[7] H. Sinn, W. Kaminsky, Ziegler-Natta Catalysis, Adv. Organomet. Chem. 18 (1980) 99–149.

[8] A. Winter, J. Rohrmann, M. Antberg, W. Spaleck, W.A. Herrmann, H. Riepl, Process for the preparation of an olefin polymer using specific metallocenes, US Patent 5504232 A, 1996.

[9] W. Kaminsky, A. Laban, Metallocene catalysis, Appl. Catal. A Gen. 222 (2001) 47–61.

[10] C.-I. Kuo, G.G.H. Patel, R.E. Pequeno, B.J. Savatsky, F.D. Hussein, Continuity additive for polyolefin polymerization processes, US Patent 9221936 B2, 2015.